Liquid Crystal Shutters for Stereoscopic Vision and 3D Dual View Application

Vinicius Nunes Henrique Silva

N° d'ordre : 2013telb0273

Sous le sceau de l'Université européenne de Bretagne

Télécom Bretagne

En habilitation conjointe avec l'Université de Bretagne-Sud

Ecole Doctorale – sicma

Liquid Crystal Shutters for Stereoscopic Vision and 3D Dual View Application

---

Thèse de Doctorat

Mention : ***"Sciences pour l'Ingénieur"***

Présentée par **Vinicius NUNES HENRIQUE SILVA**

Département : **Optique**

Directeur de thèse: Jean-Louis de Bougrenet de la Tocnaye, Professeur, Département d'optique, Télécom Bretagne

Soutenue le 23 avril 2013

Jury :

M. Jean-Baptiste de La Rivière – Directeur scientifique, Immersion (Rapporteur)
M. Jean-François Blach – Maître de conférences, Unité de catalyse et de chimie du solide (Rapporteur)
M. Jean-Louis de Bougrenet de la Tocnaye – Professeur, Télécom Bretagne
M. Jean-François Feller – Professeur, LIMATB UBS (Examinateur)
M. Laurent Dupont - Professeur, Télécom Bretagne (Examinateur)
M. Thibaut de Bougrenet – Ingénieur et chef d'entreprise, E3S (Examinateur)

M. Daniel Stoenescu - Maître de Conférences, Télécom Bretagne (Invité)

Abstract

In this thesis the main objectives were to improve the liquid crystal shutters and to develop a stereoscopic vision application called 3D Dual View. The vision quality of a 3D system based on active glasses is directly related to the performance of the liquid crystal shutters. There are a lot of parameters that play an important role in the quality of 3D glasses. Thus, efforts were concentrated in the organization of the liquid crystal molecules between the substrates and in the liquid crystal itself. We studied different configurations of shutters using nematic liquid crystal and ferroelectric liquid crystal (smectic), with and without polymer. Furthermore, the ferroelectric samples were analyzed using a full optical snapshot matrix Mueller polarimenter made by UBO (Université de Bretagne Occidentale) in partnership with Télécom-Bretagne. The second part was the development of 3D Dual View System. It is a stereoscopic vision system based on a mixture of active and passive 3D solutions which display a 3D image that can be viewed simultaneously by two spectators, but from different perspectives. To allow two different points-of-view of a scene or object in three dimensions, the system has to multiplex four images, one pair to form the 3D image for one viewer in one perspective and the other pair for the second viewer in other perspective. We describe different techniques to multiplex and demultiplex the video streams taking into account the physiological aspects, market, image quality and the crosstalk. The crosstalk between the images leads to an effect called *ghosting*, where the user sees a low intensity image that belongs to the other viewer. Then, we also characterized the ghosting effect (crosstalk) and proposed an algorithm of ghostbusting to compensate it.

Keywords: liquid crystal, optical shutters, stereoscopic vision, muelle matrix polarimeter, 3D dual view, 3D active glasses

Acknowledgments

I would like to dedicate this work to my grandparents, Mr Aloysio da Silva Nunes (in memorian), Mrs Jamyr Mendonça Nunes, Mr Carlos Henrique Silva (in memoriam) and Mrs Adair Rocha (in memorian), they gave me everything, support, knowledge and affection. It would have been impossible to reach this day without them. My other family members especially my parents, Mr Ronaldo Henrique Silva, Mrs Janilza Nunes Henrique Silva, and my sisters, Mrs Fabiana N. H. Silva and Dr Daniele N. H. Silva. All of them have been more than family members and I do not have words to express their importance.

I put her in the second paragraph, but she is the one, the most important. She is in all the pages of this thesis and in every letter there is a piece of her. I would like to thank the woman that I love, my wife Mrs Suellen Bastos Farinha. She gives me love to go on and support to reach all of our dreams until now. It was her who heard me all the days I came home without results, thinking that my PhD was going down and that I would never finished. Even without knowing anything about liquid crystal she was surer that this day would come.

I would like to express my gratitude towards Prof. Jean-Louis de Bougrenet de la Tocnaye and Mr. Thibaut de Bougrenet de la Tocnaye for giving me the opportunity to work at Télécom-Bretagne/Eyes3Shut and be able to do what I like, research. I have discovered a new world studying liquid crystals and stereoscopic vision. I had the opportunity to learn and to experience not only the research part, but also the business behind. They have been very supportive throughout this work and I would like to thank them for all this period of three and half years. In particular, Prof Jean-Louis de Bougrenet de la Tocnaye who was the person who drove my thesis, giving me the right directions. Special thanks go to Eyes3shut that gave me the financial support and all its employees.

If I had to make a choice, I would like to be a researcher like Dr Daniel Stoenescu. He conducts the research in a very meticulous way. Every step is very well calculated and it has a fundamental reason to be, he doesn't do anything without knowing all the details in advance. Besides, it is impressive his capability to explain and teach, I forgot how many times I went to him disturbing and asking question about liquid crystal and stereoscopic vision. Also, several times he came spontaneously to me to share something that he has discovered. I have no words to thank Dr Daniel Stoenescu due the amount of things that I have learned.

Prof. Laurent Dupont has been my smectic guru. His knowledge in liquid crystal area associated with patience was a blessing. He always had an answer to my question, or difficulties to understand technological and theoretical aspects. No matter what time or place, he was always listening to my doubts and crazy ideas. Thank god he has never charged me. Otherwise, I am sure that I won't have enough money.

Special thanks go to two of my best friends Luiz Felipe Maximiano, Leandro Manduca, Luiz Anet and Patricia Ruiz. Without them I would never come to France. More important than that, with their support my stay here in Brest was memorable.

I gained two things in my PhD, the title, and more important than that, the friendship of Dr.

Kedar Sathaye. Kedar is a friend for the entire life and now part of my family. We had a very good time in Brest playing football, travelling, shopping, drinking, talking nonsense, studying and working. Everything that I know about clean room is because he taught me all the steps and procedures. Further, for a long period he was my personal translator. I consider myself a very lucky person to have found a person like Kedar. Thank you very much! You are the MAN!

Also, I would like to express a word of appreciation for Dr Sylvain Rivet, Dr Philippe Babilotte and Dr Mathieu Dubreuil. We have formed a nice group of research in liquid crystals. I would like to thank Bernard Della who made my work easier in the clean room and taught me a lot of good expressions in French. Dr Andres Pablo Barbero and Dr Ricardo Marques Ribeiro, without them I would never thought to be a researcher and brave enough to leave my country.

I would like to thank my fellow colleagues and friends Dr Hani Al Hajjar (Raid partner), Dr Aurelie Chang Yong (Raid partner), Lida Sadeghioon, Dr Mervin Obegadoo, Dr Bogdan Uscumulic, Dr Charbel Nassour, Frederick Lucarz and Dr Hou Bo. I would like to express a special word of appreciation for entire staff members of Department of Optics. Especially Jennifer Romer, who is the secretary of the Department and have made the things easier for me with the French bureaucracy. Finally, I would like to thank all the members of the Vieira Marins family, especially Leonardo and Aline.

Contents

LIST OF FIGURES X
LIST OF TABLES XIII
MOTIVATION AND INTRODUCTION 1

CHAPTER 1: INTRODUCTION TO LIQUID CRYSTALS 3

INTRODUCTION 3
1. LIQUID CRYSTALS 3
1.1 NEMATIC LIQUID CRYSTAL 5
1.2 SMECTIC LIQUID CRYSTAL 5
1.2.1. Smectic A 5
1.2.2. Smectic C 6
1.2.3. Smectic C* 6
1.3 BASIC LIQUID CRYSTAL PHYSICAL PROPERTIES 7
1.3.1. Optical Anisotropy (Birefringence) 7
1.3.2. Dielectric Anisotropy 8
1.3.3. Elastic Constant and Free Energies 9
1.3.4. Viscosity 10
1.3.5. Dielectric Coupling 11
1.3.6. Ferroelectric Coupling 12
1.4 LIQUID CRYSTAL SHUTTERS/DISPLAY 13
1.4.1. Electrically Controlled Birefringence (ECB) mode 13
1.4.2. Thin Nematic 3D Shutters (TNs) 15
1.4.3. Twisted Nematic Shutters/Display 16
1.4.4. In-Plane Switching (IPS) 17
1.4.5. Surface Stabilized Ferroelectric Liquid Crystal Shutters 18
CONCLUSION 21
BIBLIOGRAPHY 22

CHAPTER 2: LIQUID CRYSTAL SHUTTERS FOR 3D CINEMA 23

INTRODUCTION 23
2.1. DEPTH PERCEPTION (BINOCULAR VISION) 24
2.2. STEREOSCOPIC VISION 24
2.2.1. 3D Techniques Without Glasses 25
2.2.1.1. Freeviewing 25
2.2.1.2. Autostereoscopy 26
2.2.2. 3D Techniques With Glasses 27
2.2.2.1. Color Multiplexing (Anaglyph) 27
2.2.2.2. Polarization Multiplexing 28
2.2.2.3. Time Multiplexing 29
2.3. STEREOSCOPIC VISION MAIN DRAWBACKS 29
2.3.1. Ghosting Effects 30
2.3.2. Color Banding 31
2.4. LIQUID CRYSTAL 3D SHUTTERS 31
2.4.1. Stabilised Ferroelectric Liquid Crystal Shutter (SFLC) 32
2.4.2. Polymer Stabilised Ferroelectric Liquid Crystal Shutter (PSFLC) 35
2.4.3. Nematic Liquid Crystal Shutter 37
CONCLUSION 43
BIBLIOGRAPHY 44

CHAPTER 3: CHARACTERIZATION OF FERROELECTRIC LIQUID CRYSTAL (FLC) SHUTTERS USING A SNAPSHOT MUELLER MATRIX POLARIMETER 46

INTRODUCTION 46
3.1. MUELLER MATRIX POLARIMETER 47
3.1.1. The principle of a Mueller Matrix Polarimeter 47
3.1.2. A Mueller Matrix Polarimeter in (e, e, 5e, 5e) configuration 47
3.1.3. The Snapshot Mueller Matrix Polarimeter (e, e, 5e, 5e) 50
3.2. SURFACE STABILIZED LIQUID CRYSTAL (SSFLC) 51
3.2.1. SSFLC in Bookshelf Geometry 51
3.2.2. SSFLC in Chevron Geometry 52
3.3. THE SSFLC AND THE POLARIMETRIC PARAMETERS 54
3.4. POLARIMETRIC EXPERIMENTAL RESULTS 55
3.4.1. The SSFLC samples and its Textures 55
3.4.2. Static Polarimetric Measurements on SSFLC cells 57
3.4.3. Dynamic Polarimetric Measurements on SSFLC cells 58
3.4.4. The Irreversible Chevron to Bookshelf Transition 61
3.4.5. Dynamic Polarimetric Measurement on PSFLC cells 65
CONCLUSION 69
BIBLIOGRAPHY 70

CHAPTER 4: 3D DUAL VIEW TECHNIQUE 72

INTRODUCTION 72
4.1. 3D DUAL VIEW TECHNIQUES 73
4.1.1. Time Multiplexing (Case 1) 74
4.1.2. Temporal and Polarization Multiplexing (Case 2.*) 76
4.1.3. Spectral Multiplexing, Anaglyph (Case 5) 78
4.1.4. Temporal and Spectral Multiplexing (Case 3.*) 79
4.1.5. Polarization and Spectral Multiplexing (Case 4) 82
4.2. 3D DUAL VIEW SETUP 84
4.2.1. Reflective Mode Setup (Télécom-Bretagne) 85
4.2.2. Transmissive Mode Setup (Immersion) 87
4.3. GHOSTING EFFECT MEASUREMENTS 88
4.3.1. Ghosting Ratio 90
4.3.2. Experimental Setup for Ghosting Evaluation (Télécom-Bretagne) 91
4.3.3. Reflective Mode Results (Télécom-Bretagne) 94
4.3.4. The Ghosting Ratio Experimental Setup (Immersion) 106
4.3.5. Transmission Mode Results (Immersion) 106
4.4. OPTICAL QUALITY AND PHYSIOLOGICAL IMPACTS 112
4.5. GHOST-BUSTING 113
CONCLUSION 118
BIBLIOGRAPHY 120

GENERAL CONCLUSION AND PERSPECTIVES 123
APPENDIX I: 126
APPENDIX II: 130

List of Figures

Figure 1 - Ilustration of (a) smectic-C, (b) smectic-A and (c) nematic liquid crystals. 4
Figure 2 - Nematic liquid crystal, the director $\vec{n}$ and a nematic under polarized microscope. 5
Figure 3 - Representation of smectic-A phase and the director n parallel to the molecules long axis 6
Figure 4 - Representation of smectic-C phase and the director $\vec{n}$ tilted according to the layers 6
Figure 5 - Representation of smectic-C phase and the rotation of the director $\vec{n}$ from layer to layer 6*
Figure 6 - Schematic of a light wave travelling inside of a birefringent medium. 8
Figure 7 - The three types of deformation: splay (a), twist (b) and bend (c). 9
Figure 8 - Liquid crystal molecule of positive and negative anisotropy under electric field. 12
Figure 9 - Spontaneous polarization on the smectic cone in an unwound smectic-C liquid crystal. 12*
Figure 10 - Schematic of an ECB cell. 14
Figure 11 - Schematic of a Thin Nematic cell and the polarizer orientation. 15
Figure 12 - Schematic of a Twisted Nematic cell. 16
Figure 13 - Schematic of an In-Plane Switching cell. 18
Figure 14 - Schematic of an SSFLC cell. 19
Figure 15 – The perspectives of an object seeing by the right and left eye. 24
Figure 16 – The lines of sight of a normal reading and seeing a 3D parallel view image. 25
Figure 17 – The crossed lines of sight of the Cross-Eye freeviewing technique. 26
Figure 18 – Illustration of the Parallax Barrier technique. 26
Figure 19 - Illustration of the lenticular Lens technique. 27
Figure 20 – The illustration of the color multiplexing technique using red and cyan filters. 28
Figure 21 – The polarization multiplexing with linear polarisers. 28
Figure 22 – Schematic of time multiplexing 3D cinema. 29
Figure 23 – Color Banding effect. 31
Figure 24 – Macroscopic schematic of FLC sample used in the experiments. 33
Figure 25 – The experimental setup to measure contrast ratio and response time. 33
Figure 26 – Pictures taken under cross polarised microscope for different twist angles. 35
Figure 27 – Pictures of the sample Felix 15/100 with 15° of twist before and after electric field. 35
Figure 28 - The light scattering of the PSFLC 13% measured with ELDIM EZLite. 37
Figure 29 – Experimental setup to measure the relaxation time in thin nematic shutters. 38
Figure 30 – The plot of the relaxation time of the different mixtures. 39
Figure 31 – Transmission versus wavelenght for the four mixtures meassured by the spectrometer. 39
Figure 32 – The transmission versus the incidence angle of the four shutter filled with the four mixtures measure by the ELDIM EZLite. 40
Figure 33 – The transmission angles improved by the MixB. 41
Figure 34 – The white dispersion of the four mixtures measured with the ELDIM EZLite. 41
Figure 35 - Polarisation Ellipse 127
Figure 36 - Examples of polarisation states: linear (a), circular (b) and elliptical (c). 127
Figure 37 - Scheme of a sample measuring polarimeter. 47
Figure 38 - Schematic of the Muller Matrix polarimeter in a (e, e, 5e, 5e) configuration. 48
Figure 39 - Experimental setup of the snapshot Mueller matrix polarimeter in the (e, e, 5e, 5e) configuration. . 50
Figure 40 - Schematic of a SSFLC in bookshelf geometry applying electric field. 51
Figure 41 - The molecule, the smectic cone and the respective parameters. 52
Figure 42 – The schematic of the chevron in SSFLC devices and the "new" position of the smectic cone. 53
Figure 43 – The liquid crystal director on a chevron structure. 53
Figure 44 – Textures under polarised microsocope of the Cell 1 (a and c) and Cell 2 (b and d) after two hours of high intensity and low frequency electric field. The dimensions are 500 x 500 μm. 56
Figure 45 – The voltages where the four static measurement a, b, c e d have been done. 57
Figure 46 – The polarimetric parameter differences α_R and R between the addresed states (a) and (b), and the memory state. The picture area is 1cm² and the vertical scale is in degrees and divided in 50 gray levels. 57
Figure 47 – Dynamics of the polarimetric parameters α_R and R between the up (a) and down (c) transition at a particular point if the cells 1 and 2. 58
Figure 48 – The liquid crystal director trajectory over the transision between the two adressed states. 59
Figure 49 – Images representing the parameter $|S|$ and τ. 59

Figure 50 – The ε_R during the transition between the two addressed states. 60
Figure 51 – (a) Hysteresis curves $\alpha_R(V)$ for 0, 10 and 90 seconds of electric field exposure, (b) and for 300 and 600 seconds. 62
Figure 52 - Hysteresis curves $\alpha_R(V)$ for 600, 1800 and 3600 seconds of electric field exposure 62
Figure 53 - Vertical width of the hysteresis curves $\alpha_R(V)$ at 0V. 63
Figure 54 – Comparison of the dynamic evolution of $\alpha_R(t)$ and $R(t)$ at different exposure time. 63
Figure 55 - Trajectory of the liquid crystal director at different time of exposure from an in-plane to a quasi-circular switching. 64
Figure 56 – (a) Hysteresis curves $\alpha_R(V)$ of the cells with different concentrations of polymer and, (b) the vertical width of the hysteresis at 0V. 66
Figure 57 – Impact of the concetration of polymer in the switching time of the liquid crystal director between the two adressed states. 66
Figure 58 – (a) The linear behaivour of the PSFLC cells, (b) and the constant switching time due to the elastic coupling of the director between 0and 5V. 67
Figure 59 – The azimuthal angle, ellipticity and the retardance polarimetric parameter for PSFLC 13%. 67
Figure 60 – Trajectories of the liquid crystal director for pure SSFLC and PSSFLC 13%. 68
Figure 61- The illustration of the two 3D video streaming and the two Viewers seeing the image of a cube from different perspectives. 73
Figure 62 - The four images multiplexed by time being projected on a regular screen. 74
Figure 63 - The goggles of Viewer 1 and Viewer 2 and their respective shutters. 75
Figure 64 - The schematic of the functionality of the 3D active goggles for the Dual View technique using time multiplexing. 75
Figure 65 - The illustration of Case 1.2 showing how the two projectors and the shutter are synchronized 76
Figure 66 - Illustration of the Case 2.1 showing the two projectors separated by polarization and the configuration of the goggles. 77
Figure 67 - Illustration of the Case 2.2 showing the two projectors synchronised and the goggles opening and closing simultaneously. 78
Figure 68 - Case 5. made with four projectors and four narrow band filter in blue and red.* 79
Figure 69- Case 3.1 showing the two projectors separated by the filter red and blue, and the configuration of the goggles. 80
Figure 70 - Case 3.2 with the two projectors synchronised and the goggles opening and closing simultaneously with the red and blue filter on each shutter. 82
Figure 71 – Scheme of Case 4.1with the passive goggles made with polarisers and color filters. 83
Figure 72 – Illustration of the Case 4.2with the passive goggles made by polarisers and color filters. 84
Figure 73 – An overall illustration of the 3D Dual View Setup at Télécom-Bretagne 85
Figure 74 – The schemnatic and the picture of the projector and polarization system with the fans to avoid overheating of the polarisers and the QWP. 86
Figure 75 – 3D glasses configuration for the cases 2.1 and 2.2. 86
Figure 76 – 3D Dual View setup at Immersion. 87
Figure 77 - The four test charts used for test ghosting evaluation. 88
Figure 78 - Superimposition of four video streams on the screen (left picture) and one of the decoded streams (right picture, taken through the glasses). 89
Figure 79 - Evaluation of Ghosting Ratio using direct comparison for the decoded stream. In this example, the upper left white stripe and the 3 other grey scales are displayed by the image that is correctly decoded, while all the other content is a consequence of the actual ghost issue. 89
Figure 80 - Example of Gamma curve of the main (continuous) and leaking image (dashed line). 91
Figure 81 – The schematic and the picture of the chromometer support with the chromameter. 92
Figure 82 – The chromameter, the projectors and the silver screen at Télécom-Bretagne. 92
Figure 83 – Illustration of the the measurement Type 1 (luminance). 93
Figure 84 - Illustration of the the measurement Type 2 (polar-ghosting). 93
Figure 85 - Illustration of the the measurement Type 3 (time-ghosting). 93
Figure 86 - Illustration of the the measurement Type 4 (polar-time ghosting). 94
Figure 87 – (a) The luminance of the main image, (b) the polar and timing ghosting, (c) the timing ghosting, (d) and the polar ghosting for the white color at versus the gray level for the white color measured at $\varphi=0°$ and $\theta=45°$ (b). 95
Figure 88 – The red color luminance distribution with respect to θ and φ (Case 2.1 – TB) 97

Figure 89– The red color polar-ghosting ratio with respect to θ and φ (Case 2.1 – TB) 97
Figure 90 - The red color time-ghosting ratio with respect to θ and φ (Case 2.1 – TB)..... 97
Figure 91 - The red color time-ghosting ratio with respect to θ and φ (Case 2.1 – TB)..... 97
Figure 92 – The green color luminance distribution with respect to θ and φ (Case 2.1 – TB)..... 98
Figure 93 – The green color polar-ghosting ratio with respect to θ and φ (Case 2.1 – TB)..... 98
Figure 94 – The green color time-ghosting ratio with respect to θ and φ (Case 2.1 – TB) 98
Figure 95 – The green color polar-time ghosting ratio with respect to θ and φ (Case 2.1 – TB)..... 98
Figure 96 – The blue color luminance distribution with respect to θ and φ (Case 2.1 – TB) 99
Figure 97 – The blue color polar-ghosting ratio with respect to θ and φ (Case 2.1 – TB)..... 99
Figure 98 – The blue color time-ghosting with respect to θ and φ (Case 2.1 – TB) 99
Figure 99 – The blue color polar-time ghosting ratio with respect to θ and φ (Case 2.1 – TB)..... 99
Figure 100 – The white color luminance distribution with respect to θ and φ (Case 2.1 – TB) 100
Figure 101 – The white color polar-time ghosting ratio with respect to θ and φ (Case 2.1 – TB) 100
Figure 102 – The white color time-ghosting ratio with respect to θ and φ (Case 2.1 – TB)..... 100
Figure 103 – The white color polar-time ghosting ratio with respect to θ and φ (Case 2.1 – TB) 100
Figure 104 – The red color luminance distribution with respect to θ and φ (Case 2.2 – TB)..... 102
Figure 105 – The red color polar-ghosting ratio distribution with respect to θ and φ (Case 2.2 – TB)..... 102
Figure 106 – The red color time-ghosting ratio distribution with respect to θ and φ (Case 2.2 – TB)..... 102
Figure 107 – The red color polar-time ghosting distribution with respect to θ and φ (Case 2.2 – TB)..... 102
Figure 108 – The green color luminance distribution with respect to θ and φ (Case 2.2 – TB)..... 103
Figure 109 – The green color polar-ghosting ratio distribution with respect to θ and φ (Case 2.2 – TB)..... 103
Figure 110 – The green color time-ghosting ratio distribution with respect to θ and φ (Case 2.2 – TB)..... 103
Figure 111 – The green color polar-time ghosting distribution with respect to θ and φ (Case 2.2 – TB)..... 103
Figure 112 – The blue color luminance distribution with respect to θ and φ (Case 2.2 – TB) 104
Figure 113 – The blue color polar-ghosting distribution with respect to θ and φ (Case 2.2 – TB)..... 104
Figure 114 – The blue color time-ghosting distribution with respect to θ and φ (Case 2.2 – TB)..... 104
Figure 115 – The blue color polar-time ghosting distribution with respect to θ and φ (Case 2.2 – TB) 104
Figure 116 – The red color luminance distribution with respect to θ and φ (Case 2.2 – TB)..... 105
Figure 117 – The red color luminance distribution with respect to θ and φ (Case 2.2 – TB)..... 105
Figure 118 – The red color luminance distribution with respect to θ and φ (Case 2.2 – TB)..... 105
Figure 119 – The red color luminance distribution with respect to θ and φ (Case 2.2 – TB)..... 105
Figure 120 - The chromometer, the projector and the silver screen at Immersion...... 106
Figure 121 – The red color luminance distribution with respect to θ and φ (Case 2.1 – Immersion) 108
Figure 122– The red color polar-ghosting ratio with respect to θ and φ (Case 2.1 – Immersion)..... 108
Figure 123 - The red color time-ghosting ratio with respect to θ and φ (Case 2.1 – Immersion) 108
Figure 124 - The red color time-ghosting ratio with respect to θ and φ (Case 2.1 – Immersion) 108
Figure 125 – The green color luminance distribution with respect to θ and φ (Case 2.1 – Immersion) 109
Figure 126 – The green color polar-ghosting ratio with respect to θ and φ (Case 2.1 – Immersion) 109
Figure 127 – The green color time-ghosting ratio with respect to θ and φ (Case 2.1 – Immersion)..... 109
Figure 128 – The green color polar-time ghosting ratio with respect to θ and φ (Case 2.1 – Immersion) 109
Figure 129 – The blue color luminance distribution with respect to θ and φ (Case 2.1 – Immersion)..... 110
Figure 130 – The blue color polar-ghosting ratio with respect to θ and φ (Case 2.1 – Immersion) 110
Figure 131 – The blue color time-ghosting with respect to θ and φ (Case 2.1 – Immersion)..... 110
Figure 132 – The blue color polar-time ghosting ratio with respect to θ and φ (Case 2.1 – Immersion)..... 110
Figure 133 – The white color luminance distribution with respect to θ and φ (Case 2.1 – Immersion)..... 111
Figure 134 – The white color polar-time ghosting ratio with respect to θ and φ (Case 2.1 – Immersion)..... 111
Figure 135 – The white color time-ghosting ratio with respect to θ and φ (Case 2.1 – Immersion) 111
Figure 136 – The white color polar-time ghosting ratio with respect to θ and φ (Case 2.1 – Immersion)..... 111
Figure 137 – The ghosting effect due to the crosstalk (a), and the ghostbusting process (b). 114
Figure 138 – Images of the 3D Dual View for with and without Ghostbusting. 117

List of Tables

Table 1 - Response time for different samples at different twist angles. 34
Table 2 – Contrast Ratio for different samples at different twist angles. 34
Table 3 – Contrast ratio and response time for PSFLC of different concentrations. 36
Table 4 – Liquid crystal mixtures. 38
Table 5 – Relaxation time of the different mixtures. 38
Table 6 – The residual light of the mixtures considering triple flash (144Hz) and a frame time of 8,33ms. 42
Table 7 - The relation between the real and imaginary magnitudes peaks with the Mueller coefficients. 49
Table 8 – All the possible configurations to separate the images of each viewer eye and isolate the viewers. 74
Table 9 – The red color luminance values with respect to θ and φ (Case 2.1 – TB) 97
Table 10 – The red color polar-ghosting ratio values with respect to θ and φ (Case 2.1 – TB) 97
Table 11 – The red color time-ghosting ratio values with respect to θ and φ (Case 2.1 – Télécom Bretagne) 97
Table 12 – The red color polar-time ghosting ratio values with respect to θ and φ (Case 2.1 – TB) 97
Table 13 – The green color luminance values with respect to θ and φ (Case 2.1 – TB) 98
Table 14 – The green color polar-ghosting ratio values with respect to θ and φ (Case 2.1 – TB) 98
Table 15 – The green color time-ghosting ratio values with respect to θ and φ (Case 2.1 – TB) 98
Table 16 – The green color polar-time ghosting ratio values with respect to θ and φ (Case 2.1 – TB) 98
Table 17 – The blue color luminance values with respect to θ and φ (Case 2.1 – TB) 99
Table 18 – The blue color polar-ghosting ratio values with respect to θ and φ (Case 2.1 – TB) 99
Table 19 – The blue color time-ghosting ratio values with respect to θ and φ (Case 2.1 – TB) 99
Table 20 – The blue color polar-time ghosting ratio values with respect to θ and φ (Case 2.1 – TB) 99
Table 21 – The white color luminance values with respect to θ and φ (Case 2.1 – TB) 100
Table 22 – The white color polar-ghosting ratio values with respect to θ and φ (Case 2.1 – TB) 100
Table 23 – The white color time-ghosting ratio values with respect to θ and φ (Case 2.1 – TB) 100
Table 24 – The blue color polar-time ghosting ratio values with respect to θ and φ (Case 2.1 – TB) 100
Table 25 – The red color luminance distribution values with respect to θ and φ (Case 2.2 – TB) 102
Table 26 – The red color polar-ghosting ratio values with respect to θ and φ (Case 2.2 – TB) 102
Table 27 – The red color time-ghosting ratio values with respect to θ and φ (Case 2.2 – TB) 102
Table 28 – The red color polar-time ghosting ratio values with respect to θ and φ (Case 2.2 – TB) 102
Table 29 – The green color luminance distribution values with respect to θ and φ (Case 2.2 – TB) 103
Table 30 – The green color polar-ghosting ratio values with respect to θ and φ (Case 2.2 – TB) 103
Table 31 – The green color time-ghosting ratio values with respect to θ and φ (Case 2.2 – TB) 103
Table 32 – The green color polar-time ghosting ratio values with respect to θ and φ (Case 2.2 – TB) 103
Table 33 – The blue color luminance distribution values with respect to θ and φ (Case 2.2 – TB) 104
Table 34 – The blue color polar-ghosting ratio values with respect to θ and φ (Case 2.2 – TB) 104
Table 35 – The blue color time-ghosting ratio values with respect to θ and φ (Case 2.2 – TB) 104
Table 36 – The blue color polar-time ghosting ratio values with respect to θ and φ (Case 2.2 – TB) 104
Table 37 – The white color time-ghosting ratio values with respect to θ and φ (Case 2.2 – TB) 105
Table 38 – The white color time-ghosting ratio values with respect to θ and φ (Case 2.2 – TB) 105
Table 39 – The white color time-ghosting ratio values with respect to θ and φ (Case 2.2 – TB) 105
Table 40 – The white color time-ghosting ratio values with respect to θ and φ (Case 2.2 – TB) 105
Table 41 – The red color luminance values with respect to θ and φ (Case 2.1 – Immersion) 108
Table 42 – The red color polar-ghosting ratio values with respect to θ and φ (Case 2.1 – Immersion) 108
Table 43 – The red color time-ghosting ratio values with respect to θ and φ (Case 2.1 – Immersion) 108
Table 44 – The red color polar-time ghosting ratio values with respect to θ and φ (Case 2.1 – Immersion) 108
Table 45 – The green color luminance values with respect to θ and φ (Case 2.1 – Immersion) 109
Table 46 – The green color polar-ghosting ratio values with respect to θ and φ (Case 2.1 – Immersion) 109
Table 47 – The green color time-ghosting ratio values with respect to θ and φ (Case 2.1 – Immersion) 109
Table 48 – The green color polar-time ghosting ratio values with respect to θ and φ (Case 2.1 – Immersion) 109
Table 49 – The blue color luminance values with respect to θ and φ (Case 2.1 – Immersion) 110
Table 50 – The blue color polar-ghosting ratio values with respect to θ and φ (Case 2.1 – Immersion) 110
Table 51 – The blue color time-ghosting ratio values with respect to θ and φ (Case 2.1 – Immersion) 110
Table 52 – The blue color polar-time ghosting ratio values with respect to θ and φ (Case 2.1 – Immersion) 110
Table 53 – The white color luminance values with respect to θ and φ (Case 2.1 – Immersion) 111
Table 54 – The white color polar-ghosting ratio values with respect to θ and φ (Case 2.1 – Immersion) 111

Table 55 – The white color time-ghosting ratio values with respect to θ and φ (Case 2.1 – Immersion) 111
Table 56 – The white color polar-time ghosting ratio values with respect to θ and φ (Case 2.1 – Immersion) . 111

Motivation and Introduction

Liquid crystals are special materials that have a huge field of applications and are present in our daily lives. The most well-know device made with liquid crystal is the LCD (Liquid Crystal Display) screen, which is a component of your television device, mobile and etc. However, liquid crystal (LC), due to its birefringence and electro-optics characteristics, has been also used in others domains of science and technology like photonics, biology and etc. Further, LC and its capacity to fast switching have helped to resurrect the 3D Cinema and consequently the stereoscopic vision market. Based on the new developments in 3D, the thesis was done at Télécom-Bretagne in a partnership with Eyes3Shut Company under the supervision of Prof. Jean-Louis de Bougrenet de la Tocnaye. The main objectives of this thesis were to improve the liquid crystal shutters and develop stereoscopic vision applications.

The vision quality of a 3D system based on active glasses, no matter if it is Cinema or TV, is directly related to the performance of the liquid crystal shutters. 3D glasses are generally composed by a plastic hull, an electronic circuit and two shutters. Basically, the shutter comprises two pieces of glass substrates with polarisers on them that confine the liquid crystal in a very thin layer. There are a lot of parameters that play an important role in the quality of 3D glasses. In this thesis the efforts were concentrated in the organization of the liquid crystal molecules between the substrates and in the liquid crystal itself. Then, we studied different configurations of shutters using nematic liquid crystal, ferroelectric liquid crystal (smectic) with and without polymer. Also, we mixed different types of nematic liquid crystal. All the shutters were fabricated in the clean room at Télécom-Bretagne and optically characterised. Furthermore, some samples were analysed using a full optical snapshot matrix Mueller polarimenter made by UBO (Université de Bretagne Occidentale) in a parternship with Télécom-Bretagne.

The second part was the development of 3D Dual View System. In general lines, it is a stereoscopic vision system, based on a mixture of active and passive 3D solutions, which displays a 3D image that can be viewed simultaneously by two spectators, but from different perspectives. To allow two different points-of-view of a scene or an object in three dimension, the system has to multiplex four images, i.e. two pairs. It means that one pair forms the 3D image for one viewer in one perspective and the other pair for the second viewer in other perspective. The viewers should wear special glasses in order to decode only their own images. Thus, the challenges were: choose the best multiplexing scheme to reduce the crosstalk and be optically comfortable to the viewer, and implement the system. The crosstalk between the images leads to an effect called *ghosting*, which the viewer sees as a low intensity image that belongs to the order viewer as if it was a ghost. Then, the work was to build the system and to characterize the ghosting effect measuring the crosstalk. More than that, it was also compared the ghosting effect between the 3D Dual View in tranmissive mode, which was made at Télécom-Bretagne, with the system in reflective mode, built at Immersion Company installed in Bordeaux. To begin with, in the first chapter, the fundamentals of the liquid crystals, exploited in this work, is introduced, their types and their basic physical properties.

The final part of this chapter is dedicated to different types of liquid crystal shutters and their electro optical properties. The shutters are detailed systemically and no details about them are given, only the necessary to understand the experiments in chapter 2.

The second chapter is a small theory about binocular vision and stereoscopy. Followed by a brief description of 3D techniques without glasses and how they emulate the perception of depth. Also, it is detailed the 3D systems with glasses showing how the images are multiplexed and decoded by the viewers. This is one of the main parts of the thesis, because it is the basis to perceive how the 3D active glasses work in a real application and, later on in Chapter 4, it helps to understand the 3D Dual View technique and the different manners to multiplex the images. We will see that the use of inappropriate 3D glasses leads to two main drawbacks in the depth perception, the ghosting effect and the color banding. Finally, it is shown the result of the characterization of different liquid crystal shutters and how each one can mitigate the cited drawbacks.

The third chapter is an extension of the previous one in the sense that it presents more deeply the behavior of the liquid crystal shutters. We did some polarimetric measurements and it was found some relation between the polarimetric parameters and the liquid crystal director. The chapter begins with the theory behind of a Mueller Matrix based polarimeter, explaining briefly polarization, the stokes vector, the mueller matrix and the polarimeter itself, made by UBO. We detailed the shutters, not in a systematic way, but describing the layers structure and the director behavior. The results reveal the relation between the liquid crystal textures with the polarimetric parameters of different shutter types.

The fourth chapter deals with the development of the 3D Dual View system application. First, we explain different processes of building 3D Dual View systems using the multiplexing technique in Chapter 2. Secondly, we describe the setup made at Télécom-Bretagne in reflective mode and, at Immersion, in transmissive mode. At Télécom-Breatgne we implemented two different cases with the same multiplexing schemes and, it is presented later on in the same chapter the optical and the ophthalmological differences between them. Since the biggest problem for this kind of system is the ghosting, we evaluated the ghosting effect using a chromameter and the results in both modes are presented. To summarize, it is suggested a ghost-busting technique to compensate the ghost effect.

It can be seen that stereoscopic vision is the soul of this work and all the applications like shutters and 3D Dual View, revolve around it. In the conclusion we have highlighted few important aspects of the work. We have also proposed few improvements, the scope and the potential for the 3D vision.

Chapter 1: *Introduction to Liquid Crystals*

Introduction

Liquid crystal is a controversial name but expresses exactly what it is. It is a special material which can behave like solid, liquid or both at the same time. In other words, besides the solid and liquid phases, liquid crystals have intermediate phases, mesophases, where it flows like liquids and concomitant possess characteristics of crystals. Due to its electro optical properties, low power consumption, slim shape and low molecular weight the liquid crystal has been widely studied and has found a commercial application in flat panel displays. The successful of liquid crystal technology is the combination of scientific disciplines such chemistry, physics, electronics and engineering. Liquid crystals can be found in many other applications beside flat panels. In this chapter we are going to introduce the liquid crystal and some of its applications that are interesting for the scope of this thesis.

1. Liquid Crystals

In 1888 a botanist, Friedrich Reinitzer, had noticed that the material cholesteryl benzoate had two "distinct melting points" [1]. He observed in his experiments that increasing the temperature of a solid sample of that material the crystal changed into a blurred liquid and after into a transparent liquid. Because of this work, the discovery of the liquid crystalline state of matter was credited to him. However, the name Liquid Crystal was suggested by Otto Lehmann, a German physicist [2]. After 1922, Georges Friedel, a French mineralogist proposed a classification based on structural properties of liquid crystals. Friedel realized the first correlation between the macroscopic structure and the LC molecular arrangement [3], introducing the term "mesophase". At that time, the Russian V. Freedericksz studied the behavior of nematic liquid crystals in the presence of electric field and the threshold effect received his name, "Freedericksz-transition" [4]. From 1960 various attempts have contributed to the development of the liquid crystal studies and the application based on electro-optical phenomena [5]. Today, LC dominate the display industry and it is used in many other fields of science.

As it was said before, the name Liquid Crystals (LC) was given because these materials have properties between those of a liquid and those of a crystal. For example, a LC in nematic phase can flow as a liquid and at the same time exhibits optical birefringence like crystalline solids. The LCs used in the experiments of this thesis were the calamitic liquid crystals which consists of elongated organic rod-like molecules in smectic and nematic phases, rigid on the long axis and strong dipoles. The smectic and nematics phases exhibited by rod-like molecules are illustrated in Figure 1.

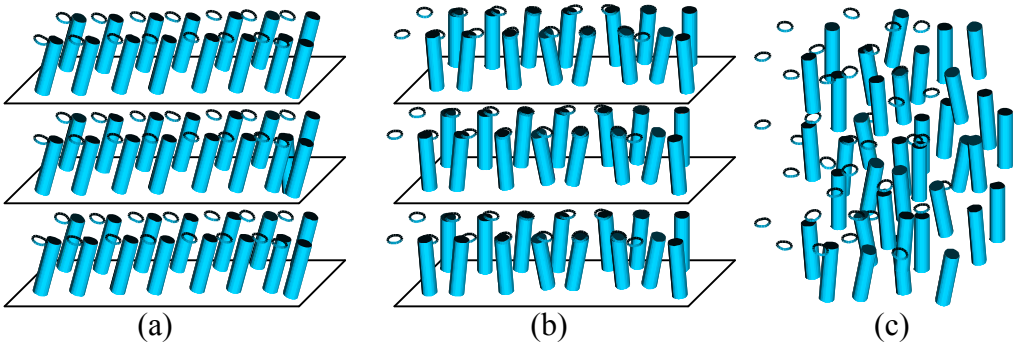

Figure 1 - Ilustration of (a) smectic-C, (b) smectic-A and (c) nematic liquid crystals.

If the temperature of the liquid crystal is kept on increasing beyond certain temperature, the orientational and positional order would break and it will behave as ordinary isotropic liquid. In this phase the molecules are free, pointing in a random direction, moving around and the material can flow like ordinary liquid. When the temperature decreases the material transforms into another phase, where the molecules have orientational order but no positional order. In this case, the molecules can still diffuse and the viscosity does not change much from the isotropic phase. However, the long axis of the molecules has a preferred direction denoted by a vector $\vec{n}$ called local director.

When the temperature is decreased further the material transforms into smectic-A. In this phase, besides the orientation order like in the nematic phase, the material acquires partially a positional order and the molecules starts to be organized in a layer structure pattern. Besides, the liquid crystal director is perpendicular to the layers. The word partially used to describe the positional order comes from the fact that the molecules are divided in a layer, but within a layer the molecules are free to move. This means that looking into a particular layer the molecules have an orientational order but not a positional order. A material in smectic-A phase has a higher viscosity rather than the water and it looks like a gel. If the temperature decreases even further the material transforms into the smetic-C phase. This phase is very similar to the smetic-A however with the liquid crystal director a little bit tilted according to the smetic layers.

At very low temperature the material is in solid (crystal) state. In this phase the molecules have positional and orientational orders but the viscosity become infinite and the molecules no longer move.

There are two main types of LC, thermotropic liquid crystals, described above, and lyotropic liquid crystals. The latter phase changes not only with the temperature but with the concentration of solvent. Another phase of liquid crystal used in many applications is the cholesteric phase. However, the cholesteric phase was not used in any of the experiments and applications included in this work. In the next sections each phase is described with their characteristics in details.

1.1 Nematic Liquid Crystal

Nematics are the most commonly studied and widely used liquid crystal. The majority of the liquid crystal display nowadays uses nematic liquid crystals. Furthermore, many other applications with nematics have been developed for telecommunication and other fields of science.

The principle characteristic of this phase is that the molecular axes are preferably oriented in one direction, defined by unitary vector know as the local director $\vec{n}$, with no positional order. Both directions of the director, $+\vec{n}$ and $-\vec{n}$, are equivalent. In ordinary nematic an optically uniaxial behavior with the optical axis parallel to the director $\vec{n}$ can be observed. Figure 2 shows a nematic liquid crystal under a polarized microscope and also a schematic presenting how the molecules organize themselves in a bulk and the director $\vec{n}$.

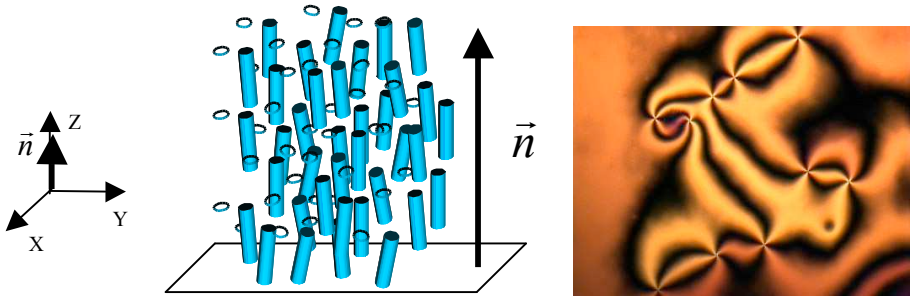

Figure 2 - Nematic liquid crystal, the director $\vec{n}$ and a nematic under polarized microscope.

In short, in the nematic liquid crystal the molecules are free to flow and their positions are randomly distributed as in a liquid, but always maintaining their directional order according to the director $\vec{n}$. Nematic liquid crystal posses a relatively low viscosity and can be easily deformed by external forces.

The nematic phase, if only weak distortions are considered, can be described by the continuum theory of nematics proposed by [6]. There are three basic types of deformation: splay, twist and bend, and they are going to be detailed in the section 1.4.3

1.2 Smectic Liquid Crystal

Like in nematic liquid crystals, the smectic liquid crystal possesses an orientational order.The big difference is that the molecules are organized in layers and not randomly distributed in the bulk. There are many types of smectic phases. However, for the purpose of this thesis only the Smectic A, Smectic C and Smectic C* phases will be presented.

1.2.1. Smectic A

The smectic-A phase, the molecules are parallel to each other and organized in layers with the thickness equal to the molecular length, Figure 3. The long axes of the molecules are perpendicular to the layer plane and they have no positional order within the layers, thus, the molecules are free to move along the layer. The smectic-A are optically positive and uniaxial with the optics axis parallel to the long axes.

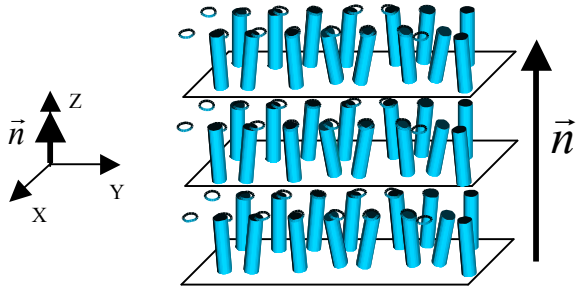

Figure 3 - Representation of smectic-A phase and the director n parallel to the molecules long axis

1.2.2. Smectic C

The smectic-C structure is similar to the structure of the smectic-A phase, but the molecules are tilted to the layer. The tilt angle for smectic-C liquid crystals is temperature dependent [7], and it is optically biaxial, Figure 4.

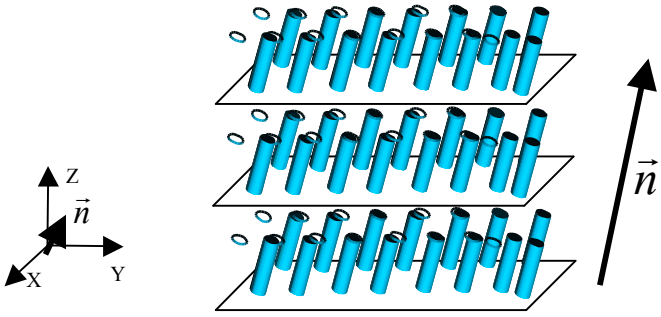

Figure 4 - Representation of smectic-C phase and the director $\vec{n}$ tilted according to the layers

1.2.3. Smectic C*

The star symbol in the smectic-C* expresses chirality. This means that the smectic-C* phase is similar to the smectic-C but with the molecules arranged in a chiral pattern, where the direction of the director rotates on the layer plane from one layer to the next, Figure 5, with the twist axis perpendicular to the layer.

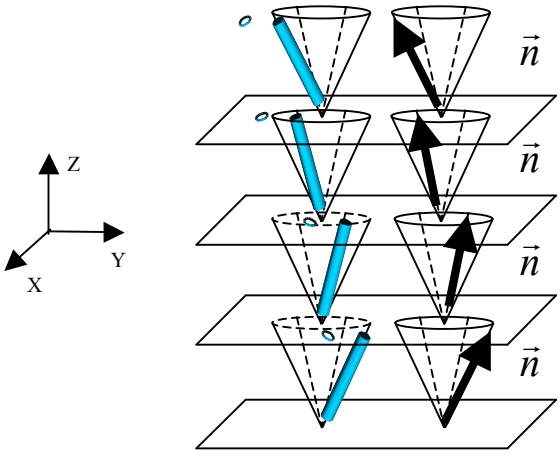

Figure 5 - Representation of smectic-C* phase and the rotation of the director $\vec{n}$ from layer to layer

This phase is optically positive, uniaxial and it has selective reflection. One of the most important characteristics of this phase is the ferroelectric properties which can appear if the

smectic helix is suppressed like in Surface Stabilized Liquid Crystals (SSFLC) devices [8].

1.3 Basic Liquid Crystal Physical Properties

The uniaxial symmetry of the liquid crystal structure around the director leads to the anisotropy of their physical properties. Anisotropy means that a physical quantity is directionally dependent i.e. they exhibit different values measured parallel or perpendicular to the director. Then, combining the anisotropic nature of the physical properties and the susceptibility to electric field to change the spatial orientation of the molecules makes the liquid crystal an important material in the display, shutters and other electro-optic devices. In the following sections we are going to discuss the major physical properties of the liquid crystal, to understand the basic principles concerning the display/shutter technology.

1.3.1. Optical Anisotropy (Birefringence)

Calamatic liquid crystals are uniaxial, polarization dependent anisotropy and therefore birefringent. This means that the refractive index of the LC has different values parallel and perpendicular to the director exhibiting different properties for the light traveling inside the LC in a perpendicular and/or in a parallel direction to the optical axis. Then, an incident polarized light parallel to the director will have a different propagation velocity than a polarized light perpendicular to the director.

These two different refractive indexes are called the ordinary refractive index (n_o) which is perpendicular to the optics axis, and the extraordinary refractive index (n_e) which is parallel to the optical axis. Thus, when a polarized light goes into a birefringent medium, like liquid crystals, the process is modeled in terms of the light being split into two perpendicular components called the ordinary (o) wave and the extraordinary (e) wave. Because of the different travelling velocities of each component the waves get out of phase and the output polarization state changes with respect to the input.

The o-wave polarization is always perpendicular to the optics axis and is related to the refractive index n_o which is constant and independent of the propagation direction. On the contrary, the e-wave polarization lie in the same plane as the optical axis and the related refractive index n_e varies with the propagation angle θ according to:

$$n_e(\theta) = \left(\frac{\cos^2 \theta}{n_o^2} + \frac{\sin^2 \theta}{n_e^2} \right)^{-1} \tag{1.1}$$

Equation 1.1 is illustrated by the refractive index ellipsoid in Figure 6.

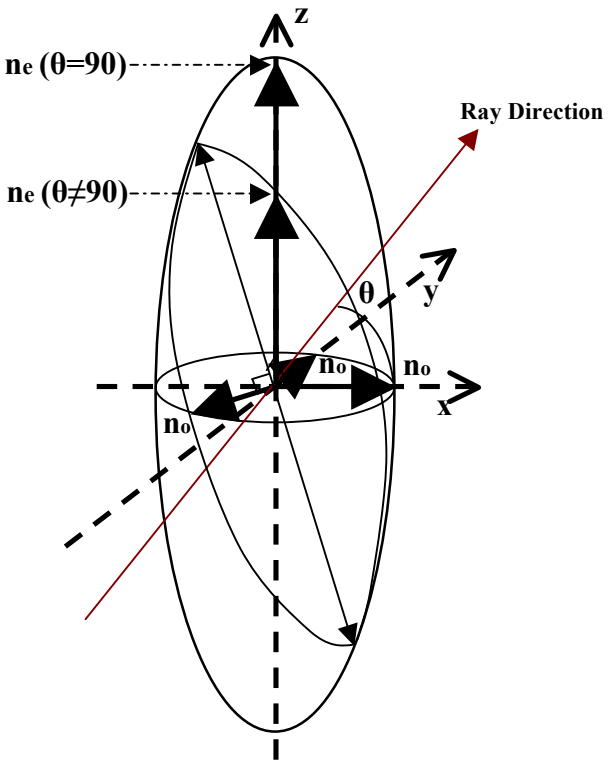

Figure 6 - Schematic of a light wave travelling inside of a birefringent medium.

The Δn of the medium is angle dependent and changes according to the propagation direction, defined as:

$$\Delta n(\theta) = n_e(\theta) - n_o \tag{1.2}$$

The birefringence of the material is defined for $\theta = 90^o$, and can be calculated by:

$$\Delta n = n_e - n_o \tag{1.3}$$

This leads to an important conclusion; as the light is split and the propagation velocities are different, the optical path for each component traveling inside a thick liquid crystal will differ. Thus, the phase difference between the ordinary and extraordinary ray transversing a liquid crystal with a birefringence of Δn and thickness d is called optical retardation and is given by:

$$\delta(\theta) = \frac{2\pi\Delta n(\theta)d}{\lambda_v} \tag{1.4}$$

where λ_v is the wavelength of the light in vacuum.

1.3.2. Dielectric Anisotropy

The interesting point about liquid crystals is their electro-optical properties. In this sense, the dielectric permittivity is one of the most important features as it relates the reorientation of the director $\vec{n}$ in the presence of an electrical field.

This relation between liquid crystal and electric field is dependent on the physical parameter permittivity. This parameter determines how an electric field affects and is affected by a

dielectric medium, also, it quantifies how easily the material polarizes in response to the applied electric field [10]. The induced polarization in non-polar LCs is divided in two parts: the electronic polarization and the ionic polarization [11]. In polar LCs, besides the two polarization mentioned before, there is the orientational polarization which represents the capability of the permanent dipoles moments to orient themselves according to the field.

The magnitude of this interaction, or polarizability, depends on the dielectric permittivity, measured parallel and perpendicular to the director, and the dielectric anisotropy which is the difference between the two measurements [12]. Therefore

$$\Delta\varepsilon = \varepsilon_{\parallel} - \varepsilon_{\perp} \tag{1.5}$$

where ε is the dielectric permittivity. When an electric field $\vec{E}$ is applied to the LC a torque on $\vec{n}$ is induced. Then, depending on the dielectric anisotropy the molecules will be oriented in a preferred direction according to the field.

An important remark is that the dielectric anisotropy is dependent on the temperature and the frequency of the applied field. Thus, as long as the temperature increases and the material start to become isotropic the dielectric constant along all the axes tends to be equal due to the isotropic comportment of the medium and the dielectric anisotropy vanishes.

1.3.3. Elastic Constant and Free Energies

The director of an aligned sample of liquid crystal can vary spatially as a result of, for example, an external applied electric field. In other words, the liquid crystal will undergo deformation in response to a external perturbation like in any solid. Three types of deformation are observed in nematics: splay, twist and bend (Figure 7).

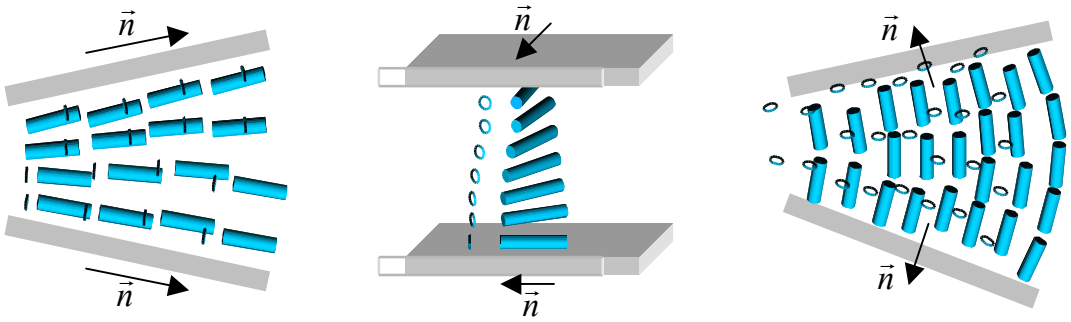

Figure 7 - The three types of deformation: splay (a), twist (b) and bend (c).

The director deformations correspond to spatial changes in $\vec{n}$, thus, the basic parameters in the deformation energies are spatial derivatives. According to the theory introduced and developed by Frank [6], the free-energy associated with the deformations are:

$$splay: f_1 = \frac{1}{2} K_{11} (\nabla \cdot \hat{n})^2 \tag{1.6}$$

$$twist: f_2 = \frac{1}{2} K_{22} (\hat{n} \cdot \nabla \times \hat{n})^2 \tag{1.7}$$

$$bend: f_3 = \frac{1}{2} K_{33} \left\| (\hat{n} \times \nabla \times \hat{n}) \right\|^2 \tag{1.8}$$

where K_{11}, K_{22} and K_{33} are the Frank elastic constants. Applying an electric field in a LC all deformations will occur and the total distortion free-energy density could be written as [9]:

$$f_d = \frac{1}{2} K_{11} (\nabla \cdot \hat{n})^2 + \frac{1}{2} K_{22} (\hat{n} \cdot \nabla \times \hat{n})^2 + \frac{1}{2} K_{33} \left\| (\hat{n} \times \nabla \times \hat{n}) \right\|^2 \tag{1.9}$$

This equation describes the deformation of the director in the bulk of nematic liquid crystal.

In Smectic-A phase the elastic energy of the deformation of the director has some crucial differences as compared to the nematic phase. Because of the layered structure the compression of the smectic layer should be included in the total distortion free-energy [11]:

$$f_{layer} = \frac{1}{2} B \left(\frac{d - d_0}{d_0} \right)^2 \tag{1.10}$$

where B is is the elastic constant for the compression of the layer, d and d_0 are the layer thicknesses after compression and the actual layer thickness, respectively. Also, due to the boundary conditions the necessary energy to change the layer thickness is too high and, in that case, the twist and the bend deformations are not allowed. Thus, the free-energy in a smectic-A is [11]:

$$f_{lelas} = \frac{1}{2} K_1 (\nabla \cdot \hat{n})^2 + \frac{1}{2} B \left(\frac{d - d_0}{d_0} \right)^2 \tag{1.11}$$

In Smectic-C the tilt of the director from the layer normal gives a freedom of rotation around the z axis. Then, it should be taken into account the energy associated with the director rotation (f_c) without layer distortion, the interlayer distortion (f_d) and a coupling between (f_{cd}). In that way, the free-energy of the system is:

$$f = f_c + f_d + f_{cd} \tag{1.12}$$

The elastic constants and free-energies are very important to understand the behavior of the liquid crystal molecules under electric field. Also, it plays a fundamental role to define the characteristics of liquid crystal devices, technologies and applications which will be explained in this thesis.

1.3.4. Viscosity

Qualitatively, viscosity describes the resistance of a fluid to flow. In other words, it is the resistance of a fluid, in our case liquid crystals, while it is being deformed by shear stress. Formally, viscosity is the ratio between the shear stress and the gradient velocity.

Like all the properties in liquid crystals, the shear viscosity is also an anisotropic property,

this means that the viscosity depends on the direction of flow. Specifically, it will rely on the direction of flow of a molecule with respect to the director within the medium. Three parameters characterize the viscosity: η_1, η_2 and η_3. The η_1 viscosity is perpendicular to the direction of flow and parallel to the velocity gradient; η_2 is parallel to the direction of flow and perpendicular to the velocity gradient; η_3 is perpendicular to the direction of flow and to the gradient velocity. These viscosities take into account that the director remains fixed during the fluid flow. Then, it only describes in a way how fast one cell can be filled by liquid crystal and/or freely moves. In more general situations the director axis reorientation often accompanies fluid flow and vice versa.

However, the viscosity coefficient which influences the optical response time in an electro-optical liquid crystal based device is called rotational viscosity (γ_1). This coefficient is associated with the movement of the molecules due to the boundary condition imposed and the applied electric field. In short, it describes how easily the molecules can move from a homogeneous planar alignment parallel to the cell surface to a homeotropic alignment under electric field.

1.3.5. Dielectric Coupling

The liquid crystals can be made of polar molecules or non-polar molecules. The difference is that polar molecules have a permanent dipole moment due to charge separation and the non-polar molecules have an induced electric dipole moment. The electric dipole moment appears when applying electric field and forces the separation of the charges into the molecule.

We saw the anisotropic characteristic of the liquid crystal. More specifically, we emphasized the dielectric anisotropy and the important relation that $\Delta\varepsilon$ has regarding an external electric field and the reorientation of the liquid crystal molecules. In this section, is described quantitatively the dielectric interaction between LC and an electric field.

For low frequency electric field E, the displacement D can be written as:

$$\vec{D} = \varepsilon_\perp \vec{E} + \left(\varepsilon_{\parallel} - \varepsilon_\perp\right)\left(\hat{n}\cdot\vec{E}\right)\hat{n} \tag{1.13}$$

Then, the dielectric energy density is:

$$-\int_0^E \vec{D}.d\vec{E} = -\frac{1}{2}\varepsilon_\perp\left(\vec{E}\cdot\vec{E}\right) - \frac{\Delta\varepsilon}{2}\left(\hat{n}\cdot\vec{E}\right)^2 \tag{1.14}$$

It can be seen that the dielectric energy density does not depend on the orientation of the director. However, the term with $-\Delta\varepsilon$ impose a preferred direction for the molecules when an electric field is applied. Thus, the torque produces is:

$$\vec{\Gamma} = \vec{D}\times\vec{E} = \Delta\varepsilon\left(\hat{n}\cdot\vec{E}\right)\left(\hat{n}\times\vec{E}\right) \tag{1.15}$$

The signal of the dielectric anisotropy and, thus, the behavior of the molecules under electric field will be defined in the way that the molecules orient themselves in the bulk. In this case of applying electric field in a liquid crystal with $\Delta\varepsilon>0$, the molecules will orient themselves

parallel to the field. For the case of $\Delta\varepsilon<0$ the molecules will orient themselves perpendicular in respect with the field. Figure 8 illustrated the two possibilities.

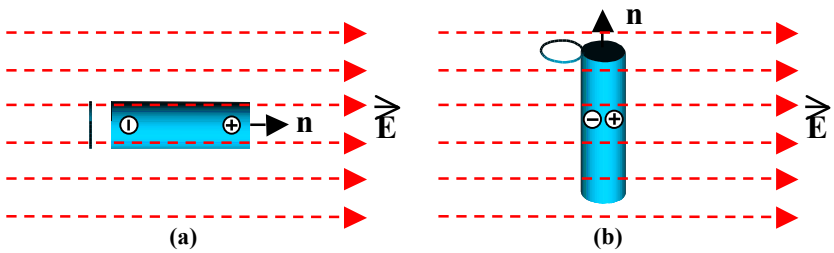

Figure 8 - Liquid crystal molecule of positive and negative anisotropy under electric field.

1.3.6. Ferroelectric Coupling

It was seen in section 1.3 that the molecules in the Smectic-C phase are tilted at an angle θ with respect to the axis normal to the layer plane. This angle is called tilt angle and, for the same mixture, it is a temperature dependent parameter. In the Smectic-C* phase, the chirality induces one helix with the axis orthogonal to the layer. Then, the director is free to rotate on the surface of a cone with 2θ of aperture and the direction of tilt making an angle φ in the azimuthal plane parallel to the layer. The result of this time-dependent alignment of the dipoles is the spontaneous polarization with a component parallel to the layer plane and orthogonal to the molecule orientation. However, due to the helical structure of the smectic-C* the spontaneous polarization is averaged to zero, Figure 5.

In SSFLC devices where the helical structure is unwound by the boundary conditions imposed by the substrates, a spontaneous polarization (P_s) with the average different to zero appears, Figure 9.

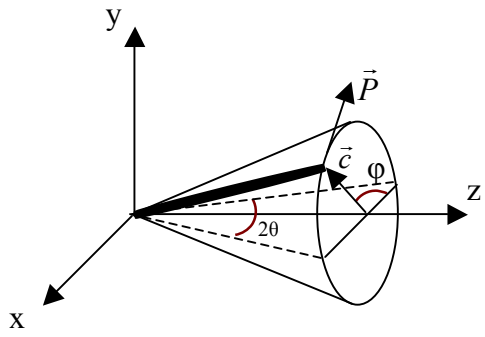

Figure 9 - Spontaneous polarization on the smectic cone in an unwound smectic-C* liquid crystal.

Then, the interaction of an electric field with the permanent polarization, referred also as ferroelectric coupling, can be written as:

$$F_p = -P_s E_y sen\varphi \tag{1.16}$$

It is important to remark that the SSFLC is a bistable device with two states that can be addressed by the electric field. This and other features, which is explained in section 1.5.5,

makes SSFLC very interesting for electro-optical applications due to the commutation velocities and other characteristics.

1.4 Liquid Crystal Shutters/Display

In general, liquid crystal shutters and display consist of a thin layer of nematic liquid crystal or smectic liquid crystal enclosed between two transparent parallel glass substrates. The plates are separated by solid spacers in order to have a uniform gap. The size of the spacers depends on the technique and the technology involved, generally between 2-10μm. Thicker cells lead to scattering and longer response time which is not interesting for shutters and displays applications. The glass substrates are coated with a whole series of thin transparent layers with different functions from conductive layer to protection layer. The conductive layer is used to apply voltage and induce electric field between the glass plates. Normally this layer is made of Indium Tin Oxide (ITO), a transparent conductor. The alignment layer, in our experiments is polyimide, is responsible to assure that the liquid crystal molecules are pointing in one preferred direction. Beside this, for many types of LCD, the substrates are placed between crossed polarizers. For some techniques, other kinds of films like retarders and compensators can be glued on the substrates. In the next sections, it is described the most important liquid crystal shutter/display technologies.

1.4.1. Electrically Controlled Birefringence (ECB) mode

The ECB mode also known as Vertical Aligned (VA) mode, as the name suggest, controls the birefringence of the liquid crystal electrically based on the Fréedericksz effect. Then, applying voltage between the substrates of an ECB cell the electric field changes the tilt angle (θ) of the molecules and consequently the birefringence according to Equation 1.2.

The ECB cell configuration is quite simple. A nematic liquid crystal of negative dielectric anisotropy is homeotropically aligned by means of an alignment layer coated in the rear and front glass plates. After, the cell is placed between crossed polarizers and the alignment of the LC molecules is modulated by dielectric coupling (Equation 1.20), with the electric field applied between the substrates previously coated with an conductive layer (ITO) as shown in Figure 10.

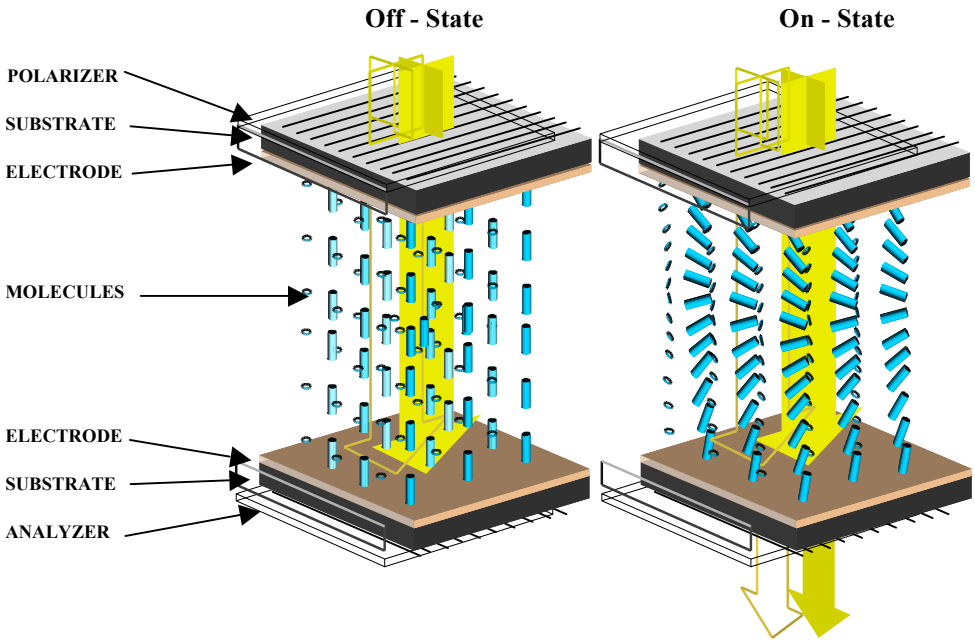

Figure 10 - Schematic of an ECB cell.

In the absence of electric field, OFF state, the polarized light emerging from the first polarizer traverse the nematic liquid crystal homeotropically aligned and is blocked by the second polarizer. There is extinction of the light and the cell appears dark.

When applying an electric filed far away from the Fréedericksz threshold the nematic director tilts away from the normal changing the birefringence of the medium. The ordinary refractive index remains unaffected, but the extraordinary refractive index increases with voltage. In this state, called ON state, some light is allowed to transverse the cell. The intensity of light depends on the optical retardation, Equation 1.4, the angle of incidence (ϕ) and is given by:

$$I = I_o \sin^2(2\phi_o)\sin^2\left(\frac{\delta}{2}\right) \tag{1.17}$$

One important factor concerning this technique is the response time of the liquid crystal molecules. This means, the time of the molecules to switch from the homeotropic alignment to the planar alignment. The rise time (τ_{ON}), plus the time of the molecules to come back to the homeotropic aligment, fall time (τ_{OFF}), is given by [14]:

$$\tau = \underbrace{\frac{\gamma_1 d^2}{\pi^2 K_1}\left(\frac{\Delta\varepsilon}{\pi^2 K_1}V^2 - 1\right)^{-1}}_{\tau_{ON}} + \underbrace{\frac{\gamma_1 d^2}{\pi^2 K_1}}_{\tau_{OFF}} \tag{1.18}$$

where γ_1 is the rotational viscosity, d is the cell thickness, K_1 is the elastic constant, V is the applying voltage and $\Delta\varepsilon$ the dielectric anisotropy.

Unfortunately, this technique for display technology has some drawbacks. Intrinsically, it has a poor angle of view due to the molecules orientation. Besides, to obtain withal a low response time, a good light transmission in the visible spectrum and cells of 5-6 micron

thickness, the liquid crystal should fulfill conflicting specifications. For example, from Equation 1.2 the light intensity depends on the birefringence. However, high values of Δn lead to very viscous liquid crystal materials increasing the response time.

Also, the molecules can tilt towards any direction slowing down the response time and reducing the viewing angle. In order to impose a pre-determined tilt direction and improve the technology some solutions have been proposed like Multi-Domain Vertical Alignment (MVA) and Patterned Vertical Alignment (PVA) [15][16].

1.4.2. Thin Nematic 3D Shutters (TNs)

The Thin Nematic Shutters are a half-wave plate with the same operational principle as ECB cells though having some peculiar differences. First, the rear and front substrates are coated with a planar alignment layer and both rubbed in the same direction. The substrates are assemble with the alignment layers facing each other in a parallel alignment. Second, the cell thickness is between 1-2 microns. Third, the cell is placed between cross polarizers in 45 degrees with respect to the optical axis to allow light transmission in the off state as show in Figure 11. In the on state the liquid crystal molecules aligned themselves parallel to the electric field changing the alignment to homeotropic and the material losses the birefringence property. Thus, the polarized light from the first polarizer is blocked by the second polarizer and the cell becomes dark.

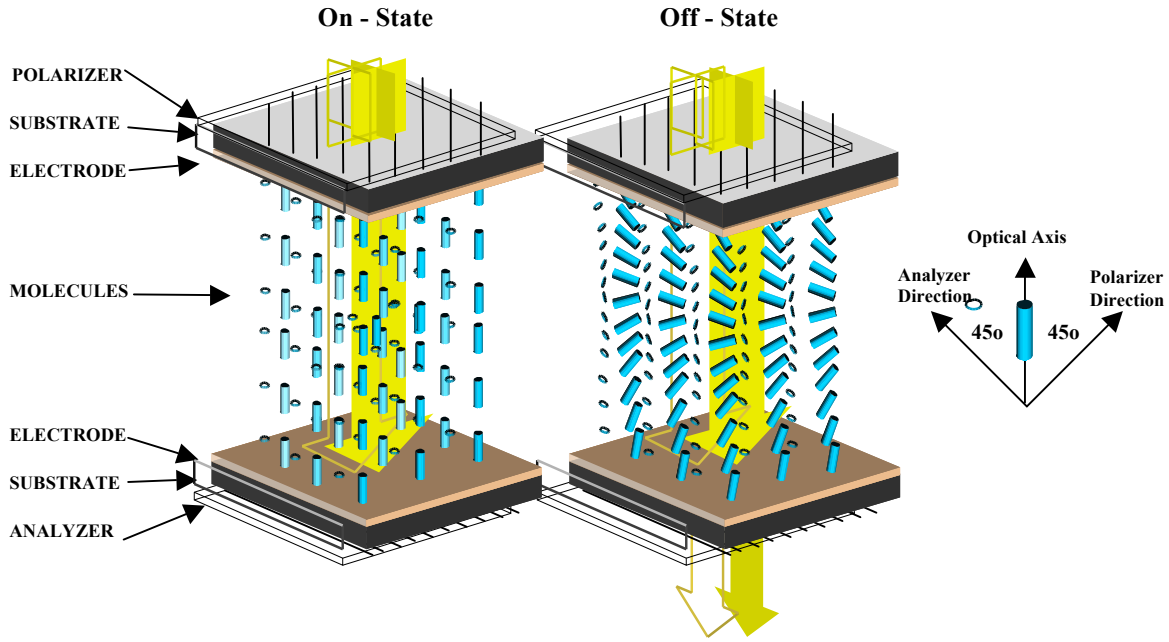

Figure 11 - Schematic of a Thin Nematic cell and the polarizer orientation.

One important point is the thickness of the cells. It was seen in Equation 1.18 that the response time depends upon the viscosity, the dielectric anisotropy, the applied electric field and the distance (*d*) between the substrates. Hence, the only physical parameter which can improve the relaxation time of the shutters and adequate them to cinema theater specifications is the thickness (*d*). However, since the thickness also impacts the viewing angle, the chromatic response and the transmission spectra, a suitable birefringence material should be

chosen to maintain the half-wave plate characteristics.

Thin Nematic cell, as the ECB cell, has the birefringence of the medium changed by applying voltage and has the same disadvantages as the ones presented in the ECB section. Nevertheless, TNs are reliable for 3D cinema and easy to manufacture.

1.4.3. Twisted Nematic Shutters/Display

The Twist Nematic (TN) field effect was introduced by Schadt and Helfrich [17]. After mid 1970s it was rapidly adopted as the display technology in portable instruments. The advantageous characteristics of the TN is low power consumption, low operating voltages, low threshold, high contrast for narrow viewing angles and better viewing angles in comparison with the ECB mode. However, the main disadvantages are long response times and an angle dependent contrast.

A TN cell is a nematic liquid crystal sandwiched between two glass plates with rubbed polyimide alignment layers placed between cross polarizers. What distinguishes from the ECB like cells is, in the TN configuration the front and the rear alignment layers substrates are orthogonally placed to induce a twist in the liquid crystal molecules as shown in Figure 13.

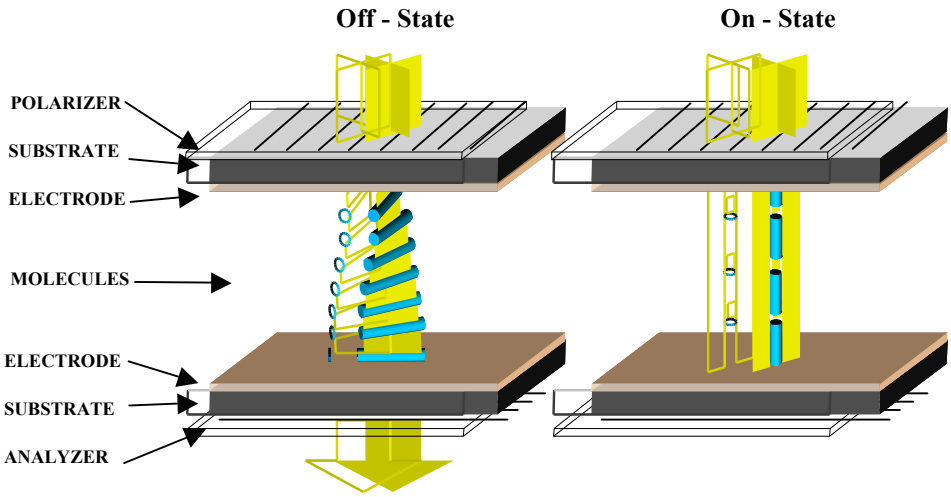

Figure 12 - Schematic of a Twisted Nematic cell.

In the OFF state, the visible light passes through the first polarizer and it is guided by the twisted nematic medium due to the wave-guide effect if the condition $\Delta nd >> 0{,}5\lambda$ is met [18]. The wave-guide action turns the plane of polarization of the incoming visible light allowing the light to pass through the second polarizer. Thus, without electric field the cell is transparent.

In the ON state, or when a voltage above the threshold is applied and considering a liquid crystal with positive anisotropy, the molecules start to tilt to align parallel to the electric field vector. As a result, the effective birefringence is almost zero and, in consequence, the polarized light from the first polarizer no longer rotate and it is absorbed by the second polarizer. The threshold voltage, or tilt voltage, is defined by the equation:

$$V_{th} = \pi \left[\frac{1}{\varepsilon_0 \Delta\varepsilon} \underbrace{\left(K_1 + \frac{K_3 - 2K_2}{4} \right)}_{k} \right]^{\frac{1}{2}} \tag{1.19}$$

where K_1, K_2 and K_3 are the Frank elastic constants, ε_0 is the dielectric constant of the vacuum and $\Delta\varepsilon$ is the dielectric anisotropy of the nematic liquid crystal. Removing the applied voltage the molecules come back to the twist configuration. The time to untwist, τ_{ON}, and to twist, τ_{OFF} are given by:

$$\tau_{off} = \frac{\gamma_1 d^2}{\Delta\varepsilon E - k\pi^2} \tag{1.20}$$

$$\tau_{off} = \frac{\gamma_1 d^2}{k\pi^2} \tag{1.21}$$

As it was mentioned before, the TN technique has some crucial disadvantages. The contrast is asymmetric and it depends on the viewing angle and the direction of view in respect to the director. Some molecules do not completely turn in the direction of the electric field, leading to a light leakage in the on state.

1.4.4. In-Plane Switching (IPS)

The In-Plane Switching mode was developed by Hitachi in 1996 in order to improve the display technology which, at that time, was predominantly TN [19]. The idea was to enhance the view angle and the image quality.

An IPS cell has in principle the same configuration as a Thin Nematic cell. However, two main differences can be observed. The direction of the applied voltage is parallel to the substrate surface by placing two electrodes on the same substrate as shown in Figure 13, and both substrates are rubbed at a certain angle with the electrodes.

In the OFF state, when no voltage is applied, the director is uniformly oriented and the polarization direction of the light does not change, since the cell is placed between crossed polarizers the light is blocked by the second polarizer. In the ON state, the parallel electric field with respect to the substrate drives the molecules to rotate in the substrates plane, orienting them along the field direction. Hence, the light phase changes and can pass through the second polarizer,

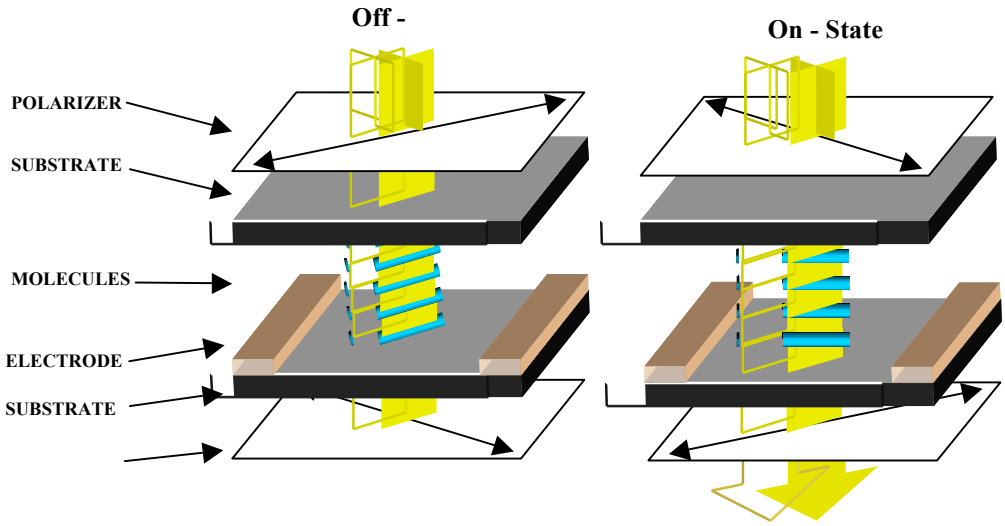

Figure 13 - Schematic of an In-Plane Switching cell.

For IPS technique the fall time is defined as:

$$\tau_{off} = \frac{\gamma_1 d^2}{\pi^2 K_2} \tag{1.22}$$

where γ_1 is the viscosity, K_2 is the Frank elastic constants and d is the cell thickness.

The rise time is more complicated because it depends on the applied voltage and the rubbing direction. However, after a small-angle approximation, the most commonly know equation, is:

$$\tau_{off} = \frac{\gamma_1}{\varepsilon_0 |\Delta\varepsilon| E^2 - \frac{\pi^2}{d^2} K_2} \tag{1.23}$$

where ε_0 is the dielectric constant of the vacuum and $\Delta\varepsilon$ is the dielectric anisotropy of the nematic liquid crystal.

The principal advantages of IPS is the color accuracy due to the small gamma and color shifts, and since the director lies in the substrate plane, the viewing angle is large and symmetric. The big problem in IPS is the low contrast ratio and the color angle dependency. To overcome the initial problems regarding the technology, several improvements were done leading to new types, like: Super-IPS, Advanced Super-IPS and IPS-Pro.

1.4.5. Surface Stabilized Ferroelectric Liquid Crystal Shutters

SSFLC was invented by Clark and Lagerwall at the Chalmers University [8]. The basic idea is, considering the discovery of ferroeletricity in smectic C*, to suppress the helix of smectic C* phase by using thin cells. Since the gap of the cell is very small the substrates oblige the molecules to position their molecular axis in the plane of the cell. This situation gives two equivalent states on the smectic cone separated by 2θ, where θ is the layer tilt angle. If an electric field is applied it is possible to switch the position of the molecules between the two states and after the field removal the switched state remains, creating a bistable memory

effect. Then, placing a SSFLC cell between crossed polarizers with the molecules director parallel to one of the absorption axes a switchable half-wave plate is generated.

The SSFLC cell is a layer of smectic C* enclosed by two rubbed substrates with conductive layers. Ideally, the smectic layers should be orthogonal forming a bookshelf configuration like in smectic A phase. However, due to the shrinkage the bookshelf geometry is replaced by a chevron geometry that will be explained latter in this thesis. The cell gap is of the order of 1-2μm and then the smectic C* helix is unwound by the surface forces, causing the molecules long axes to lie in the plane of the cell with a small pretilt angle. The crossed polarizers, as said before, are fixed with one polarizer parallel to the optic axis of one of the bistable states, or offset at a fixed angle. The schematic of SSFLC cell can be seen in Figure 14.

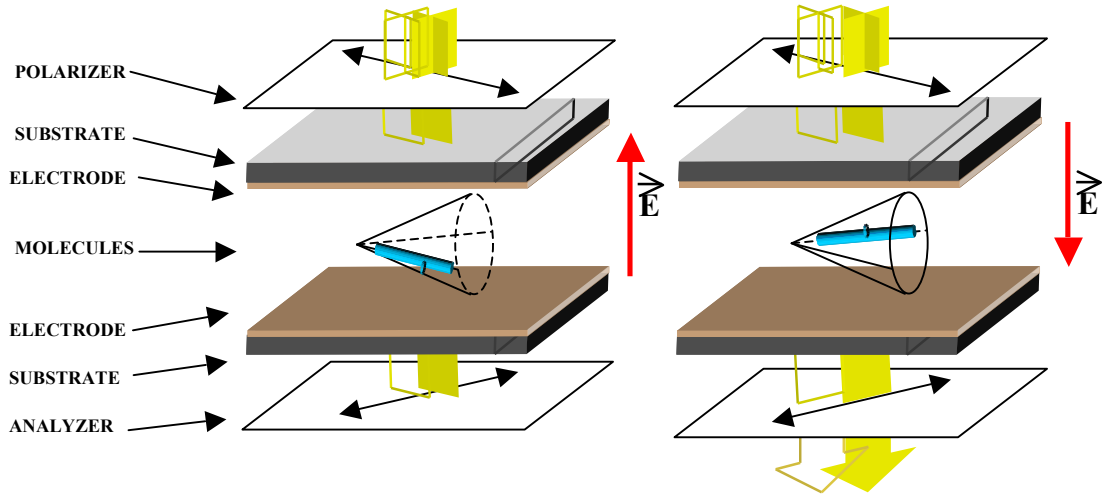

Figure 14 - Schematic of an SSFLC cell.

The dark state (down state) is obtained by applying the electric field and switching the molecules to the position parallel to the polarizer on the top which the light is coming from. In the up state (bright state) the electric field is applied in opposite direction changing the position of the molecules according to the bottom polarizer and one component of the polarization is retarded by 180 degrees, thereby allowing light to pass through the analyzer on the bottom. The transmission of the SSFLC cells is given [20]:

$$I = I_o \sin^2 4\theta \sin^2\left(\frac{\pi \Delta n d}{\lambda}\right) \tag{1.24}$$

where I_o is the incident light intensity, λ the wavelength and Δn is the birefringence. It can be noted that the maximum transmission is reached when θ is 22,5 degrees. A good dark state and a contrast ratio will depend on the birefringence of the liquid crystal and consequently the cell gap. For the liquid crystal Felix 100/015 used in our experiments with a $\Delta n = 0{,}16$ it requires a cell gap nearby ≈1,7μm to maximize the contrast ratio.

The great advantages for SSFLC shutters/display are the wide viewing angle and the response time. The switching times are shorter in comparison of the others technique with nematic liquid crystals and is given by [21]:

$$\tau = \frac{\gamma_{eff}}{P_S E} \tag{1.25}$$

where γ_{eff} is the viscosity, P_S the spontaneous polarization and E the electric field.

Some issues and several limitations have restricted the use of SSFLC as shutters and displays. To align ferroelectric liquid crystal it is necessary to increase the temperature until the isotropic phase and cool down slowly passing through nematic phase, smectic A phase and then into smectic C* phase. However, because of the shrinkage the chevron structure is normally encountered with two opposite tilt angles. The chevron structure results in zigzag defects separating the cells in different domains with inhomogeneous orientation of the director reducing the contrast ratio. These issues associated with the fragility and the complex alignment procedure has taken this technique out of the market.

Conclusion

Liquid Crystal is a very well-known material because of its birefringence, selective reflection and electro-optical characteristics. From the time it was discovered in 1888 by the botanist Friedrich Reinitzer until now, liquid crystal has been studied by specialist from different areas of knowledge and applied in a wide spectrum of applications. The most famous application was in flat panels which consequently revolutionized the industry of mobiles, TVs and related. However, it is not only in the display technology, but liquid crystal has opened a field that concerns biology, telecommunication and etc.

In this chapter, we have discussed the fundamentals about liquid crystals material and its electro-optical characteristics. Also, we have introduced some techniques used by the flat panel industry to manufacture display/shutters based on liquid crystal, pointing the advantages and the disadvantages of each one. Our purpose is to give an overall idea about what can be done in terms of shutters and give the base to understand our experiments which have been done by applying some of these techniques in order to improve the 3D glasses for cinema, TV and DLP projections. Our aim is to enhance 3D glasses and to improve the quality of the 3D vision.

In the next chapter we explain why we see in 3D and some techniques to simulate the 3D using two static 2D images and the 3D TV/Cinema. After we highlight the two major issues for the 3D cinema, ghosting and color banding effect, and what are the mechanisms which make them appear for each 3D cinema technique. The final part is the experiments and characterization of different types of liquid crystal shutters in order to improve the 3D vision trying to get rid of the ghosting and color banding effect.

Bibliography

[1] F. Reinitzer, *"Beiträge zur Kenntniss des Cholesterins"*, Monatshefte fur Chemie, Vol. 9, Issue 1, pp. 421-441, 1888.

[2] O. Lehmann, "Flüssige Krystalle", NATURE, Vol IXX, p.622, 1904.

[3] G. Friedel, "The Mesomorphic States Of Matter", Annales de Physique, Vol. 18, pp. 273-474, 1922.

[4] V. Fréedericksz, V. Zolina, "Forces causing the orientation of an anisotropic liquid", Trans. Faraday Soc., Vol. 29, pp 919-930, 1933.

[5] D. Dunmur, T. Sluckin, "Soap, Science, and Flat-screen TVs: a history of liquid crystals", Oxford University Press, pp. 20-7, 2011.

[6] Frank, F. C. 1958. Discuss. Faraday Soc. 25:19.

[7] Pikin, S. A., and V. L. Indenbom. 1978. Ferroelectrics. 20:151.

[8] Noel A. Clark, Sven T. Lagerwall, "Surface-stabilized ferroelectric liquid crystal electro-optics: New multistate structures and devices", Ferroelectrics, 59, Iss. 1, 1984.

[9] S. V. Pasechnik, V. G. Chigrinov and D. V. Shmeliova, "Liquid Crystals – Viscous and Elastic Properties", Wiley-VCH, German, 2009.

[10] M. G. Clark et al, "Measurement of the permittivity of nematic liquid crystals in magnetic and electric fields using extrapolation procedures", J. Phys. D.: Appl. Phys. Vol. 13, pp. 2151, 1980.

[11] Shin-Tson Wu, Deng-Ke Yang, "Fundamentals of Liquid Crystal Devices", Wiley Series in Display Technology, 1st Edition, 2006.

[12] deGennes, P. G. 1974, "The Physics of Liquid Crystals", Oxford: Claredon Press.

[13] I. Sage, "Thermochromic liquid crystal devices", in Liquid crystals–applications and uses, Vol. 3, ed. B.

[14] W. Helfrich, Mol. Cryst. Liq. Cryst. 21, 187, 1973.

[15] Y. Koike and K. Okamoto, "A super high quality MVA-TFT liquid crystal displays", in SID Dig., pp. 206-209, 1999.

[16] K. H. Kim, "Advance of PVA Technology for Multi-media Applications", SID Digest, 40.4 1208, 2003.

[17] M. Schadt and W. Helfrich, "Voltage-dependent optical activity of twisted nematic liquid crystal", Appl. Phys. Lett., vol. 18, pp. 127-128, 1971.

[18] C. H. Gooch and H. A. Tarry, Ellectron. Lett. 10, 2, 1974

[19] M. Oh-e and K. Kondo, "Electro-optical characteristics and switching behavior of the in-plane switching mode", Appl. Phys. Lett., vol. 67, pp. 3895-3897, 1995.

[20] N. A. Clark and S. T. Lagerwall, Appl. Phys. Lett. 36, 899, 1980.

[21] C. Escher, T. Geelhaar, and E. Bohm, Liq. Cryst. 3, 469, 1988

Chapter 2: *Liquid Crystal Shutters for 3D Cinema*

Introduction

In 1830 Charles Wheatstone created a device called the "reflecting mirror stereoscope" [1]. At that time he wanted to prove the fundamental that we see in 3-D because we have two eyes with binocular vision. The expression "Stereoscope" comes from the Greek words *skopion* plus *stereo* which means "to see - solid". The device consisted of two mirrors at 45 degrees with one reflecting the image of the left eye and the other of the right eye in order to produce a stereoscopic image[1]. In the beginning, to prove his theory he used stereoscopic drawings made by himself. He published his historical article concerning the stereoscope vision in 1838. The commercial interest in Wheatstone theory came with the invention of photography. In 1841 M. Fizeau and M. Claudet produced the first daguerreotypes[2] for stereoscope. Another huge contribution in stereography was made by David Brewster, who also claims to be the one that discovered the stereoscope vision and not Charles, he established technical aspects about camera lenses [2]. However, his most popular invention was the lenticular stereoscope.

One important contribution to the stereoscopic vision which has affected directly the 3D cinema was made by J. C. Almeida in 1856. He projected slides of stereoscopic images successively using colored red, green filters and the spectators were using goggles with red and green filters on the lenses. In this way, the green image could be seen by the eye covered by the green filter and the red image could be seen by the eye covered by the red filter forming a 3D image. Then, from 1850 to 1890 a lot of studies were done to improve stereoscopic photography and stereoscopic images in motion [3]. In 1891 Ducons du Hauron invented the anaglyph stereoscopic print and reproduced stereoscopic photographs. Soon after, 1901, Claude Grivolas patented a projector for 3D which two reels of film were simultaneously projected, one through a lens with a blue filter and the other through a lens with a red filter [4]. The audience used a goggle with red and blues filters to combine the two images in perspective. The first 3D system which persisted into the market for almost all XX century was born.

In order to understand the 3D cinema today there are two more very important inventions. The first one was in 1922, Laurens Hammond and William F. Cassidy changed the way to present 3D images [5]. It was the first active technology for 3D projection. Their process required two reels of film (right eye and left eye) each one projected separately by different projectors. The projectors were electronically synchronized to produce alternating left and right images on the screen. Thus, to make a stereoscopic image each spectator had to sit

[1] It is two images of the same subject slightly offset of each other to create the illusion of depth.
[2] A photographic process which the image is positive made in the camera on a silver plate.

behind a “televiewer”, a mechanical shutter driven by an electric motor synchronized with the projectors. The aim of the shutter was to block the view of one eye while the image destined to the other eye was on the screen. This technique failed due to the expenses of installation. However, the principle remains and it is used today as a solution for stereoscopic vision systems. The second invention, which impacted the 3D cinema industry, was the Polaroid filters, in other words, the polarisers in 1932 by Edwin H. Land [6]. The images of the left and right eye were encoded with orthogonal polarization and projected on the screen and the audience had to use polarized goggles.

Today, all the 3D cinema systems follow the same principles as in the beginning of the last century, the anaglyph, the active (shutter) and passive (polarized) techniques. The development of all these solutions during the last century along with the evolution in electronics has helped to have motion stereoscopic images with high quality. In this Chapter is presented an introduction of the techniques to stereoscopic vision in motion and its drawbacks as ghosting effect and color banding. Finally, some measurements and improvements of different liquid crystal shutters are shown.

2.1. Depth Perception (Binocular Vision)

The vision represents 75% of our perception of everything that surrounds us. The eyes are responsible to “collect” the light and transform it in electrical pulses that are decoded by our nervous system leading us to see. The binocular vision is a result of having two horizontally aligned eyes that allows us to see the same object from two slightly different perspectives. The central nervous system processes these two perspectives giving the notion of depth [7]. Then, the depth perception is given by integration of the visual information captured by the eyes and interpreted by the brain. The Figure 15 shows an object and the two perspectives of it.

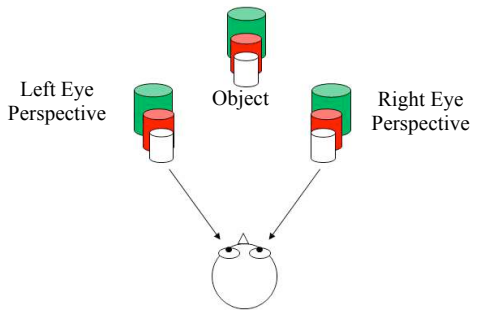

Figure 15 – The perspectives of an object seeing by the right and left eye.

The term stereoscopic is a three dimensional visualization of the same element from two slightly different points of view, each one captured by only one eye.

2.2. Stereoscopic Vision

Why not take the advantage of our binocular vision and apply on photography and cinematography? In a strict sense, used in this thesis, the stereoscopy is the enhancement of

the illusion of depth, in photographs or movies, presenting two 2D (two dimension) images of the same object (or scenario) from slightly different perspectives to each eye of a viewer. These 2D images are combined in the brain giving the perception of depth and forming one 3D image. Several techniques were developed in photography and in cinematography to achieve the perception of depth. In the following section we describe some of them emphasizing current techniques in the cinema, television and projection market. We do not pretend to explain in details all the 3D techniques but the minimum to understand how the 3D vision works, our experiments and the results with the liquid crystal 3D shutters.

2.2.1. 3D Techniques Without Glasses

The challenge is to allow the left eye to see the image intended for the left eye and the right eye only the image intended for it without using 3D glasses or any kind of headgear.

2.2.1.1. Freeviewing

In Freeviewing technique both the images, left and right, are always visible to both eyes. In that case the viewer should learn how to point each eye to the correct image to see the 3D effect. There are two main techniques: Parallel View and Crossed-eye View.

- Parallel View

The image in parallel view is formed by two images: one left image (IMG-L) disposed on the left side for the left eye and one right image (IMG-R) disposed on the right side for the right eye (IMG-L). Normally, when we read a written piece of paper automatically we aim our eyes directly to the paper surface and read it. However, to see the 3D effect looking at a parallel view image on the paper the lines of sight of the eyes have to move outward towards parallel in a way that the left eye sees only the left image and the right eye the right image. The figure below show the difference between the lines of sight while you read a paper and while you see a 3D image using parallel view technique.

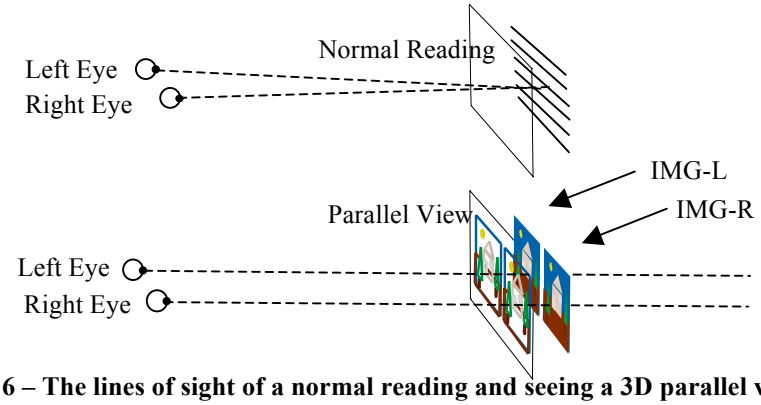

Figure 16 – The lines of sight of a normal reading and seeing a 3D parallel view image.

- Cross-Eye View

In cross eye viewing the left image is on the right side and the right image is one to the left side. In this situation the viewer has to cross the lines of sight in order to the right eye see the right image which is on the left side and the left eye to see the left image that is on the right side (Figure 17).

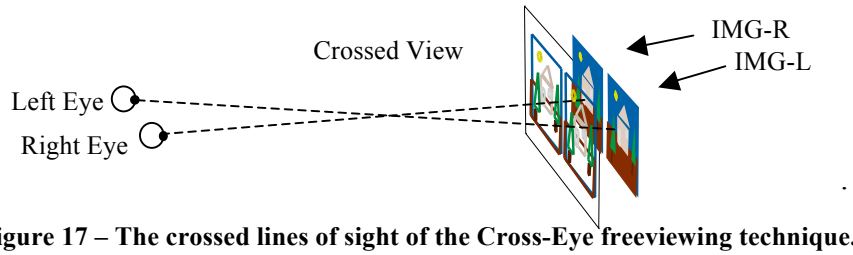

Figure 17 – The crossed lines of sight of the Cross-Eye freeviewing technique.

The freeviewing technique is possible to implement on pictures and photographs but not in movies. Maintaining the eyes strained to keep the parallel or crossed view for long periods is almost impossible and will fatigue the eyes.

2.2.1.2. Autostereoscopy

Autostereoscopic is a display technology which uses optical components inside of the displays to enable each eye to see the intended images and creates the sensation of depth. The principle of the autostereoscopy technologies is that the viewers do not have to wear special headgears to see in 3D. The optical components splits each image, left and right, into the viewer's eyes. One of the drawbacks of this technology is that the viewing angle is limited and the viewers, to achieve the stereoscopic effect, should be in front of the screen in a specific position [8]. To overcome the issue Automultiscopic displays has been done which provide different views of the same scene [9]. There are two main types of automultiscopic displays: head-tracking, as the name suggest the system tracks the viewer, and multi views display [10][11], the projection is made by sections and the viewer while moving see different perspectives of the scene. Below we describe the most well known techniques of Autostereoscopy.

- Parallax Barrier

The parallax barrier was invented by August Berthier in 1986. Today, in terms of market, the portable game Nintendo 3Ds is one of the most successful devices which use the parallax barrier technique. The technique consists of dividing the horizontal resolution of a display, typically liquid crystal display, into two sets. One horizontal column of pixels displays the left image and the other column the right image. Then, a barrier with precision slits is placed in front of the display in a way that one viewer in front of the screen in a well-defined spot can see a 3D image. Figure 18 illustrates how the viewer's eyes receive the "correct" images from the display by putting a barrier in front of it to have the stereoscopic effect.

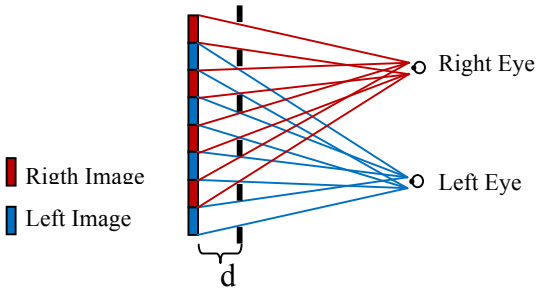

Figure 18 – Illustration of the Parallax Barrier technique.

The distance (d) between the barrier and the pixels depends on the viewing distance normal to

the screen, the pixel pitch and the eyes separation [12], limiting the angle of view.

- Lenticular Lens (arrays)

This technique was first implemented in pictures with the name of lenticular printing (LP) [13]. The LP process consists of creating a lenticular image from two images and combine with a lenticular lens. The images are interlaced on a substrate and after covered with an array of lenses to direct the light from each image to different spots. The Lenticular Lens 3D display follows the same principle. The display pixels are divided in two sets of columns, one column projects the right image, the other column the left image and an array of cylindrical lenses are stick on the display directing the light from adjacent pixels columns to different viewing angles slots. In Figure 19, it illustrates the Lenticular Lens technique.

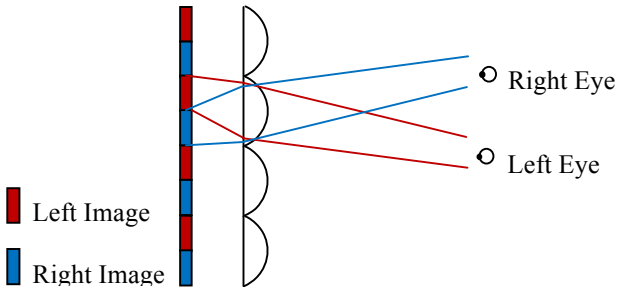

Figure 19 - Illustration of the lenticular Lens technique.

2.2.2. 3D Techniques With Glasses

In this section it is described the current 3D techniques which requires the viewers to wear special 3D glasses in order to perceive the stereoscopic effect.

2.2.2.1. Color Multiplexing (Anaglyph)

Anaglyph is the classic method of visualization in 3D. It is a very low-cost solution and can be easily implemented in any common color display devices. 3D anaglyph images are achieved by combining the two images, for the left and right eyes, using complementary color coding [14]. Typically, the method uses the red and cyan channel for the left and right eye, respectively. The viewers have to wear colored glasses so that the eyes receive only the corresponding images. The main disadvantages are the loss of color information, crosstalk and chromatic adaptation problems [15][16]. Figure 20, illustrates the color multiplexing technique using red and cyan filters for 3D cinema. Note that the representation with two projectors on Figure 20 and Figure 21 is for didactical purposes, these techniques can be achieved using only one projector.

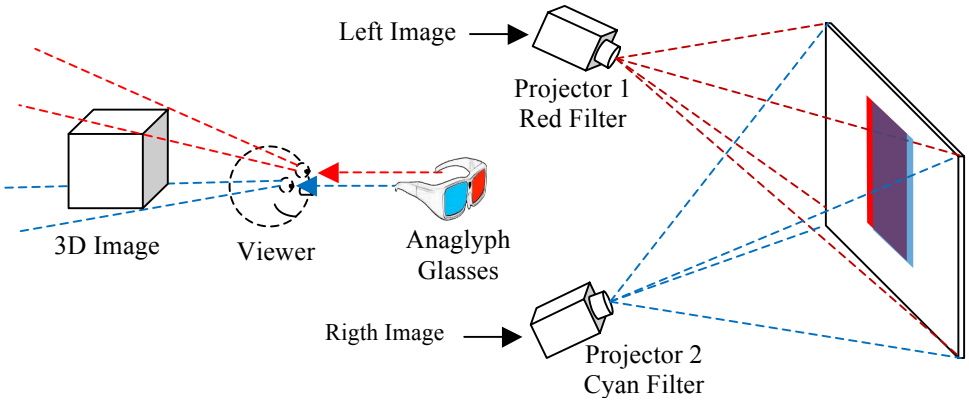

Figure 20 – The illustration of the color multiplexing technique using red and cyan filters.

In 2001, a technique called ColorCode 3D was patented to produce full color 3D images, which uses amber and blue colored filters on the glasses [17]. The main point of the ColorCode was the improvement of the color of 3D images. Another technique with relatively high image quality was made by Infitec GmbH [18]. They use narrowband interference filters both with the spectral response in red, green and blue but slightly shifted in wavelength. It has low crosstalk and requires a color gamut transformation algorithm [19]. The same company implemented a wheel-based approach to reduce the number of projectors to one, instead of two. The left and right images are sequentially displayed.

2.2.2.2. Polarization Multiplexing

This technique encodes the left and the right images in orthogonal polarization states. It can be used in linear and circular polarization, but the latter allows the viewer to tilt their heads without noticing the ghosting effect, and the viewers have to wear polarized glasses. Two projectors produce the images, the first one projects either the left or the right image in one polarization state while the other projects in a orthogonal polarization state. The disadvantage of this technique is the necessity of a special screen to preserve the polarization states, like a silver screen. Figure 21 shows a schematic of the polarization multiplexing using linear polarisers.

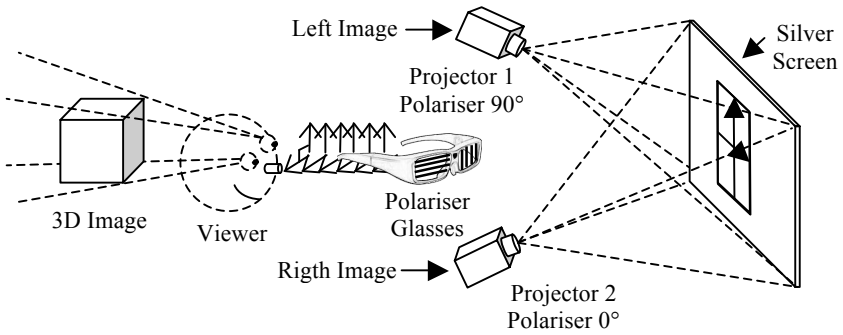

Figure 21 – The polarization multiplexing with linear polarisers.

The use of two projector increases the cost and power consumption. Furthermore, the aligning of the projectors is not simple. One solution is using a polarization modulator in front of the projector, eliminating the second projector. The company RealD proposes similar technique which is available and called ZScreen [20].

The drawbacks of the polarization multiplexing are the chromatic aberration and the ghosting effect introduced by the polariser filters. The ghosting effect is also due to the quality of the silver screen and the projection system. The ghosting is deeply investigated in the last chapter.

2.2.2.3. Time Multiplexing

The time multiplexing technique exploits the persistence of vision phenomena. The left and right images are displayed on the screen alternatively at high frame rate, typically 120Hz. The viewers have to wear glasses with active shutter which are synchronised to the displayed image. While the left images are on the screen the right shutter of the goggle is closed and the left shutter is open, and vice versa. In a way that one eye sees only the image which is intended to it. The synchronization is done by infrared emitters or DLP Link, which flashes are sent to the screen between the right and left frame are reflected from the screen and are detected by the shutter glasses. The disadvantage is the cost of the active glasses and the video bandwidth compared to a 2D video stream. However, the technique does not need a silver screen, just a regular screen, and only one projector with sufficient bandwidth is necessary. Nowadays, this technique is implemented in cinema theatres, TV displays and it has also been deployed in immersive displays [21]. Figure 22 illustrates how the 3D Cinema theatres using the time multiplexing technology works.

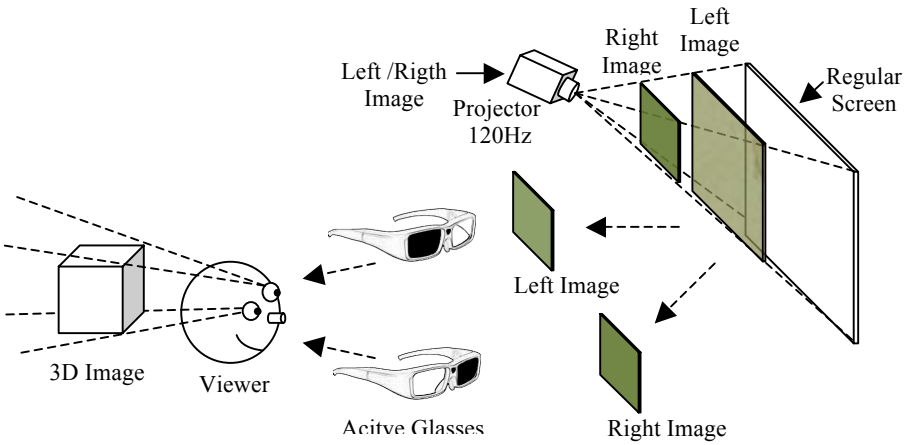

Figure 22 – Schematic of time multiplexing 3D cinema.

Each technology has its own advantages and limitations. The choice depends on the application and the budget. For example, deploying a polarizer system with polarization modulators in home theaters or in cinema theaters could be a lower cost solution in terms of glasses. However, in this case the ghosting effect is higher due to the imperfect polarizer and silver screens, and the screens are normally expensive.

In the next section, the ghosting effect, also known as crosstalk, and the color banding, the two main factors that reduce the quality of the 3D solutions techniques are described.

2.3. Stereoscopic Vision Main Drawbacks

There is a huge development in the 3D market ranging from the quality of the projection

systems and the quality of the content. In this direction it is necessary to provide to the viewers high quality 3D experience. The two major factors which play an important role in the quality of the stereoscopic vision are the ghosting and color banding effects.

2.3.1. Ghosting Effects

The crosstalk in stereoscopic displays in simple words is the leakage of the left image into the right image and vice versa. The crosstalk causes loss of contrast, loss of the 3D effect and viewer discomfort [22]. Ghosting Effect is the visible effect caused by the crosstalk between the stereoscopic images. In Stereoscopic systems with high levels of crosstalk the viewer's eyes see not only the image that is intended for one eye but some of the image which is intended for the other eye.

There are several reasons for which the ghosting effect occurs and it depends on the stereoscopic display technology. Since it is not possible and also it is not the aim of this thesis to discuss all the existing technologies, in this section it is described only the general reasons of the ghosting effect for the mentioned techniques: color multiplexing, polarization multiplexing and time multiplexing.

- Time Multiplexing Ghosting Effect Factors

In active displays and active 3D cinema the ghosting effect is directly related to the optical performance of the liquid crystal shutters. It means that the shutters ought to have a very good dark state, i.e. when the shutter is closed the amount of light passing through it should be insignificant. The display or the projector has to be in perfect synchronization with the active glasses. Also, the shutters have to be fast enough to open (rise time) and close (fall time) while the image which is intended to it is being displayed, because supposing that the shutter has a high fall time the displayed image may change before the shutter is completely closed and the viewer eye will see the image that is not intended to see.

- Polarization Multiplexing Ghosting Effect Factors

The simple method to implement 3D projection involves the use of two projectors, a polariser in front of each projector, a silver screen and polarised glasses for the viewers. Taking into account this setup the principal factors that may influence the ghosting effect are the optical performance of the polarisers which includes the transmittance and the extinction factor with respect to the orthogonal polarization state, the capability of the silver screen to maintain the polarization states that comes from the projection system and the orientation of the coding and decoding polarisers. The polariser 3D solution that uses polarisation modulators has two additional factors: the phase of the polarisation according to the display and the optical quality of the modulator.

- Color Multiplexing Ghosting Effect Factors

The important contributor to ghosting effect in 3D displays, which codes the left and right images with complementary colors, is the spectral quality of the color filters. The first filters used to implement the anaglyph techique were red and cyan. These filters were not narrow enough and both, red and cyan, had small part of the spectral response invading the green

region of the spectrum causing the ghosting effect. In projection system and in display system the filters selectivity determine the level of ghosting and the image quality.

2.3.2. Color Banding

The color banding is the inappropriate color representation of the image. In active 3D cinema if the switching time of the shutters is too long there is possibility of losing color information due to the incapability of the viewer to see all the shades of a color. In fact, the shutter is not completely opened while the image is on the screen. In Figure 23 the dot line represents the switching time of the shutters with the left and right images on the background. It can be seen that part of the information of the color is lost for the viewer eye.

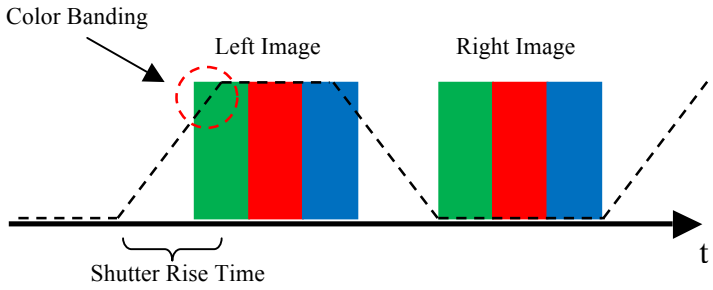

Figure 23 – Color Banding effect.

The color banding and the ghosting effects degrade the quality of 3D vision in term of image quality and eye strain if the viewer wears the glasses for long time. In order to reduce the amount of ghosting and color banding it is necessary to understand the mechanisms which provoke the effect.

In the active 3D solution it has been seen that the glasses are the ones which need more attention with respect to the ghosting effect and color banding. In the next section, we have performed a detailed analysis of the electro-optical performance of different liquid crystal shutters to find out possible solutions to avoid the cited effects improving the 3D vision sensation.

2.4. Liquid Crystal 3D Shutters

The actual active 3D glasses based on liquid crystals provide the highest quality in terms of 3D vision with relatively low levels of ghosting and color banding. The disadvantages of the glasses are that the glasses are heavy and the cost is higher because of the electronics, the liquid crystal shutters and the power supply. The main technical aspects involved are switching times, contrast ratio and residual light [23]. It was seen that the switching time is directly linked to the image quality. Slow shutters would imply ghosting, color banding and consequently a bad 3D experience.

The dark time, the time between the right and left image in time multiplexing systems, is defined with respect to the existing active glasses' switching time and varies between 1 to 2ms. This time interval in a way defines the brightness of the images because it limits the time that one frame, right or left image, remains on the screen. Currently, the active 3D systems

that are on the market use shutters based on a nematic liquid crystal with a switching time close to 1 millisecond, contrast ratio of 1:200 and a transmittance of 32% [23]. The question is why we don't use ferroelectric liquid crystal? The ferroelectric liquid crystal has a switching time around 100 microseconds and it is symmetrically bi-stable [24]. Thus, it is possible to reduce the dark time improving the brightness and avoiding the color banding. The remaining aspects to not put the ferroelectric liquid crystal on the shops' shelves are the poor contrast ratio and inability to sustain shocks. We should not forget that the 3D glasses should let pass as much light as possible on the bright state and block everything in dark state to avoid ghosting. Besides, users have to be able to handle the glasses without damaging the shutters.

In the following section different types of ferroelectric liquid crystal shutters are described and are characterized, showing how it is possible to improve them and the reason that they are not yet on the market. Finally, since ferroelectric cannot be used as shutters due to the upcoming conclusions in that chapter, a new nematic liquid crystal mixture was tested and improved the currently 3D active glasses.

2.4.1. Stabilised Ferroelectric Liquid Crystal Shutter (SFLC)

The important features about ferroelectric liquid crystal (FLC) which makes it suitable for 3D glasses are the possibility to built high speed optical shutters with a wide view angle. The most interest FLCs for shutter applications are chiral smectic C phases. However, one of the problems is to obtain homogeneous and/or bi-stable alignment because smectic phase are very sensitive to surface interactions. Besides, when confined smectic liquid crystals pass from the smectic-A phase to smectic-C it shrinks the smectic layers forming chevron defects type C1 and/or C2 [25]. One of the two possible chevron defects can be avoided making the liquid crystal cells in parallel fashion rather than in the anti parallel [25]. The other chevron can be irreversibly removed by applying low frequency and high amplitude electric field, leading to a bookshelf structure which is not suitable for optical shutters.

To avoid the chevron defects to appear, it is proposed a twist structure of FLC induced by a twist in rubbing direction on the cell substrates. It was proved that the spatial distortion of the director is coupled to the spatial distortion of the tilt of the smectic layers [26], and assuming that the normal of the layers is parallel to the median axis of the rubbing direction, the layer thickness (l) shrinks in the smectic-A phase mitigating the chevron formation in smectic-C phase. The relative layer shrinkage is evaluated as

$$\frac{\Delta l}{l} \cong \frac{\Psi^2}{8}$$

where Ψ is the induced twist angle.

Several twist FLC cells have been done and optically characterised to see the influence of the twist of the director on the chevron structure and how it changes the texture and the electro-optical properties. The experiments were done with different Twisted Surface Stabilised Liquid Crystal (TSSFLC) cell at various twist angles varying from 0° to 45°, inclusive of a

regular SSFLC cell (0°).

- The Liquid Crystal Samples

The TSSFLC samples used in the experiments consist of two glasses (20 x 20mm) coated with transparent electrode indium tin oxide (ITO). Both glasses were spin coated with a thin film of polyimide (~100nm) Nissan SE410 forming the front and the rear substrate (FS and RS). After hard-bake (2h at 180°C), the polyimide film of the front substrate and rear substrate were rubbed in angle (Ψ) with a velvet cloth to induce a planar alignment of the liquid crystal molecules. The cell gap was maintained flat by using glass-bead-spacers of about 1.5µm. Then, by capilarity, the cells were filled with the smectic liquid crystal at a temperature well above the nematic-isotropic transition and slowly cooled down (cooling rate of 0,1°C/min) to room temperature in order to have a uniform cell. Figure 24 is the schematic of the TSSFLC cell used in this thesis.

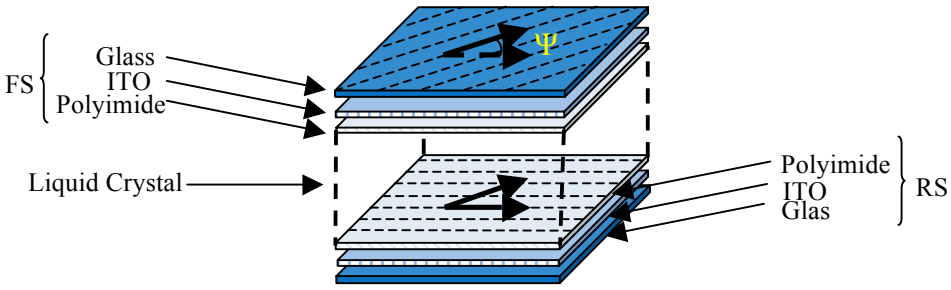

Figure 24 – Macroscopic schematic of FLC sample used in the experiments.

- The Liquid Crystal Samples Optical Characterization

The samples were characterized by taking pictures to see the difference in the texture, by measuring the contrast ratio (CR) and the response time (RT). The measurements of CR and RT were performed using a He-Ne laser (LD), a function generator (FG), an oscilloscope (OS), two linear polarisers (LP), a photodetector (D) and a power meter (PM). The cells were put between the crossed polariser and connected to the function generator. The waveform applied to the cells was a square wave at 1 KHz frequency with 50% of duty cycle and 20V peak-to-peak. The function generator and the power meter were connected to the oscilloscope to check the waveform applied to the cells, to measure the response time and the contrast ratio of the samples. Figure 25 is the experimental setup to characterize the liquid crystal samples.

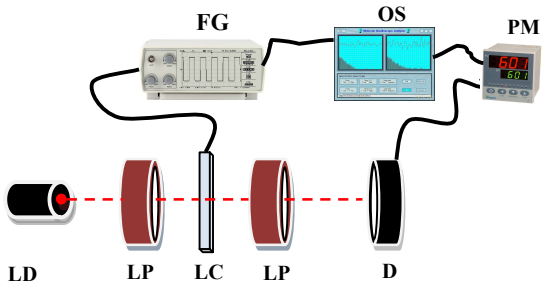

Figure 25 – The experimental setup to measure contrast ratio and response time.

The measurements were done for several samples with different liquid crystals: Felix 15/100, Felix 19/100 and W206D. Table 1 has the response time behaviour as a function of the twist

angle for all the tested liquid crystals.

	Time (µs)		
Twist Angle (°)	**W206D**	**Felix 15/100**	**Felix 19/100**
0	260	37	32
5	250	32	30
10	220	72	33
15	300	35	30
20	266	37	36
25	425	35	35
30	315	40	33

Table 1 - Response time for different samples at different twist angles.

It can be seen from Table 1 that the twist angle has a very weak influence on the response time. This was expected because the smectic cone does not change with the twist and the liquid crystal director switches the same way for all the listed samples.

In the next table there are the results of the contrast ratio measured in the sample mentioned in Table 1:

	Contrast Ratio		
Twist Angle (°)	**W206D**	**Felix 15/100**	**Felix 19/100**
0	973	967	1762
5	1138	916	2273
10	2727	2364	1149
15	2242	2080	1494
20	125	1531	2086
25	268	683	1653
30	72	141	1489

Table 2 – Contrast Ratio for different samples at different twist angles.

The three liquid crystals were chosen to find out if there was a relationship between the twist angle and the effective angle of the ferroelectric liquid crystal. We thought that with the twist it would be possible to introduce a coupling between the director and the smectic layer tilt, which would restrict the chevron defects. However, in terms of contrast ratio and response time we could not find a direct relation between the induced twist and the electro-optical characteristics. The contrast ratio of the sample W206D and the Felix 15/100 are optimal between 10° and 15° and for Felix 19/100 at 5°. However, the texture of the twisted cells were more uniform in comparison with a regular surface stabilized liquid crystal cell (0°) and was defects free, as it can be seen in the pictures below. Only the pictures with the liquid crystal Felix 15/100 are shown, because the results in terms of texture are the same for other liquid crystals. The pictures were taken under cross polarised microscope using lens Nikkon with aperture of 0,13 and 5x zoom. The area of the pictures is 100 x 100 micrometers.

0° **10°** **15°**

Figure 26 – Pictures taken under cross polarised microscope for different twist angles.

Besides the contrast ratio, response time and texture, the biggest issue is the susceptibility of surface stabilized ferroelectric liquid crystal (SSFLC) for pressure and long periods of applying voltage. It was observed that there were changes in the FLC texture modifying its electro-optical characteristics after long period of applying voltage (2h). The chevron, the roof-top and the stripes texture start to slowly reappear as long as the electric field is applied. To check the dependence of the twisted cells texture with the electric field, the Felix 15/100 with 15° of twist underwent the electric field during 2h (20V peak-to-peak @ 1KHz) and two pictures before and after were taken.

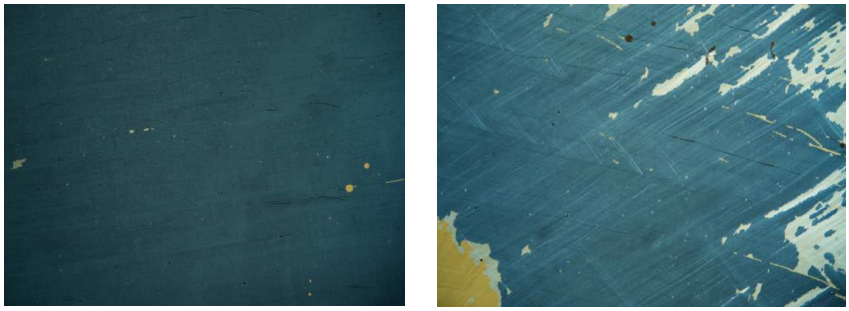

Before **After**

Figure 27 – Pictures of the sample Felix 15/100 with 15° of twist before and after electric field.

The texture changed after the electric field and the roof-top defects and chevron started to appear. To overcome these problems and make the shutters more robust a mixture of FLC and polymer was done. After all, the contrast ratio and response time results were good and suits perfectly the 3D glasses requirements. The idea was to make sure that the texture will not change due to pressure and long periods of applying voltage.

2.4.2. Polymer Stabilised Ferroelectric Liquid Crystal Shutter (PSFLC)

The samples were done by making a mixture of Felix 015/100 with liquid crystal based polymer (Merck-RM257) and photoinitiator (Igracure 651). Three mixtures were prepared with 1%, 5% and 13% of RM257 by weight, 13% is the limit of solubility. The photoinitiator was used to start the polymerization and the concentration was about of 0,1%. The fabrication of the cell is exactly the same as it is done with the SSFLC which we have seen in the last section. The only steps that change are the filling process and the polymerisation to form the polymer network. The PSFLC cells are filled above the isotropic temperature and when is

completely filled it is cooled down till the nematic phase temperature. After the cell is completely in nematic phase, a ultra-violet lamp is placed on it and the cell is polymerised during one hour at 0,1mW/cm². The energy is enough to polymerize the sample with RM257. The contrast ratio and the response time were measured using the same experimental setup used for SSFLC with and without twist (Figure 25). However, the voltage required to completely switch the liquid crystal director in a PSFLC sample is higher due to the polymer network as the network hinges the free movement of liquid crystal molecules. Then, we applied to the cell 30V peak-to-peak.

RM257 (%)	Contrast Ratio	Response Time (µs)
1	967	39
5	433	85
13	685	93

Table 3 – Contrast ratio and response time for PSFLC of different concentrations.

The concentration of 1% is not sufficient to form the polymer network. The PSFLC at 1% behaves as a pure SSFLC and the results are almost the same than the ones in Table 3 and Table 1 for the Felix 015/100 with 0° twist. However, the contrast ratio and the response time for the 5% and 13% change. The samples become slow when the concentration of RM257 increases as the polymer network is denser. The denser is the polymer network the transmission of the light in the dark reduces and the contrast ratio increases.

In fact, the polymer stabilised ferroelectric liquid crystal (PSFLC) shutters are more rigid and resistant. No changes have been noticed after applying electric field for 2h but the samples scatter the light. The scattering can be caused due to the presence of any dust particle inside the cell or, in our case, due to the polymer network. When the domain size of the polymer network is much higher than the wavelength, then the light is scattered. Then, we have increased the concentration of polymer to 13% in order to decrease the domain size of the polymer network. The scattering leads to two major problems when it concerns 3D glasses. First, on the bright state if the shutter scatters the light the viewer will see a blurry image without sharpness. Second, on the dark state some amount of light leaks and the viewer might see the ghosting effect.

To measure the scattering the ELDIM EZLite colorimeter was used with white light as the source. The ELDIM is based on Fourier optics. In fact, the ELDIM focuses the light which passes through the sample and refocuses on the Fourier plane at a position according to the incident and azimuthal angles. Thus, it is possible to measure the scattering and its angular dependence. The Figure 28 shows the scattering lobes for the sample with 13% of polymer.

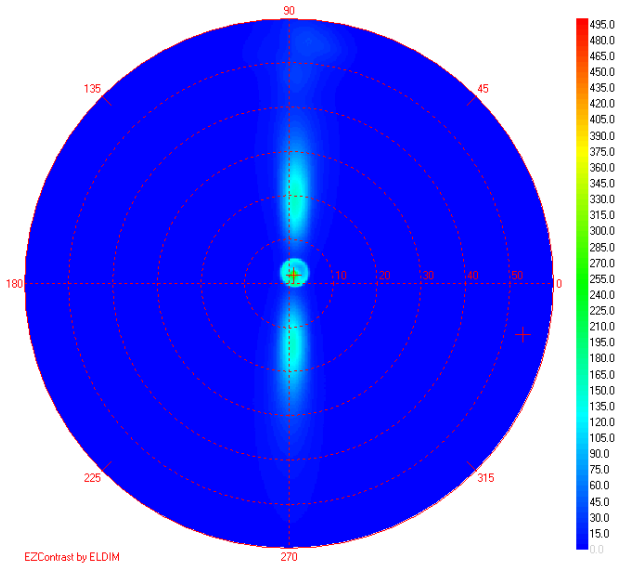

Figure 28 - The light scattering of the PSFLC 13% measured with ELDIM EZLite.

2.4.3. Nematic Liquid Crystal Shutter

The results have proven that use SSFLC, with and without twist, and PSFLC could be a solution to improve the stereoscopic vision in active 3D systems. They have excellent contrast ratio and a fast response time, but some issues have to be mitigated before going to the market. The SSFLC cells cannot support electric voltages for long periods without changing the texture and they are very fragile to mechanical shocks. The PSFLC shutter was a solution to overcome these problems, but it scatters the light and the viewer sees the ghosting effect.

Considering the results with FLC and PSFLC we decided to go back to the traditional technique of the nematic described in section 1.4.2. It is well-know that this type of shutter has very good contrast, it can support electric field and mechanical shocks, and it has acceptable response time and light transmission. It was seen in Chapter 1, from Equation 1.17 that the transmission of nematic shutters for a given wavelength depends on the thickness (d) and the birefringence (Δn) of the liquid crystal. The thickness of 1,5µm is the mechanical limit that large scale industry can achieve. However, there are some techniques like phase-separation which can reduce the thickness of the shutter to less than 1µm [27][28], but it is not implemented yet on the industry and still have some drawbacks to overcome. So to have good transmission over the entire visible spectrum a high birefringent LC is required. On the other hand, high birefrigent LCs are viscous and consequently the response time increases (Equation 1.18). The point is how to make shutter with better transmission, higher Δn, and at the same time fast enough to be used in currently active 3D systems.

The glasses that we want to improve belongs to Eyes3Shut (E3S) the sponsor of this thesis and the partner in the project of active shutters and 3D vision. E3S fabricates and sells active glasses for 3D cinema and DLP projectors. The glasses' characteristics are: liquid crystal LCE3S-A, not viscous with a birefringence of 0,11, shutter thickness of 1,5µm and the response time is approximately 1ms. Basically, the aim is to improve the Δn to have better transmission without slowing down the switching.

Then, the idea was to mix another liquid crystal (LCE3S-B) which has a high birefringence (Δn=0,16) with the liquid crystal LCE3S-A used by E3S. Two mixtures have been done and the principal characteristics are listed in Table 4. Note that the concentration of the liquid crystals was done by weight.

Liquid Crystal	LCE3S-A	LCE3S-B	Δn
LCE3S-A	100%	0%	0,11
MixA	60%	40%	0,13
MixB	40%	60%	0,14
LCE3S-B	0%	100%	0,16

Table 4 – Liquid crystal mixtures.

Once the mixtures were prepared, four cells of 1,5µm thickness with the same characteristics explained in Section 1.4.2 were filled and then were characterized. The thicknesses of the cells were calculated using retardation measurements done by a Berek compensator. The characterization of stereoscopic 3D vision shutters have to cover at least four aspects: relaxation time, transmission, viewing angle and white dispersion. The relaxation time is related to the reduction of the ghosting effect, the viewing angle is important to the maintenance of the contrast with respect to the angle of vision and, the transmission and white dispersion are associated with brightness and color fidelity.

- Relaxation Time

The relaxation time was measured using a different apparatus from before. Instead of using a laser to measure like we used for the SSFLC cells, a crossed polarised microscope was used. The cell was placed on the stage and illuminated by the microscope lamp and the intensity collected by an avalanche photodetector attached to the microscope. The cell was connected to a function generator and the avalanche detector to the oscilloscope. Essentially, the function generator had the functionality to open the shutter, which means to turn the liquid crystal molecules to a homeotropic alignment (bright state), and measure the time (relaxation time) that the molecules need to come back to the planar alignment (dark state). Figure 29 is the experimental setup.

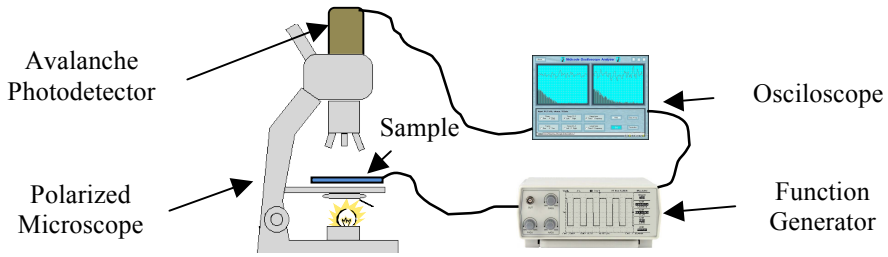

Figure 29 – Experimental setup to measure the relaxation time in thin nematic shutters.

The results are listed in Table 5 and represented graphically in Figure 30:

Liquid Crystal	Thickness (µm)	Δn	τ(ms)
LCE3S-A	1,5	0,11	0,95
MixA	1,5	0,13	1,08
MixB	1,5	0,14	1,27
LCE3S-B	1,5	0,16	1,38

Table 5 – Relaxation time of the different mixtures.

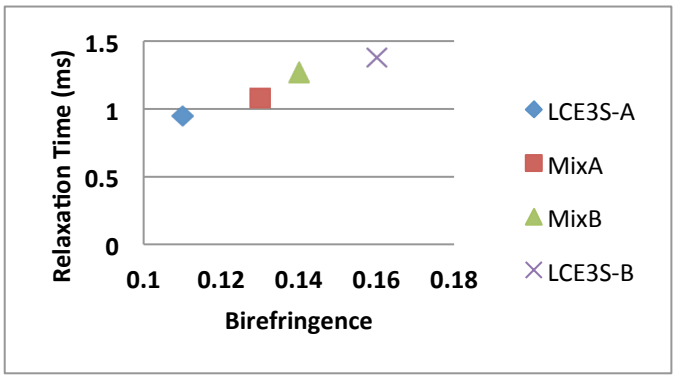

Figure 30 – The plot of the relaxation time of the different mixtures.

The relaxation time from the liquid crystal (LCE3S-A) used in the actual glasses as compared to the MixA has increased by 13,6% and for the MixB by 33,6%. This happened because the LC3S-B is more viscous and the amount of it is higher in MixB.

- Light Transmission and Viewing Angle

The transmission of each mixture was measured using the Ocean Optics spectrometer to observe the amount of light that passes through the sample as a function of the wavelength, and also with the ELDIM EZLite the transmission was measured with respect to the viewing angle. A good transmission has to be associated to a widening viewing angle to have a good 3D shutter. Figure 31 shows the transmission and the pictures of each sample as a function of the wavelength measured by the spectrometer.

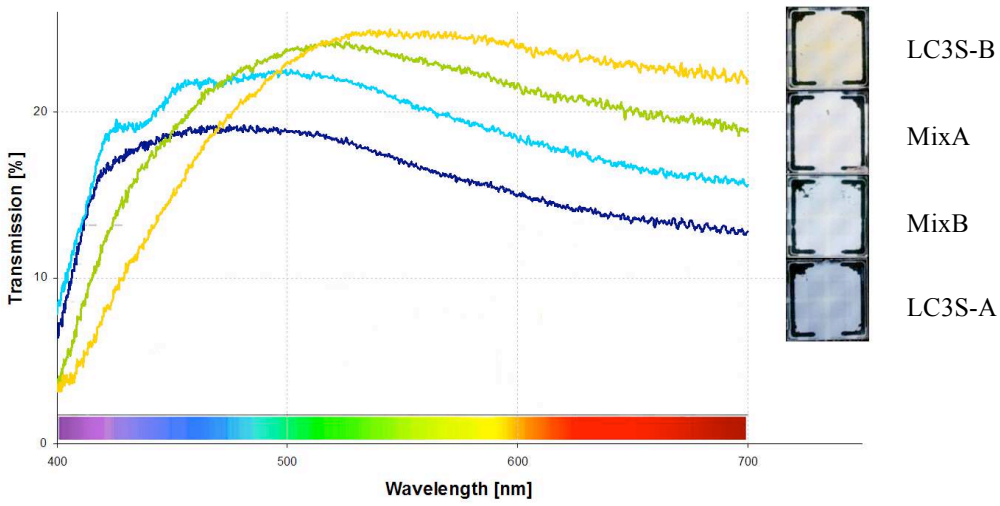

Figure 31 – Transmission versus wavelenght for the four mixtures meassured by the spectrometer.

The transmission measured with the ELDIM EZLite:

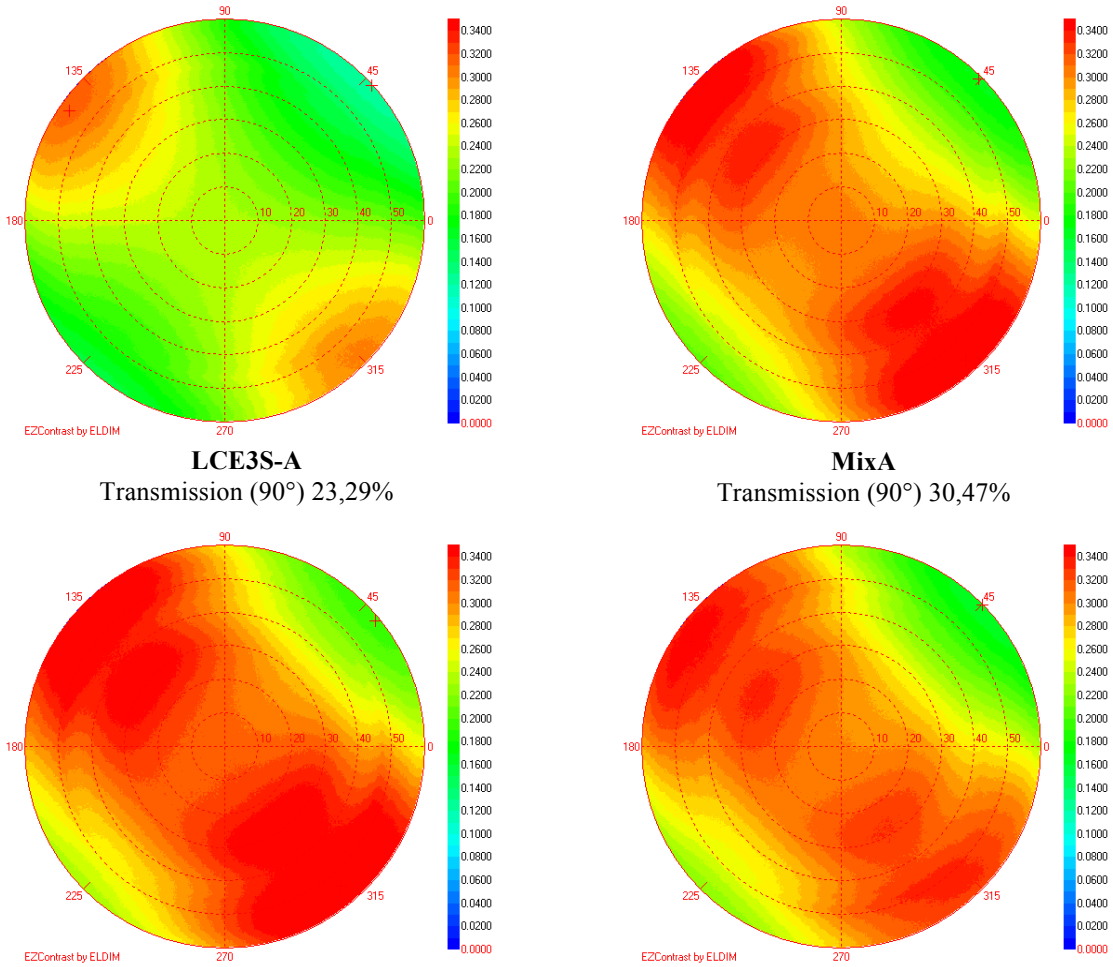

LCE3S-A
Transmission (90°) 23,29%

MixA
Transmission (90°) 30,47%

MixB
Transmission (90°) 31,77%

LCE3S-B
Transmission (90°) 30,08%

Figure 32 – The transmission versus the incidence angle of the four shutter filled with the four mixtures measure by the ELDIM EZLite.

The MixB has enhanced the optical properties as compared to the liquid crystal used in the actual glasses. The transmission, Figure 32, measured normal to the shutters has improved from 23,29% to 31,77%, which means an improvement of 36%. Also, the transmission as a function of the angles has improved widening the viewing angle and becoming more uniformly distributed than the others mixtures. In Figure 31 it can be seen that MixB has a more flat response and higher transmission between 430nm and 500nm (Blue). Figure 33 shows the angles where the MixB have improved.

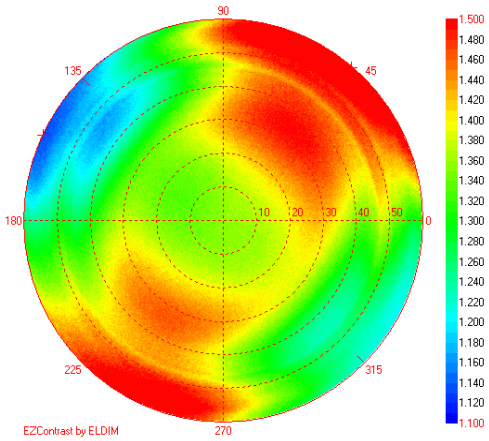

Figure 33 – The transmission angles improved by the MixB.

- White Dispersion

In optics, dispersion is the phenomena where the phase velocity of a light wave depends on its frequency. When you illuminate a piece of glass, with a pure white light each wavelength see the medium in a different way. The refractive index of the medium depends on the wavelength. This means, that the phase velocity of each incident wavelength is changed by the medium causing different colors to refract at different angles, as a consequence the colors will change according to the viewing angle. Then, the white dispersion leads to a degradation of the images. Figure 34 shows the white dispersion of the four mixture measured with ELDIM EZLite.

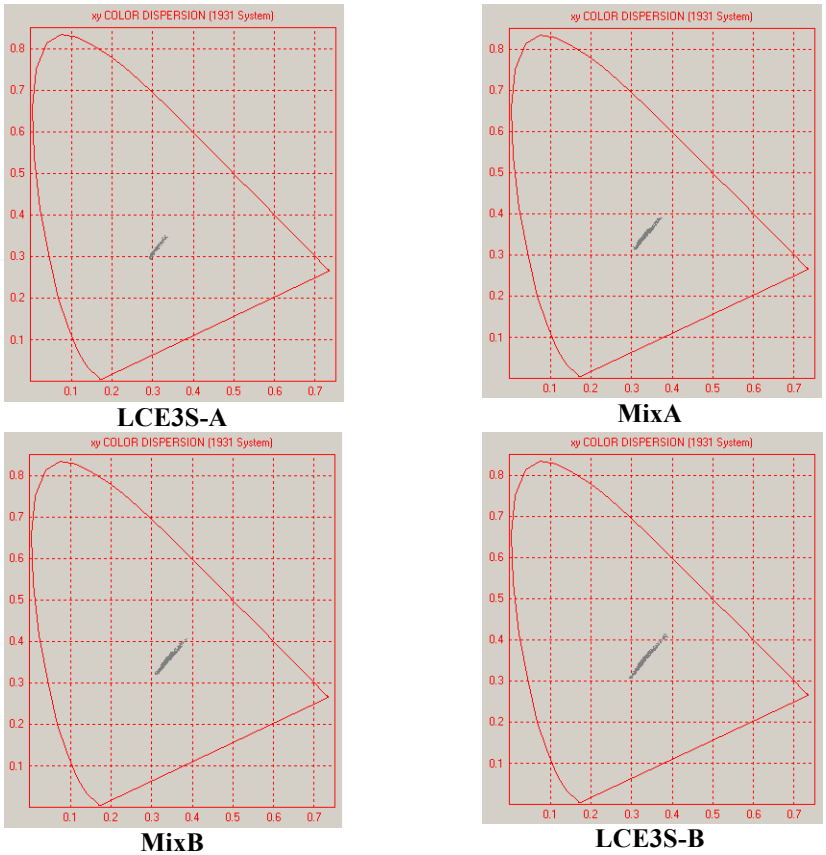

Figure 34 – The white dispersion of the four mixtures measured with the ELDIM EZLite.

The white dispersion of MixB and MixA are almost the same (white reference x=y=1/3). The only difference between the mixture and the LCE3S-A is that the later tend to the blue.

Another factor for Active 3D vision is the residual light (RL). Some parameters play an important role in the RL amount: the transmission, flash duration and the dark time. The transmission was measured using the ELDIM and the residual light was calculated at a triple flash frequency (144Hz). The frames into triple flash can have a maximum duration of 8,33ms and using LCE3S-A, MixA, MixB and LCE3S-B the frame duration decreases due to the relaxation time and are respectively: 7,38ms, 7,25ms, 7,06ms and 6,96ms. Since we know the transmission of each mixture from Figure 32, the RL is easily determined and it is shown in Table 6.

Liquid Crystal	Residual Light
LCE3S-A	20,63%
MixA	26,52%
MixB	26,92%
LCE3S-B	25,13%

Table 6 – The residual light of the mixtures considering triple flash (144Hz) and a frame time of 8,33ms.

Once all, MixB evolves as a good solution to improve the shutters without losing efficiency due to the increasing of the relaxation time.

Conclusion

In this Chapter we have described some stereoscopic techniques pointing the advantages and the disadvantages of each of them. Even the solution without glasses, which is not the objective of this thesis, is interesting to contextualize the stereoscopic. The small theory about the 3D with glasses, passive and active, is important because it provides the basic information to understand the last part of this chapter which concerns the experiments and characterization of the shutters, and also Chapter 4. The ghosting and color banding effects are introduced since they are the drawbacks to be mitigated to lead to high quality 3D images. To summarize this thesis in a few words it would be: the improvement of stereoscopic systems avoiding the ghosting and color banding effect.

Concerning the active 3D many alternatives to develop new glasses with better quality were studied and tested. First, shutters based on SSFLC cells were done, characterized and they have presented excellent response time but it is very unlikely to have cell with free of chevron defects. Furthermore, we tried to do Twisted SSFLC samples, the concept behind this method was to reduce the layers in smectic A phase to prevent the shrinkage of the layer when the liquid crystal passes to the smectic C. Several samples with different twist were done and the chevron defects were completely removed, as a consequence the contrast ratio got better because no more light was escaping due to the defects. However, SSFLC, twisted or not, has a serious problem against shocks and the application of electric field for long periods. After one hour of applying the minimum voltage to address the liquid crystal director between the two states the roof-top and chevron texture starts to appear in some areas. Thus, introducing a small quantity of polymer and doing PSFLC cells the problem of shock and texture change have been solved, but the polymer scatters the light reducing considerably the quality of the 3D images. Hence, we have decided to take the conventional way of using the nematic liquid crystal glasses which are already on the market and have good contrast ratio, response time and no problems of shocks or texture change. A new mixture of nematic liquid crystal was prepared, tested and shutters made of this new material were characterized with respect to its optical properties. The glasses of Eyes3Shut, our partner and the sponsor with Télécom-Bretagne of this thesis, were improved and consequently improving the 3D experience of the users.

Further studies should be done involving SSFLC based shutters with twist and polymer. They are promising and can drastically change the 3D vision due to the high contrast ratio and fast response time. Thus, it would be interesting to circumvent the scattering, shock and texture problems. In the next chapter we are going to show some polarimetric measurements with SSFLC cells using a Snapshot Matrix Mueller Polarimenter. The aim is to understand thoroughly how these cells work to try to overcome the listed issues.

Bibliography

[1] Charles Wheatstone, *"Contributions to the Physiology of Vision.—Part the First. On Some Remarkable, and Unobserved, Phenomena of Binocular Vision"*, Philosophical Transactions of the Royal Society of London, Vol. 128, pp. 371-394, Royal Society 1838.

[2] Sir David Brewster, *"The stereoscope: its history, Theory and Construction, with its Application to the Fine and Useful Arts and Education"*, J. Murray, 1856.

[3] A. Claudet F. R. S., "XXXVI. On moving photographic figures, illustrating some phenomena of vision connected with the combination of the stereoscope and the phenakistoscope by means of photography", Philosophical Magazine Series 4, Vol. 30, Issue 203, 1865.

[4] Ray Zone, *"Stereoscopic Cinema & the Origins of 3-D Film, 1838-1952"*, University Press of Kentucky, 2007.

[5] The Teleview Corporation, *"Stereoscopic Motion-Eectuke Device"*, U. S. Patent, no. 1,506,524, Aug. 1924.

[6] Edwin H. Land et al, *"Display Device Employing Polarized"*, U. S. Patent, no. 2,165,974, July 1939.

[7] Nakayama K., Shimojo S. and Silverman GH., *"Stereoscopic depth: its relation to image segmentation, grouping, and the recognition of occluded objects."*, Perception, Vol. 18, pp. 55-68, 1989.

[8] Dodgson, N.A.; , *"Autostereoscopic 3D Displays,"* Computer , vol.38, no.8, pp. 31- 36, Aug 2005.

[9] Hirota, K.; Tagawa, K.; Suzuki, Y.;, *"Automultiscopic display by revolving flat-panel displays,"* Virtual Reality Conference, 2008. VR '08. IEEE, vol., no., pp.161-168, 8-12 March 2008.

[10] Borner, R.; Duckstein, B.; Machui, O.; Roder, H.; Sinnig, T.; Sikora, T.; , *"A family of single-user autostereoscopic displays with head-tracking capabilities,"* Circuits and Systems for Video Technology, IEEE Transactions on , vol.10, no.2, pp.234-243, Mar 2000.

[11] Yan Zhang; Quanmin Ji; Wenshuai Zhang; , *"Multi-view autostereoscopic 3D display,"* Optics Photonics and Energy Engineering (OPEE), 2010 International Conference on , vol.1, no., pp.58-61, 10-11 May 2010.

[12] Sexton, I., *"Parallax barrier display systems,"* Stereoscopic Television, IEE Colloquium on , vol., no., pp.5/1-5/5, 15 Oct 1992.

[13] D.E. Roberts, *"History of Lenticular and Related Autostereoscopic Methods"*, white paper, Leap Technologies, LLC, 2003.

[14] W. Rollman, Zwei neue stereoskopische methoden, Annalen deer Physik und Chemie,vol. 90, pp. 186–187, 1853.

[15] A. J. Woods and T. Rourke, *"Ghosting in anaglyphic stereoscopic images"*, in Proc. SPIE V Stereoscopic Displays and Virtual Reality Systems XI, A. J. Woods, J. O. Merritt, S. A. Benton, and M. T. Bolas, Eds., 2004, pp. 354–365.

[16] I. Ideses and L. Yaroslavsky, *"Three methods that improve the visual quality of color anaglyphs"*, J. Opt. A, Pure Appl. Opt., vol. 7, pp. 755–762, 2005.

[17] S. E. B. Sorensen, P. S. Hansen, and N. L. Sorensen, *"Method for recording and viewing stereoscopic images in color using multichrome filters"*, U.S. Patent 6 687 003, 2004.

[18] H. Jorke, A. Simon, and M. Fritz, *"Advanced stereo projection using interference filters"*, J. Soc. Inf. Display, vol. 17, no. 5, pp. 407–410, 2009.

[19] D. Gadia, C. Bonanomi, M. Rossi, A. Rizzi, and D. Marini, *"Color management and color perception issues in a virtual reality theatre"*, Proc. SPIE, A. J. Woods, N. S. Holliman, and J. O. Merritt, Eds., 2008, no. 1, p. 68030S.

[20] L. Lipton and M. Cowan, B., *"Zscreen modulator with wire grid polarizer for stereoscopic projection"*, U.S. Patent 7 633 666, 2009.

[21] C. Cruz-Neira, D. J. Sandin, T. A. DeFanti, R. V. Kenyon, and J. C. Hart, *"The CAVE: Audio visual experience automatic virtual environment"*, Commun. ACM, vol. 35, no. 6, pp. 64–72, 1992.

[22] F. L. Kooi, A. Toet, "*Visual comfort of binocular and 3D displays"* in Displays, vol. 25, pp. 99-108, 2004.

[23] Abhishek K. Srivastava, J. L. de Bougrenet de La Tocnaye, and Laurent Dupont, *"Liquid Crystal Active Glasses for 3D Cinema",* Journal of Display Technology, Vol. 6, Issue 10, pp. 522-530, 2010.

[24] S. T. Lagerwall, *Ferroelectric and Antiferroelectric Liquid Crystals*, WILEY-VCH, 1999.

[25] C. Wang and P. J. Bos, *"Bistable C1 ferroelectric liquid crystal device for e-paper application"*, Displays, vol. 25, pp. 187-194, 2004.

[26] L. Limat, "A Model of Chevron in Smectic C* Liquid Crystals: Uniform and Twisted "Soliton" States", J. Phys. II France, vol. 5, pp. 803-822, 1995.

[27] T. Qian, JH. Kim, S. Kumar and P. L. Taylor, *"Phase-separated composite films: Experiment and theory"*, Physical Review E, vol. 61, n. 4, pp. 4007-4010, 200.

[28] V. Vorflusev, JH. Kim and S. Kumar, *"Phase separated composite films of liquid crystals"*, Science, v. 283, n. 5409, pp. 1903-1905, 1999.

Chapter 3: *Characterization of Ferroelectric Liquid Crystal (FLC) shutters using a Snapshot Mueller Matrix Polarimeter*

Introduction

The description of the static and dynamic behaviour in surface stabilised ferroelectric liquid crystal (SSFLC) cells has been widely investigated since their first implementation by Clark and Lagerwall [1]. The simplest way to understand qualitatively the texture of such cells is to examine them under a polarising microscope [2]. Furthermore, electro-optical characterisation can be made by measuring the light intensity between crossed polarisers with a temporal resolution in the order of microseconds. However, to have a complete description of the director distribution and the layer structure, it is necessary more complex models. In the other hand, others model-independent methods and devices were used and developed to characterise liquid crystals (LCs). Among them, X-ray diffraction which details the layer structure of the liquid crystals cells [3], and optical guided modes [4], which access the director in-depth distribution. These last two methods, lateral spatial resolution as well as temporal resolution are often poor.

A snapshot Mueller matrix polarimeter (SMMP) [5] was recently developed by our partners, and further used to carry out time-resolved analyses of reorientations in FLC cells [6]. This tool has many advantages for optical characterisation of LCs. First, the lateral spatial resolution is about the optical beam size (~500µm here). Second, the temporal resolution, equal to the detector acquisition time (~µs here), is the best one among the current Mueller polarimeters. Moreover, with the SMMP it is possible to have independently the polarimetric properties of the sample: dichroism, birefringence and depolarisation.

It is well known that when a high-intensity and low-frequency electric field is applied to a surface-stabilised ferroelectric liquid crystal (SSFLC) cell, its texture evolves from an uniform texture with zigzag defects to a uniform striped texture by passing through a most complicated 'rooftop' texture [7][8][9][10]. The change of texture is associated to the irreversible straightening out of the smectic layers due to the coupling of the spontaneous polarisation with the applied electric field. Our work was aimed to establish a strong correlation between the static and dynamic polarimetric properties (issued from Mueller matrix measurements) and the texture of SSFLC cells. It will be shown that the trajectory of the optic axis of the cell between the two addressed states depends on the texture. Additionally, experiments with PSFLC and twisted SSFLC cells have been done to

characterize and have a better understanding about that type of shutters.

In the next sections, the experimental setup is described. Besides, the polarimetric parameters issued from the Mueller matrix are explained and associated to the director distributions. After, it is presented the basics concerning the SSFLC textures followed by the related static (at fixed voltage) and the dynamic (upon field reversal) polarimetric parameters. Finally, the results and the conclusions of the experiments carried out on the SSFLC, PSFLC and twisted SSFLC samples.

3.1. Mueller Matrix Polarimeter

3.1.1. The principle of a Mueller Matrix Polarimeter

Polarimetry is the science of measuring polarization and polarimeter is the optical instrument used for determining the polarization properties. This type of device is used in many technological fields as, astronomy [14], spectroscopic of materials, biology [15], and etc. Two main types of polarimeter exist: light measuring polarimeters and, in our case, sample measuring polarimeters. The sample measuring polarimeters relates the polarization states between incident and exiting light beam for a sample. The basic block diagram of a sample measuring polarimeter is shown in Figure 35.

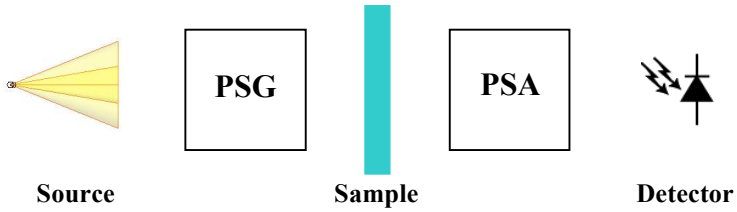

Figure 35 - Scheme of a sample measuring polarimeter.

where PSG and PSA are the polarization state generator and the polarization state analyzer, respectively. The principle is the light from the source passes through the PSG defining a set of polarization states which are incident on a sample, mathematically; the PSG defines a sequence of well known Stokes vectors S_n. Just in sequence, the polarization states, represented in terms of the vectors Sn, are modified by the sample and the exiting vectors are MS_n. These exiting states are analysed by the PSA, A_n, and the measurements is $B_n = A_n MS_n$. Then, the sample's Mueller matrix can be calculated according to Equation 3.1:

$$M_n = A_n^{-1} B S_n^{-1} \tag{3.1}$$

The measurements are assumed to be linear in relation to the Mueller matrix of the sample. However, it is far more complex to obtain the Mueller matrix because of the complexity of the data reduction equations, the quantities of measurements to have a precise result and the polarization elements are not ideal.

3.1.2. A Mueller Matrix Polarimeter in (e, e, 5e, 5e) configuration

A lot of polarimeters with different experimental configurations have been built to determine

the Mueller matrix of a sample. For example, dual rotating retarder polarimeter [16] and dual rotating polarizer polarimeter [17]. Unfortunately, it generally includes mechanical or active elements which require extra care to maintain the stability in the measurements. The SMMP used in our experiments was carefully conceived to avoid these kinds of elements and determines the Mueller matrix of a sample by measuring the spectrum of the exiting light. The polarimeter is based on polarization coding by wavelength. This means that the device associates one polarization state to a given wavelength of the broadband spectral source. Many devices and techniques have been developed using polarization coding, including polarimeters, ellipsometer and etc [18][19].

The coding system (PSG) consist of a linear polarizer at 0° and two wave plates whose thickness is *e* and their optical axis respectively at 45° and 0°. The decoding system (PSA) is made of two wave plates whose thickness is *5e* and their optical axis at 0° and 45°, and a linear polarizer at 90°. Figure 36 shows the Mueller Matrix Polarimeter in a (e, e, 5e, 5e) configuration.

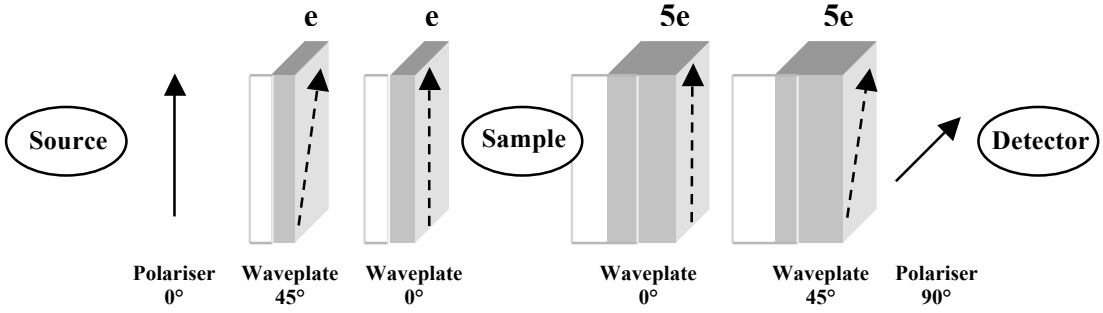

Figure 36 - Schematic of the Muller Matrix polarimeter in a (e, e, 5e, 5e) configuration.

Using the Mueller calculus (Equation 3.1) and modelling the propagation of polarization states through the system, the Stokes vector in front of the detector is therefore given by:

$$\vec{S}_s = \left[P(90°)\right]\cdot\left[R(5\phi,45°)\right]\cdot\left[R(5\phi,0°)\right]\cdot\left[M\right]\cdot\left[R(\phi,0°)\right]\cdot\left[R(\phi,45°)\right]\cdot\left[P(0°)\right]\cdot\vec{S}_i \tag{3.2}$$

where $\left[P(\theta)\right]$ is the Mueller matrix of a linear polariser oriented at θ degrees, $\left[R(\phi,\theta)\right]$ is the Mueller matrix of a birefringent retarder whose retardation is ϕ and the fast axis is at θ degrees with respect to the reference axis and, M is the Mueller matrix of the sample. Therefore, considering a narrow spectrum source, the retardation can be expressed in the first order approximation as:

$$\phi \approx \phi_0 + 2\pi f_0 \lambda \tag{3.3}$$

where f_0 and ϕ_0 are the fundamental frequency and the retardation associated, respectively. Thus, each wavelength from the source will have its own retardation and polarization state. The light intensity is the first parameter of the Stokes vector (S_0) and, taking into account Equation 3.2 and 3.3, it can be written as:

$$
\begin{aligned}
32I(\lambda) = {} & 8m_{00} + 4m_{02} - 4m_{20} - 2m_{22} + (8m_{01} - 4m_{21})\cos(2\pi f_0\lambda) \\
& - (4m_{02} - 2m_{22})\cos(2\times 2\pi f_0\lambda) + 2m_{12}\cos(3\times 2\pi f_0\lambda) - 4m_{11}\cos(4\times 2\pi f_0\lambda) \\
& - (8m_{10} - 4m_{12})\cos(5\times 2\pi f_0\lambda) - 4m_{11}\cos(6\times 2\pi f_0\lambda) + 2m_{12}\cos(7\times 2\pi f_0\lambda) \\
& - (m_{22} - m_{33})\cos(8\times 2\pi f_0\lambda) + 2m_{21}\cos(9\times 2\pi f_0\lambda) + (4m_{20} - 2m_{22})\cos(10\times 2\pi f_0\lambda) \\
& + 2m_{21}\cos(11\times 2\pi f_0\lambda) - (m_{22} - m_{33})\cos(12\times 2\pi f_0\lambda) - (4m_{03} - 2m_{23})\sin(2\times 2\pi f_0\lambda) \\
& - 2m_{13}\sin(3\times 2\pi f_0\lambda) + 2m_{13}\sin(7\times 2\pi f_0\lambda) + (m_{23} + m_{32})\sin(8\times 2\pi f_0\lambda) \\
& - 2m_{13}\sin(9\times 2\pi f_0\lambda) - (4m_{30} + 2m_{32})\sin(10\times 2\pi f_0\lambda) - 2m_{31}\sin(11\times 2\pi f_0\lambda) \\
& - (m_{23} - m_{32})\sin(12\times 2\pi f_0\lambda)
\end{aligned}
\tag{3.4}
$$

where m_{ij} are the Mueller matrix coefficients of the sample.

The retarder thickness was carefully chosen in order to generate 12 frequencies multiples of the fundamental frequency. The Fourier transform of the detected signal $I(\lambda)$ creates 12 peaks, real and imaginary, whose magnitudes are linear combination of the Mueller matrix coefficients m_{ij} of the sample (Table 7).

Frequency	Real Part (Magnitude x 64)	Imaginary Part (Magnitude x 64)
0	$16m_{00} + 8m_{02} - 8m_{20} - 4m_{22}$	0
f_0	$8m_{01} - 4m_{21}$	0
$2f_0$	$-4m_{02} + 2m_{22}$	$-4m_{03} + 2m_{23}$
$3f_0$	$2m_{12}$	$-2m_{13}$
$4f_0$	$-4m_{11}$	0
$5f_0$	$-8m_{10} - 4m_{12}$	0
$6f_0$	$-4m_{11}$	0
$7f_0$	$2m_{12}$	$2m_{13}$
$8f_0$	$-m_{22} + m_{33}$	$m_{23} + m_{32}$
$9f_0$	$2m_{21}$	$-2m_{31}$
$10f_0$	$4m_{20} + 2m_{22}$	$-4m_{30} - 2m_{32}$
$11f_0$	$2m_{21}$	$-2m_{31}$
$12f_0$	$-m_{22} - m_{33}$	$m_{23} + m_{32}$

Table 7 - The relation between the real and imaginary magnitudes peaks with the Mueller coefficients.

Then, to retrieve the coefficients it was defined a vector $\vec{V}$ composed by the real and imaginary peaks, and from Table 1 the transformation matrix [P]. Thus, it can be written:

$$\vec{V} = [P]\vec{X} \tag{3.5}$$

where $\vec{X}$ is the vector with the m_{ij} coefficients. Finally, the Mueller matrix coefficients can be calculated doing a pseudo inversion of Equation 3.5:

$$\vec{X} = ([P]^T.[P])^{-1}.[P]^T.\vec{V} \tag{3.6}$$

3.1.3. The Snapshot Mueller Matrix Polarimeter (e, e, 5e, 5e)

In general, a Muller matrix polarimeter has two main parts. One part placed before the medium in study, in our case the liquid crystal (LC) sample, and the other part after the medium. The first part generates the polarization state and the second part analyse the polarization state modified by the medium. The polarimeter SMMP used in this study is described in [5], it is a device based on polarization coding by wavelength. This means that the states of polarization are generated by each wavelength of the light source. Indeed, the aim is to assign a polarization state to a given wavelength. Still, for comprehensive purposes, it is possible to subdivide the polarimeter in several parts, the light source, the coding system, the decoding system and the detection system as it is shows in the Figure 37. The coding system and the decoding system are composed by a linear polarizer (LP) and two retarders (RET). The detection system is comprised by two lenses, L1 and L2, a scattering medium (ST), an optical fibre and a CCD camera. The full polarimetric response, the Mueller matrix of the sample, is defined indirectly, measuring the spectrum I(λ) by a CCD camera.

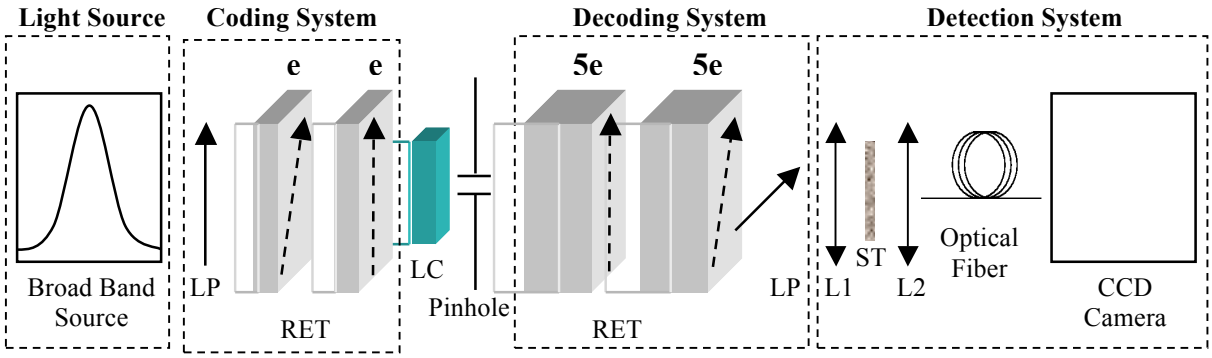

Figure 37 - Experimental setup of the snapshot Mueller matrix polarimeter in the (e, e, 5e, 5e) configuration.

The 15-nm-broad source is a superluminescent diode (B&WTek®) with a central wavelength at 829 nm. The beam size, initially around 1 mm, has been reduced to 500 μm by using an afocal system composed of two lenses. The polarisers (ColorPol®), made of nanoparticles, have an extinction ratio of 100,000:1 and an angular acceptance of 20°. The retarders are made up of calcite ($\Delta n = 0{,}1661$), and have a thickness e = 2,08 mm for the coding system, whereas the thickness of those used for the decoding system is 5e = 10,4 mm. The lens, L1, images the sample on the scattering medium in order to avoid coherence effects, whereas the lens, L2, images the light from the scattering medium at the optical fibre entrance. Thus, the light is collected by a multimode optical fibre, and is injected into a dispersive system composed of a 1200 grooves/mm grating and a 512 × 512 pixels charge-coupled device (CCD) camera (ICCD-Max®). Given that only one dimension of the CCD is used (wavelength axis), a binning is made in the other direction (intensity axis), which enhances the signal-to-noise ratio. The temporal characteristics of the camera for data acquisition are as follows: a gate width that is adjustable over a time range from the *ns* to the *s* and a repetition rate around 1 kHz. A full Mueller matrix is included in a single spectrum, I(λ), and is thus recorded under the previous conditions, which are the best ones achievable among current

Mueller polarimeters. The Mueller matrix is evaluated at the wavelength λ_0, which is the central wavelength of the detection range. Techniques for the reconstruction of Mueller matrices and calibration of the device are described in [20].

3.2.Surface Stabilized Liquid Crystal (SSFLC)

3.2.1. SSFLC in Bookshelf Geometry

The Surface Stabilized Liquid Crystal (SSFLC) was conceived and it has been extensively studied by Clark and Lagerwall [1]. The principle is to unwiund the helix of a smectic C* and obtain a uniform state with a macroscopic spontaneous polarization without electric field. The SSFLC device is a smectic C* liquid crystal in which the layers are confined by two glass plates coated with an alignment layer. The principle is to associate the distance (d) between the plates, which should be smaller than the helical period, and the anchoring energy of the alignment layer which forces the director in a preferred direction. Thus, the surface breaks the helical structure of the bulk forming two energetically equivalent states which leads to a symmetric bistability of the molecules in the smectic cone. In the ideal case, due to the planar alignment, the smectic layers are positioned perpendicular to the substrate surface in bookshelf geometry. Figure 38 gives a general description of a SSFLC device in bookshelf geometry and the laboratory coordinates.

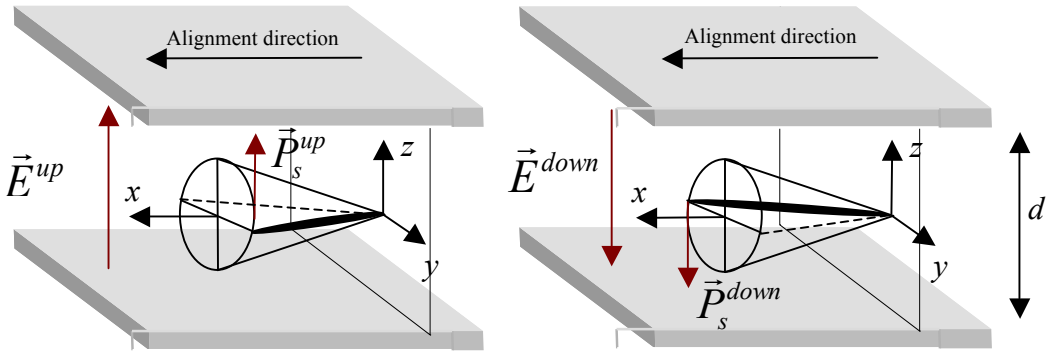

Figure 38 - Schematic of a SSFLC in bookshelf geometry applying electric field.

The spontaneous polarization $\vec{P}_S$ associated is tangent to the smectic cone and due to the bistability can have two orientations, “up” and “down” [21]. Applying an electric field perpendicular to the alignment layers the $\vec{P}_S$ will align parallel to it. Thus, the liquid crystal director can moves according to the electric field.

In fact, the liquid crystal molecules can move between two saturated states forming an angle θ in the smectic cone. Then, it is important, to better understand the dynamics involved, defining the position of the liquid crystal director with respect to the azimuthal angle (φ) and to the $\vec{P}_S$ (Figure 39).

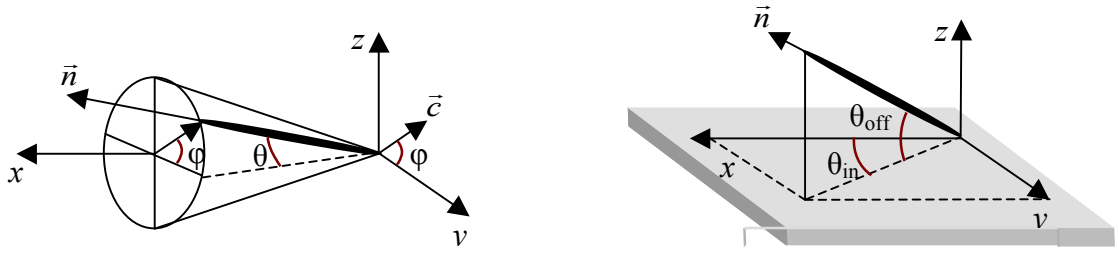

Figure 39 - The molecule, the smectic cone and the respective parameters.

The $\vec{P}_S$ is perpendicular to the vector $\vec{c}$, which defines the position of the liquid crystal director in the cone, and φ is the angle between the spontaneous polarization and $\vec{E}$ while applying electric field ($\vec{E}$). Therefore, the liquid crystal director and the spontaneous polarization as a function of θ and φ in bookshelf geometry can be written as:

$$\vec{n}(x,y,z) = \begin{pmatrix} \cos\theta \\ \sin\theta\cos\varphi \\ \sin\theta\sin\varphi \end{pmatrix} \tag{3.7}$$

$$\vec{P} = \alpha(\vec{n} \times \vec{x}) \tag{3.8}$$

$$\vec{P}_S = P_S(0, -\sin\varphi, \cos\varphi) \tag{3.9}$$

In Figure 38, it can be seen that the position "up" and "down" of the molecules are related to the electric field $\vec{E}^{up}$ and $\vec{E}^{down}$, respectively. In that case, the azimuthal angle is 0 for the "up position" and π for the "down position". However, for the polarimetric measurements, it is interesting to define the liquid crystal director in terms of θ_{in} and θ_{off}, whose are the angle between the projection of the director $\vec{n}$ and the alignment direction, and the angle between this director $\vec{n}$ and the XY plane, respectively.

$$\vec{n}(x,y,z) = \begin{pmatrix} \cos\theta_{in}\cos\theta_{off} \\ \sin\theta\cos\theta_{off} \\ \sin\theta_{off} \end{pmatrix} \tag{3.10}$$

3.2.2. SSFLC in Chevron Geometry

In Practice, the boundary condition imposed by the glass plates and the shrinkage of the layers changes the texture of the SSFLC cells [22]. Basically, the samples are made by filling very thin cells (1,5μm) with ferroelectric liquid crystal (smectic-C*) in isotropic phase and cooling down slowly (0,1°C/min) until room temperature. When the liquid crystal reaches the temperature corresponding to the smectic A phase, the alignment layers induce what is called bookshelf geometry with the director normal to the smectic layer. If the temperature is decreased further until the smectic-C* phase, the director tilts inducing a compression of the smectic layers forcing the chevron texture to form. The chevron structure allows the layer spacing to decrease while maintaining the number of layers fixed. Figure 40 shows the

chevron structure and the respective "new" position of the smectic cone.

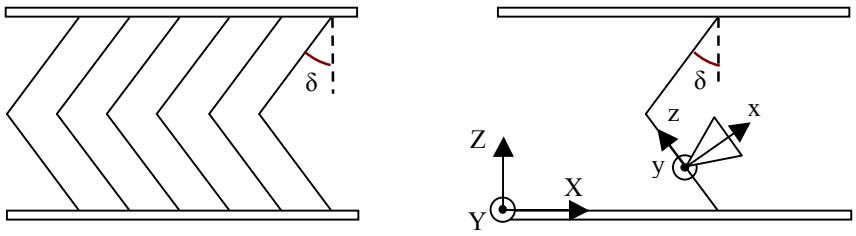

Figure 40 – The schematic of the chevron in SSFLC devices and the "new" position of the smectic cone.

In the thesis the chevron angle (δ) is considered constant over the entire cell. Thus, the chevron forces modifications in the relations described by equations 3.9. In fact, the smectic cone is turned by the angle δ (Figure 41).

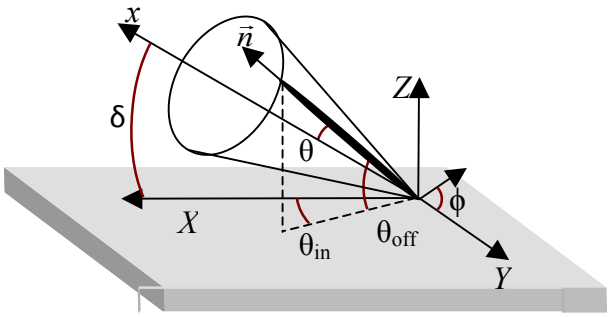

Figure 41 – The liquid crystal director on a chevron structure.

Then we have the following relations:

$$\vec{n}(X,Y,Z) = \begin{pmatrix} \sin\theta\sin\phi_{(z)}\sin\delta + \cos\theta\cos\delta \\ \sin\theta\cos\phi_{(z)} \\ \sin\theta\sin\phi_{(z)}\cos\delta - \cos\theta\sin\delta \end{pmatrix} \tag{3.11}$$

$$\vec{P}_s(X,Y,Z) = \begin{pmatrix} \cos\phi_{(z)}\sin\delta \\ -\sin\phi_{(z)} \\ \cos\phi_{(z)}\cos\delta \end{pmatrix} \tag{3.12}$$

$$\theta_{in}(Z) = \tan^{-1}\left(\frac{\sin\theta\cos\phi_{(z)}}{\sin\theta\sin\phi_{(z)}\sin\delta - \cos\theta\cos\delta}\right) \tag{3.13}$$

$$\theta_{off}(Z) = \sin^{-1}\left(\sin\theta\sin\phi_{(z)}\cos\delta - \cos\theta\sin\delta\right) \tag{3.14}$$

The liquid crystal director in the chevron interface has a fixed orientation and all the molecules are aligned uniformly with an azimuthal angle ϕ_0. However, applying an electric field the molecules align perpendicular to the field and the azimuthal angle is equal to zero.

3.3. The SSFLC and the Polarimetric Parameters

All the polarimetric properties of a SSFLC sample are in its Mueller matrix. It consist of dichroism, birefringence and depolarisation. Since the liquid crystal analysis by the polarimeter is done under normal incidence no dichroism is expected. Although, as already mentioned, the LC has a strong birefringence which can be associated to a retarder. The depolarisation is the random action of amplitude and phase and its effect results from a spatial averaging of polarimetric properties over the section of the beam or/and temporal over the acquisition time. However, in the setup described in Figure 37 a pinhole to avoid the detector to capture scattered/diffracted light. Thus, the depolarization caused by the scattering due to the presence of spatial inhomogeneities in the samples is not detected. The depolarisation, P_d [23], is used to control the aperture time of the CCD camera.

The polarimetric effects are obtained decomposing the experimental Mueller matrix using the Lu and Chipman decomposition [24]. The obtained three matrices, diattenuation, retardance and depolarisation correspond to the polarimetric effects: dichroism, birefringence, depolarisation, respectively. However, only the retardance matrix was exploited because of the birefringence characteristic of the medium. One of the advantages of measuring the whole Mueller matrix of the sample and performing the Lu and Chipman decomposition is that the birefringence properties are obtained from the resolution of an over-determined and noise-filtered system. Three experimental parameters of the retarder associated to the LC cell are extracted from the retardance matrix: retardance (R, phase difference between the two eigenstates of the retarder), the azimuth angle (α_R, the direction of the fast axis of the retarder) and the ellipticity angle (ε_R, ellipticity of the retarder). Those parameters are model-independent and they describe how the polarisation is modified by the medium. The first two parameters, R and α_R, are used to represent the optic axis of the retarder into the laboratory coordinate system (X, Y, Z), as shown in Figure 40.

Generally, a LC cell can be described as an elliptical birefringent medium where the direction of the optic axis is defined by the angles θ_{in} (in-plane angle) and θ_{off} (off-plane angle). These two angles are linked to R and α_R as:

$$\alpha_R = \theta_{in} \tag{3.15}$$

$$R = \frac{2\pi\Delta n(\theta_{off})d}{\lambda_0} \tag{3.16}$$

$$\Delta n(\theta_{off}) = \frac{n_e n_o}{\sqrt{n_e^2 \sin^2(\theta_{off}) + n_o^2 \cos^2(\theta_{off})}} - n_o \tag{3.17}$$

where λ_0 = 829 nm, d is the thickness of the SSFLC cell and n_e and n_o are, respectively, the extraordinary index and the ordinary index of the liquid crystal. Thus, the parameter α_R is

equal to θ_{in} which is the angle between the projection of the optic axis in the plane of the glass plates and the rubbing direction. R is linked to θ_{off} which is the angle between the optic axis and the glass plate. Assuming a uniform in-depth molecular distribution, the optic axis is aligned with the long axis of the liquid crystal director.

The parameter ε_R is linked to the in-depth molecular distributions along Z. It was shown that along the direction of the light propagation a superposition of linear retarder slabs with their optic axis in different directions is equivalent to an elliptic retarder [25]. This is the case for 'twist' or 'splayed' molecular distributions along the depth. Although, the ε_R is not sufficient to have an in-depth-resolved description of the molecular orientation, it gives an insight into the global shape of the distribution. For example, simulations has been done to quantify the ellipticity parameter in a 1.5 μm planar aligned cell, with a tilt angle θ= 25.5°, with a uniform distribution and the ellipticity is 0° (linear birefringent). In a quasi-uniform, but symmetric chevron distribution [26], the ellipticity is also 0◦ because the perfect compensation of the twist between the two halves of the cell. A splayed distribution with a linear variation of the azimuthal angle ϕ between the two surfaces the ellipticity parameter is about 8.7°, and for a half-splayed distribution the ellipticity parameter is about 6.7° [27].

Notice that the optical parameters result from an averaging over the optical beam size and thanks to spatial filtering, the scattered/diffracted light is not analysed. In the case of SSFLC cells, layer defects leads to scattering and a horizontal chevron structure (stripes) creates diffraction. The optical parameters are not sensitive to these last two effects.

3.4. Polarimetric Experimental Results

In the following section we present the experimental results obtained with different SSFCL and PSFLC samples using the SnapShot Mueller Matrix Polarimeter. It is discussed and the polarimetric parameters are associated with the SSFLC textures and the structure of the smectic layers. The irreversible chevron to bookshelf transition is also addressed showing the behavior of the liquid crystal director under electric field for both cases. Moreover, the impact of the concentration of polymer in PSFLC is studied evidencing how the polymer changes the electro-optical characteristics.

3.4.1. The SSFLC samples and its Textures

The samples under study were three SSFLC cells made of the same liquid crystal Felix 015/100 from Clariant®. They were prepared as the same way as it was explained in Section 2.4.1. Two glass substrates coated with transparent electrodes of indium tin oxide (ITO) and then spin-coated with a layer of polyimide. After hard bake (2h at 180°) the polyimide was rubbed in order to have a planar orientation of the LC. The gap between the substrates was controlled by glass-bead spacers of 1,8 μm (cell 1) and 1,5 μm (cell 2). The Felix 015/100 was introduced into the cell by capillarity at isotropic temperature and cooled down slowly to the chiral smectic C (SmC*) phase, at room temperature. A high-intensity and low-frequency electric field treatment (10 Hz – ±20V square wave voltage during 2 hours) was applied to

each cell in order to change its texture. Because of different thicknesses two different textured cells were formed. Indeed, since it was applied ±20V the electric field seen by the LC was lower in cell 1 rather than in cell 2. Figure 42 shows the pictures taken under a polarised microscope of two regions of both cells after electric field treatment.

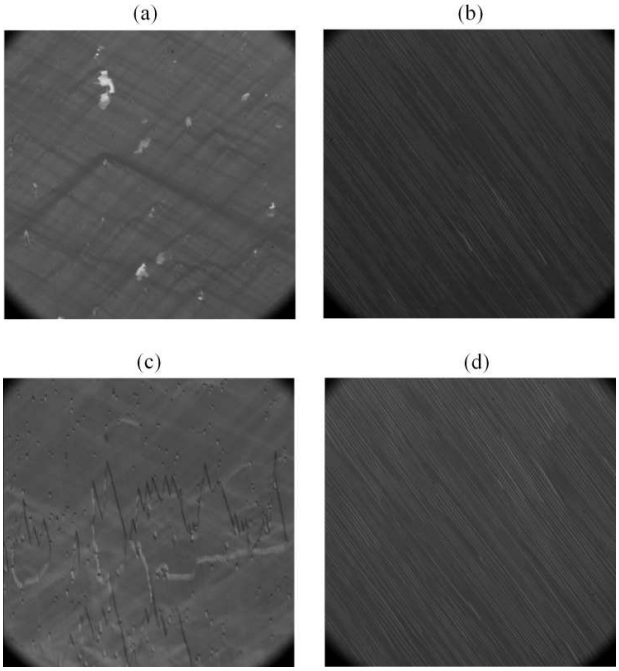

Figure 42 – Textures under polarised microsocope of the Cell 1 (a and c) and Cell 2 (b and d) after two hours of high intensity and low frequency electric field. The dimensions are 500 x 500 µm.

It is observed in the Cell 1 the 'rooftop' defects and a small area with zigzag lines (Figure 3(a) and Figure 3(c)). Cell 2 has a more uniform texture with stripes (Figure 3(b) and (d)).

Such texture can be explained. The boundary condition imposed by the glass plates and the shrinkage of the layers changes the texture of the SSFLC cells. When the ferroelectric liquid crystal (smectic-C*) in isotropic phase is cooling down slowly until room temperature, there is a temperature where the liquid crystal change to the smectic A phase and the alignment layers induce what is called bookshelf geometry with the director normal to the smectic layer. If the temperature is decreased further until the smectic-C* phase, the director tilts inducing a compression of the smectic layers forcing the chevron texture to form. The chevron structure allows the layer spacing to decrease while maintaining the number of layers fixed. In the case of a chevron structure, the polarization vector $\vec{P}_s$ is tilted at the chevron interface.

Then, applying electric field normal (along Z direction) to the substrates and since $\vec{P}_s$ is not collinear to the field $\vec{E}$, there is a torque $\vec{P} \times \vec{E}$ tending to straighten up the chevron to an upright direction forming, at first, the 'rooftop' texture. This texture suggests a local variation of the chevron angle. Increasing the electric field (or the exposure time) the smectic layers evolves to the so-called quasi-bookshelf structure leading to the formation of a horizontal chevron structure seen as stripes under the polarising microscope. This irreversible behaviour has been widely supported by both optical, and X-ray diffraction measurements [28][29].

3.4.2. Static Polarimetric Measurements on SSFLC cells

Two types of polarimetric measurements have been done. The first type the polarimetric parameters were analysed applying fixed voltages to the sample. It was called static measurements. Second, the measurements were done applying an alternate voltage and we called as dynamic measurements.

In the static measurements, the detection system and the driving voltage were synchronized in order to measure the polarimetric properties when the cells were submitted to a four specific voltage values: +15V (a), 0V (b), –15V (c) and 0V (d) again. In Figure 43 it is shown the four voltages values.

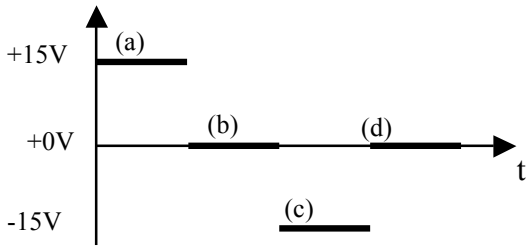

Figure 43 – The voltages where the four static measurement a, b, c e d have been done.

The liquid crystal director addressed states are at +15V (a) and –15V (c) and the memory states are at 0V (b) and 0V (d). To have an insight of the spatial distribution of the polarimetric parameters all over the cell a polarimetric image was constructed by moving the sample on a two-dimensional (2D) translation stages and measuring its Mueller matrix for each probing position. The distance between two probing positions was 500 μm and the image was composed of 400 'pixels' (20 × 20 pixels), which means 1 cm². Notice that the independent behavior of the four states (a, b, c and d) is not as useful as the comparison between the addressed and the memory states. Figure 44 is the variations of α_R and R parameters between the (a) and (b) states.

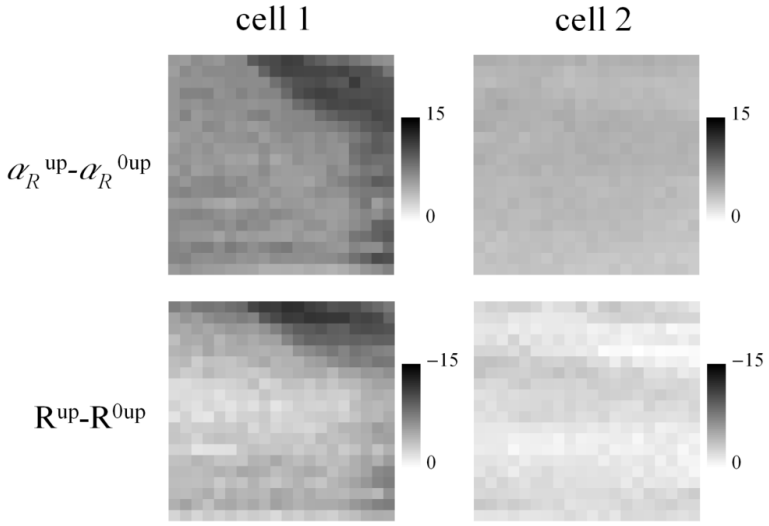

Figure 44 – The polarimetric parameter differences α_R and R between the addresed states (a) and (b), and the memory state. The picture area is 1cm² and the vertical scale is in degrees and divided in 50 gray levels.

The average values of the polarimetric parameters differences measured in Cell 1 are $< R_{(up)} - R_{(0up)} > = -4{,}90°$ and $< \alpha_{R(up)} - \alpha_{R(0up)} > = 7.20°$. In cell 2 are $< R_{(up)} - R_{(0up)} > = -1{,}68°$ and $< \alpha_{R(up)} - \alpha_{R(0up)} > = 4{,}15°$. The memory states in cell 2 are closer to the addressed states in cell 1. This means that the difference was reduced by the electric field treatment.

3.4.3. Dynamic Polarimetric Measurements on SSFLC cells

The switching dynamics from the 'up' (a) to the 'down' (c) states ('up/down' transition) were measured applying a ±15V @ 100 Hz square wave signal. The repetition rate of the CCD camera is 1 kHz and the switching times for the SSFLC cells are around 100 µs. Then, the dynamic evolution of the polarimetric properties cannot be studied over a single period. The camera had to be synchronised with the applied voltage to reconstruct the transition step-by-step lengthening of the acquisition delay. The acquisition time for one point and the step of the delay were both set equal to 5 µs. Figure 45 illustrates the dynamic evolutions of the polarimetric parameters, α_R and R, at one particular position (one pixel).

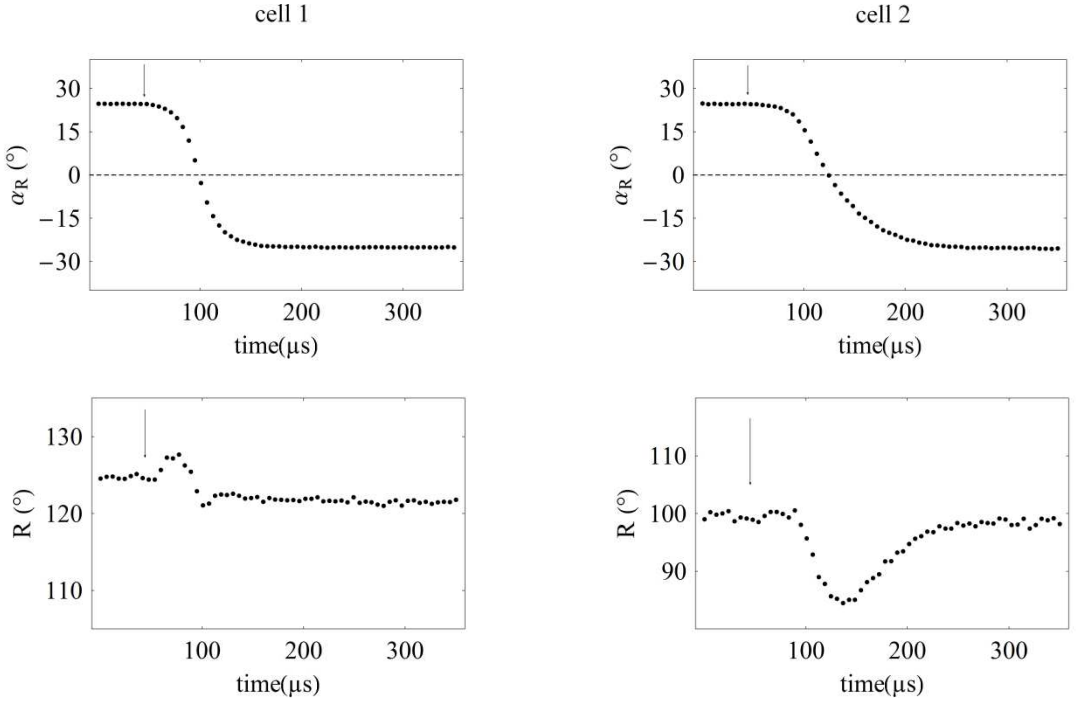

Figure 45 – Dynamics of the polarimetric parameters α_R and R between the up (a) and down (c) transition at a particular point if the cells 1 and 2.

The depolarisation index was close to 1, meaning that the acquisition time was short enough to avoid temporal averaging. Notice that the measurements of α_R and R in the addressed states are in perfect agreement with the sample specifications; tilt angle θ = 25,5° and thicknesses 1,8 and 1,5 µm for cell 1 and 2, respectively. The dynamic behaviours of α_R and R are very different between the two cells. The duration of the transition between the two addressed states is shorter in cell 1 and the R(t) curves also shows two distinct behaviours. An interesting way to represent α_R and R is to draw the trajectory of the liquid crystal director

over the transition once that the polarimetric parameter are linked to the angles θ_{in} and θ_{off}. The trajectories corresponding to the experiments illustrated in Figure 45 are plotted in Figure 46. Note that this calculation is done under the assumption that the refractive indexes do not change during the transition.

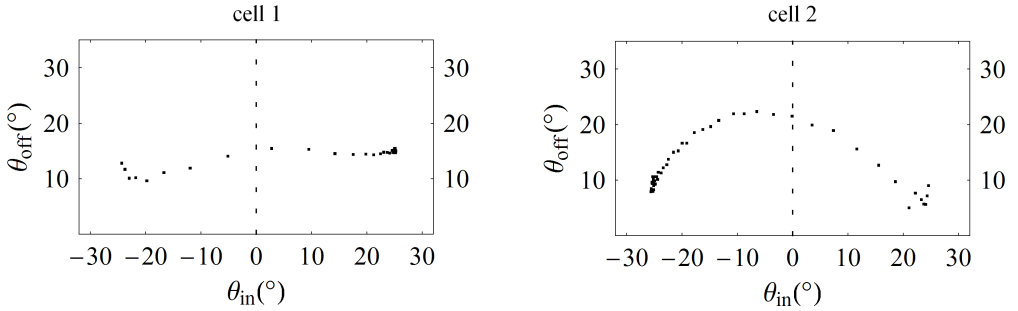

Figure 46 – The liquid crystal director trajectory over the transision between the two adressed states.

In Figure 46 the director trajectory in cell 1 is flat-shaped and in cell 2 is more circular. Two parameters, |S| and τ, were used to quantify the presented dynamic behaviour. The parameter |S|, in degrees, represents the flatness of the trajectory and it is defined as:

$$|S| = \sum_i (\theta_{off}^i - \theta_{off}^0) \tag{3.18}$$

where θ_{off}^0 is the off-plane angle in the addressed state and θ_{off}^i is the off-plane angle for the *i*-th acquisition of the transition. The parameter τ, in microseconds, is the switching time of the transition, obtained by an adjustment of the equation $\tan\theta_{in}(t) = \tan\theta \tanh\left[\frac{t}{\tau} - \ln\left(\tan\frac{\phi_0}{2}\right)\right]$ [30]. The values were calculated for each position of the cells and the results are represented in the format of an image (Figure 47) with the same spatial resolution as in Figure 44.

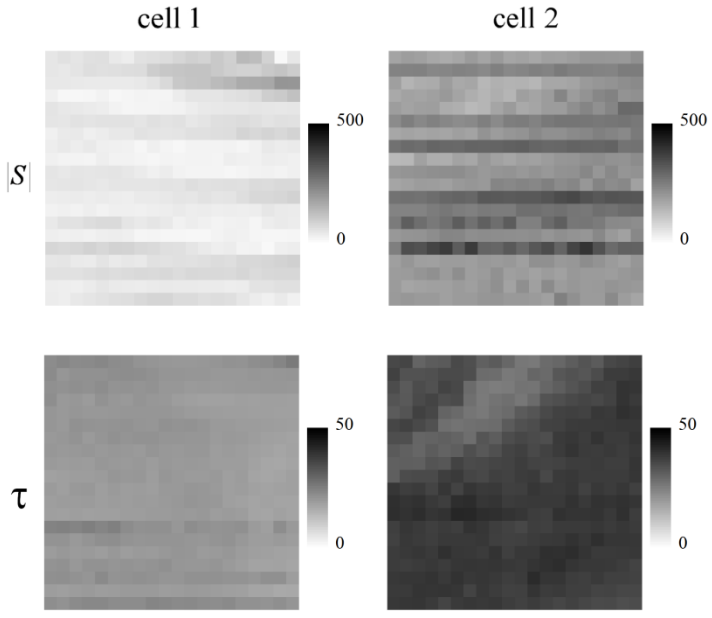

Figure 47 – Images representing the parameter |S| and τ.

The Figure 47 shows that the liquid crystal director of cell 1 has a more flattened trajectory

during the transition and that the rise time is shorter for cell 1. Later in this thesis is presented with more details the relation between the liquid crystal director trajectory and the structure of the SSFLC samples.

When applying electric field to the cells the LC director moves around the smectic cone. Assuming a perfect bookshelf structure for the smectic layers and a uniform molecular distribution, the trajectory of the liquid crystal director into the (Y, Z) plane has to be a perfect circle. However, if the layers are tilted in a symmetric chevron structure, the director trajectory is distorted because of the projection of the smectic cone system with respect to the laboratory coordinates. Supposing that the layers are fixed it is very unlikely that the switching of the director (in chevron structure) will have a flat-shaped trajectory over the transition between the addressed states. Thus, it is possible that the smectic layers reorient reversibly while the director is moving around the cone [31][32]. According to the experiments reported in [33], no reversible smectic layer movement upon field reversal was observed and it was suggested that the smectic layers remains unchanged and the in-depth distribution of the molecules is quasi-uniform. This behaviour cannot result in our observation of a flat-shaped trajectory. Also, we proposed the formation of half-splayed states during switching, but it would generate a high ellipticity parameter ε_R which we never observed in this study (Figure 48).

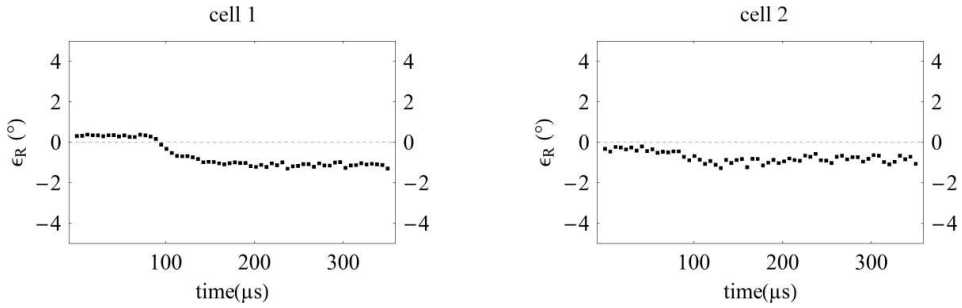

Figure 48 – The ε_R during the transition between the two addressed states.

In a recent study [34], the reversible reorientation of the smectic layers was observed in high-resolution time-resolved X-ray experiments. Such experiments are totally model-independent and give direct access to the organization of the layers and are in perfect agreement with the results that we have found.

The strong anchoring energy due to the alignment layer forces a planar orientation of the molecules in the whole cell. Additionally, the director rotates on the smectic cone. Then, to satisfy both last statements, during switching the smectic layers have to move while the molecules are switching around the cone keeping them in a planar orientation over the transition. However, the chevron angle at the surfaces must be fixed, which probably results in a complicated deformed layer structure during the switching motion, as shown experimentally in static measurements [29]. This behavior also agrees with a previous description by Hartmann et al. [31]. When the smectic layers are irreversibly straightened out due to the application of the electric field they become fixed in a quasi-bookshelf structure. As a consequence, the layers remain unchanged, steady during the switching process and the

trajectory of the liquid crystal director becomes almost a perfect circle. We discuss more the irreversible straightened out of the smectic layer in the next sections. The above conclusions assume a uniform or quasi-uniform distribution of the molecules and the case of the non-uniform distribution cannot be excluded. In that case, the representation of the trajectory of the optic axis is no more valuable, because the refractive indexes are time-dependent.

3.4.4. The Irreversible Chevron to Bookshelf Transition

Some techniques and computer simulations which characterize and describes the reorientation of the director and the layers dynamics of SSFLC samples have been published in the scientific literature [35][36]. As it was said before, the SSFLC texture changes after applying a low frequency electric field for long periods. The changes in the texture are due to the motion of the smectic layers from chevron to bookshelf geometry that culminates in an irreversible transition after a certain period of applied voltage. Then, for the moment we are interested in study this irreversible chevron to bookshelf transitions by using the same Snapshot Mueller Matrix Polarimeter.

In chevron geometry the electric field not only reorients the liquid crystal director but also dynamically change the layer configuration. Then, to characterize all the switching mechanism the layer movement should be included in the description. The polarimetric results show the movement of the smectic layer while switching and the irreversible change in the texture of SSFLC cells from chevron to bookshelf while applying a high electric field. The polarimetric parameters clearly describe the trajectory of the director evolving from an in-plane switching (chevron) to a quasi-circular switching (bookshelf) as long as a strong electric field is applied. Observe that our experiments to understand the chevron to bookshelf transition have been done with SSFLC cell with the same configuration as the sample described in Section 2.4.1.

The basic idea of the experiment is to apply a high electric field at low frequency in the samples during predefined time intervals $(T_{\exp o})$ to force the straight-up of the smectic layers and measure the polarimetric parameters between these intervals with a low electric field at high frequency to analyze the behavior along the time. Thus, three different voltages formats have been applied to the cell. The first one was a rectangular voltage of 40V (±20V) peak-to-peak at 10Hz applied during exposition times of 0, 10, 90, 300, 600, 1800 and 3600 seconds. These exposition times were chosen in order to gradually change the texture of the samples from chevron to bookshelf. Then, to do the characterization with the SMMP, between the exposition intervals a rectangular voltage of 9,6V (±4,8V) peak-to-peak at 100Hz was applied to study the fast switching of the director, and a triangular voltage of 9,6V (±4,8V) peak-to-peak at 0,5Hz was applied to analyze the progressive switching of the director. All the applied voltages are supposed to provide experimental results without disturbing the layer organization, which is supposed to be affected only by the first rectangular voltage (±20V, 10Hz).

Hysteresis curves $\alpha_R(V)$ at different time of exposure $(T_{\exp o})$

The hysteresis curves $\alpha_R(V)$ were measured for different exposition times by applying the triangular voltage after the preliminary exposition of the sample to the rectangular voltage (±20V, 10Hz), which modifies the layer structure of the liquid crystal. The evolution of the hysteresis can be described into three phases: first, between 0s and 90s, the hysteresis curve is tilted with respect to the main axis and the width at 0V increases significantly until reaching a quasi-perfect hysteresis shape at 90s, as can be seen in Figure 49(a). Between 300s and 600s, the area of the hysteresis cycle seems to continue increasing at 0V and this evolution is shown in Figure 49(b).

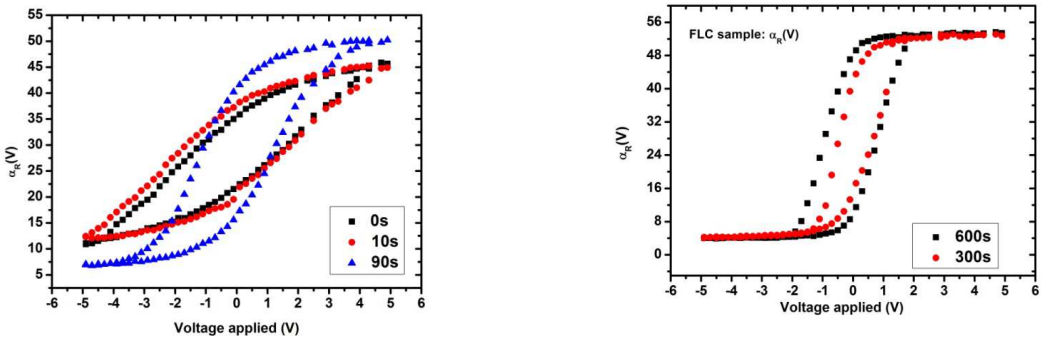

(a) (b)

Figure 49 – (a) Hysteresis curves $\alpha_R(V)$ for 0, 10 and 90 seconds of electric field exposure, (b) and for 300 and 600 seconds.

After 600, 1800 and 3600 seconds the curve seems to stabilize and no relevant change can be noticed above 600s, Figure 50. The lateral expansion of the hysteresis curve confirms a clear chevron/bookshelf structure transition.

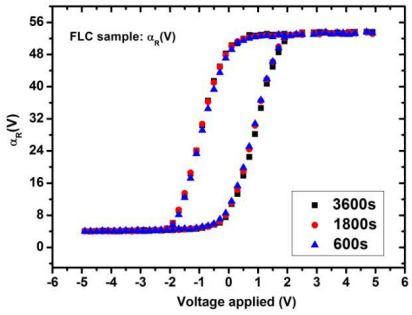

Figure 50 - Hysteresis curves $\alpha_R(V)$ for 600, 1800 and 3600 seconds of electric field exposure

To clearly express the behaviour of the hysteresis curves along the time, it is possible to plot the vertical width at 0V(Figure 51). At 0s, due to the chevron the layers and consequently the smectic cone are tilted by the angle δ. Then, since the cell is planar aligned, in the absence of electric field the director lies on the surface of the cell with an azimuthal angle φ, where φ≠0°,90°. Then, the angle (α_R) between the two addressed states on the surface is smaller than the liquid crystal tilted angle and the hysteresis curve width at 0V is thin. Applying

electric field and stretching the smectic layers, this apparent tilt angle increases and also the hysteresis width. At 600s, the layers are completely stretched (bookshelf) by the electric field, the smectic cone is not tilted anymore, the director azimuthal angle is φ=0°,90° and the apparent tilt angle has the same value of the liquid crystal tilt angle. The results show that the SSFLC, in the beginning in a chevron configuration, had its structure irreversible changed by the application of the strong electric field.

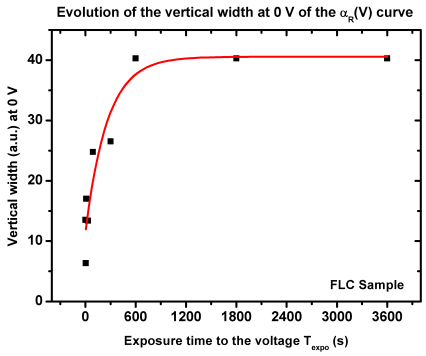

Figure 51 - Vertical width of the hysteresis curves $\alpha_R(V)$ at 0V.

Evolution of the polarimetric coefficients $\alpha_R(t)$ and $R(t)$.

In agreement with the hysteresis curves and in order to show the changes in the layer configuration of SSLFC devices, the polarimetric coefficients $\alpha_R(t)$and $R(t)$were measured for 300s of exposure time until 3600s. As it can be seen in Figure 52, there is a significant change in the behaviour of the parameters α_R and R between 300s and 600s.

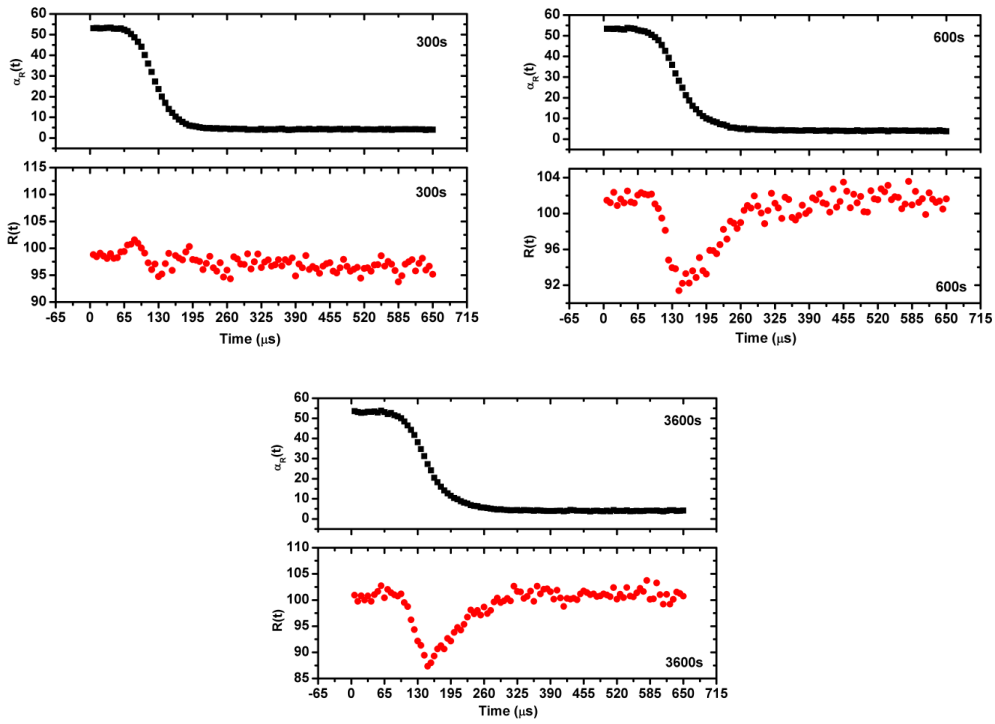

Figure 52 – Comparison of the dynamic evolution of $\alpha_R(t)$ and $R(t)$ at different exposure time.

For instance, the duration of the transition between the two addressed states for 300s is shorter

in comparison with the exposure times above 300s. Besides, since the polarimetric coefficients α_R and R are related with the angles θ_{in} and θ_{off}, it is possible to map the trajectory of the liquid crystal director while switching (Figure 53) like we have shown in Figure 46 in the last section.

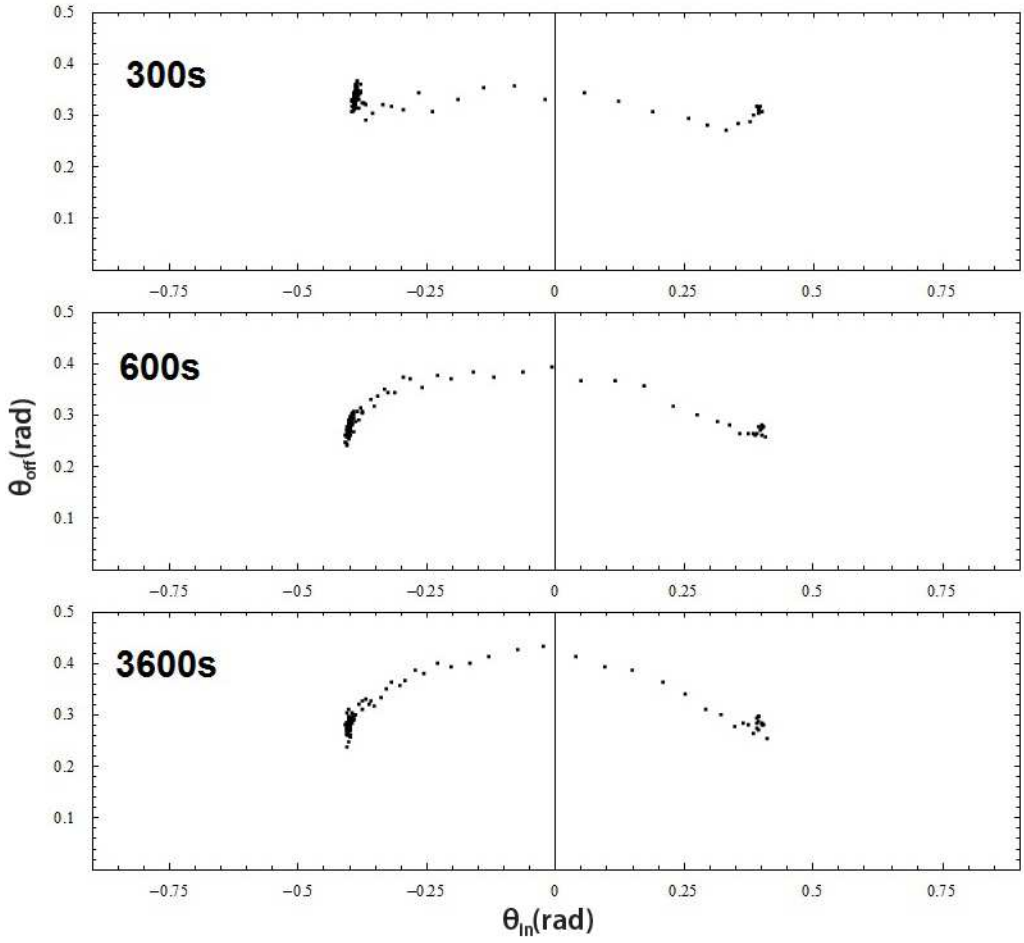

Figure 53 - Trajectory of the liquid crystal director at different time of exposure from an in-plane to a quasi-circular switching.

Notice that the results shown in the figure above are in agreement with Figure 46. The trajectory of the director is in a plane parallel to the substrates for 300s of exposition. This is due the switching of the director between the two addressed states around the smectic cone and, concomitantly, the movement of the layer from the chevron to the bookshelf texture while applying electric field. In other words, the director and the layers move at the same time leading the director to move in the plane of the cell. Above 300s, the trajectory of the director changes to a quasi-circular switching, but not completely. The smectic layer stretches up a little but not permanently to a bookshelf structure and, as it was seen before, might corresponds to the roof-top texture. Before the complete stretching (chevron) the torque on the layers produced by the electric field leads to a reversible reorientation of the layer while switching (t<300s). Thus, the orientation of the director along the cone is superimposed by the reversible reorientation of the layers. Above 600s the results in Figure 53 shows that the tilted smectic layers (chevron) is irreversibly stretched and the layers reach the bookshelf state.

Then, in the bookshelf case, the director follows the uniform reorientation along the smectic cone (t>600s).

3.4.5. Dynamic Polarimetric Measurement on PSFLC cells

In order to understand the PSFLC cells and the role that the concentration (%C) of polymer impacts its behaviour, polarimetric measurements using the SMMP were done for different concentrations. Furthermore, the results obtained on the PSFLC sample are compared with those already measured for pure SSFLC (Surface Stabilized Ferro-electric Liquid Crystal). Three mixtures were done and were made of the liquid crystal Felix 015/100 (Clarian) mixed with RM257 (Merck) in different concentrations (by weight): 3%, 5% and 13%. The higher rate, 13%, corresponds to the maximum value of solubility. Indeed, above this limit, the mixture becomes bi-phasic and two phases co-exists, one of pure polymer and the other of pure liquid crystal. The photo-initiator Irgacure 651 with percentage less than 1% was used as a starter to the polymerization.

To compare the PSSFLC cells with the pure SSFLC cell all the samples have received the electric field treatment as it was done with the experiments with the SSFLC samples. Thus, a rectangular voltage of ±20V @ 10Hz was applied in all the cells during more than 3600s. This was done to be sure that the pure SSFLC had completely modified to a bookshelf structure and no more changes in the texture could be observed and in the PSFLC to allow the comparison with the pure one. Reminds that other two voltages were used: on rectangular voltage ±10V @ 100Hz to study the switching of the liquid crystal director between the addressed states and a triangular voltage ±10V @ 0,5Hz to observe the progressive director reorientation (Figure 54)

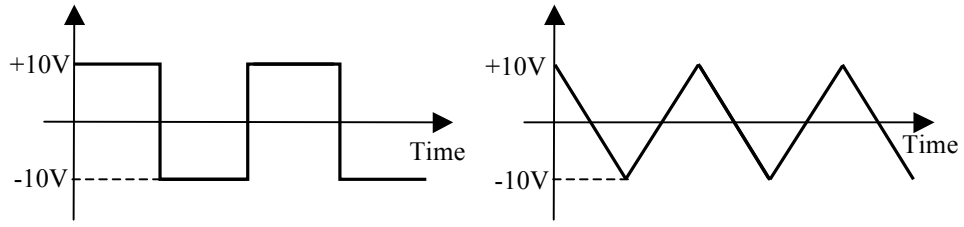

Figure 54 – The rectangular voltage (±10V @ 100Hz) in order to study the switching and the triangular voltage (±10V @ 0,5Hz) to observe the director reorientation.

Hysteresis curves $\alpha_R(V)$ for different polymer concentrations.

We have measured the polarimetric parameter α_R as funciotn of time and voltage while applying the triangular voltage. This parameter is related to the physical parameter θ_{in}, which is the projection of the liquid crystal director on the cell plane. Typically hysteresis for SSFLC in a bookshelf geometry have an "open" curve due to the fact that the layers are stretched, immobile and the director while switching "travels" on the smectic cone. However, when the concentration of polymer increases the vertical width (W), at 0V of the hysteresis curve, start to become thinner and it is almost cancelled at 13% (W=0,1), Figure 55.

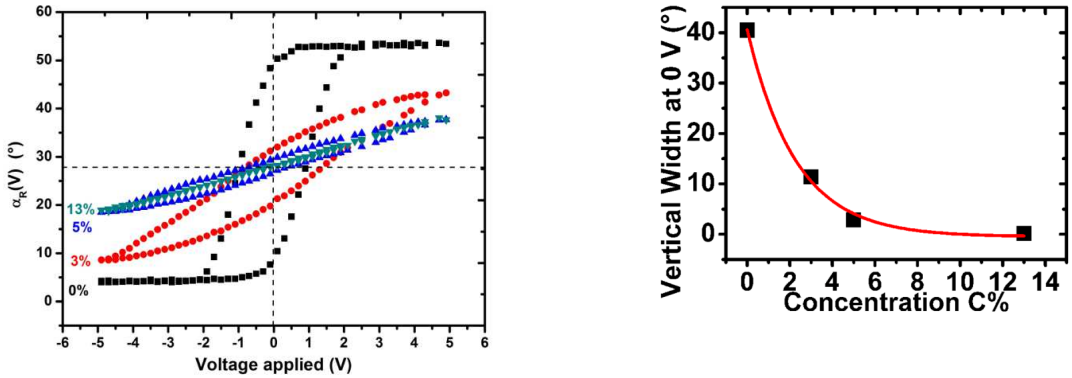

(a) (b)

Figure 55 – (a) Hysteresis curves $\alpha_R(V)$ of the cells with different concentrations of polymer and, (b) the vertical width of the hysteresis at 0V.

The presence of polymer eliminates the hysteresis loop because the bulk effect becomes more predominant comparing to the surface effect. In fact, the elastic energy associated to the concentration of polymer start to be more important than the ferroelectric energy. Also, the presence of polymer increase the viscosity of the medium and the switching of the director does not anymore obey Equation 1.25 for pure SSFLC. In simple words, the director has more difficulties to move and the switching time decrease for higher concentrations, Figure 56.

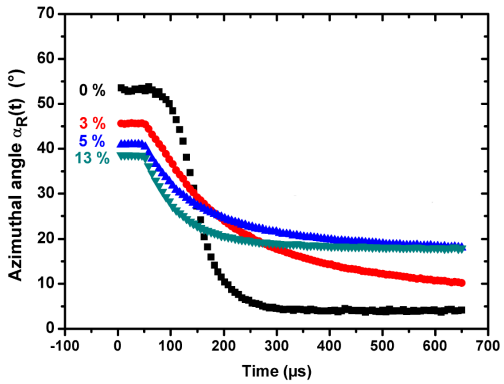

Figure 56 – Impact of the concetration of polymer in the switching time of the liquid crystal director between the two adressed states.

When the viscosity reaches the maximum value, at 13% of concentration of RM257, the switching time (τ) is constant as a function of the applied electric field. The elastic coupling is more important than the ferroelectric coupling and the liquid crystal director switching time remains the same between 0 and 5V. In the Figure 57 shows the optical power measured while the sample was switching and the τ with respect to the applied voltage. Note that these measurements in Figure 57 were not done with SMMP but with the same experimental setup used to measure the contrast of the shutters in Figure 25.

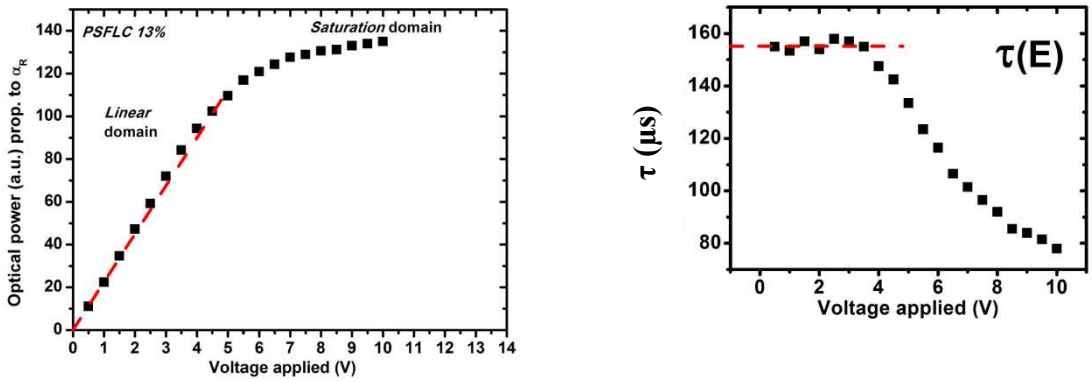

(a) (b)

Figure 57 – (a) The linear behaivour of the PSFLC cells, (b) and the constant switching time due to the elastic coupling of the director between 0and 5V.

After 5V the ferroelectric coupling becomes more important than the elastic coupling and the cell behaves like a normal SSFLC cell.

Evolution of the polarimetric coefficients $\varepsilon_R(t)$, $\alpha_R(t)$ *and* $R(t)$.

Concerning polarimetric parameter R(t), for pure SSFLC, we found a clear decrease of R(t) corresponding to a pure ferroelectric behaviour which is correlated to the rotation of the liquid crystal director around the smectic cone in the bookshelf structure. For 13%, we found that there is no change in the amplitude of R(t) meaning that we have a planar commutation of the director. This is a clear impact of the presence of polymer in the birefringence of the medium. Additionally, the $\varepsilon_R(t)$ polarimetric coefficient has a low variance in amplitude. We can consider this low value to a nearly homogeneous in-depth structure. Nevertheless, it is possible that this small variation is linked to inhomogenities of the bulk created by the polymer network which could have been collapsed in some areas [50][51]. The measurements with the SMMP do not give a conclusive answer about what happen in the volume, but just a glimpse. Figure 58 shows the behaviour of $\varepsilon_R(t)$, $\alpha_R(t)$ and $R(t)$.

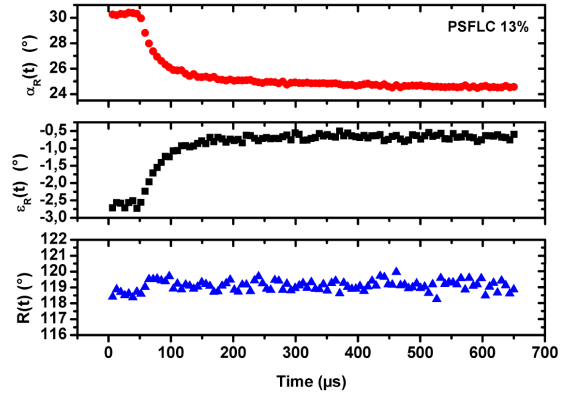

Figure 58 – The azimuthal angle, ellipticity and the retardance polarimetric parameter for PSFLC 13%.

Like we have done with the pure SSFLC, the trajectory between two states of the director can be easily mapped using the polarimetric parameters $\alpha_R(t)$ and $R(t)$. The trajectory of the

director for the PSFLC 13% is not like the pure SSFLC in bookshelf geometry, but is quasi-linear like the one measured for the SSFLC with chevron structure. Figure 59 shows the trajectory of the director for PSFLC 13% and the pure SSFLC in bookshelf.

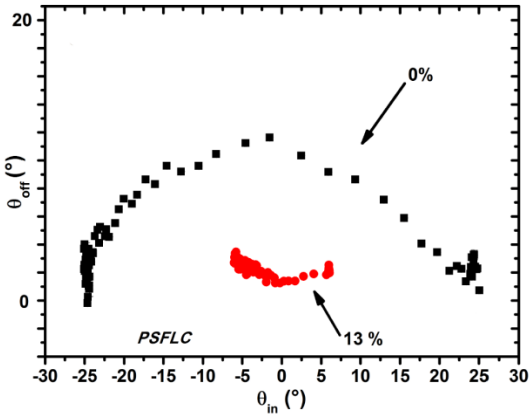

Figure 59 – Trajectories of the liquid crystal director for pure SSFLC and PSSFLC 13%.

The result above show that the director move in a plane switching. This happened because after the electric filed treatment the layers have not changed to a bookshelf geometry. In fact, the necessary energy to stretch up the layers in a PSFLC should be higher due to the presence of polymer. Besides, the applied voltage to verify the dynamics was also not sufficient to move the director completely between the two addressed states, but it was enough to check the behaviour of the switching.

Conclusion

In the first part we have established a correlation between the static and dynamic polarimetric properties with the textures of SSFLC cells. For a cell exhibiting a texture with 'rooftop' and zigzag defects (chevron structure), the difference between addressed and memory states was found to be high. Moreover, the trajectory of the optic axis during the 'up/down' transition proved to be flat-shaped. On the contrary, in a cell with a striped texture (quasi-bookshelf structure), the difference between addressed and memory states was lower, and the trajectory during the 'up/down' transition was more circular. Assuming a collective movement for the molecules, the shape of the trajectories could be explained by a reversible motion of the smectic layers, simultaneously to the rotation of the molecules on the smectic cone.

In the second part we established a link between the polarimetric properties with the layer structure and the liquid crystal director of surface stabilized ferroelectric liquid crystal cells showing the irreversible chevron to bookshelf transition. We have shown typical hysteresis curves for SSFLC devices in chevron and bookshelf geometry, and the behavior while applying high electric fields at different time of exposure to see the gradual change in the structure of the layers. The measured polarimetric parameters are in perfect agreement with the theoretical movement of the liquid crystal director, the movement of the smectic layers and the irreversible change of the smectic layer configuration from chevron to bookshelf geometry.

The last part was a link between the polarimetric paramentes and the concentration of polymer in PSFLC cells. It was seen that while you increase the concentration of polymer the elastic coupling becomes more important than the ferroelectric coupling and the cells start to operate in a linear regime for certain values of the applied voltage. The ellipiticity measurement presents a possibility that the concentration of polymer could have lead to a non-uniform structure of the bulk, but it is just a hypothesis and could not be confirmed with the obtained results. The hysteresis curves and trajectory of the PSFLC 3% director shows that the structure would remain like the pure SSFLC in a chevron geometry. This leads to an important conclusion that maybe the polymer masks the chevron, since the pictures under crossed polariser have not shown zigzag defects.

We have done some measurement with twisted surface stabilized ferroelectric liquid crystal but the results were lacking in consistency and we have decided to not introduce in this thesis. However, we have demonstrated that the SMMP used is suitable to characterize SSFLC and PSFLC cells with an excellent temporal and spatial resolution. It is a beneficial tool and can lead to a better knowledge of dynamic behaviours in LC devices

Bibliography

[1] Clark, N.A.; Lagerwall, S.T. Appl. Phys. Lett. 1980, 36, 899-901.

[2] Derking, I. “Texture of Liquid Crystals”, Wiley-VCH: Weinheim 2003.

[3] Rieker, T.P.; Clark, N.A.; Smith, G.S.; Parmar, D.S.; Sirota, E.B.; Safinya, C.R. Phys. Rev. Lett. 1987, 59, 2658–2661.

[4] Elston, S.J.; Sambles, J.R.; Clark, M.G. J. Mod. Opt. 1989, 36, 1019–1025.

[5] Dubreuil, M.; Rivet, S.; Le Jeune, B.; Cariou, J. Opt. Express 2007, 15, 13660–13668.

[6] Dubreuil, M.; Rivet, S.; Le Jeune, B.; Dupont, L. Opt. Lett. 2010, 35, 1019–1021.

[7] Hartmann, W.J.A.M.; Luyckx-Smolders, A.M.M. J. Appl. Phys. 1990, 67, 1253–1261.

[8] Shao, R.F.;Willis, P.C.; Clark,N.A. Ferroelectrics 1991, 121, 127–136.

[9] Verhulst, A.G.H.; Stommels, F.J. Ferroelectrics 1991, 121, 79–90.

[10] Patel, J.S.; Lee, S.-D.; Goodby, J.W. Phys. Rev. A: At., Mol., Opt. Phys. 1989, 40, 2854–2856.

[11] E. Collett, “Field Guide to Polarization”, SPIE Field Guides vol. FG05, SPIE (2005)

[12] R. M. A. Azzam, "Propagation of partially polarized light through anisotropic media with or without depolarization: A differential 4 × 4 matrix calculus," J. Opt. Soc. Am. 68, 1756-1767 (1978).

[13] William H. McMaster (1961). "Matrix representation of polarization". Rev. Mod. Phys. 8: 33.

[14] Tom Gehrels, “Planets Stars and Nebulae Studied with Photopolarimetry”, University of Arizona Press, 1974.

[15] F. Boulvert et al, “Analysis of the Depolarizing Properties of Irradiated Pig Skin”, J. Opt. A: Pure Appl. Opt. 7 21.

[16] Dennis H. Goldstein, "Mueller matrix dual-rotating retarder polarimeter," Appl. Opt. 31, 6676-6683 (1992).

[17] P. A. Williams, A. H. Rose, and C. M. Wang, "Rotating-polarizer polarimeter for accurate retardance measurement," Appl. Opt. 36, 6466-6472 (1997).

[18] Azzam, R. M. A., ‘‘Photopolarimetric Measurement of the Mueller Matrix by Fourier Analysis of a Single Detected Signal, ’’ Opt. Lett. 2: 148 – 150 (1978).

[19] Azzam , R. M. A. (ed.) , ‘‘Ellipsometry , ’’ Soc . Photo - Opt. Instrum. Eng. Milestone Series, MS27 (1991).

[20] M. Dubreuil, S. Rivet, B. Le Jeune and J. Cariou, “Systematic errors specific to a snapshot Mueller matrix polarimeter”, Appl. Opt., 48, pp. 1135-1142, 2009.

[21] W. J. A. M. Hartmann and A. M. M. Luyckx-Smolders, “The bistability of the surface-stabilized ferroelectric liquid-crystal effect in electrically reoriented chevron structures”, J. Appl. Phys. 67, 1253 (1990).

[22] T. P. Rieker, N. A. Clark, C. R. Safinya, “Chevron layer structures in surface stabilized ferroelectric liquid crystal (SSFLC) cells filled with a material which exhibits the chiral nematic to smectic C* phase transition”, Ferroelectric, 113 (1), 1991.

[23] Gil, J.J.; Bernabeu, E. J. Mod. Opt. 1986, 33, 185–189.

[24] S.Y. Lu and R.A. Chipman, “Interpretation of Mueller matrices based on polar decomposition”, J. Opt. Soc. Am. A, 13, pp. 1106-1113, 1996.

[25] Scharf, T. Polarized Light in Liquid Crystals and Polymers; JohnWiley & Sons, Inc.: Hoboken, NJ, 2007.

[26] Maclennan, J.E.; Handschy, M.A.; Clark, N.A. Liq. Cryst. 1990, 7, 787–796.

[27] M. Dubreuil, “Développement d'un polarimètre de Mueller instantané par codage en longueur d'onde. Application à la caractérisation de cristaux liquides ferroélectriques.”, Université de Bretagne occidentale, Brest 2010.

[28] Y. Takahashi, A. Iida, Y. Takanishi, T. Ogasawara, M. Nakata, K. Ishikawa and H. Takezoe, “Dynamic local-layer response of surface-stabilized ferroelectric liquid crystals to a high electric field by time-resolved x-ray microdiffraction”, Phys. Rev. E, 67, 051706-1, 2003.

[29] M. Oh-e, M. Isogai and T. Kitamura, “X-ray studies on layer structure and bistability in ferroelectric liquid crystals”, Liq. Cryst., 11, pp. 101-109, 1992.

[30] Handschy, M.A.; Clark, N.A. Ferroelectrics 1984, 59, 69–116.

[31] Hartmann, W.J.A.M.; Vertogen, G.; Gerritsma, C.J.; Sprang, H.A.V.; Verhulst, A.G.H. Ferroelectrics 1991, 113, 257–268.

[32] Giesselmann, F.; Zugenmaier, P. Mol. Cryst. Liq. Cryst. 1993, 237, 121–143.

[33] Willis, P.C.; Clark, N.A.; Safinya, C.R. Liq. Cryst. 1992, 11, 581–592.

[34] Gleeson, H.F.; Bryant, G.K.; Morse, A.S. Mol. Cryst. Liq. Cryst. 2001, 362, 203–215.

[35] W.J.A.M. Hartmann, G. Vertogen, C.J. Gerritsma, H.A.V. Sprang and A.G.H. Verhulst, “SSFLC field-induced director pattern modulation described in terms of smectic layer bending” , Ferroelectrics, vol. 113, Iss. 1, 1991.

[36] Dubal, H.R., Escher, C., Ohlendorf, D., “Electro-optical behaviour of ferroelectric liquid crystal (FLC) mixtures”, Electrets, 1988. (ISE 6) Proceedings, 6th International Symposium on (IEEE Cat. No.88CH2593-2), pp. 334-338.

[37] B. Caillaud, L. Dupont, J.L. de Bougrenet de la Tocnaye, Mol. Cryst. Liq. Cryst. 469 (9), (2007) 59-68.

[38] J. Li, Z. Wang, Y. Cai, X. Huang, Ferroelectric 213, (1998) 91-99.

Chapter 4: *3D Dual View Technique*

Introduction

The Dual View technique is an intrinsic capability of TVs or 3D video-projector that displays in a single screen two video streaming which can be seen separately by at least two different viewers [1]. For instance, Samsung recently presented at the CES its Dual-View TV [2]. Dual-View TVs basically play two full HD image streams that can be tuned by the viewers wearing compatible glasses. This means that two users watching the same TV can watch different channels in full HD. In other words, the stereo pair is used to separate the streams for two different viewers. Consequently, watching 3D view requires at least four independent frames projection or display. The content of each 3D streaming can be unrelated, an example of this might be displaying two different TV shows, or movies, or one 3D streaming displays a movie and the other a football match. The content can be also related: in that case, the projectors display two 3D streaming of the same scene but from different view angles. This provides the advantage of free viewpoint projection [3], which is not possible with conventional 3D contents as soon as several users have to be considered, since no side views are possible (despite having different physical viewpoints on the screen and associated 3D content, all the viewers see the same scene, which is computed from the same virtual 3D point of view). This technique is, therefore, interesting because allowing the viewers to share a vision of the same scene, but from their own perspectives. For example, in the military domain two officers can plan a better strategy of defence or attack exchanging different visual information looking for a 3D map having different points of view, or in telemedicine the doctors can also exchange different information during a surgery having two different views of the same patient. Even if the 3D Dual View technique is promising and has a huge range of applications, some drawbacks, mainly the ghosting effect, should be mitigated to avoid the interference between the two 3D streaming and consequently the misunderstanding of the scene. Also, some physiological aspects regarding the spectators have to be considered for long-term use.

One of the biggest issues of the 3D Dual View, that is the same for all the 3D stereoscopic system, is how to code four 2D pictures in order to have two stereo images with less ghosting effect as possible [4]. Several coding solutions can be proposed and in this chapter will be presented the different configurations to implement the 3D Dual View technique using DLP Link 3D projectors with special active goggles and, its advantages and disadvantages of each configuration. Following, we demonstrated the implementation of the 3D Dual View in two different configurations working in two different modes, reflective mode that was implemented in Télécom-Bretagne (TB), and transmittive mode that was implemented by Immersion, our partner. Finally, we will show some ghosting effect measurements which have been done for both modes and we proposed a technique to compensate it.

4.1. 3D Dual View Techniques

As it was explained briefly in the introduction, the 3D Dual View technique, in a few words, is the technique which displays two 3D video streaming on a screen of two different 3D scenes or one 3D scene with two different points of view (Figure 60) to be seeing by two different viewers. In our case, we are interested to project a 3D scene with different points of view for two specific Viewers. Thus, the basic idea is to place these two viewers in front of a screen and allow them to see an image, of an object for example, from different perspective. Figure 60 shows a simple illustration of the two 3D video streaming that forms a cube and two Viewers standing in front of the screen and their respective vision of the projected scene.

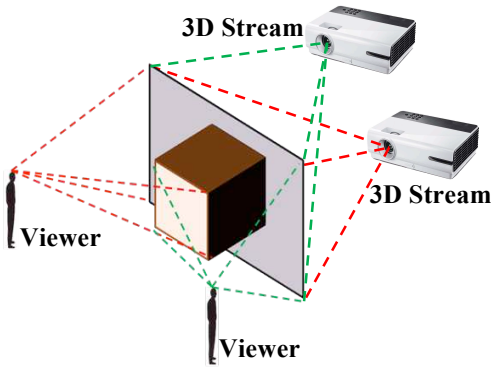

Figure 60- The illustration of the two 3D video streaming and the two Viewers seeing the image of a cube from different perspectives.

Projecting two different 3D streams on a screen for different Viewers is not simple as it is. In Chapter 2 was discussed that one 3D image is nothing but two 2D images of the same subject taking from two slightly different angles [5], one image for the right eye and the other image for the left eye. This means that projecting a 3D video implies in projecting two 2D video streams, one for each eye of the viewer with the minimum ghosting. Then, since the 3D Dual View technique has the aim to display two 3D video contents, it is necessary to encode and decode four 2D video streams in a way that they do not interfere with each other. Beyond the ghosting effect that appears between the right and the left images on traditional 3D, the 3D Dual View ought to avoid the ghosting between the viewers, i.e. the left and right image of one viewer cannot interfere in the images of the other viewer and vice-versa.

Thus, the challenge is to choose the best manner to encode and decode the four 2D streams. Since is possible to code the 3D stream by color (spectral multiplexing - anaglyph), polarization and time (time multiplexing), we can combine these three techniques and code two 3D images to do the 3D Dual View. More than separating the eyes of each viewer using the mentioned techniques, it is necessary to isolate the viewers from each other. Table 8 show the possibilities to separate the images of each eye and the viewers at the same time combining the mentioned techniques.

Viewers Eyes Separation Technique	Viewers Separation Technique			
		Time	Polarization	Anaglyph
	Time	Case 1	Case 2.1	Case 3.1
	Polarization	Case 2.2	-	Case 4.1
	Anaglyph	Case 3.2	Case 4.2	Case 5

Table 8 – All the possible configurations to separate the images of each viewer' eye and isolate the viewers.

For example, in the Case 2.1 the viewers are separated by polarization and the viewers eyes are separated by time. The case "polarization x polarization" cannot be done since only two orthogonal polarization states are possible.

In the next subsections is presented the different possible configurations of 3D Dual View employing a combination of the existing techniques showed in Table 8, including the solutions which we have chosen to implement.

4.1.1. Time Multiplexing (Case 1)

One immediate solution that normally comes in our mind is to use one simple 3D cinema concepts and try to apply in the 3D Dual View. The Dual View cannot be done with all the cinema solutions, specially the passive solution which circular or linear polarisers cannot encode four images separately by polarization. However, the 3D active solution can be adapted to encode and decode four different images. In theory, many time-multiplexing configurations are achievable, but we will describe two configurations that are more suitable due to the current technology. We have chosen based on the products available and expected on the market to show realizable solutions.

- Time Multiplexing with 240Hz projector

The first proposed configuration to implement the Dual View technique take the advantage of a 240Hz projector which can project 60 images per second for each viewers eye to create the sensation of depth for the two viewers using active 3D goggles. The projector display successively four images, the right and left image, IMG-R1 and IMG-L1, for the Viewer 1 and the right and left image, IMG-R2 and IMG-L2, for the Viewer 2 and projects on a regular screen, as can be seen in Figure 61.

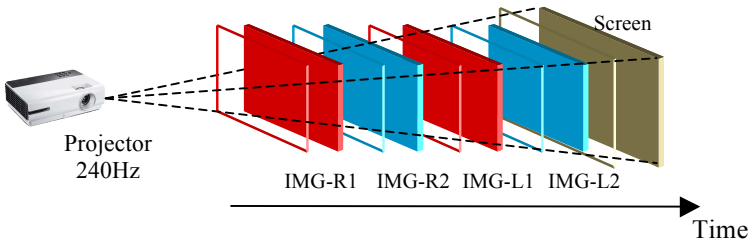

Figure 61 - The four images multiplexed by time being projected on a regular screen.

The viewers, in order to see the two 3D images designated for them, have to wear special 3D

active goggles synchronised with the projector. The goggle is composed by two shutters, for the Viewer 1 we call the right and left shutter as SHT-R1 and SHT-L1, and for the Viewer 2 the right and the left shutter as SHT-R2 and SHT-L2 as can be seen in Figure 62.

Figure 62 - The goggles of Viewer 1 and Viewer 2 and their respective shutters.

The shutter is responsible to let only one eye to see the image which is being projected on the screen that belongs to that eye. Then, when the image IMG-R1 is on the screen the shutter SHT-R1 is open and all the other shutters are closed, only the right eye of the Viewer 1 can see the projected image. To create one different 3D scene for each viewer, the 240Hz projector send a synchronization signal (sync) followed by the four images and the shutters open and closes according to the projected image. The Figure 63 illustrates how the two goggles behave while the images are being projected showing how it is possible to one viewer to see only the 3D scene designated to him.

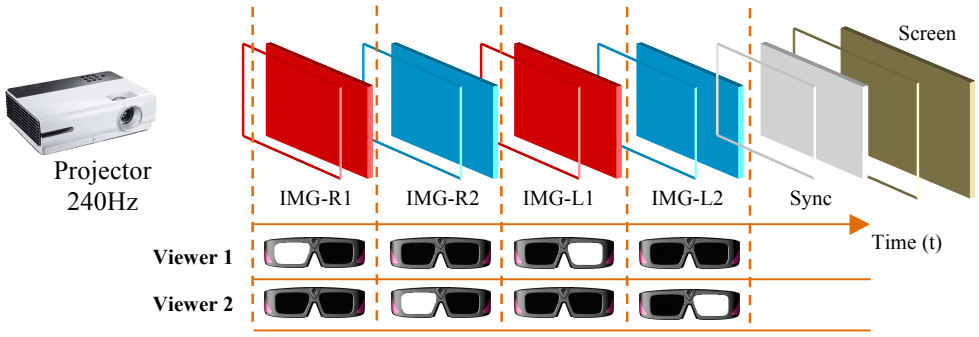

Figure 63 - The schematic of the functionality of the 3D active goggles for the Dual View technique using time multiplexing.

What was described until now and resumed in Figure 63 is nothing but the 3D cinema active solution using 3D projector operating at 240Hz. In fact, the projector time-multiplexes two different 3D video streams which synchronised with the goggles can realize the 3D Dual View. The advantage of this solution is that it uses one single projector to display the two 3D streams and is a pure active solution which can be done with goggles based on liquid crystal. However, the biggest issue of this approach is, besides the rumours, there is no 240Hz projector available on the market. Also, increasing the operating frequency of the projector the luminance is reduced in comparison with projectors operating at 60Hz, the 240Hz projectors will have eight times less luminance.

- Time Multiplexing with two 120Hz projector

There is no 3D projector operating at 240Hz on the market. To overcome this issue and still implement the 3D Dual View technique with time multiplexing, we can use, for example two "normal" 3D DLP Link projectors. As "normal", we understand as two projectors operating at 120Hz. The only difference is the manner how the synchronization is made. Now, not only the goggles have to be synchronized with the image which is being displayed, but also the two

projectors should be synchronized between them.

One projector (P1) is dedicated to the Viewer 1 and the other projector (P2) is dedicated to the Viewer 2. The projectors display the images out of phase with each other and the shutters close according to the image which is on the screen. Figure 64 illustrates the solution showing the behaviour of the shutter according to the displayed image.

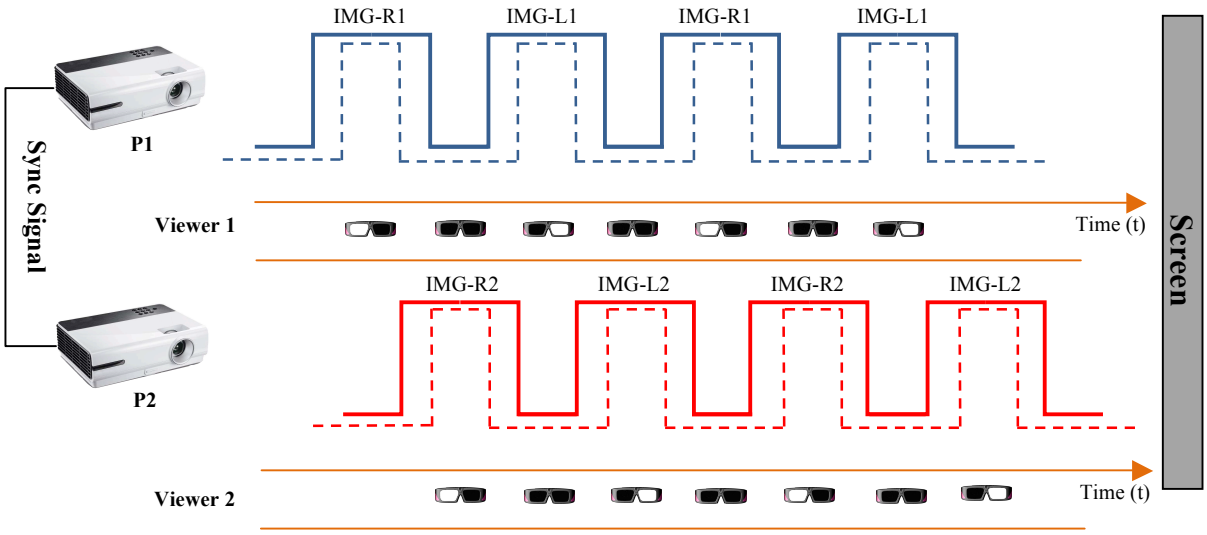

Figure 64 - The illustration of Case 1.2 showing how the two projectors and the shutter are synchronized

The important part of the two projector solution is it can be done with commercial 3D DLP Link projector and it remains an active solution with the viewers wearing active goggles. However, the projector should have a synchronization output and input, the active goggles have to be reprogrammed and the luminance is reduced by a factor of 8. Theoretically, the 3D Dual View using only the active solution can be done using more than two projectors, for example four 60Hz projector out of phase, but the luminance is drastically reduced and the complexity to manage the synchronization of the projectors increases. The next two solutions is a mixture between the Active 3D and Passive 3D commercial solution for 3D cinema.

4.1.2. Temporal and Polarization Multiplexing (Case 2.*)

Four video streams cannot be encoded by polarization, thus the 3D Dual View technique cannot be reproduced using only polarisers. However, the 3D Dual View technique is possible to realize if we combine polarization with time-multiplexing. The attractive point of the next two solutions is that polarization and time multiplexing, as a solution for 3D vision, already exists on the cinema market, television and data-show projectors.

We have seen until now that one 3D DLP Link projector is enough to encode temporally two 2D video streams and display a 3D video on a regular screen with the viewers wearing active goggles. Also, we know from Chapter 2, that one 3D video projection can be also achieved with two 2D video streams encoded by polarization and displayed on a silver screen with the viewers wearing passive goggles. However, we are looking for two 3D video, which means four 2D video streams with related content. In that case, we mixed the two solutions to accomplish the 3D Dual View technique.

- Independent Projection (Case 2.1)

The first idea that naturally comes when you start to think in mixing the polarization solution with the time solution is to separate the viewers using polarisers. Then, using two 3D projectors and placing a right circular polarizer (RCP) in front of one projector and a left circular polariser (LCP) in front of the other projector we encode the 3D stream of each projector in opposite (orthogonal) polarization states. The viewers, in order to decode only one stream and watch the video from one projector, should wear special active goggles. These special active goggles are regular active goggles used with 3D DLP Link projector with a polariser glued on it. Thus, the same that was done with the projectors should be done with the viewers goggle, a right circular polarizer has to be placed on one goggle, on both shutters, and a left circular polariser has to be placed on the other goggle, also on both shutters. The synchronization of the goggles with the projectors can be done in two different ways. The polarisers can also be placed on the goggles photodetector and the synchronization can be done independently by the synchronization signal of each projector, in that case each projector will be responsible to synchronize its goggle. Or we synchronize the projectors and only one synchronization signal is sent to the screen, in that case the polarisers on the photodetectors are not anymore needed. The biggest disadvantage of the Case 2.1 is that a silver screen has to replace the regular screen in order to maintain the polarization states for the viewers goggle.

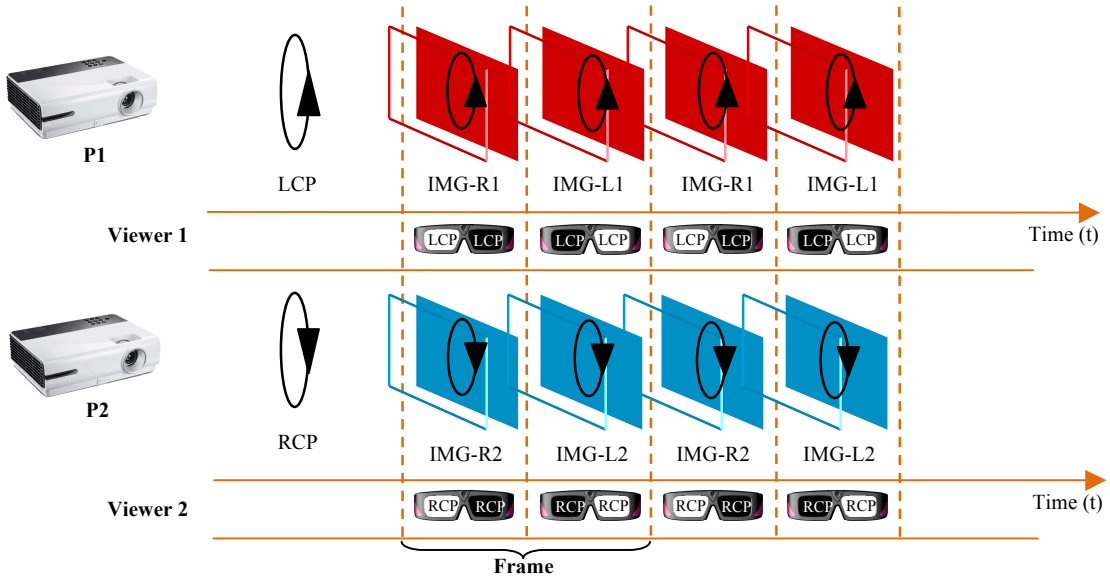

Figure 65 - Illustration of the Case 2.1 showing the two projectors separated by polarization and the configuration of the goggles.

Clearly in Figure 65 it is possible to see that the images, IMG-R1 and IMG-L1, are encoded by the LCP and the images, IMG-R2 and IMG-L2, are encoded by the RCP, and only the Viewer 1 are able to watch the video stream projected by P1 and the Viewer 2 the video stream projected by P2. The idea is simple, however to build up the configuration set-up is not an easy task and the system becomes complex, as we will be seen later in this chapter.

- Synchronised Projection (Case 2.2)

Basically the configuration set-up for the Case 2.2 is identical to the case 2.1. The differences are in how the images are sent, the functionality and the configuration of the active goggles. In this case the projector P1 projects the right images (IMG-R1 and IMG-R2) and the other projector P2 projects the left images (IMG-L1 and IMG-L2). The projectors ought to be synchronised to send at one instant *t* the right image and the left image of one viewer, for example P1 projects IMG-R1 and P2 projects IMG-L1 for the Viewer 1, and at the instant t_{t+1} the right and the left image of the other viewer, now P1 projects IMG-R2 and P2 projects IMG-L2 for Viewer 2. Then, the viewers are separated by time and the viewer eyes are separated by polarization. The shutters of one goggle open and close simultaneously and that one RCP should be placed on the right shutter of the active goggle and one LCP has to be placed on the left shutter of the active goggles in order to isolate the viewer's eyes. Figure 66 illustrates the Case 2.2.

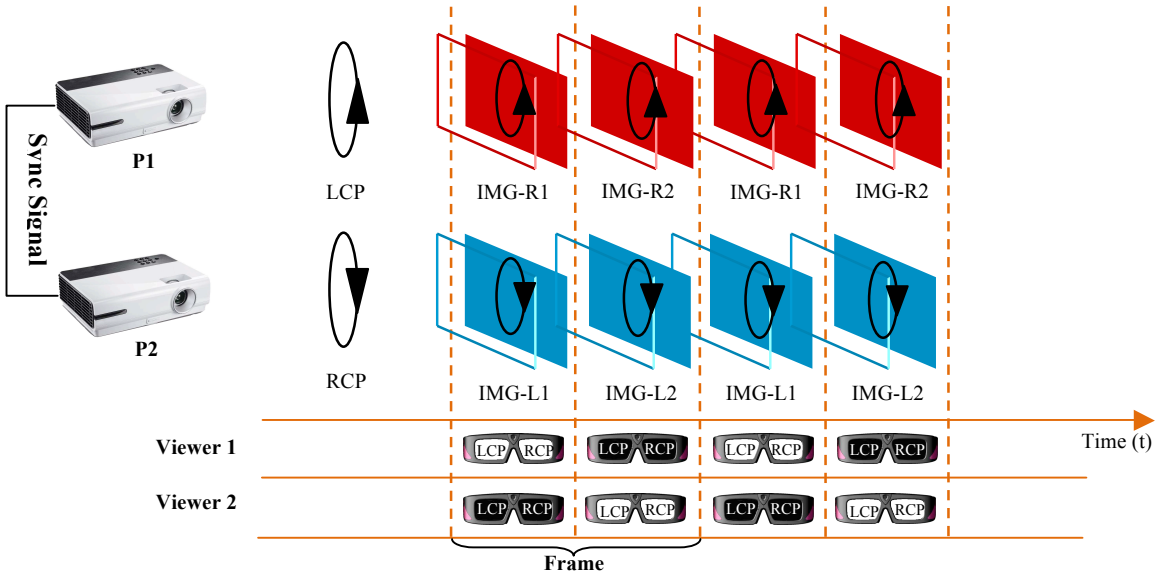

Figure 66 - Illustration of the Case 2.2 showing the two projectors synchronised and the goggles opening and closing simultaneously.

The most interesting point about this case which differs from last case is how the goggles works and, still the big disadvantage is the necessity of the silver screen to maintain the polarization.

4.1.3. Spectral Multiplexing, Anaglyph (Case 5)

The Anaglyph was one of the first techniques used to achieve the stereoscopic 3D effect [6]. Then, why it could not be used to implement the 3D Dual View? In fact, the Dual View can be done using only the spectral multiplexing with different kinds of configuration. However, we did not implement this technique due to the same issues that one day the 3D cinema market stopped using the anaglyph, issues that will be detailed in that section.

As seen in Chapter 2, the stereoscopic 3D effect is achieved by means of encoding each eye's image using filter of different colors, normally complementary colors, typically blue (cyan)

and red. Therefore, if we use very narrow band filters it is possible to encode, for example, four 2D videos streams, or two 3D videos streams. Notice that the number of video streams that can be encoded by the anaglyph technique is directly related to the quality of the filter and its selectiveness. Now, supposing that we have four narrow band filters, two red filters (RF1 and RF2) and two blue filters (BF1 and BF2) not centred at the same wavelength but slightly shifted, it we can encode the four 2D video streams and implement the 3D Dual View. The viewers should wear passive goggles with the respective filters placed on it. Figure 67 illustrate the 3D Dual View using the anaglyph technique by means of four regular projectors.

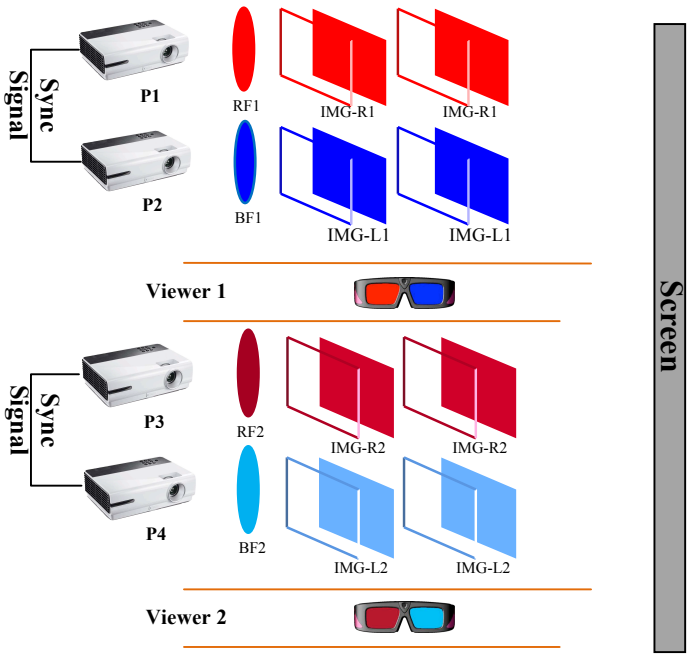

Figure 67 - Case 5.* made with four projectors and four narrow band filter in blue and red.

The example above, using four projectors, was done in order to explain the concept of the 3D Dual View using the anaglyph technique. However, it can be done using two or even one projector, but the solution becomes more complicated to realize. To project two 3D images of projectors should be synchronised in pairs. The advantages of using anaglyph are that there is no need of a silver screen and since it is a passive technology it uses passive goggles. The biggest problem about the anaglyph method is the quality of the color, one filter tint everything red and the other tint everything cyan and the result to the viewer is a poor quality image. Also, for the 3D Dual View the filters should be high quality and have a narrow band to avoid the ghosting effect, like it has done by Infitec and cited in Chapter 2. Thus, the goggles and the system become more expensive.

4.1.4. Temporal and Spectral Multiplexing (Case 3.*)

In the last section we saw that the anaglyph goggles and the projection system due to the quality of the filters become more expensive. To reduce the cost and still use the anaglyph technique we can mix the 3D active solution with the anaglyph 3D passive solution. The basic idea is almost the same expressed in section 4.1.2, but instead of using polarisers we use red and blue filters on the goggles and in the projection system. The use of active goggles reduces

the ghosting effect compared with the pure anaglyph solution. Besides, as we will be seen, the projection system is simpler and does not need to be modified. Projectors at 120Hz are already on the market, thus it is only necessary to place the color filters in front of each one.

- Independent Projection (Case 3.1)

This case follows the same principle of the Case 2.1, but instead of polarisers it mixes the color filters with the time multiplexing. The viewers are separated by colored filters and not by polarization. Then, using two 3D DLP Link projectors and placing a red filter (RF) in front of one projector and a blue filter (BF) in front of the other projector we encode the 3D stream of each projector in different spectral ranges. To decode the video stream from one projector, the viewers should wear active goggles with the red or the blue filter on both shutters, depending on each 3D stream the viewer wants to watch. Like the Case 2.1, the synchronization of the goggles with the projectors can be done in two different ways, placing on the goggles photodetector the red or the blue filter and the synchronization is done independently by the synchronization signal of each projector, in that case each projector synchronize its goggle. Or we synchronize the projectors and only one synchronization signal is sent to the screen, in that case the filters are not necessary. Figure 68 illustrates the Case 3.1.

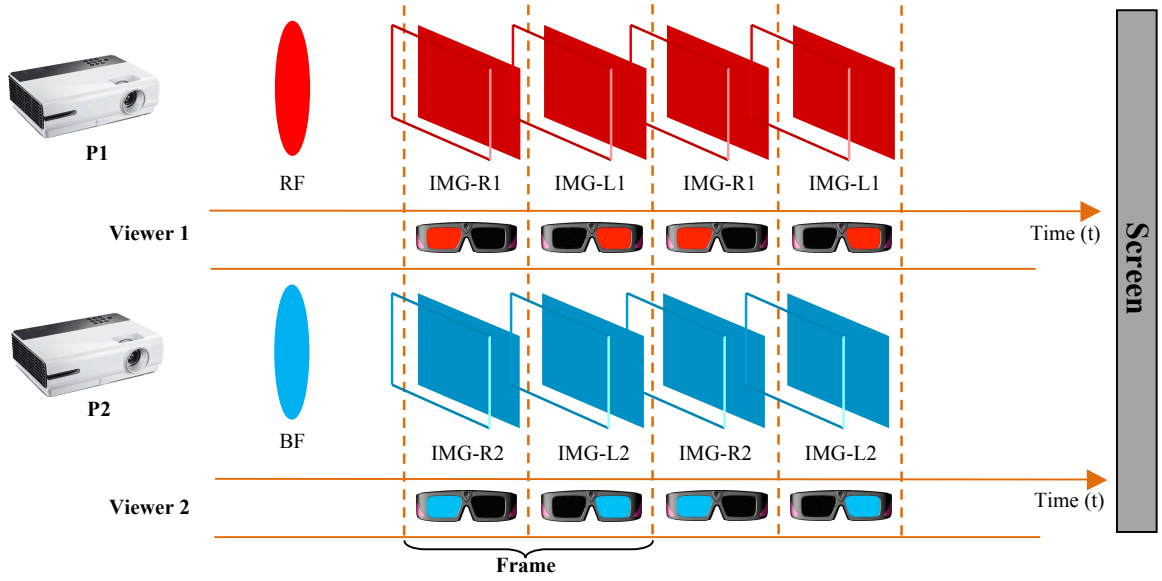

Figure 68- Case 3.1 showing the two projectors separated by the filter red and blue, and the configuration of the goggles.

In Figure 68 we see that the images, IMG-R1 and IMG-L1, are encoded by the RF and the images, IMG-R2 and IMG-L2, are encoded by the BF, and only the Viewer 1 are able to watch the video stream projected by P1 and the Viewer 2 the video stream projected by P2. The advantages is that the Case 3.1 does not need a silver screen and since it uses active goggles, and filters placed on the shutters, it has a better quality with respect to the ghosting effect. The goggles are cheaper than case 5.* because the filters do not need to be very selective. However, still the biggest issue it is that the anaglyph method has a poor color reproduction leading to a bad image quality.

- Dependent Projection (Case 3.2)

The configuration set-up for the Case 3.2 is identical to the case 3.1. The differences are in how the images are sent, the functionality and the configuration of the active goggles. In fact, the operational of this case is the same as the Case 2.2. The projector P1 with the filter RF projects the right images (IMG-R1 and IMG-R2) and the other projector P2 with the filter BF projects the left images (IMG-L1 and IMG-L2). The projectors are synchronised to display during one period Δt the right and the left images of one viewer, for example P1 projects IMG-R1 and P2 projects IMG-L1 for the Viewer 1, and during Δt_{t+1} the right and the left image of the other viewer, P1 projects IMG-R2 and P2 projects IMG-L2 for Viewer 2. Then, the viewers are separated by time and the viewer eyes are separated by color. The shutters of the goggles open and close and the RF is placed on the right shutter of the active goggle and the BF is placed on the left shutter to isolate the eyes from each other. Figure 69 illustrates the Case 3.2.

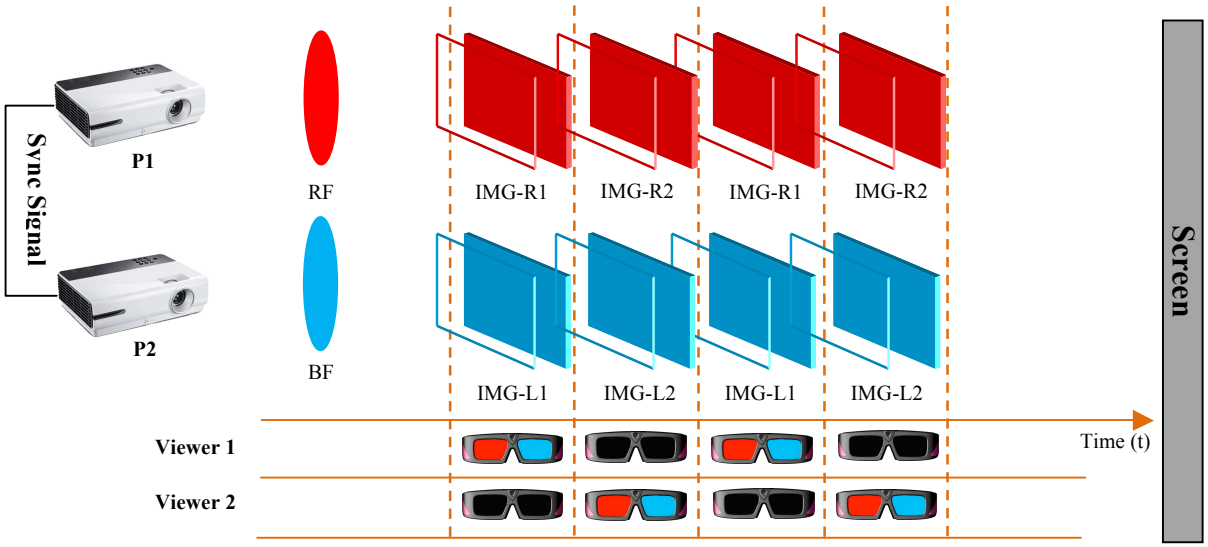

Figure 69 - Case 3.2 with the two projectors synchronised and the goggles opening and closing simultaneously with the red and blue filter on each shutter.

The operational of this case is the same as the Case 2.2, the most important point is how the goggles work. The advantages are the same as for the independent projection, excepting the need to synchronise the two projectors, and the disadvantages in all the cases that uses anaglyph remains the same, the color and consequently the bad image quality that tint the images according to the filters color.

4.1.5. Polarization and Spectral Multiplexing (Case 4)

The next 3D Dual View solution that will be described below mixes polarization and spectral multiplexing. However, it was seen that the anaglyph solution or become expensive due to the narrow band filters trammelling the commercialization, or cheap but with a bad quality increasing the ghosting [7][8], and the color quality is poor. Besides, it is inherent the ghosting effect in the polarization system due to the non ideal polarisers [9], fact that leads all the passive 3D commercial solutions to implement techniques to overcome this issue [10]. Because of this, the section 4.1.5 about the Case 4 was written just to complement and

indicate that it is a possible solution but will not be implemented due to the already cited reasons that leads to a poor image quality.

There are two manners to realize this solution. It can be done separating the viewers by polarization and the viewer eyes by color, or the viewers by color and the eyes by polarization. The only advantages, but not sufficient to put it into practice, is that it uses a regular screen and the goggles are passive. It means that the goggles do not have batteries, the synchronization is not necessary and it is not expensive in comparison with active goggles.

- Polarised Projection (Case 4.1)

The polarised projection separates the viewers by polarization. Thus, using two 3D DLP Link projectors and placing a right circular polarizer (RCP) in front of one projector and a left circular polarizer (LCP) in front of the other projector we encode the 3D stream of each projector in opposite (orthogonal) polarization states. To separate the viewer eyes, each eye's image (IMG-R1, IMG-L1, IMG-R2 and IMG-L2) are encoded using filters of different colors, usually complementary, normally red and blue (cyan). In order to decode only one stream and watch the video from one projector, the viewer should wear special passive goggles. Both lenses of the goggles are made by a polariser, one goggle with RCP and the other with LCP, with a red filter (RF) on top of the polariser in the right side and a blue filter on top of the polariser in the left side. Figure 70 illustrates the Case 4.1.

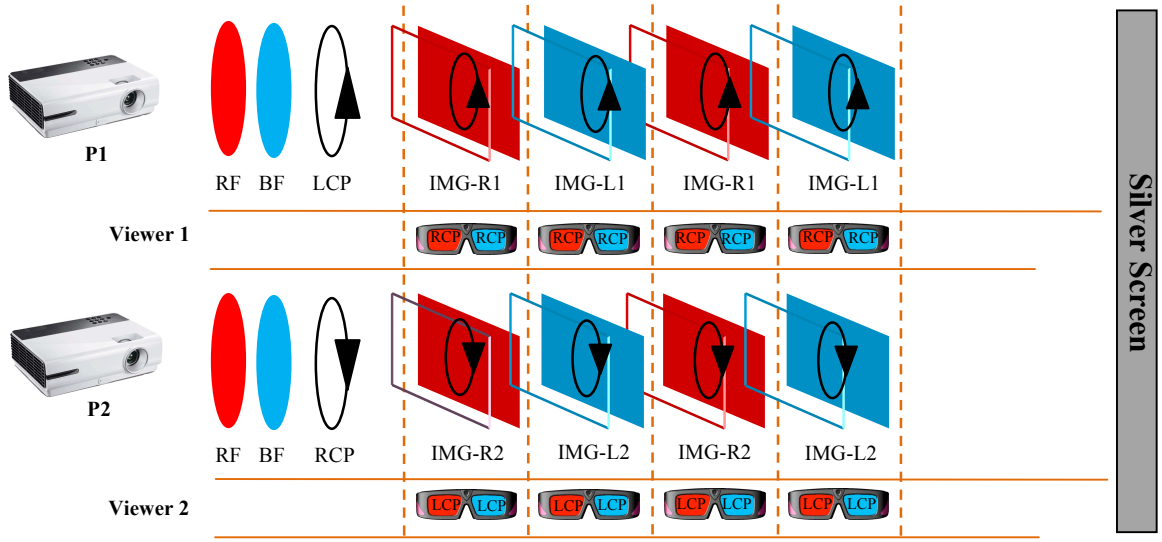

Figure 70 – Scheme of Case 4.1with the passive goggles made with polarisers and color filters.

- Color Projection (Case 4.2)

The case 4.2 is the inverse of the last case (Case 4.1). The color projection separates the viewers by color. Thus, using two 3D DLP Link projectors and placing a red filter (RF) in front of one projector and a blue filter (BF) in front of the other projector we encode the 3D stream of each projector in opposite color. To separate the viewer eyes, each eye's image (IMG-R1, IMG-L1, IMG-R2 and IMG-L2) are encoded using circular polarisers in orthogonal polarization states. To decode only one stream and watch the video from one projector, the viewer should wear special passive goggles. The goggles are different from the Case 4.1.

First, one goggle has a red filter in both lenses and the other a blue filter. Second, instead of placing a RCP in one goggle and a LCP in the other goggle, it is placed a RCP and a LCP in both goggles but each polariser on one lens. Figure 71 illustrates the Case 4.2.

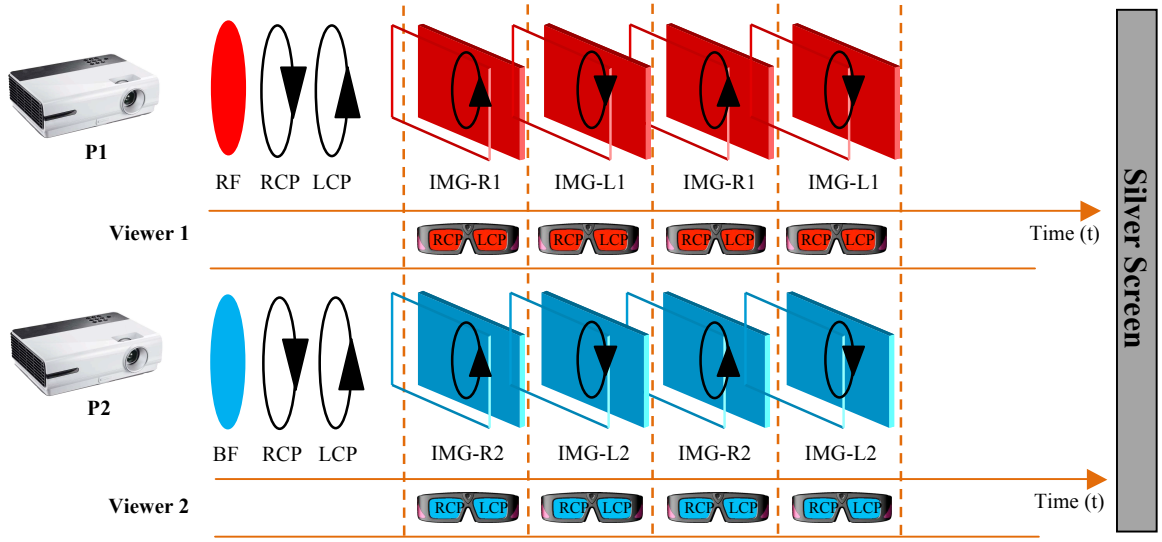

Figure 71 – Illustration of the Case 4.2with the passive goggles made by polarisers and color filters.

Another drawback of the Case 4.2 is that a polarizing modulator [11], like ZScreen [12], has to be added to change the polarization according to the image projected image, increasing the complexity of the system.

4.2. 3D Dual View Setup

We have chosen to implement the 3D Dual View technique for the Case 2.1 and 2.2 because of two main reasons. First, it concerns to the image quality. In this sense, as it was seen before any case that uses color filters (anaglyph), cases 3, 4 and 5, was put a side. Second, it regards to the commercial facilities. The active and passive solution for regular 3D vision already exists on the market. The DLP projectors operating at 120Hz, the screen and the goggles are easily found and can have affordable prices for further commercial applications. However, there are few disadvantages. The existing projection system and the available goggles do not suit all our needs and they have to be modified to accomplish the 3D Dual View.

The 3D Dual View setup is divided in three parts: projection system, projection medium and visualization system. The projection system is composed by the projectors to display the images, an optical setup to transform the light of each projector in circular polarised light and a computer to manage the images and the 3D video streams. The projection medium is the screen and it will be responsible to maintain and to not change the polarization states from the projection system. Finally, we have the visualization system that comprises the 3D Dual View goggles.

Two modes are proposed to implement the technique, the reflective mode that was done by our team at Télécom-Bretagne (TB) and the transmitive mode which was implemented and it

is commercially available from Immersion company. The biggest difference between them is in the visualization system, at TB it is used a screen that reflects the light from the projector to the viewers eyes maintaining the polarization states and at Immersion the screens let the light passes through it without disturbing the polarization states. Still there are some small differences like, the way that the goggles are synchronized and the components which are from different brands. The ghosting effect was measured for the cases 2.1 and 2.2 at Télécom-Bretagne and only the case 2.1 at Immersion, because of technical reason that is explained later. In the next subsections it is described the 3D Dual View setups at Télécom-Bretagne and Immersion showing each part of the whole system in details.

4.2.1. Reflective Mode Setup (Télécom-Bretagne)

The objective of the project at TB is to display two 3D video streams on a silver screen placed on a table for two viewers who stand in front of it to see the same 3D images but from different points of view. The projection system consist of two DLP Link projectors Optoma HD67, two linear polarisers (Thorlabs LPVISE200), two quarter wave-plate films, two fans and one computer with processor Intel Core i7 3.5Ghz, one powerful video card NVidia Quadro 4000 and a software, developed by our team, installed to manage the two 3D video streams. The projectors are connected to the computer with HDMI cables to display the images. The quarter wave-plates (QWP) and the linear polariser (LP) are placed in front of the projectors to circularly polarise the images displayed by the projectors. The fast axis of one QWP are placed at 45° with one linear polariser placed at 0°, to have left handed circular polarization, and the other LP at 90° to have the right handed circular polarization. Since the polarisers plus the QWP have to be close enough to the projectors to cover all the output light, the fans are strategically disposed to avoid overheating and damage the polarization system. The visualization medium is a silver screen Screen-Tech that reflects the light without changing the polarization state from the projection system to the viewers. In section 4.1.2 it was seen that the cases 2.1 and 2.2 use the same configuration setup, the only changes are in how the images are sent to the screen and how the goggles work. Figure 72 shows an overall schematic of the 3D Dual View at Télécom-Bretagne.

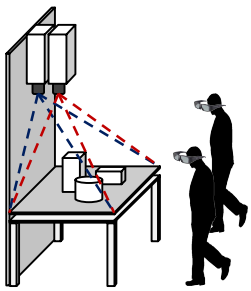

Figure 72 – An overall illustration of the 3D Dual View Setup at Télécom-Bretagne

Thus, to put the projectors and the circular polariser in a vertical position with respect to the silver screen, as it can be seen in the figure above, one support for the projector plus the polarization system was designed and realized by our group (Figure 73). The support is able

to move in θ and φ to align the displayed images on the screen.

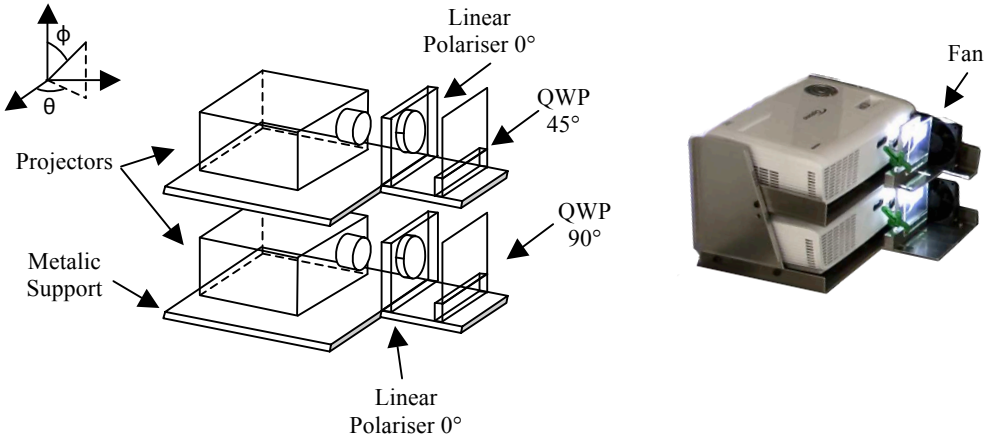

Figure 73 – The schemnatic and the picture of the projector and polarization system with the fans to avoid overheating of the polarisers and the QWP.

The visualization system is composed by active goggles plus a QWP stick on it to make active goggles with circular polariser and a photodetector to synchronize the goggles with the DLP Link projectors. For the case 2.1 the QWP is stick on the left shutter with the fast axis at 45° with respect to the front linear polariser, to have an active left handed circular polariser, and on right shutter at -45° to have an active right handed circular polariser. The case 2.2 both shutters of one goggle have the same circular polarisers. Then, the QWP fast axis is stick on the left and on the right shutter at 45° in one goggle and at -45° in the other goggle. **Figure 74** shows the goggles for the case 2.1 and 2.2.

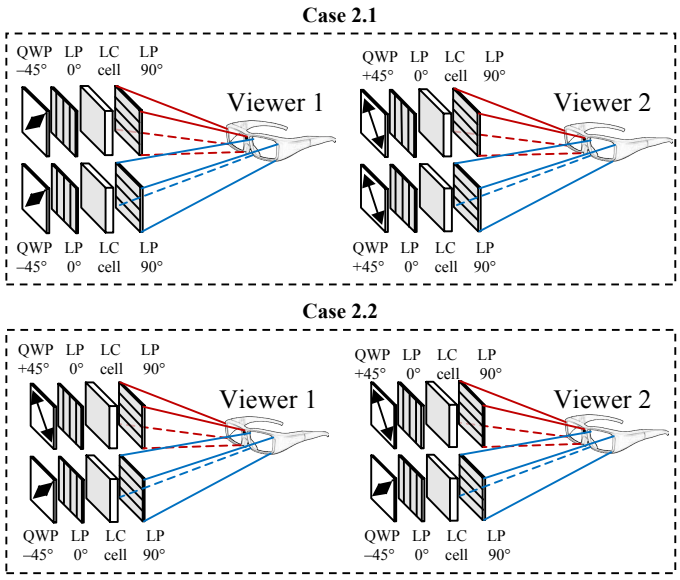

Figure 74 – 3D glasses configuration for the cases 2.1 and 2.2.

The goggles synchronization is made by the DLP Link projector and a photodetector mounted on the goggles. In fact, the DLP projector sends, during the darktime, a flash light to the screen that reflects on it reaching the photodetector, triggering a circuit which command the shutters to open and close at the right time according to the displayed image. The advantage is that DLP Link projector does not need an external emitter to synchronise the goggles with the

videos streams. Furthermore, the 3D Dual View for the case 2.1 requires that one goggle (Viewer 1) have to be synchronised with one projector (P1) and the other goggles (Viewer 2) with the other projector (P2). First, we have tried to put orthogonally circular polariser in front of each photodetector goggles and synchronise them separately. The projector (P1) signal synchronising the Viewer 1 and the projector (P2) signals the Viewer 2. However, because of the weak depolarization of the screen, the goggles were detecting both signals and the shutters were opening and closing at the wrong moment. The solution that we choose was to synchronise the projector putting the flash light of the projectors in phase. This was done via software. The program that controls the video streams starts the projection in phase and consequently the synchronisation signal.

4.2.2. Transmissive Mode Setup (Immersion)

The two main features of the 3D Dual View setup at Immersion are the screen and the synchronization of the goggles. There it is used a transmissive screen disposed horizontally on a table with the two projectors under it to display the two 3D images for two viewers standing in opposite sides of the table. The projection system consist of two DLP Link projectors, two circular polarisers (right and left handed), a computer, one powerful video cards and a software developed by Immersion that manages the two 3D video streams. The projectors are also connected to the computer with HDMI cables to display the images and the circular polarisers are placed in front of it. A ventilation system was installed to avoid overheating and damage the projection lamp and the polarization system. The visualization medium is a transmissive screen that let the light pass through it without changing the polarization state from the projection system to the viewers. Figure 75 shows an overall schematic of the 3D Dual View at Immersion.

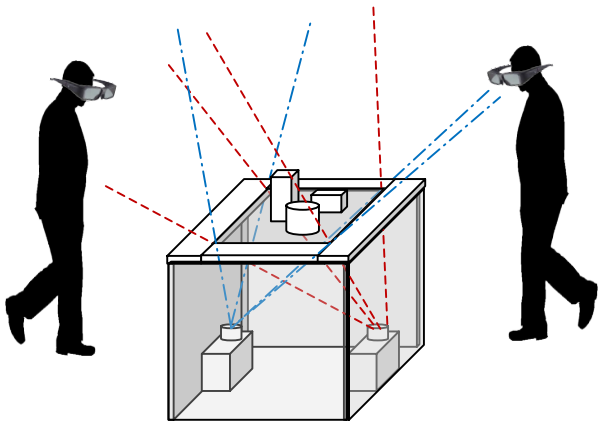

Figure 75 – 3D Dual View setup at Immersion.

The goggles synchronization at Immersion is made by the infrared emitters. The emitters are synchronised with the projectors and send a signal to the goggles which have an infrared photodetector on it. The goggles are triggered and the shutters open and close according to the displayed image.

4.3. Ghosting Effect Measurements

Crosstalk is a critical factor that impacts the image quality for stereoscopic 3D vision [13], and causes visual discomfort [14]. Also known as ghosting, the effect can make the 3D images hard to fuse, lacking in fidelity. Hence, it is crucial in the development of a high quality 3D system, to achieve low levels of crosstalk. It was seen in Chapter 2 that in regular 3D systems the crosstalk, or ghosting, is the leakage of the left image into the right eye and the right image into the left eye due to an incomplete isolation of the right and left channels (2D video streams). However, in the 3D Dual View the crosstalk becomes worst and even more complicate to measure and compensate, because it deals with two 3D streams, which means four 2D video streams. Thus, not only the left and right eyes of one viewer should be isolated, but also the left and right eyes of the second viewer. The images intended to one viewer cannot interfere in the images of the other viewer and vice versa.

The quality of the 3D Dual View is strongly related to the levels of crosstalk. Then, it is necessary to measure the ghosting effect in order to compensate it. It is already published in the literature several methods, simple or complex, to measure the crosstalk in stereoscopic system and also techniques to compensate. It can be done qualitatively using Test Charts [15], or quantitatively using CCD cameras [16]. Qualitatively, one test charts is sent through one video channels and a gray level scale is sent through the other video channel and the viewer compares the gray level which are leaking with the scale. Quantitative, it is used cameras and image treatment to evaluate "how much" of one image is interfering in the other image. All of them are based on the same idea: the stereo streams display static images containing a bright zone and a grey scale. For each image the bright region is placed in a distinct part of the display and the grey scale goes along the whole bright region of the other image in order to evaluate the crosstalk leakage by direct comparison. We implemented a similar technique to mitigate the crosstalk effects. The four static images we used are presented in Figure 76

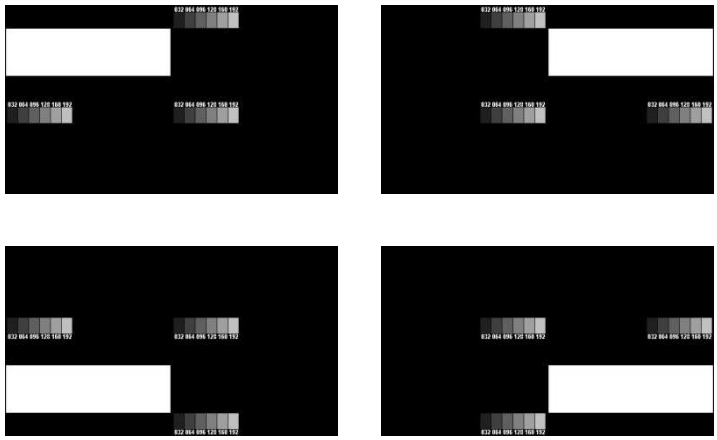

Figure 76 - The four test charts used for test ghosting evaluation

For each one, the bright region is in a distinct corner. Without glasses, the image of the screen is a simple superimposition of the four images, as seen in the Figure 77. A few photometric measures have been required to balance the luminance and color temperature of projectors.

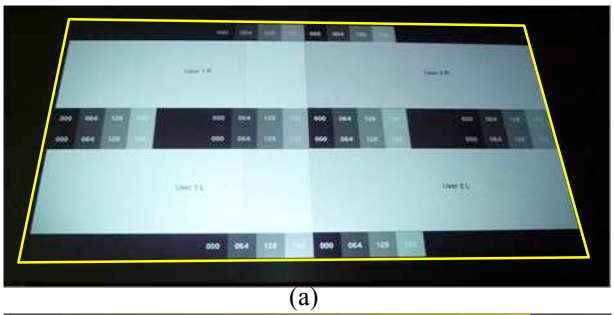

(a)

(b)

Figure 77 - Superimposition of four video streams on the screen (left picture) and one of the decoded streams (right picture, taken through the glasses).

Using appropriate glasses, each video stream could be decoded but, due to the crosstalk effect, the decoded stream contains leakage traces of the three others. As we can see in Fig.8, the evaluation of the ghosting ratio can be done for each stream by a simple comparison of the ghost images with the neighboring grey scales, which are placed here for reference.

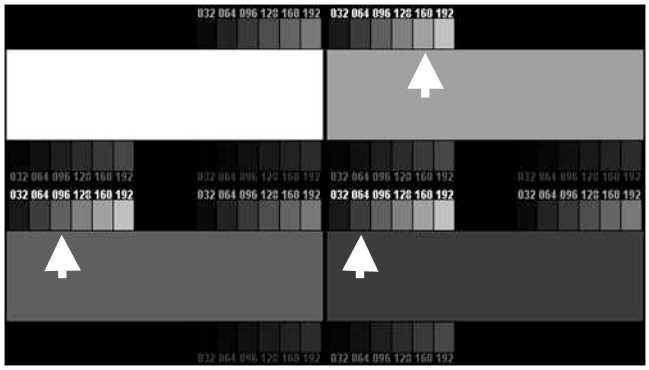

Figure 78 - Evaluation of Ghosting Ratio using direct comparison for the decoded stream. In this example, the upper left white stripe and the 3 other grey scales are displayed by the image that is correctly decoded, while all the other content is a consequence of the actual ghost issue.

For applications where the viewers are located far from the screen and the viewing angle do not change much (home TV for example), this simple technique allows a fast evaluation of the ghosting. Its main drawback is the fact that ghosting evaluations are made at different points of the screen. If we want to let the viewers free to walk around the screen, the Ghosting Ratio should be assessed for each point of the screen and for each possible position of the viewers, position that is described by polar angles. In addition, human eyes are non-linear sensors with color sensitivity and dependence between the light perception and the light intensity that is far from linear. Not only the eye shows a spectral sensitivity but the sensitivity changes when the light intensity changes. For all these reasons, we developed a more dedicated ghosting ratio evaluation methodology taking into account those specificities.

In this thesis it is proposed a simple method to measure the ghosting using a chromometer attached to a mechanical arm to evaluate the crosstalk for different angles, polar angle (φ) and azimuth angle (φ). However, before showing the experimental setup and the results it is necessary to introduce the concept of Ghosting Ratio.

4.3.1. Ghosting Ratio

The ghosting or crosstalk can be used as a metric to express how much leakage occurs in a stereoscopic system display. This metric is called by some authors as "crosstalk ratio", or ghosting ratio [17][18]. There are in the literature many mathematical definitions for the crosstalk ratio. Chu, et al defined the crosstalk as [19]:

$$Crosstalk = \frac{luminance - measured - at - one - eye}{luminance - measured - at - the - other - eye} \tag{4.1}$$

Hong, et al provides this definition calculating the ghosting ratio using one test image consisting of black data for the even horizontal lines and white data for the odd horizontal lines, and one test image of black data for the odd horizontal lines as white data for even horizontal lines. The ratio of the luminance of these two images was called by them as 3-D crosstalk [20]. The issues of this definition is that it is not included the effect of black level. There are some projectors which are unable to outputting zero luminance for the full black. Nevertheless, some author takes into consideration the non-zero black level subtracting the black level luminance [21]. Normally, black and white images are used in the measurements using the second definition. In this thesis is proposed a slightly different definition as it will be seen it.

Digital image processing is based on the use of grey-scales. Generally, grey-scales are chosen to ensure for each grey level a proportional level of light perception. Due to the eye non-linear response, the relation between the light intensity and the perceived grey level is given by a Gamma curve. This is why we measured, for each projector, the dependence of the light intensity (I) on the grey level (n_g) of the displayed image to determine the γ values, approximated by $I = a \cdot n_g^{\gamma}$. Measures have been made with an ISO-Tech 1335 light-meter, in a dark room, to avoid any influence of the external light. Our experiments have shown that $\gamma = 2.0 \pm 0.04$ for each primary color (red, green, blue). As shown later on, this value simplifies the evaluation of the ghosting ratio.

Due to the crosstalk, the leaking image having a gray level $n_{IMG-LKG}$ will produce a ghosting which is equivalent to a gray level $n_{IMG-MAIN}$ of the main image. Fig.9 gives an example of the luminance curves of the main image represented by the continuous curve and one of the three leaking images (dashed curve).

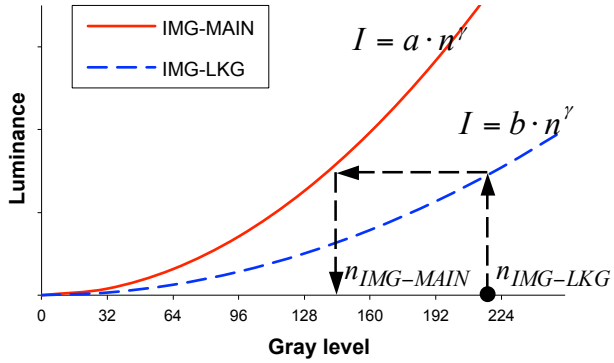

Figure 79 - Example of Gamma curve of the main (continuous) and leaking image (dashed line).

In the particular case when the luminance dependence on the gray level follows a Gamma curve for each stream, we obtain:

$$I_{SHT} = a \cdot n_{IMG-MAIN}^{\gamma} = b \cdot n_{IMG-LKG}^{\gamma} \tag{4.2}$$

where a and b are constants and n is the gray level of each displayed image. Then, the ratio between the two gray levels is a constant, allowing to predicting for all gray levels of the leaking image the effect on the main image. We define for each pair of video streams the Ghosting Ratio (GR) as:

$$GR = \frac{n_{IMG-MAIN}}{n_{IMG-LKG}} = \sqrt[\gamma]{b/a} \tag{4.3}$$

The subunitary value of GR depends on the quality of stream separation. Therefore, it should be reciprocal: this means the GR from a first video stream to a second one should be the same as the GR from the second to the first one.

The definition of ghosting ratio is in agreement with Chu, et al but adapted to the 3D Dual View setup and with the experiments that were done. In the next section it will be explained and demonstrate the experimental setup which were used to measure the ghosting ratio with respect to different viewing angles to map the ghosting for the reflective mode (Télécom-Bretagne) and the transmissive mode (Immersion).

4.3.2. Experimental Setup for Ghosting Evaluation (Télécom-Bretagne)

To measure the ghosting and its angle dependence the chromameter Minolta CS-100 was placed on an arm. The arm was designed and fabricated by our team allowing the device to move and measure the crosstalk in all the possible relevant view angles established by the 3D Dual View setup in reflective mode (Télécom-Bretagne) and transmissive mode (Immersion). Figure 80 shows a schematic of the arm and a picture of the chromometer attached to the arm.

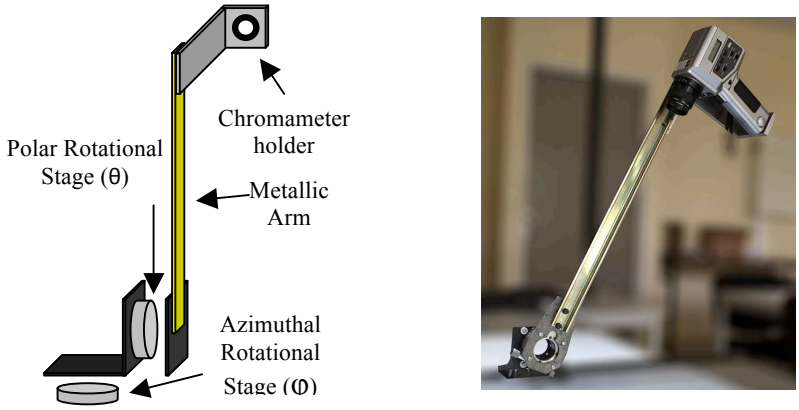

Figure 80 – The schematic and the picture of the chromometer support with the chromameter.

The rotational stages in θ, polar angle, allows the arm to move between 90° and 0° degree and the rotational stage in φ, azimuthal angle, between -180° and 180° degrees. The chromometer is placed on a metalic support fixed at the end of the yellow arm and fixed with a screw thread to not move during the experiments. The chromameter support was fixed on a metallic surface which was put on the table where the experiments were taken place. Figure 81 demonstrates how the chromameter covers all the relevant angles, how it can measure the reflected luminance of the projectors at a fixed point on the silver screen and the projectors illuminating the silver screen with the chromameter on it.

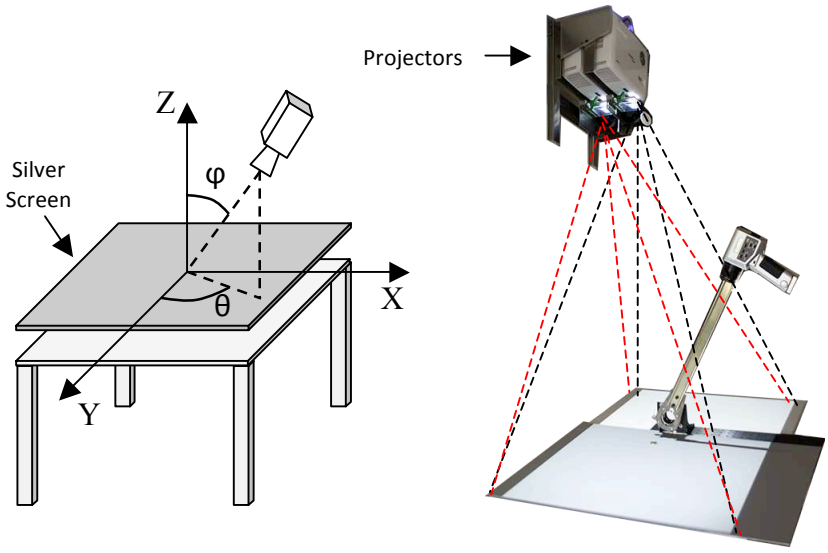

Figure 81 – The chromameter, the projectors and the silver screen at Télécom-Bretagne.

To qualitatively evaluate the ghosting it is necessary to place one shutter in front of the chromameter and measure the light that passes through it, which is leaking from the undesirable images. For example, to measure the ghosting in the SHT-R2 (right shutter of the Viewer 2) due to IMG-L1, we project only the IMG-L1 on the screen and measure the light that passes through the SHT-R2. This measurement is the amount of light from the IMG-L1 that is leaking through the shutter SHT-R2. Thus, four types of luminance measurements are done for the case 2.1:

- *Type 1 :*

It is projected only the IMG-R2, the main image of the shutter SHT-R2, on the screen and it is measured the luminance through the SHT-R2. In that case, the SHT-R2 is open and the image has the same polarization as the shutter. In this case, it is measured the luminance which is not a leakage, but the useful amount of light for that shutter (Figure 82).

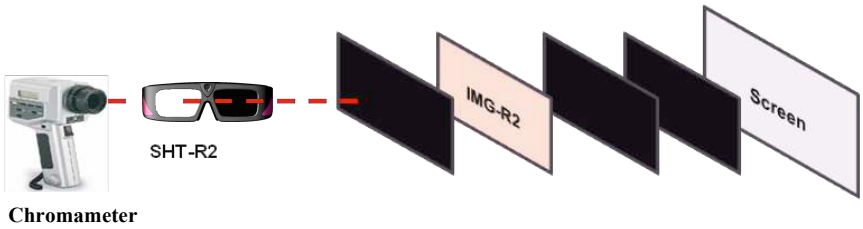

Figure 82 – Illustration of the the measurement Type 1 (luminance).

- *Type 2 :*

It is projected only the image IMG-R1, image designated to the right eye of viewer 1, on the screen and it is measured the luminance through the SHT-R2. In that case, the SHT-R2 is in the opposite polarization and the SHT-R2 is open. Thus, it is measured the ghosting by polarization (Figure 83).

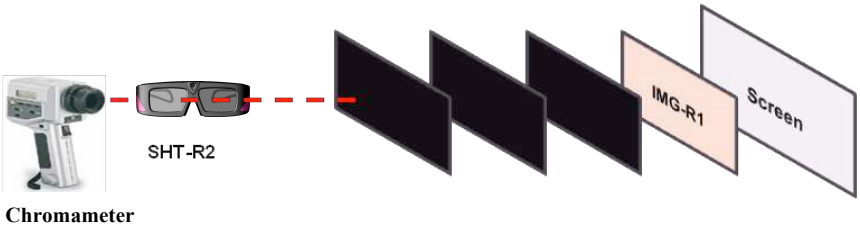

Figure 83 - Illustration of the the measurement Type 2 (polar-ghosting).

- *Type 3 :*

It is projected the image IMG-L2 and it is measured the luminance through the shutter SHT-R2. The image and the shutter are in the same polarization but the shutter is closed. Then, it is measured the ghosting due timing (Figure 84).

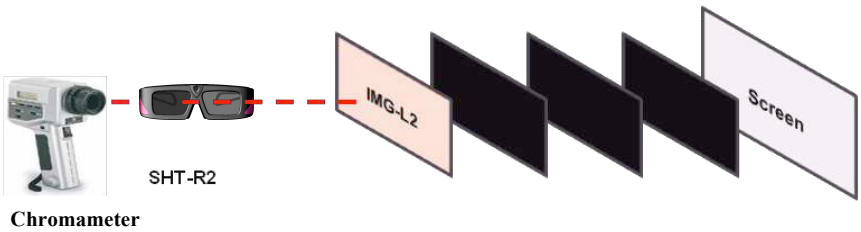

Figure 84 - Illustration of the the measurement Type 3 (time-ghosting).

- *Type 4 :*

It is projected the image IMG-L1 and it is measured the luminance through the shutter SHT-R2. The image is encoded in the opposite polarization as the shutter, and the SHT-R2 is closed. It is measured the ghosting by time and polarization (Figure 85).

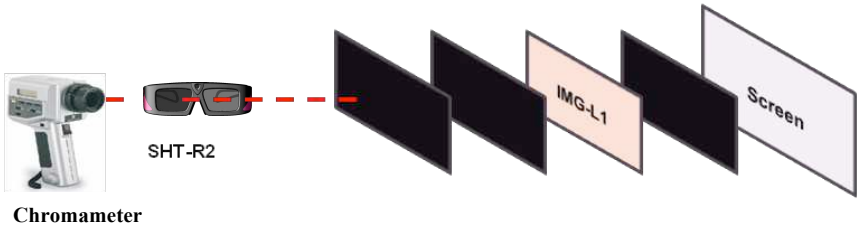

Figure 85 - Illustration of the the measurement Type 4 (polar-time ghosting).

In the following section it will be seen that the ghosting was measured for all the three additive colors red (R), green (G), blue (B) and the white (W) at different viewing angles. Then, all the four types of measurements were done for each color. The aim is to know which color introduces more ghosting to the system and the dependence according to the view angle.

4.3.3. Reflective Mode Results (Télécom-Bretagne)

The ghosting ratio (GR) is calculated after doing the four types of measurements described in the last section. The images are projected one at a time, varying the gray level from 0 to 255 and the luminosity is measured through one shutter with the chromometer Minolta. Notice that it is presented the result of the ghosting of only one shutter (SHT-R2), because the results in the other shutters have been the same. The ghosting ratio has been measured for the red, green, blue and white colors and for the angles: φ equal to -90°, -60°, -30°, -0°, 30°, 60°, 90° and θ equal to 30°, 60° and 90°. Also, the light distribution reflected by the silver screen is measured to help the analysis of the ghosting effect. All the obtained curves have been approximated a parabola to calculate the coefficients *a* and *b* of the ghosting ratio. The measurements were done in complete darkness. To give an example, Figure 86 show the curves of the luminance passing through the shutter versus the gray level for the white color with the chromameter pointing to the centre of the silver screen with the mechanical arm at θ=0° and φ=45°, the luminance passing through the shutter SHT-R2 due to the IMG-R1 (Type 2 – polarization ghosting), the luminance due to the IMG-L2 (Type 3 – timing ghosting) and due to the IMG-L1 (Type 4 – timing and polarization ghosting).

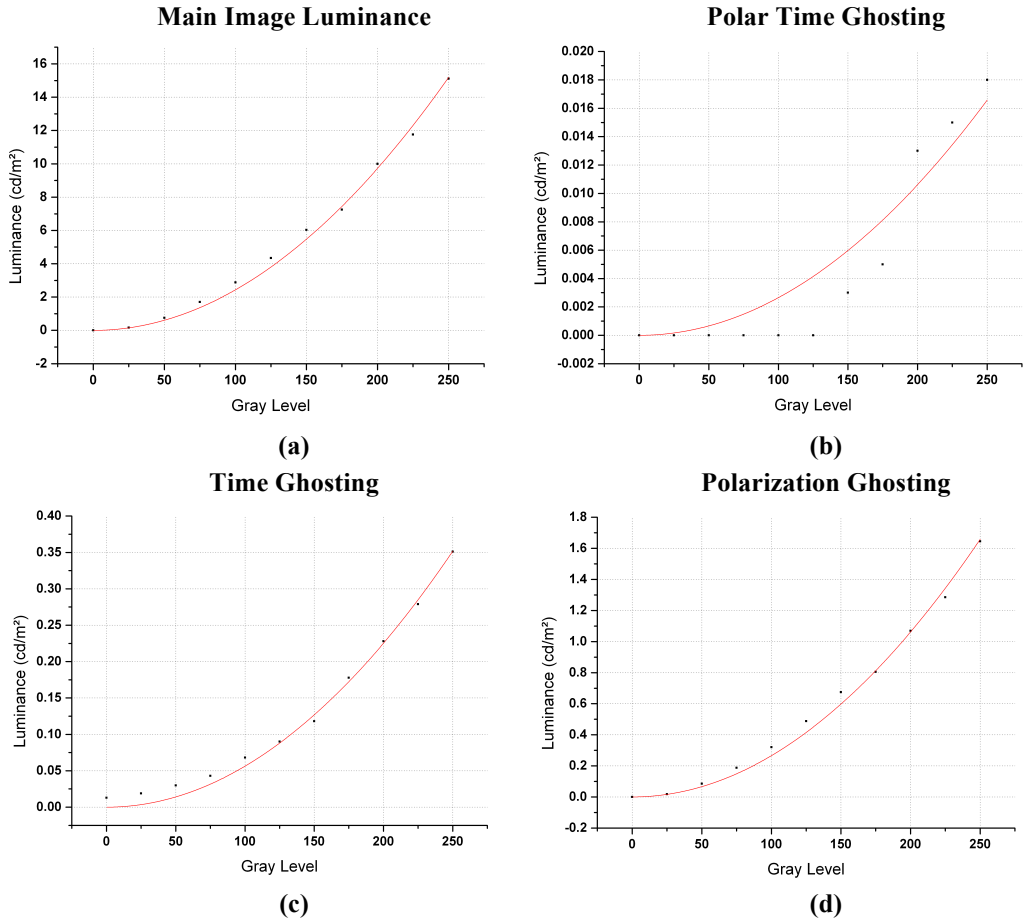

Figure 86 – (a) The luminance of the main image, (b) the polar and timing ghosting, (c) the timing ghosting, (d) and the polar ghosting for the white color at versus the gray level for the white color measured at φ=0° and θ=45° (b).

After, fitting the curves (Figure 86) with a Gamma function and using Equation 4.3, three ghosting ratios are calculated, the polarization ghosting ration (GRP), the timing ghosting ratio (GRT) and the polar-time ghosting ratio (GRPT). In the case above (Figure 86), the ghosting ratio for the white color at θ=0° and φ=45° are: GRP=0,338, GRT=0,087 and GRPT=0,033.

The measurements were made for the listed colors (RGB) and for four projected images. Due to the quantity of data to be retrieved, the experiment with the Minolta CS-100 was impossible to perform manually. A software was developed to synchronize the chromameter with the system projection. The images were projected sequentially varying the gray level and the chromameter was measuring each image while they were being displayed. The data were automatically saved in a text file for further analysis. Only the mechanical arm to change the angles and the alignment of the chromameter, to be sure that it was pointing to the same location, was done manually. The text files with the saved data, the curves, were analysed and fitted using the software Origin (release 6.0).

- Case 2.1 Results (Independent Projection)

It is presented the result obtained at Télécom-Bretagne (TB) for the Case 2.1, where the viewers are separated by polarization and the viewer's eyes by time. Reminding that the shutters open and close alternately, they have the same polarisers on it, the right shutter with a RCP and the left shutter with a LCP, and each projector displays the images for one viewer.

The results are organised by colors; for each color there are four results: the luminance (Type 1) and the ghosting ratio as a function of the angles (θ and φ) due to the polar-ghosting (Type 2), time ghosting (Type 3), and polar-time ghosting (Type 4). The results are in the format of a table, with the numerical value of the ghosting ratio for each Type, and plotted as a surface to map and interpret the results easily.

○ Red (R) - Case 2.1 (Télécom-Bretagne)

Luminance

θ\ϕ	-90	-60	-30	0	30	60	90
0	7,415	5,478	4,483	4,368	4,268	3,893	4,185
30	3,593	3,005	4,128	3,900	2,363	2,110	1,895
45	1,138	1,773	2,468	2,275	1,568	1,223	1,075
60	0,705	1,253	1,463	1,248	1,053	0,823	0,700

Table 9 – The red color luminance values with respect to θ and φ (Case 2.1 – TB)

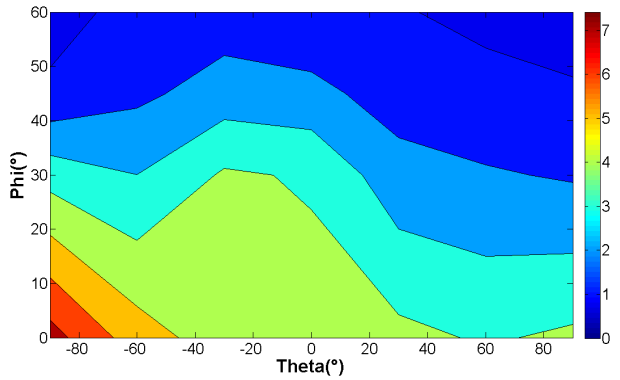

Figure 87 – The red color luminance distribution with respect to θ and φ (Case 2.1 – TB)

Polar Ghosting Ratio

θ\ϕ	-90	-60	-30	0	30	60	90
0	0,191	0,306	0,349	0,337	0,274	0,270	0,256
30	0,240	0,271	0,273	0,341	0,385	0,363	0,313
45	0,363	0,351	0,333	0,393	0,443	0,438	0,413
60	0,455	0,402	0,410	0,451	0,518	0,533	0,514

Table 10 – The red color polar-ghosting ratio values with respect to θ and φ (Case 2.1 – TB)

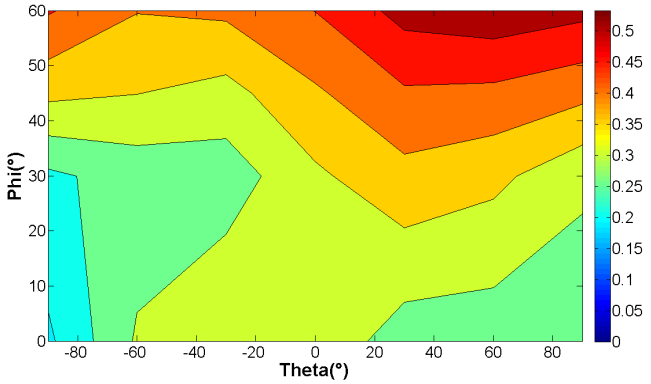

Figure 88– The red color polar-ghosting ratio with respect to θ and φ (Case 2.1 – TB)

Time Ghosting Ratio

θ\ϕ	-90	-60	-30	0	30	60	90
0	0,094	0,078	0,063	0,076	0,068	0,068	0,069
30	0,065	0,070	0,089	0,086	0,060	0,054	0,033
45	0,000	0,070	0,070	0,070	0,037	0,022	0,000
60	0,000	0,000	0,020	0,000	0,000	0,000	0,000

Table 11 – The red color time-ghosting ratio values with respect to θ and φ (Case 2.1 – Télécom Bretagne)

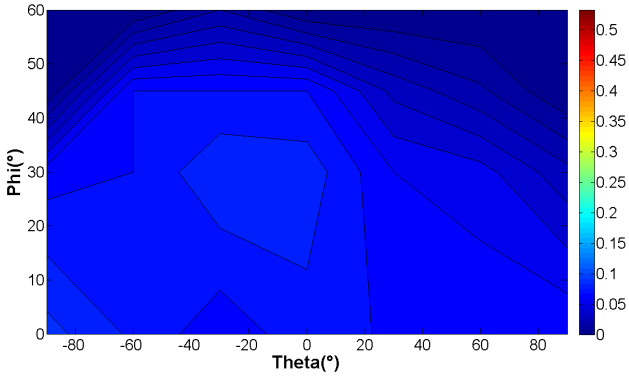

Figure 89 - The red color time-ghosting ratio with respect to θ and φ (Case 2.1 – TB)

Polar Time Ghosting Ratio

θ\ϕ	-90	-60	-30	0	30	60	90
0	0,052	0,043	0,033	0,059	0,059	0,129	0,089
30	0,000	0,000	0,032	0,046	0,023	0,000	0,000
45	0,000	0,000	0,000	0,019	0,000	0,000	0,000
60	0,000	0,000	0,000	0,000	0,000	0,000	0,000

Table 12 – The red color polar-time ghosting ratio values with respect to θ and φ (Case 2.1 – Télécom Bretagne)

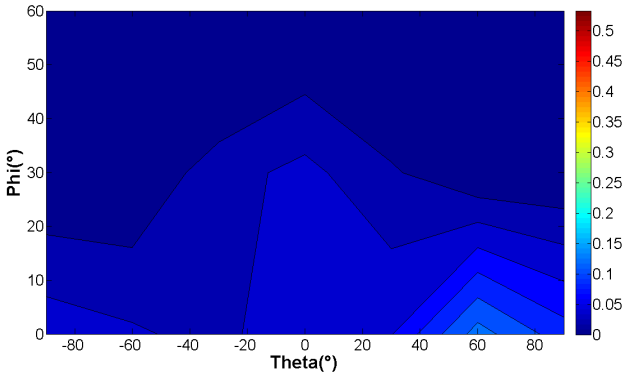

Figure 90 - The red color time-ghosting ratio with respect to θ and φ (Case 2.1 – TB)

○ Green (G) - Case 2.1 (Télécom-Bretagne)

Luminance

θ\ϕ	-90	-60	-30	0	30	60	90
0	21,070	15,890	13,390	13,160	12,510	10,890	11,870
30	9,093	8,313	11,630	11,670	7,030	6,265	5,305
45	3,213	4,920	6,933	6,890	4,638	3,615	3,055
60	2,008	3,485	4,035	3,755	3,143	2,398	2,010

Table 13 – The green color luminance values with respect to θ and φ (Case 2.1 – TB)

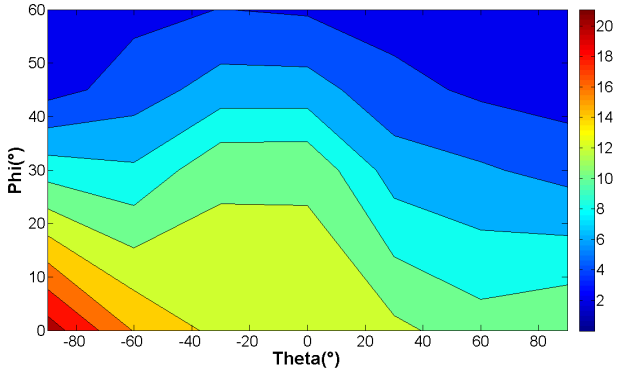

Figure 91 – The green color luminance distribution with respect to θ and φ (Case 2.1 – TB)

Polar Ghosting Ratio

θ\ϕ	-90	-60	-30	0	30	60	90
0	0,188	0,240	0,255	0,247	0,237	0,272	0,246
30	0,273	0,263	0,255	0,259	0,296	0,300	0,320
45	0,382	0,350	0,322	0,329	0,369	0,388	0,421
60	0,479	0,419	0,412	0,405	0,455	0,495	0,517

Table 14 – The green color polar-ghosting ratio values with respect to θ and φ (Case 2.1 – TB)

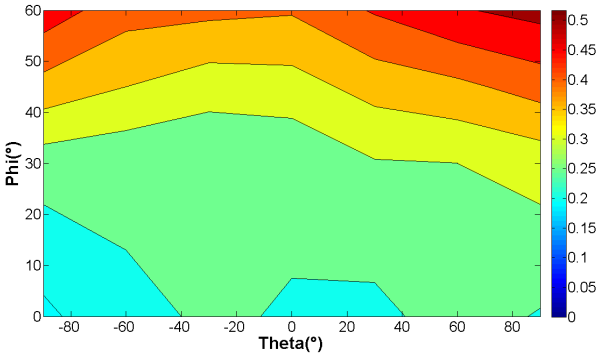

Figure 92 – The green color polar-ghosting ratio with respect to θ and φ (Case 2.1 – TB)

Time Ghosting Ratio

θ\ϕ	-90	-60	-30	0	30	60	90
0	0,092	0,083	0,086	0,086	0,089	0,083	0,089
30	0,092	0,089	0,100	0,098	0,091	0,094	0,081
45	0,067	0,103	0,092	0,090	0,079	0,079	0,063
60	0,031	0,081	0,081	0,072	0,066	0,061	0,050

Table 15 – The green color time-ghosting ratio values with respect to θ and φ (Case 2.1 – Télécom Bretagne)

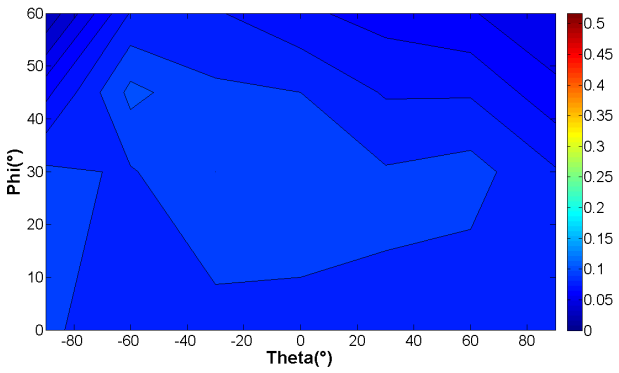

Figure 93 – The green color time-ghosting ratio with respect to θ and φ (Case 2.1 – TB)

Polar Time Ghosting Ratio

θ\ϕ	-90	-60	-30	0	30	60	90
0	0,038	0,035	0,037	0,048	0,051	0,097	0,079
30	0,024	0,021	0,031	0,043	0,030	0,014	0,000
45	0,000	0,017	0,025	0,030	0,000	0,000	0,000
60	0,000	0,000	0,000	0,017	0,000	0,000	0,000

Table 16 – The green color polar-time ghosting ratio values with respect to θ and φ (Case 2.1 – Télécom Bretagne)

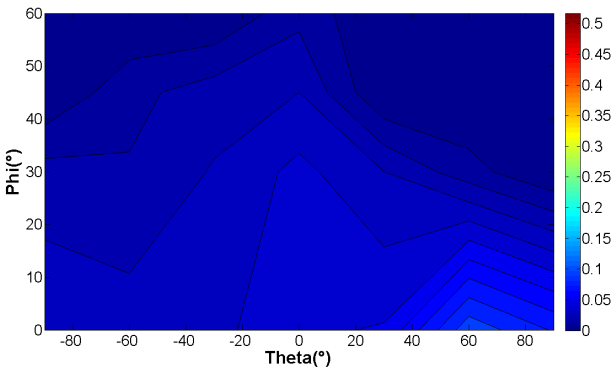

Figure 94 – The green color polar-time ghosting ratio with respect to θ and φ (Case 2.1 – TB)

○ Blue (B) - Case 2.1 (Télécom-Bretagne)

Luminance

θ\ϕ	-90	-60	-30	0	30	60	90
0	4,183	3,150	2,268	2,628	2,460	2,140	2,335
30	2,310	1,603	2,263	2,325	1,395	1,243	1,035
45	0,625	0,930	1,355	1,380	0,920	0,715	0,588
60	0,383	1,603	0,783	0,743	0,623	0,473	0,383

Table 17 – The blue color luminance values with respect to θ and φ (Case 2.1 – TB)

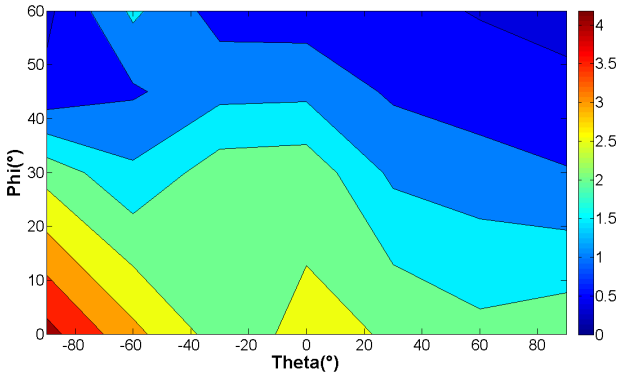

Figure 95 – The blue color luminance distribution with respect to θ and φ (Case 2.1 – TB)

Polar Ghosting Ratio

θ\ϕ	-90	-60	-30	0	30	60	90
0	0,206	0,238	0,297	0,285	0,273	0,265	0,225
30	0,224	0,254	0,245	0,276	0,303	0,311	0,312
45	0,352	0,330	0,305	0,337	0,361	0,377	0,392
60	0,433	0,391	0,388	0,402	0,431	0,460	0,479

Table 18 – The blue color polar-ghosting ratio values with respect to θ and φ (Case 2.1 – TB)

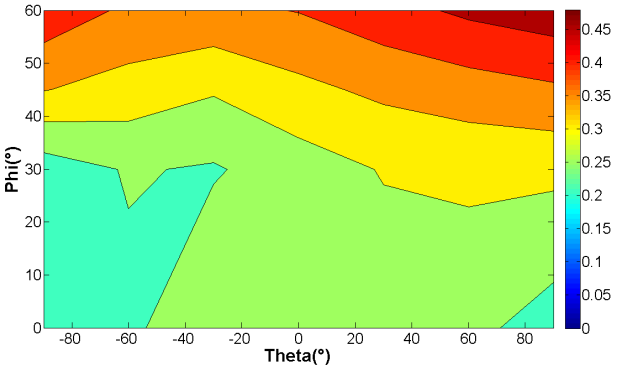

Figure 96 – The blue color polar-ghosting ratio with respect to θ and φ (Case 2.1 – TB)

Time Ghosting Ratio

θ\ϕ	-90	-60	-30	0	30	60	90
0	0,105	0,085	0,076	0,076	0,073	0,068	0,075
30	0,073	0,060	0,085	0,091	0,043	0,058	0,034
45	0,000	0,036	0,055	0,071	0,000	0,041	0,000
60	0,000	0,000	0,000	0,402	0,000	0,000	0,000

Table 19 – The blue color time-ghosting ratio values with respect to θ and φ (Case 2.1 – TB)

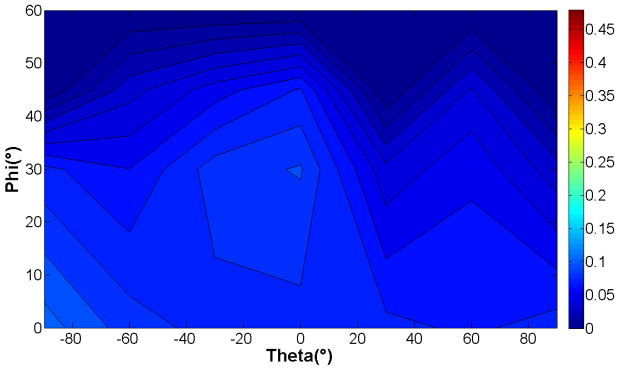

Figure 97 – The blue color time-ghosting with respect to θ and φ (Case 2.1 – TB)

Polar Time Ghosting Ratio

θ\ϕ	-90	-60	-30	0	30	60	90
0	0,064	0,040	0,047	0,044	0,035	0,084	0,059
30	0,002	0,022	0,049	0,062	0,000	0,000	0,000
45	0,000	0,000	0,000	0,000	0,000	0,000	0,000
60	0,000	0,000	0,000	0,000	0,000	0,000	0,000

Table 20 – The blue color polar-time ghosting ratio values with respect to θ and φ (Case 2.1 – TB)

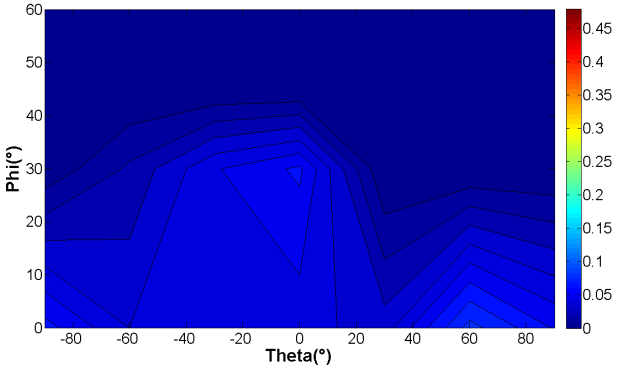

Figure 98 – The blue color polar-time ghosting ratio with respect to θ and φ (Case 2.1 – TB)

○ White (W) - Case 2.1 (Télécom-Bretagne)

Luminance

θ\ϕ	-90	-60	-30	0	30	60	90
0	22,630	34,850	29,340	28,740	27,230	24,160	26,060
30	21,340	18,310	25,490	25,320	15,370	13,710	11,680
45	7,108	10,750	15,260	15,110	10,190	7,905	6,728
60	4,428	7,701	8,933	8,213	6,880	5,258	4,443

Table 21 – The white color luminance values with respect to θ and φ (Case 2.1 – TB)

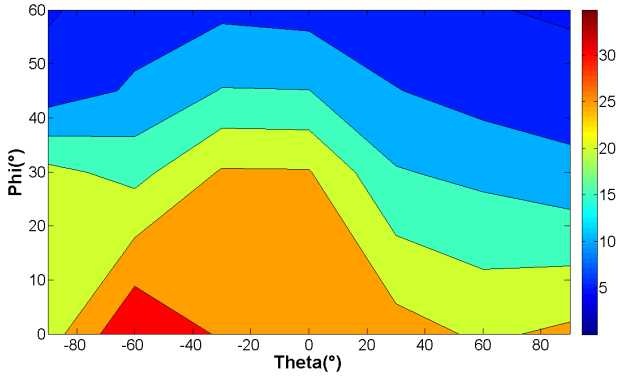

Figure 99 – The white color luminance distribution with respect to θ and φ (Case 2.1 – TB)

Polar Ghosting Ratio

θ\ϕ	-90	-60	-30	0	30	60	90
0	0,270	0,249	0,267	0,267	0,247	0,268	0,245
30	0,249	0,262	0,254	0,273	0,313	0,311	0,319
45	0,372	0,348	0,320	0,338	0,380	0,396	0,417
60	0,475	0,414	0,408	0,414	0,463	0,500	0,513

Table 22 – The white color polar-ghosting ratio values with respect to θ and φ (Case 2.1 – TB)

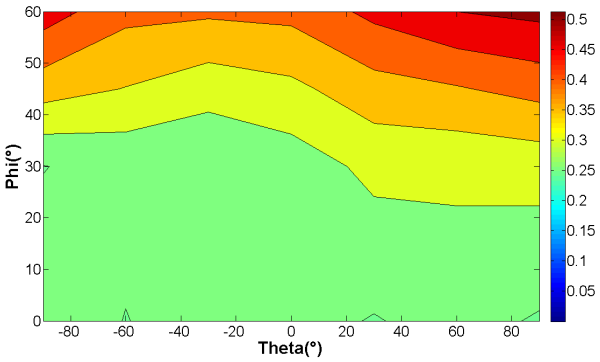

Figure 100 – The white color polar-time ghosting ratio with respect to θ and φ (Case 2.1 – TB)

Time Ghosting Ratio

θ\ϕ	-90	-60	-30	0	30	60	90
0	0,125	0,079	0,076	0,078	0,081	0,079	0,080
30	0,073	0,087	0,096	0,095	0,092	0,089	0,080
45	0,073	0,108	0,095	0,087	0,083	0,091	0,057
60	0,064	0,092	0,082	0,075	0,075	0,069	0,073

Table 23 – The white color time-ghosting ratio values with respect to θ and φ (Case 2.1 – TB)

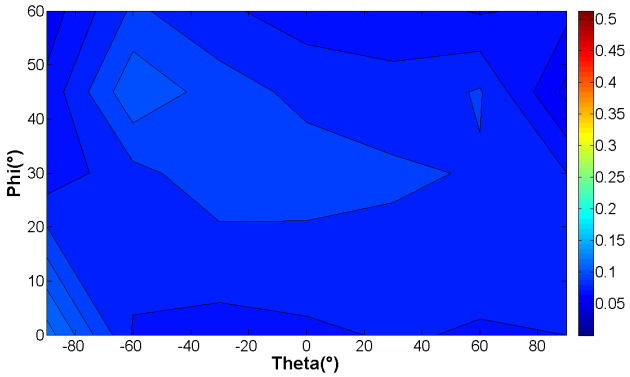

Figure 101 – The white color time-ghosting ratio with respect to θ and φ (Case 2.1 – TB)

Polar Time Ghosting Ratio

θ\ϕ	-90	-60	-30	0	30	60	90
0	0,049	0,031	0,026	0,046	0,051	0,119	0,078
30	0,020	0,027	0,032	0,036	0,028	0,021	0,022
45	0,013	0,023	0,029	0,033	0,024	0,023	0,000
60	0,016	0,016	0,018	0,019	0,017	0,020	0,016

Table 24 – The blue color polar-time ghosting ratio values with respect to θ and φ (Case 2.1 – TB)

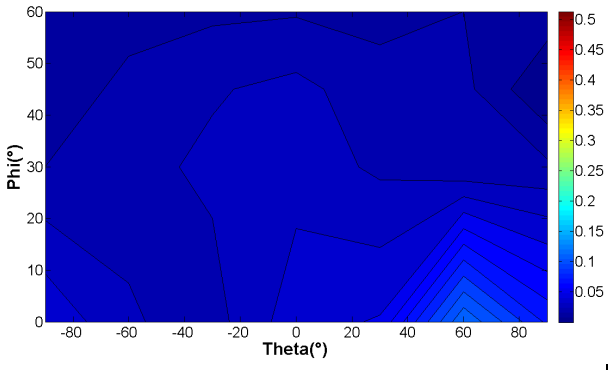

Figure 102 – The white color polar-time ghosting ratio with respect to θ and φ (Case 2.1 – Télécom Bretagne)

It was expected that the luminance measured for each color were different, because the projectors are balanced to match with the eye sensitivity. Also, the results have shown that the ghosting by polarization is the most important followed by the time-ghosting and the polar-time ghosting. The polar-ghosting ratio has a maximum value around 0,500 (50%) and a minimum value around of 0,250 (25%). This happens because the silver screen is not ideal depolarising part of the incoming light and due to the fact that the polarisers are not perfect [22]. Then, some part of the light which is reflect by the screen and reaches the viewers are not polarised and consequentely is not blocked by the goggles polarisers. The ghosting by timing is less important due to the quality of the active shutter, the high contrast and the non-dependence with polarization [23]. When one shutter is closed only a few amount of light passes through it and, even if the shutter is at the same polarization as the reflected light, the ghosting ratio has a maximum around 0,10 (10%) and a minimum around 0,05 (5%). When the shutter is closed and the light is at the opposite polarization, polar-time ghosting, the ghosting ratio is even less, it has a maximum around 0,05 (5%) and a minimum at 0,01 (1%). Analysing the Figure 88, Figure 92 and Figure 96 it is observed that the polar-ghosting ratio increases for higher values of θ and it can be considered as uniform with respect to φ. Observing Figure 100, polar-ghosting ratio for the white color, it is confirmed the angle dependence of the polar-ghosting according to the angles θ and the uniformity in φ. Notice that the polar-ghosting ratio encreases while the luminances (Figure 87, Figure 91 and Figure 95) decreases, because the luminosity of the undeserible images passing through the shutter start to increase approximating to the luminosity of the main image. In fact, the depolarization becomes more relevant for higher values of φ. The time-ghosting ratio and the polar-time ghosting ratio is considered uniform and angle independent, as it can be seen in the results with the white color (Figure 101, Figure 102).

- Case 2.2 Results (Independent Projection)

Now, it is presented the results obtained at Télécom-Bretagne for the Case 2.2, where the viewers are separated by time and the viewer's eyes by polarization. Both shutters open and close alternately, they have orthogonal polarisers on it, the right shutter with a RCP and the left shutter with a LCP. One projector displays the left images and the other the right images for both viewers.

The results are organised by colors and in each color there are four results: the luminance of the main stream and the ghosting ratio as a function of the angles (θ and φ) due to the polar-ghosting, time ghosting, and polar-time ghosting. The results are in the format of a table, with the numerical value of the ghosting ratio for each Type and plotted as a surface to map and facilitate the interpretation of the results.

○ Red (R) – Case 2.2 (Télécom-Bretagne)

Luminance

θ\ϕ	-90	-60	-30	0	30	60	90
0	8,731	5,955	5,438	4,715	4,068	4,128	4,740
30	2,098	2,480	3,203	3,013	2,655	2,113	1,775
45	1,110	1,410	1,798	1,983	1,605	1,238	1,028
60	0,718	0,868	1,125	1,288	0,990	0,788	0,675

Table 25 – The red color luminance distribution values with respect to θ and φ (Case 2.2 – TB)

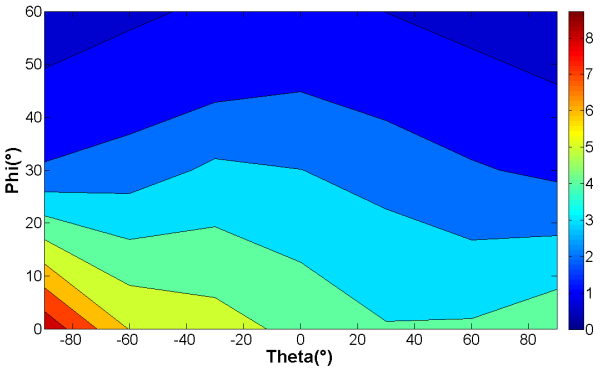

Figure 103 – The red color luminance distribution with respect to θ and φ (Case 2.2 – TB)

Polar Ghosting Ratio

θ\ϕ	-90	-60	-30	0	30	60	90
0	0,333	0,304	0,230	0,266	0,360	0,395	0,382
30	0,423	0,348	0,284	0,330	0,411	0,472	0,446
45	0,484	0,417	0,346	0,382	0,485	0,532	0,517
60	0,560	0,498	0,440	0,473	0,573	0,612	0,590

Table 26 – The red color polar-ghosting ratio values with respect to θ and φ (Case 2.2 – TB)

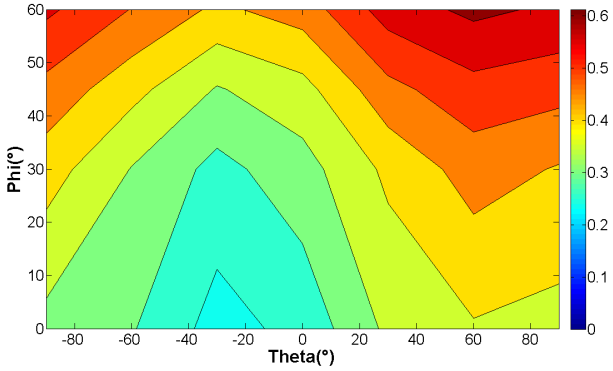

Figure 104 – The red color polar-ghosting ratio distribution with respect to θ and φ (Case 2.2 – TB)

Time Ghosting Ratio

θ\ϕ	-90	-60	-30	0	30	60	90
0	0,362	0,358	0,356	0,355	0,346	0,365	0,360
30	0,357	0,354	0,353	0,348	0,349	0,349	0,348
45	0,349	0,345	0,346	0,354	0,347	0,352	0,339
60	0,340	0,344	0,350	0,345	0,345	0,344	0,333

Table 27 – The red color time-ghosting ratio values with respect to θ and φ (Case 2.2 – TB)

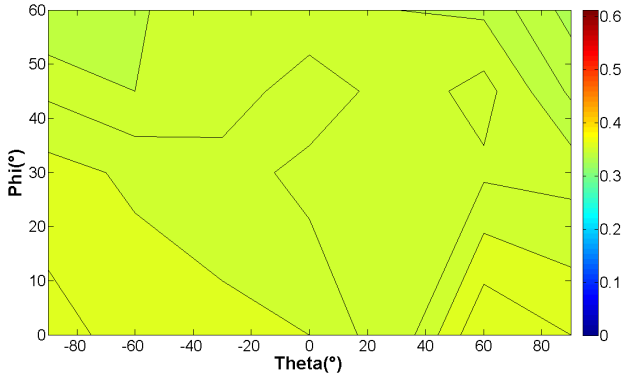

Figure 105 – The red color time-ghosting ratio distribution with respect to θ and φ (Case 2.2 – TB)

Polar Time Ghosting Ratio

θ\ϕ	-90	-60	-30	0	30	60	90
0	0,163	0,149	0,129	0,130	0,155	0,170	0,164
30	0,176	0,149	0,131	0,147	0,166	0,182	0,168
45	0,178	0,164	0,135	0,151	0,185	0,180	0,185
60	0,179	0,152	0,149	0,183	0,183	0,205	0,163

Table 28 – The red color polar-time ghosting ratio values with respect to θ and φ (Case 2.2 – TB)

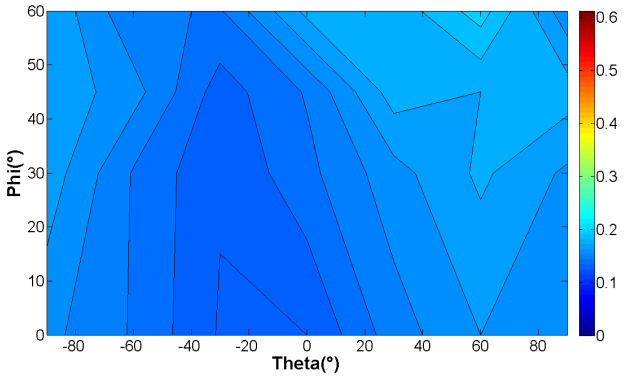

Figure 106 – The red color polar-time ghosting distribution with respect to θ and φ (Case 2.2 – TB)

○ Green (G) - Case 2.2 (Télécom-Bretagne)

Luminance

θ\ϕ	-90	-60	-30	0	30	60	90
0	31,10	20,680	18,460	16,340	14,470	14,810	16,86
30	7,448	8,568	10,880	10,400	9,428	7,648	6,318
45	3,955	4,883	6,110	6,883	5,720	4,490	3,670
60	2,558	2,990	3,860	4,490	3,593	2,888	2,413

Table 29 – The green color luminance distribution values with respect to θ and φ (Case 2.2 – TB)

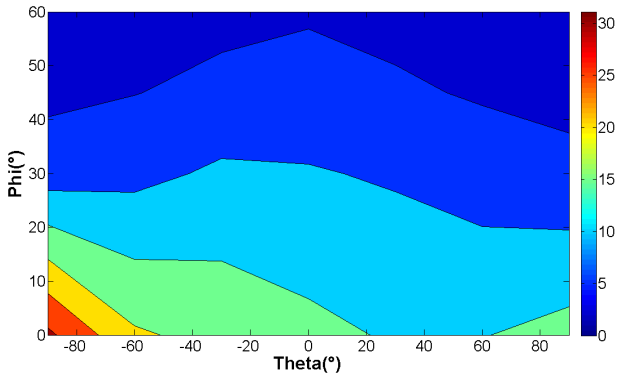

Figure 107 – The green color luminance distribution with respect to θ and φ (Case 2.2 – TB)

Polar Ghosting Ratio

θ\ϕ	-90	-60	-30	0	30	60	90
0	0,220	0,233	0,212	0,242	0,280	0,282	0,266
30	0,333	0,296	0,264	0,301	0,335	0,035	0,358
45	0,427	0,382	0,349	0,365	0,412	0,440	0,455
60	0,522	0,488	0,454	0,456	0,511	0,537	0,552

Table 30 – The green color polar-ghosting ratio values with respect to θ and φ (Case 2.2 – TB)

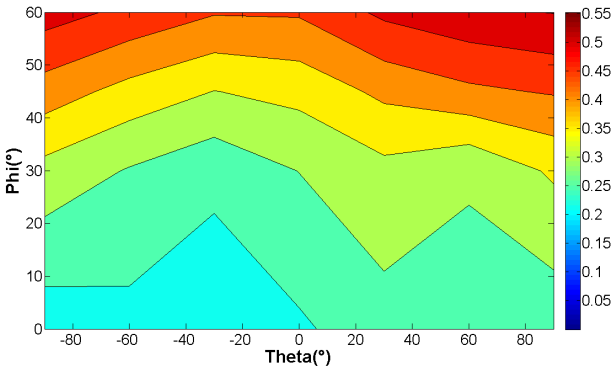

Figure 108 – The green color polar-ghosting ratio distribution with respect to θ and φ (Case 2.2 – TB)

Time Ghosting Ratio

θ\ϕ	-90	-60	-30	0	30	60	90
0	0,113	0,113	0,113	0,113	0,112	0,135	0,130
30	0,116	0,108	0,109	0,109	0,107	0,104	0,105
45	0,098	0,104	0,105	0,104	0,105	0,098	0,098
60	0,099	0,088	0,099	0,100	0,099	0,089	0,086

Table 31 – The green color time-ghosting ratio values with respect to θ and φ (Case 2.2 – TB)

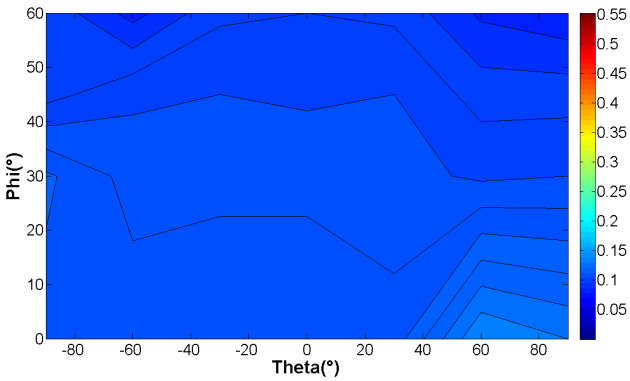

Figure 109 – The green color time-ghosting ratio distribution with respect to θ and φ (Case 2.2 – TB)

Polar Time Ghosting Ratio

θ\ϕ	-90	-60	-30	0	30	60	90
0	0,068	0,065	0,066	0,067	0,067	0,069	0,067
30	0,076	0,067	0,059	0,064	0,065	0,066	0,060
45	0,050	0,061	0,064	0,064	0,066	0,058	0,064
60	0,063	0,052	0,051	0,058	0,060	0,032	0,046

Table 32 – The green color polar-time ghosting ratio values with respect to θ and φ (Case 2.2 – TB)

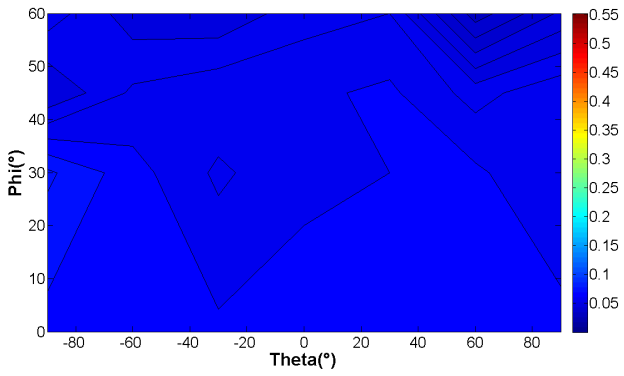

Figure 110 – The green color polar-time ghosting distribution with respect to θ and φ (Case 2.2 – TB)

○ Blue (B) - Case 2.2 (Télécom-Bretagne)

Luminance

θ\ϕ	-90	-60	-30	0	30	60	90
0	4,530	3,013	2,275	2,450	2,178	2,183	2,468
30	1,073	1,243	1,595	1,563	1,423	1,138	0,913
45	0,568	0,695	0,895	1,030	0,858	0,663	0,528
60	0,365	0,425	0,558	0,673	0,535	0,413	0,343

Table 33 – The blue color luminance distribution values with respect to θ and φ (Case 2.2 – TB)

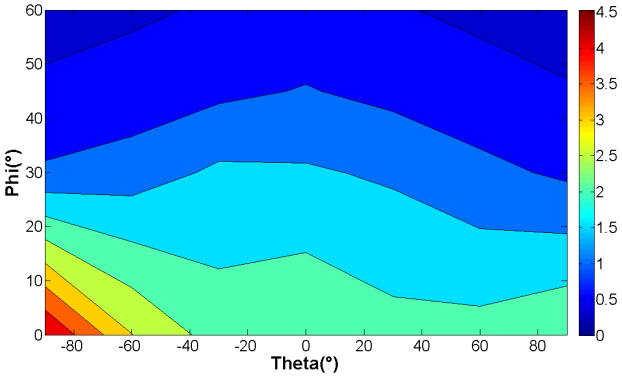

Figure 111 – The blue color luminance distribution with respect to θ and φ (Case 2.2 – TB)

Polar Ghosting Ratio

θ\ϕ	-90	-60	-30	0	30	60	90
0	0,257	0,279	0,296	0,288	0,305	0,309	0,295
30	0,368	0,342	0,317	0,330	0,356	0,375	0,392
45	0,484	0,429	0,403	0,394	0,432	0,456	0,492
60	0,556	0,553	0,497	0,480	0,526	0,567	0,579

Table 34 – The blue color polar-ghosting ratio values with respect to θ and φ (Case 2.2 – TB)

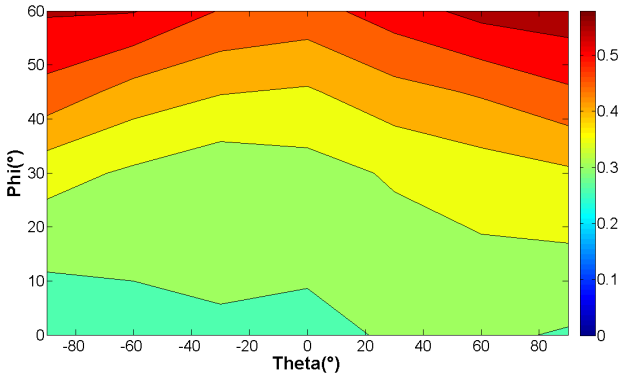

Figure 112 – The blue color polar-ghosting distribution with respect to θ and φ (Case 2.2 – TB)

Time Ghosting Ratio

θ\ϕ	-90	-60	-30	0	30	60	90
0	0,201	0,198	0,208	0,192	0,183	0,206	0,204
30	0,181	0,179	0,182	0,184	0,174	0,175	0,159
45	0,133	0,120	0,167	0,165	0,153	0,087	0,097
60	0,091	0,108	0,073	0,139	0,137	0,085	0,000

Table 35 – The blue color time-ghosting ratio values with respect to θ and φ (Case 2.2 – TB)

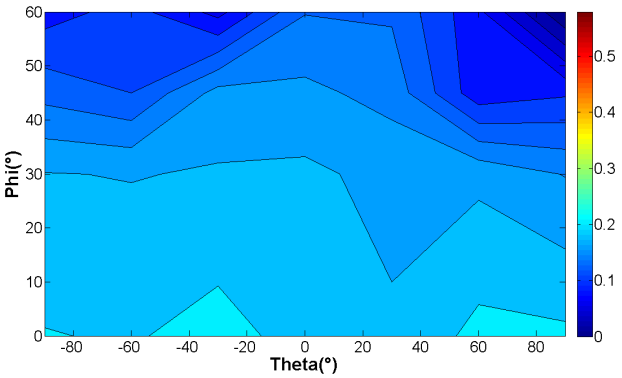

Figure 113 – The blue color time-ghosting distribution with respect to θ and φ (Case 2.2 – TB)

Polar Time Ghosting Ratio

θ\ϕ	-90	-60	-30	0	30	60	90
0	0,165	0,161	0,169	0,163	0,156	0,151	0,156
30	0,137	0,136	0,148	0,145	0,140	0,148	0,128
45	0,073	0,137	0,106	0,139	0,123	0,123	0,075
60	0,000	0,000	0,095	0,109	0,075	0,000	0,000

Table 36 – The blue color polar-time ghosting ratio values with respect to θ and φ (Case 2.2 – TB)

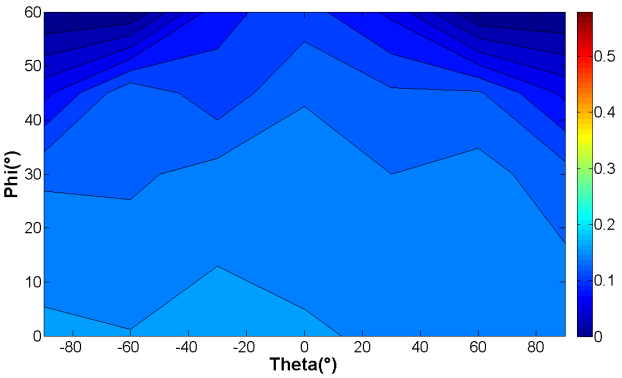

Figure 114 – The blue color polar-time ghosting distribution with respect to θ and φ (Case 2.2 – TB)

○ White (W) - Case 2.2 (Télécom-Bretagne)

Luminance

θ\ϕ	-90	-60	-30	0	30	60	90
0	59,740	39,900	35,870	31,510	27,830	28,510	32,230
30	14,320	16,560	21,150	20,140	18,160	14,650	12,140
45	7,600	9,431	11,210	13,300	11,030	8,618	7,063
60	4,940	5,789	7,495	8,671	6,915	5,553	4,670

Table 37 – The white color time-ghosting ratio values with respect to θ and φ (Case 2.2 – TB)

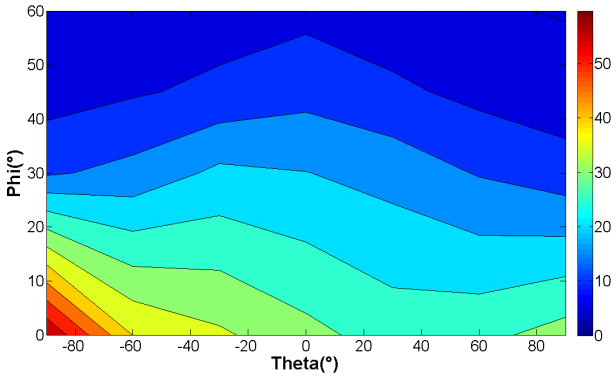

Figure 115 – The red color luminance distribution with respect to θ and φ (Case 2.2 – TB)

Polar Ghosting Ratio

θ\ϕ	-90	-60	-30	0	30	60	90
0	0,236	0,243	0,212	0,244	0,292	0,300	0,285
30	0,351	0,307	0,265	0,306	0,348	0,380	0,376
45	0,444	0,394	0,364	0,371	0,425	0,461	0,472
60	0,538	0,501	0,460	0,464	0,527	0,557	0,568

Table 38 – The white color time-ghosting ratio values with respect to θ and φ (Case 2.2 – TB)

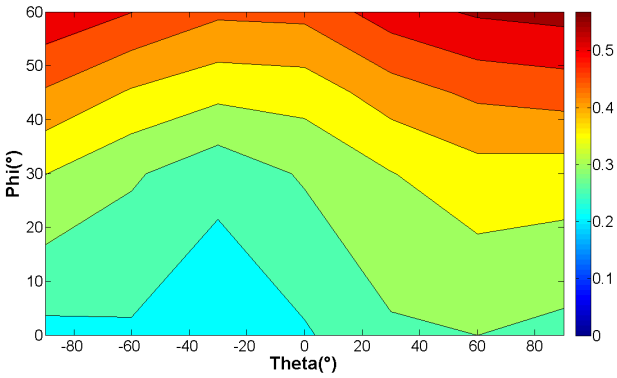

Figure 116 – The red color luminance distribution with respect to θ and φ (Case 2.2 – TB)

Time Ghosting Ratio

θ\ϕ	-90	-60	-30	0	30	60	90
0	0,172	0,172	0,172	0,173	0,168	0,187	0,183
30	0,178	0,173	0,171	0,169	0,166	0,169	0,167
45	0,169	0,171	0,175	0,170	0,168	0,168	0,168
60	0,170	0,170	0,167	0,168	0,165	0,163	0,162

Table 39 – The white color time-ghosting ratio values with respect to θ and φ (Case 2.2 – TB)

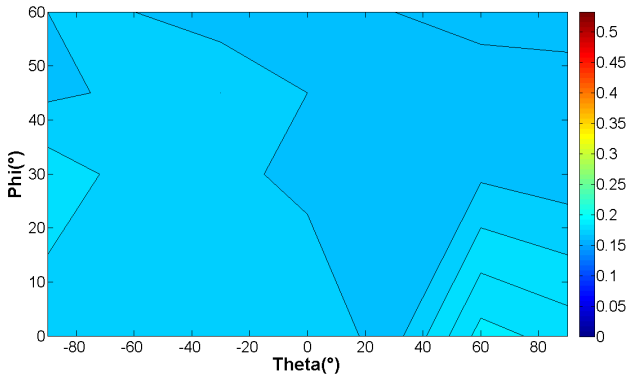

Figure 117 – The red color luminance distribution with respect to θ and φ (Case 2.2 – TB)

PolarTime Ghosting Ratio

θ\ϕ	-90	-60	-30	0	30	60	90
0	0,069	0,066	0,059	0,063	0,070	0,076	0,074
30	0,093	0,072	0,062	0,066	0,075	0,081	0,078
45	0,084	0,083	0,069	0,075	0,084	0,090	0,088
60	0,095	0,088	0,077	0,083	0,092	0,100	0,093

Table 40 – The white color time-ghosting ratio values with respect to θ and φ (Case 2.2 – TB)

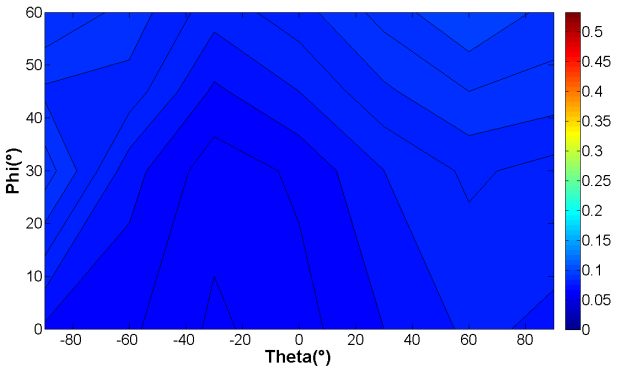

Figure 118 – The red color luminance distribution with respect to θ and φ (Case 2.2 – TB)

The results for the case 2.2 reassured that the ghosting by polarization is the most important, followed by the time-ghosting and the polar-time ghosting. However, the main difference between the case 2.1 and case 2.2 was in the strength of the ghosting ratio, but the behavior remained the same. The polar-ghosting ratio for the case 2.2 has a maximum value around 0,55 (55%) and a minimum value around of 0,25 (25%). It still due to the silver screen, but the increasing of the ghosting ratio is probably due to the difference between the goggles since the quarter-wave plates were manually placed and a reduction in the contrast of the shutters due to the new functionality that both shutters open and close at the same time. The time-ghosting ratio has a maximum around 0,17 (17%) and a minimum around 0,16 (16%), the polar-time a maximum at 0,01 (10%) and a minimum at 0,06 (6%). Analyzing the white color (Figures 50, 51 and 52) it is observed that the polar-ghosting ratio increases for higher values of θ and almost uniform in φ, with a small increasing of ghosting at the centre of the screen. The case 2.2 and 2.1 in terms of ghosting have the behavior.

4.3.4. The Ghosting Ratio Experimental Setup (Immerssion)

The same experimental setup to measure the ghosting at Télécom-Bretagne was used at Immerssion, the same chromameter Minolta CS-100 attached to the mechanical arm and placed on a metallic support (Figure 80). The difference is that the 3D Dual View setup at Immersion consists of two projectors placed under a transmissive screen and it projects the images to the viewers through a transmissive and diffusive screen. In that case the metallic support was placed on the transmissive screen. The experiments were done in completely darkness. Figure 119 shows how the mechanical arm was placed with respect to the transmissive screen and an illustration of the immersion 3D Dual View setup product.

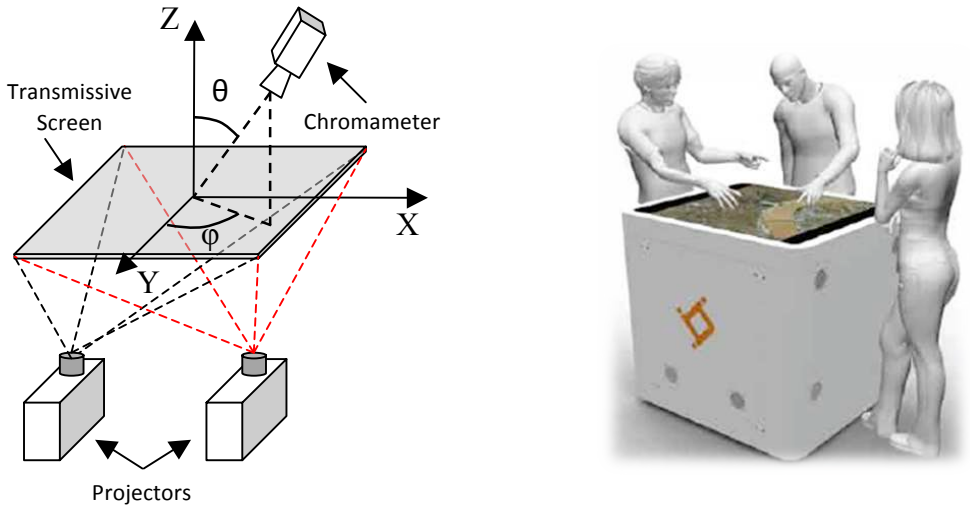

Figure 119 - The chromometer, the projector and the silver screen at Immersion.

The measurements made for the reflection mode are the same as for the transmission mode, the only difference between them is how the images are projected and the goggles. Apart of that, is still the measurement of the ghosting by polarization, time and polar-time.

4.3.5. Transmission Mode Results (Immersion)

The ghosting ratio (GR) is calculated after doing the four types of measurements described in

section 4.3.2. The images are projected one at a time, varying the gray level from 0 to 255 and the luminosity is measured through one shutter with the chromameter Minolta. The ghosting has been measured for the red, green, blue and white colors and for the angles: φ equal to -90°, -60°, -30°, -0°, 30°, 60°, 90° and θ equal to 0°, 30°, 45° and 60°. The same that was done for the silver screen, in the reflection mode, was done in transmission mode, the light distribution from the projectors that traverse the transmissive screen was measured. The obtained curves were approximated by the Gamma function and the coefficients *a* and *b* (Figure 79) were obtained in order to calculated the ghosting ratio using Equation 4.3.

- Case 2.1 Results (Independent Projection)

The results obtained at Immersion (IM) for the Case 2.1, where the viewers are separated by polarization and the viewer's eyes by time. The shutters open and close alternately, they have the same polarisers on it, the right shutter with a RCP and the left shutter with a LCP, and each projector displays the images for one viewer.

The organization of the results remains the same. It is organized by colors and in each color there are four results: the luminance and the ghosting ratio as a function of the angles (θ and φ) due to the polar-ghosting, time ghosting, and polar-time ghosting. The results are in the format of a table, with the numerical value of the ghosting ratio for each Type, and plotted as a surface map for interpreting the results.

○ Red (R) – Case 2.1 (Immersion)

Luminance

θ\ϕ	-90	-60	-30	0	30	60	90
0	2,103	1,960	1,175	1,293	1,175	1,268	1,178
30	1,048	2,213	3,010	3,193	2,340	1,295	0,740
45	0,650	1,490	2,62	3,065	2,050	0,983	0,455
60	0,318	0,903	1,860	2,260	1,450	0,628	0,230

Table 41 – The red color luminance values with respect to θ and φ (Case 2.1 – Immersion)

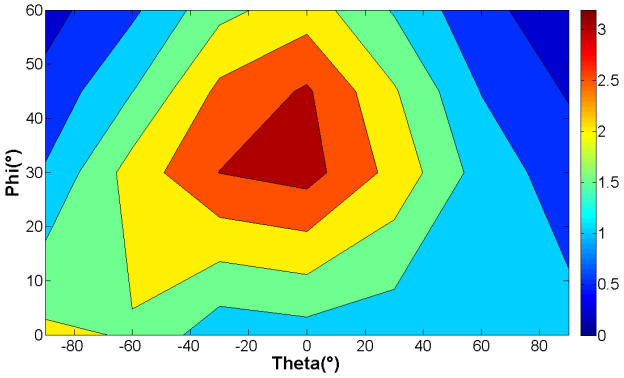

Figure 120 – The red color luminance distribution with respect to θ and φ (Case 2.1 – Immersion)

Polar Ghosting Ratio

θ\ϕ	-90	-60	-30	0	30	60	90
0	0,227	0,156	0,351	0,245	0,351	0,380	0,3 0
30	0,229	0,139	0,115	0,131	0,161	0,219	0,287
45	0,228	0,118	0,113	0,123	0,131	0,186	0,256
60	0,203	0,134	0,109	0,108	0,115	0,176	0,278

Table 42 – The red color polar-ghosting ratio values with respect to θ and φ (Case 2.1 – Immersion)

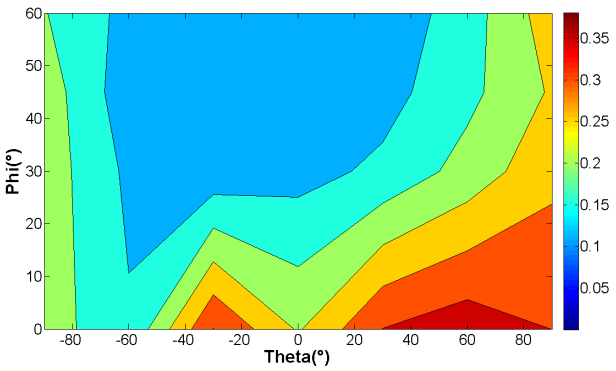

Figure 121– The red color polar-ghosting ratio with respect to θ and φ (Case 2.1 – Immersion)

Time Ghosting Ratio

θ\ϕ	-90	-60	-30	0	30	60	90
0	0,120	0,124	0,095	0,087	0,095	0,116	0,123
30	0,065	0,123	0,125	0,128	0,126	0,107	0,084
45	0,000	0,103	0,118	0,126	0,122	0,088	0,000
60	0,000	0,037	0,114	0,117	0,093	0,000	0,0 0

Table 43 – The red color time-ghosting ratio values with respect to θ and φ (Case 2.1 – Immersion)

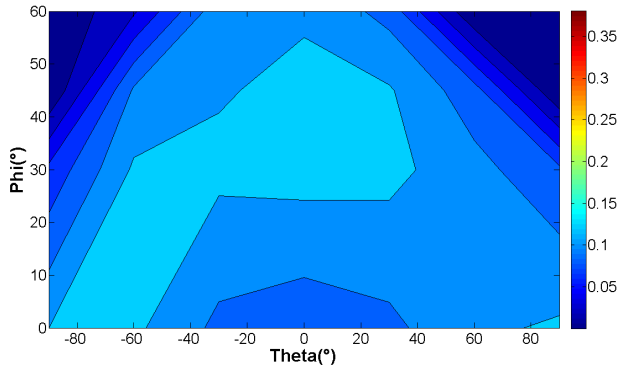

Figure 122 - The red color time-ghosting ratio with respect to θ and φ (Case 2.1 – Immersion)

Polar Time Ghosting Ratio

θ\ϕ	-90	-60	-30	0	30	60	90
0	0,096	0,105	0,053	0,046	0,053	0,075	0,079
30	0,056	0,104	0,096	0,102	0,105	0,089	0,000
45	0,000	,086	0,095	0,106	0,099	0,045	0,000
60	0,000	0,000	0,078	0,083	0,071	0,000	0,000

Table 44 – The red color polar-time ghosting ratio values with respect to θ and φ (Case 2.1 – Immersion)

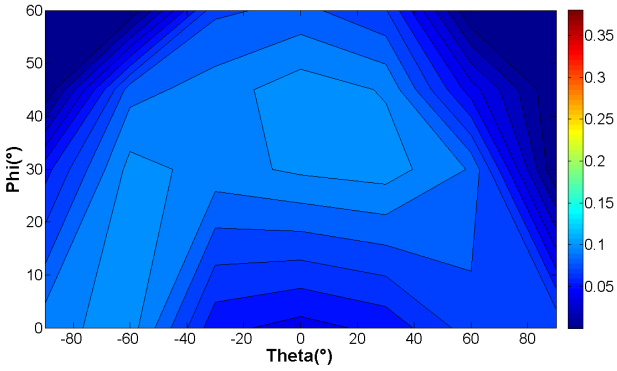

Figure 123 - The red color time-ghosting ratio with respect to θ and φ (Case 2.1 – Immersion)

○ Green (G) – Case 2.1 (Immersion)

Luminance

θ\ϕ	-90	-60	-30	0	30	60	90
0	8,691	8,073	5,070	5,413	5,070	5,570	5,175
30	4,518	8,998	11,860	12,690	9,611	5,570	3,288
45	2,878	6,115	10,320	12,130	8,491	4,263	2,033
60	1,438	3,790	7,425	9,176	6,043	2,755	1,068

Table 45 – The green color luminance values with respect to θ and φ (Case 2.1 – Immersion)

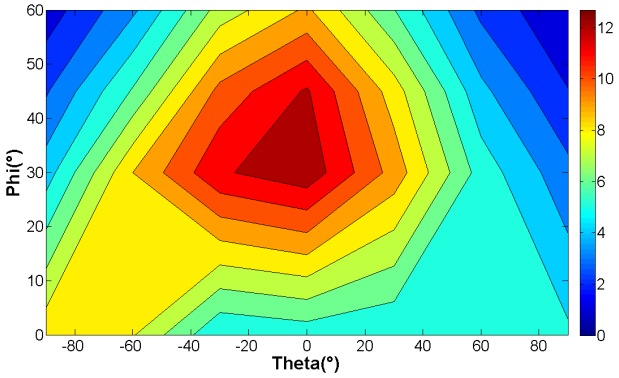

Figure 124 – The green color luminance distribution with respect to θ and φ (Case 2.1 – Immersion)

Polar Ghosting Ratio

θ\ϕ	-90	-60	-30	0	30	60	90
0	0,172	0,122	0,283	0,229	0,283	0,272	0,238
30	0,177	0,103	0,091	0,097	0,122	0,165	0,230
45	0,196	0,111	0,083	0,089	0,103	0,157	0,257
60	,243	0,127	0,083	0,084	0,104	0,170	0,329

Table 46 – The green color polar-ghosting ratio values with respect to θ and φ (Case 2.1 – Immersion)

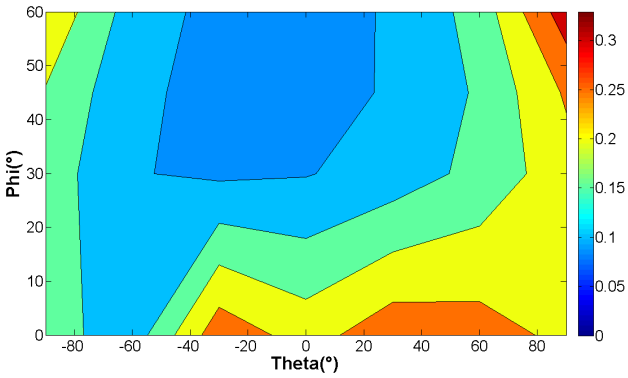

Figure 125 – The green color polar-ghosting ratio with respect to θ and φ (Case 2.1 – Immersion)

Time Ghosting Ratio

θ\ϕ	-90	-60	-30	0	30	60	90
0	0,087	0,088	0,079	0,075	0,079	0,080	0,078
30	0,075	0,090	0,087	0,090	0,086	0,079	0,058
45	0,061	0,085	0,088	0,091	0,083	0,070	0,040
60	0,000	0,075	0,080	0,085	0,082	0,054	0,000

Table 47 – The green color time-ghosting ratio values with respect to θ and φ (Case 2.1 – Immersion)

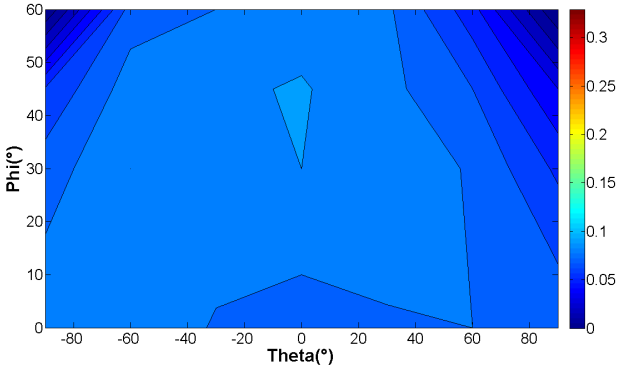

Figure 126 – The green color time-ghosting ratio with respect to θ and φ (Case 2.1 – Immersion)

Polar Time Ghosting Ratio

θ\ϕ	-90	-60	-30	0	30	60	90
0	0,049	0,051	0,048	0,025	0,048	0,043	0,047
30	0,037	0,052	0,052	0,055	0,055	0,044	0,025
45	0,000	0,047	0,051	0,053	0,046	0,000	0,000
60	0,000	0,028	0,039	0,046	0,032	0,000	0,000

Table 48 – The green color polar-time ghosting ratio values with respect to θ and φ (Case 2.1 – Immersion)

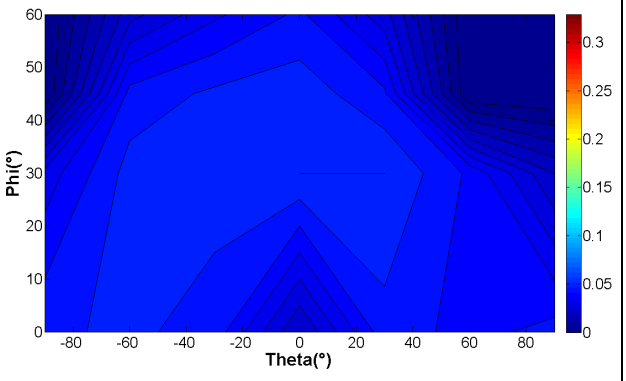

Figure 127 – The green color polar-time ghosting ratio with respect to θ and φ (Case 2.1 – Immersion)

○ Blue (B) – Case 2.1 (Immersion)

Luminance

θ\ϕ	-90	-60	-30	0	30	60	90
0	1,763	1,620	1,085	1,148	1,085	1,188	,075
30	0,945	1,805	2,378	2,575	1,978	1,153	0,678
45	0,595	1,233	2,068	2,453	1,728	0,880	0,420
60	0,290	0,765	1,498	1,860	1,233	0,560	0,213

Table 49 – The blue color luminance values with respect to θ and φ (Case 2.1 – Immersion)

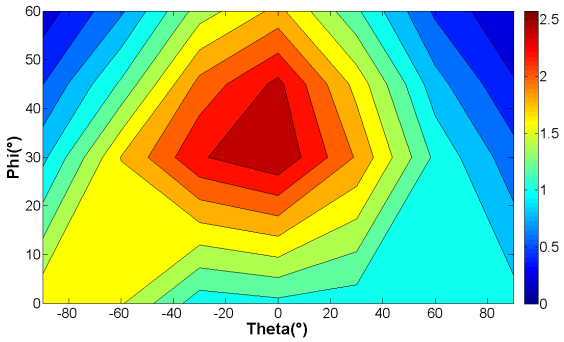

Figure 128 – The blue color luminance distribution with respect to θ and φ (Case 2.1 – Immersion)

Polar Ghosting Ratio

θ\ϕ	-90	-60	-30	0	30	60	90
0	0,175	0,175	0,180	0,158	0,180	0,186	0,194
30	0,179	0,147	0,135	0,135	0,132	0,129	0,205
45	0,150	0,140	0,134	0,131	0,125	0,125	0,209
60	0,174	0,114	0,116	0,118	0,109	0,099	0,178

Table 50 – The blue color polar-ghosting ratio values with respect to θ and φ (Case 2.1 – Immersion)

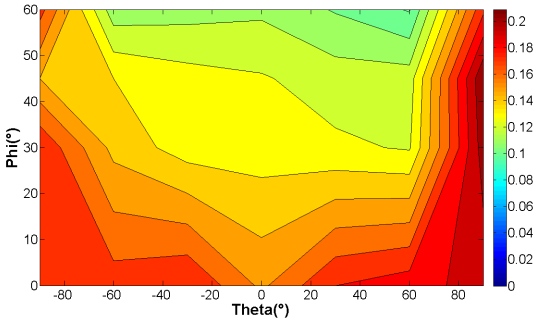

Figure 129 – The blue color polar-ghosting ratio with respect to θ and φ (Case 2.1 – Immersion)

Time Ghosting Ratio

θ\ϕ	-90	-60	-30	0	30	60	90
0	0,132	0,129	0,092	0,082	0,092	0,112	0,102
30	0,075	0,132	0,128	0,139	0,132	0,107	0,022
45	0,000	0, 22	0,131	0,137	0,119	0,081	0,000
60	0,000	0,070	0,101	0,129	0,106	0,000	0,000

Table 51 – The blue color time-ghosting ratio values with respect to θ and φ (Case 2.1 – Immersion)

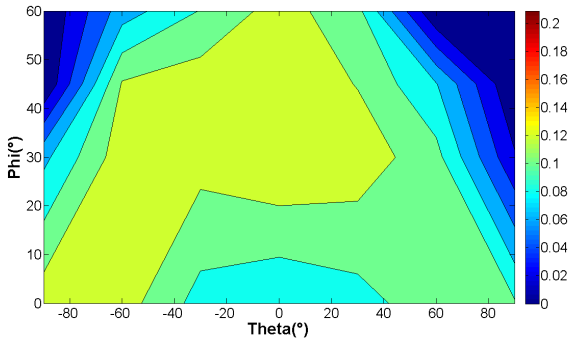

Figure 130 – The blue color time-ghosting with respect to θ and φ (Case 2.1 – Immersion)

Polar Time Ghosting Ratio

θ\ϕ	-90	-60	-30	0	30	60	90
0	0,106	0,111	0,026	0, 39	0,026	0,077	0,058
30	0,018	0,113	0,105	0,120	0,102	0,088	0,000
45	0,000	0,095	0,098	0,108	0,103	0,000	0,000
60	0,000	0,020	0,078	0,102	0,075	0,000	0,000

Table 52 – The blue color polar-time ghosting ratio values with respect to θ and φ (Case 2.1 – Immersion)

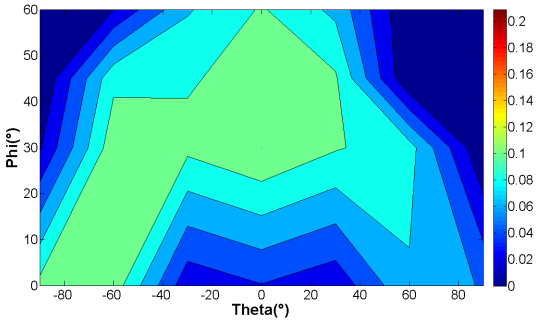

Figure 131 – The blue color polar-time ghosting ratio with respect to θ and φ (Case 2.1 – Immersion)

○ White (W) – Case 2.1 (Immersion)

Luminance

θ\ϕ	-90	-60	-30	0	30	60	90
0	12,740	11,810	7,430	7,983	7,430	8,136	7,530
30	6,598	13,200	17,450	18,710	14,100	8,136	4,783
45	4,208	8,971	15,190	17,880	12,420	6,233	2,965
60	2,110	5,553	10,940	13,470	8,848	4,028	1,573

Table 53 – The white color luminance values with respect to θ and φ (Case 2.1 – Immersion)

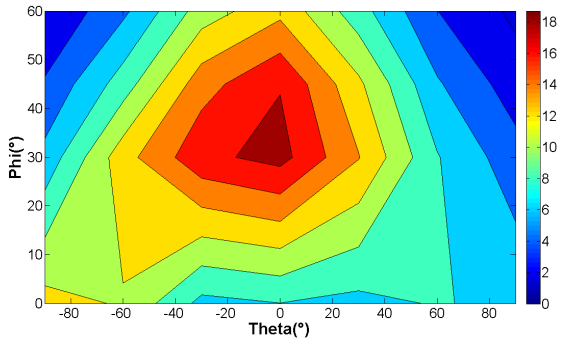

Figure 132 – The white color luminance distribution with respect to θ and φ (Case 2.1 – Immersion)

Polar Ghosting Ratio

θ\ϕ	-90	-60	-30	0	30	60	90
0	0,174	0,126	0,282	0,222	0,282	0,279	0,252
30	0,18	0,100	0,085	0,091	0,118	0,167	0,242
45	0,209	0,105	0,079	0,079	0,096	0,162	0,268
60	0,250	0,125	0,081	0,076	0,097	0,168	0,334

Table 54 – The white color polar-ghosting ratio values with respect to θ and φ (Case 2.1 – Immersion)

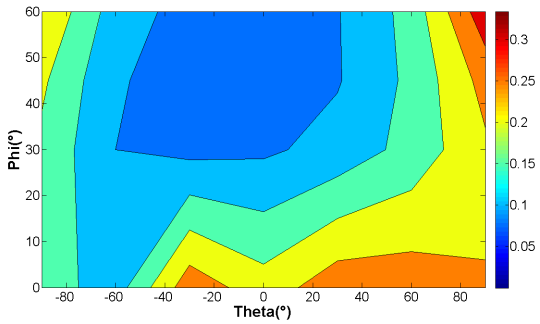

Figure 133 – The white color polar-time ghosting ratio with respect to θ and φ (Case 2.1 – Immersion)

Time Ghosting Ratio

θ\ϕ	-90	-60	-30	0	30	60	90
0	0,084	0,083	0,086	0,077	0,074	0,079	0,082
30	0,075	0,085	0,084	0,084	0,082	0,080	0,076
45	0,063	0,080	0,083	0,085	0,082	0,071	0,058
60	0,000	0,074	0,077	0,083	0,079	0,068	0, 00

Table 55 – The white color time-ghosting ratio values with respect to θ and φ (Case 2.1 – Immersion)

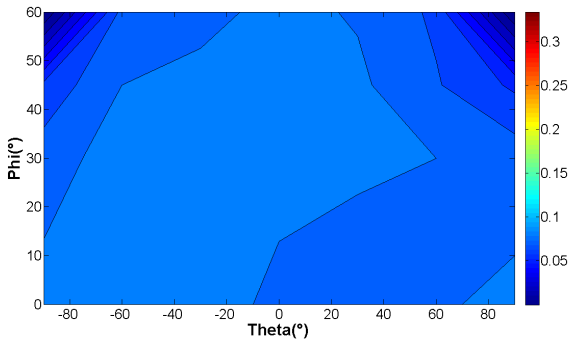

Figure 134 – The white color time-ghosting ratio with respect to θ and φ (Case 2.1 – Immersion)

Polar Time Ghosting Ratio

θ\ϕ	-90	-60	-30	0	30	60	90
0	0,043	0,044	0,049	0,029	0,049	0,043	0,039
30	0,019	0,041	0,044	0,045	0,045	0,035	0,000
45	0,0 0	0,035	0,043	0,043	0,043	0,007	0,000
60	0,000	0,000	0,029	0,039	0,037	0,000	0,000

Table 56 – The white color polar-time ghosting ratio values with respect to θ and φ (Case 2.1 – Immersion)

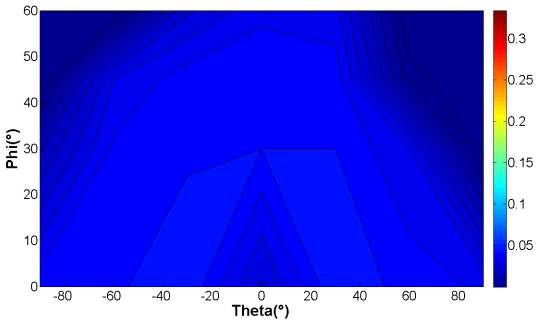

Figure 135 – The white color polar-time ghosting ratio with respect to θ and φ (Case 2.1 – Immersion)

As it was expected, since the measurement at TB and Immersion was done with the same shutter, that the ghosting by polarization is the most harmful followed by the time-ghosting and polar-time ghosting. The time-ghosting and polar-time ghosting did not change

significantly. The worst measured time-ghosting at TB is 0,10 and at Immersion is 0,08, and the worst measured polar-time ghosting at TB is 0,046 and 0,043 at Immersion, which means that both cases TM and RM has the same ghosting by time and polar-time. The light distribution in the transmissive mode (TM) is completely different for the reflective mode (RM). As a result the ghosting effect by polarization also changes its configuration. Observe in Figure 132 that the light distribution in RM is not symmetric having more light at $\theta<0°$. Then, the other projector has more light at $\theta>0°$, consequently, the ghosting by polarization (Figure 133) is higher at $0°<\theta<90°$ because the light of the opposite projectors becomes more intense at that region. Remind that the projectors at Immersion are placed one in front of the other (Figure 119). In fact, while the viewer walks around the table in the direction of the other viewer the light from the other projector becomes more intense and the ghosting increases. The polar-ghosting ratio encreases while the luminances decreases, because the luminosity of the undeserible images passing through the shutter start to increase approximating to the luminosity of the main image. There is a small difference of the ghosting effect between the colors and this happened also for the Case 2.2 and 2.1 at TB, it is due to the eye sensibility. Other remark wich is notable is the difference in intensity among the polar-ghosting at TB and Immersion. The worst measured ghosting at TB for the white color is 0,51 and 0,33 at Immersion. There are two major factors which contributes to this considerable difference. First, since the projector and the viewers are placed one in front of the other at Immersion the light from each projector is much more directive to the viewers. Is like it has the two different projectors displaying at different screen and each viewer is in front of its screen. In the contrary, at Télécom-Bretagne the viewers are placed side by side and both receives light from the two projectors with the same intensity.

4.4.Optical Quality and Physiological Impacts

Even if, quantitatively, both solutions are impacted by a comparable amount of ghosting, they are not similar, after a closer look, in particular when considering possible eye unbalances. In the case 2.2, when the shutters are opened, only the images intended to the associated viewer are displayed (Figure 66), thus the polarization ghosting perceived by the viewer is the leakage of his left image on his right eye, and his right image on his left eye. Indeed, the viewer sees the intended image, plus the ghosting of the same image. In the case 2.1, the shutters open and close alternatively and images intended to both viewers are simultaneously displayed on the screen (Figure 65). In that case, the viewer sees the polarization ghosting related to the image of the other viewer and vice-versa. Consequently, these images being synthesized from viewpoints far from each other and being associated to different users, their content may be quite different and the ghosting perception could be stronger. In this case, the first viewer sees the intended image, plus the ghosting of the second viewer image with less intensity but shifted in another perspective. This could result in some added fatigue. Furthermore, in the case 2.2 the projectors have to be equally calibrated. A difference between the light intensities of each projector will generate left and right images with different brightness, leading to different light intensity in the viewer's eyes. In an extreme scenario, one

projector with more brightness than the other could result in complex physiological impacts as it will be seen. Additionally, the same happens with the ghosting, since the stronger is the luminosity difference between the projectors, the stronger is the intensity difference between ghosting effects in the viewer's eyes. This may cause visual fatigue and discomfort.

This last consideration should not be underestimated, in particular for a viewer long exposure to such conditions. The consequence, when such an unbalance is maintained for a long time, is a possible risk of amblyopia or lazy eye [24]. Amblyopia is a neurologically active process, resulting from a constant unilateral different vision/prescription in each eye. This can be due to constant turn of one eye (strabismus) or anisometropia (for instance blur), and/or blockage of an eye due to trauma, lid droop, etc [24]. If one eye sees clearly and the other sees a blur, the good eye and brain will inhibit (block, suppress, ignore) the eye with the blur. This inhibition process can result in a permanent decrease in the vision. Among various serious consequences, amblyopia can cause a permanent loss of vision, with associated loss of stereopsis (3D perception). The case here (ghosting unbalance) does not correspond directly to three identified causes for amblyopia. However, a difference in image quality on both retinas and an image corrupted by another will make difficult the correlation process between images during the sensitive phase. This could result in visual anomalies associated with amblyopia, such as image doubling, which can be related to chromatic optical defocus. This will be particularly true when a viewer is using such a system for a long time. Further investigations are in progress to confirm this point. This should be an interesting strength of the 2.1 configuration.

Another important factor, differentiating cases 2.1 and 2.2, has to be mentioned. In the case 2.1, where the shutters open and close alternatively, at one moment the viewer sees the right image of the 3D frame and, after the time needed to close the right shutter and open the left shutter, the left eye will see the left image of a subsequent 3D frame and not the left image of the original frame. This does not occur in the case 2.2, where both shutters open and close at the same time. This possible distortion in depth perception of stereoscopic 3D movies, due to the delay introduced between each image of the video pair, has been observed and studied [25]. This is, of course, related to object motions in a scene and in particular to motion in depth, which explains the recent attention paid to the High Frame Rate (HFR) standard, to prevent some motion artifacts in the perception of distances, related to the motion direction which could, in some cases, result in parallax inversion [25] or loss of the 3D perception. From this point of view, 2.1 (alternated vision) and 2.2 (simultaneous vision) are quite different, and therefore the 2.2 configuration seems particularly interesting.

4.5.Ghost-Busting

Ghost-Busting also known as crosstalk cancellation is a technique to reduce the ghosting effect in stereoscopic vision systems. The ghost-busting did not remove the crosstalk between the images, but hides the ghosting by using image processing before display. Some Ghost-Busting techniques for stereoscopic vision in passive and active systems are already published [26][27][28], and all of them follow the same basic principles. The technique is a "pre-

distortion" of the displayed image before displaying it. The leakage that is expected to occur from the unintended image to the intended image is measured, like what we have done with the chromometer and shown in the last sections. After, this amount of leakage is subtracted from the intended image creating a modified intended image. The processed image is displayed on the screen and the processed image plus the leakage (crosstalking) from the unintended image results in the original intended image. The schematic bellow exemplifies the ghosting effect and the ghostbusting process in 3D Dua View System.

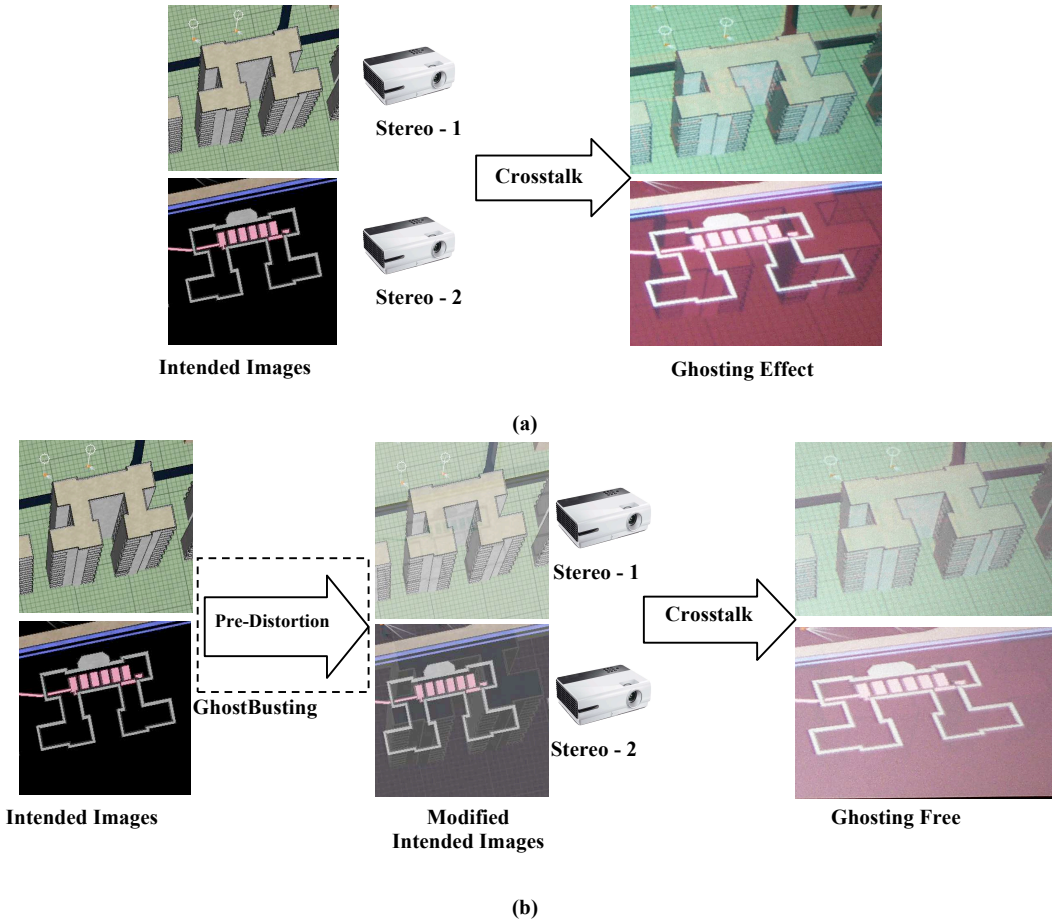

Figure 136 – The ghosting effect due to the crosstalk (a), and the ghostbusting process (b).

For the 3D Dual View the ghost-busting technique becomes more complicated. Instead of having one stereo image with two images interfering, in the 3D Dual View there are two stereo images, which mean four images, interfering and leaking in each other. The principle of the ghost-busting technique remains the same as it was explained before. However, it requires much more computer processing to modify the intended image before display, because three types of ghosting have to be compensated.

To understand the ghostbusting processing algorithm in the 3D Dual View let's start considering three ghosting coefficients: time ghosting coefficient (C_{Tn}), polar ghosting coefficient (C_{Pn}) and polar-time ghosting coefficient (C_{PTn}), and they are defined as:

$$C_{Tn} = GR_{Tn}^{\gamma} \tag{4.4}$$

$$C_{Pn} = GR_{Pn}^{\gamma} \tag{4.5}$$

$$C_{PTn} = C_{Tn} \cdot C_{Pn} \tag{4.6}$$

where n is the viewer number (n=1,2), GR_T is the time ghosting ratio, GR_P is the polar ghosting ratio and γ is the projection system gamma value. Then, the ghostbusting can be done by solving the following equation system:

$$\begin{pmatrix} L_1 \\ R_1 \\ L_2 \\ R_2 \end{pmatrix} = M \begin{pmatrix} L_1' \\ R_1' \\ L_2' \\ R_2' \end{pmatrix} \text{ or } \begin{pmatrix} L_1' \\ R_1' \\ L_2' \\ R_2' \end{pmatrix} = M^{-1} \begin{pmatrix} L_1 \\ R_1 \\ L_2 \\ R_2 \end{pmatrix} \tag{4.7}$$

where M is the ghosting coefficients matrix, L_1 and R_1 are the intended stereo images for the viewer 1, L_2 and R_2 are the intended stereo images for the viewer 2, L_1' and R_1' are the modified (ghostbusted) stereo images for the viewer 1 and, L_2' and R_2' are the modified (ghostbusted) stereo images for the viewer 1. Remind that L_n and R_n are the light intensity of the left and right images, and are defined by Equation 4.2. For the case 2.1, for example, the left intended image of viewer 1 (L_1) can be written as a sum of the modified left images of the viewer 1 (L_1'), plus the leakage due to the time ghosting of the modified right image of viewer 1 ($C_{T1}R_1'$), plus the leakage due to the polar ghosting of the modified left image of viewer 2 ($C_{P1}L_2'$) and plus the leakage due to the polar-time ghosting of the modified right image of viewer 2 ($C_{PT1}R_2'$):

$$L_1 = L_1' + C_{T1}R_1' + C_{P1}L_2' + C_{PT1}R_2' \tag{4.8}$$

Following the same procedure for the other three images, the M matrix for the case 2.1 can be written as:

$$M_{2.1} = \begin{pmatrix} 1 & C_{T1} & C_{P1} & C_{PT1} \\ C_{T1} & 1 & C_{PT1} & C_{P1} \\ C_{P2} & C_{PT2} & 1 & C_{T2} \\ C_{PT2} & C_{P2} & C_{T2} & 1 \end{pmatrix} \tag{4.9}$$

In the case 2.2 the viewers are separated by time and the images are separated by polarization. So, to have the M matrix it only needs to swap the places of the polar ghosting coefficient with the time ghosting coefficient in the matrix $M_{2.1}$:

$$M_{2.2} = \begin{pmatrix} 1 & C_{P1} & C_{T1} & C_{PT1} \\ C_{P1} & 1 & C_{PT1} & C_{T1} \\ C_{T2} & C_{PT2} & 1 & C_{P2} \\ C_{PT2} & C_{T2} & C_{P2} & 1 \end{pmatrix} \tag{4.10}$$

Since one image is composed by the primary colors (red, green and blue), the ghostbusting is achieved solving the system Equation 4.7 for all the three colors. Also, to ghostbust the

images the solution of system has to be written in terms of gray level. Then, solving the equation system for the case 2.2 and considering the luminance as function of the gray level (Equation 4.2), we have, for example, for one image the following solution:

(4.11)

where n'_{L1} is the modified gray level.

The problem is when the intended image has pixels which obliges the algorithm to force the intended image to go darker than black before being displayed. In this case, the gray level of the image should be raised before the ghostbusting process, reducing the dynamic range of the image and losing contrast, but hiding the ghosting effect. From equation 4.11 and getting the two negative terms we can obtain the minimum value of the gray level that the image has to be raised. For the case 2.2 it is:

$$n_{\min} = 255 \sqrt[\gamma]{C_{P1} + C_{T1} \frac{1 - C_{P1}^{\ 2}}{1 - C_{P2}^{\ 2}}} \cong 255 \sqrt[\gamma]{C_{P1} + C_{T1}} \tag{4.12}$$

The reduction of the dynamic range degrades the contrast of the displayed images. Figure 137 illustrates the degradation of the process, which is done for all the displayed images.

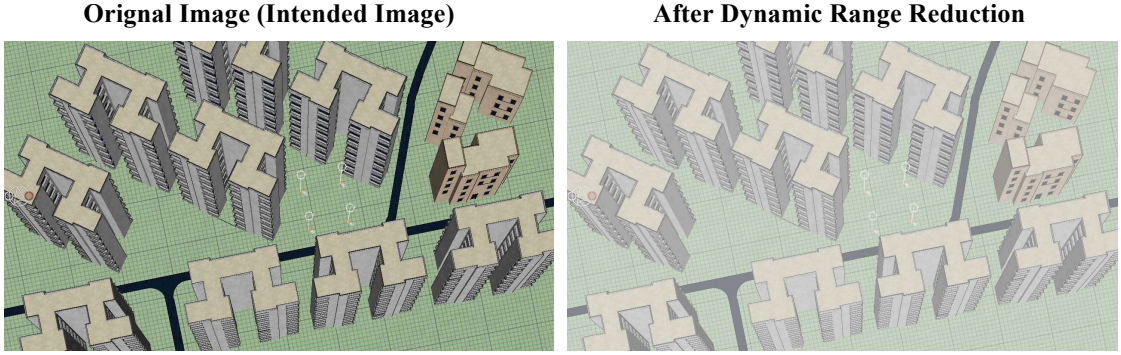

Figure 137 – The original image before and after dynamic range reduction.

After the dynamic reduction, the images are processed to remove the ghosting. Then, to solve the equation system and ghostbust the images, a software was done with MATLAB. It is important to keep in mind that the complexity of the solution of the equation system comes from the fact that the ghosting is angle dependent and varies with respect to the color. Thus, the software has to be capable to solve the equation system for each color and according to the position of the viewers. The algorithm was tested statically, which means that the images were ghostbusted offline and after displayed.

In Figure 138 the result of the ghostbusting for the case 2.2. First, a rough picture of the ghosbusting technique considering the viewer 1 in front of the table (θ=0°) looking at 45° (φ) and viewer 2 at θ=-60° also looking at 45°. Second, it has an overview picture of the ghostbusting over the entire reflective screen.

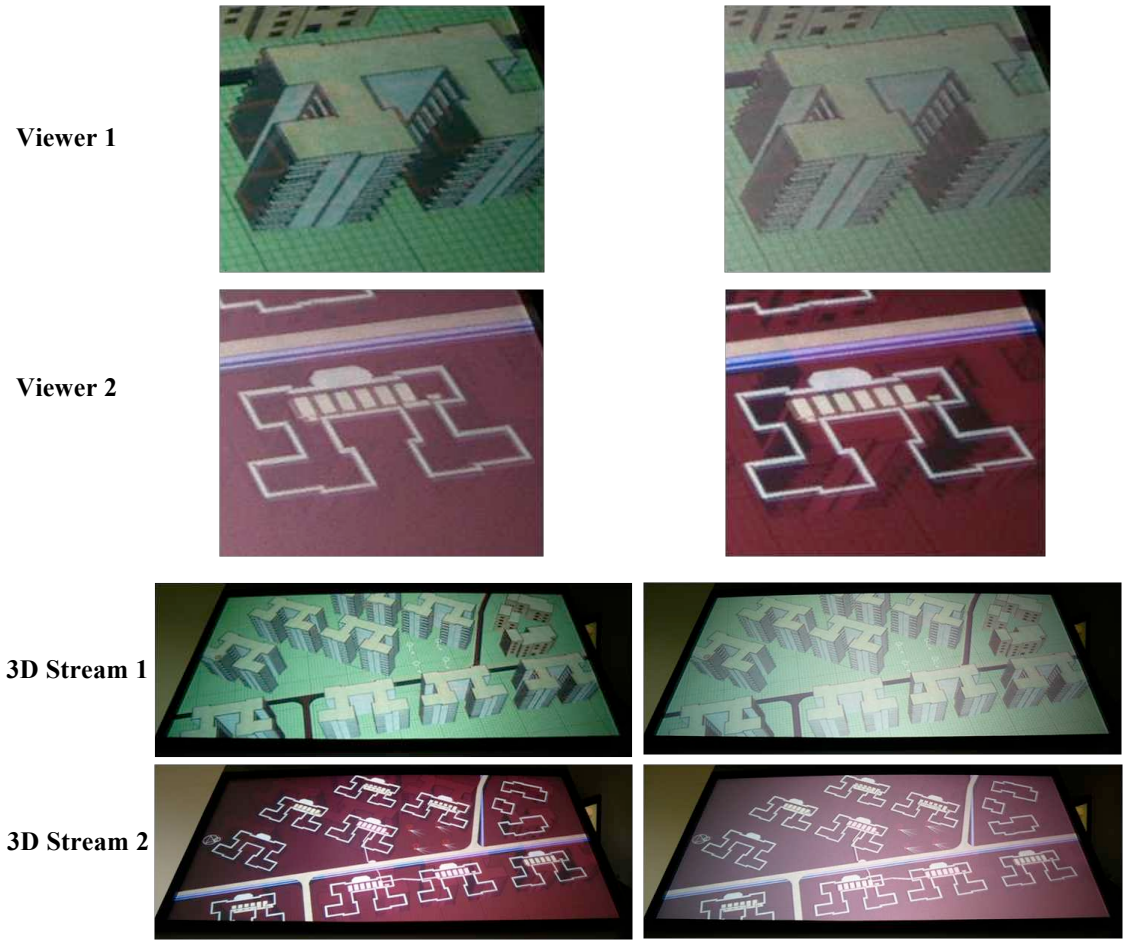

Figure 138 – Images of the 3D Dual View for with and without Ghostbusting.

The big advantage of this technique is the reduction of the ghosting effect. Then, the viewers do not see the images which not belong to them avoiding fatigue and the misunderstanding of the scene. The big disadvantages of this technique are the reduction of the dynamic range of the images losing considerably the contrast and, since the ghosting ratio is angle dependent, the dynamic range of the images changes while the viewers move. Then, if one viewer remains at his place and the other moves, the luminosity of the image of the moving viewer will dynamic change disturbing the stopped viewer (Equation 4.13). The latter can be attenuated according to the ghostbusting policy. For example, the ghosting ratio in reflective mode is almost constant for all θ which eliminates the problem of the viewer moving around the table.

Conclusion

The 3D Dual View can be implemented in several ways mixing different stereoscopic techniques like anaglyph (color multiplexing), polarization multiplexing and time multiplexing. Each one has its own limitations and drawbacks that should be mitigated to delivery high quality 3D vision experience. It has been chosen to mix time-multiplexing with polarization multiplexing due to the facilities to find on the market materials and devices concerning these techniques, and because color multiplexing has bad color fidelity delivering poor image quality to the viewers. It could been done using the color multiplexing explained in Chapter 2 that uses narrowband color filters but it would have increased the budget of our "final system". Also, our partner Immersion have had already implemented the 3D Dual View using the same techniques but in transmission mode and It was an opportunity to measure the ghosting in both solutions, using transmissive and reflective screen, and compare them.

It has shown two possibilities, Case 2.1 and 2.2, to implement the 3D Dual View setup. Both cases were in reflective mode and mixing polarization and timing multiplexing. The subtle difference is in how the images are displayed and the glasses functionality. The left and the right image of one viewer are projected by one projector in case 2.1 and in Case 2.2 the left image is project by one projector and the right by the second projector. The shutters of regular active glasses open and close one after the other, like in Case 2.1, and in Case 2.2 both open and closes at the same time. The viewers, in Case 2.2, are more susceptible to differences in the light intensity of the projectors leading to amblyopia if the system is used for long periods. In the other hand, the Case 2.1 causes discomfort and fatigue due to the ghosting by polarization which is not related to its image. The interesting advantage of Case 2.2 is less depth distortion when you have fast moving objects being displayed.

At Télécom-Bretagne the ghosting effect was measured for the Case 2.1 and 2.2 in transmission mode, by means of a silver screen, and at Immersion in reflective mode only for the Case 2.1. It makes no sense to do the Case 2.2 at Immersion because the projectors are facing each other and the light received by one viewer due to one projector is more intense than the other projector and the left and right image would have unbalanced intensities. It was proved that the ghosting by polarization is the most harmful for 3D Dual View systems for several reasons and sources. First, the quarter wave plates were manually glued on the glasses linear polarisers and on the projection system linear polarisers to make the circular polarisers. Second, the quarter wave plates are not ideal and are wavelength depended. Third, the silver and the transmissive screen depolarize part of the incoming light. The color dependency of the ghosting is small, the red, green and blue colors presented the same angular behaviour but with a slight change in the ghosting intensity. The time and the polar-time ghosting are less damaging to the system because the Eyes3Shut glasses have a contrast ratio higher than 200 and a good dark state. In a way comparing the Case 2.1 in transmission mode and reflective mode is unfair and it could be said: without purpose. The light distribution is not the same and, as it was mentioned before, the position of the projector with respect to the screen is completely different. The time and the polar-time ghosting are the same for both modes and

the polar ghosting is stronger in the transmission mode due to the position of the projectors. Nonetheless, some point can be highlighted. At Immersion the ghosting has a stronger angular dependency which means that walking around the table the ghosting changes, and the same does not happen at Télécom-Bretagne. The interesting point in not having an angular dependency is that the ghost-busting can be implemented independent of the position of the viewers. Otherwise, a tracking system has to be used to know where the viewers are and compensate the ghosting according to their positions.

The ghostbusting technique was implemented in offline mode. It was possible to remove the ghosting effect improving the quality of the 3D system. However, the algorithm obliges the images to have the dynamic range reduced leading to a low contrast. A lot of work has been done to implement the 3D Dual View, measure the ghosting effect and ghostbust the images. Nevertheless, a lot of work still has to be done to improve the 3D Dual View technique and deliver high quality images to the viewers. First, tests in other screens have to be done to improve the quality of the projection, avoiding the crosstalk by improving the devices and components reduce image processing (ghostbusting). Second, the ghosbusting technique has to be implemented online and with respect to the viewer's position by using a tracking system.

Bibliography

[1] Kunio Sakamoto, Masayuki Yoshigi, “Dual-View display: dual-layer LCDs high-resolution full-screen viewing”, Proc. SPIE 6312, Applications of Digital Image Processing XXIX, 63121D, August 2006.

[2] Samsung Dual-View OLED HDTV, CES, January 2012, Las Vegas

[3] A. Smolic, K. Mueller, P. Merkle, C. Fehn, P. Kauff, P. Eisert, and T. Wiegand, *”3D Video and Free Viewpoint Video”*, Technologies, Applications and MPEG Standards, at IEEE International Conference on Multimedia and Expo (ICME'06), Toronto, Ontario, Canada, July 2006.

[4] James S. Lipscomb, Wayne L. Wooten, *“Reducing crosstalk between stereoscopic views”*, Proc. SPIE 2177, Stereoscopic Displays and Virtual Reality Systems, p. 92, April 1994.

[5] Szabo, C.; Sobota, B.; Sincak, S.; *"Depth maps and other techniques of stereoscopy in 3D scene visualization,"* Intelligent Systems and Informatics (SISY), 2011 IEEE 9th International Symposium on, vol., no., pp.207-210, 8-10 Sept. 2011.

[6] G. M. Wheelwright, *“Possibilities of Stereoscopic Motion Pictures”*, SMTPE Motion Imaging Journal, Vol. 29, pp. 603-613, December 1937.

[7] A. J. Woods, C. R. Harris, *“Comparing levels of crosstalk with red/cyan, blue/yellow, and green/magenta anaglyph 3D glasses”*, Proceedings of SPIE Stereoscopic Display and Application XXI, vol. 7253, pp. 0Q1-0Q12, January 2010.

[8] Jorke Helmut, Fritz Markus, *“INFITEC-A New Stereoscopic Visualisation Tool by Wavelength Multiplex Imaging”*, Journal of Three Dimensional Images, Vol. 19, no. 3, pp. 50-56, 2005.

[9] Lili Wang; Teunissen, K.; Yan Tu; Li Chen; Panpan Zhang; Tingting Zhang; Heynderickx, I.;, *"Crosstalk Evaluation in Stereoscopic Displays"*, Display Technology, Journal of , vol.7, no.4, pp.208-214, April 2011

[10] Klimenko S., Frolov P., Nikitina L., Nikitin I., *“Crosstalk reduction in passive stereoprojection systems”*, Eurographics 2003, pp. 235-240, 2003.

[11] L. Lipton, J. J. Hanlon, *“Polarizing Modulator for an Electronic Stereoscopic Display”*, US Patent 6,975,345. December 2005.

[12] M. Cowan, J. Greer, L. Lipton, J. Chiu, *“Enhaced Zscreen Modulator Techniques”*, US Patente 7,760,157. July 2010.

[13] Liyuan Xing; Junyong You; Ebrahimi, T.; Perkis, A.; , *"A perceptual quality metric for stereoscopic crosstalk perception,"* Image Processing (ICIP), 2010 17th IEEE International Conference on , vol., no., pp.4033-4036, 26-29 Sept. 2010.

[14] S. Pala, R. Stevens, P. Surman, “Optical crosstalk and visual comfort of a stereoscopic display used in a real-time application” in Proc. SPIE Stereoscopic Displays and Virtual Reality Systems XIV, 6490, pp. 1101-1112, 2007.

[15] Michael A. Weissman, Andrew J. Woods, *"A Simple Method for Measuring Crosstalk in Stereoscopic Displays"*, Proc. SPIE 7863, Stereoscopic Displays and Applications XXII, 786310, February 2011.

[16] Vermeirsch, K.; Van Hoey, G.; van Beurden, M.; Surman, P.; , *"Measurement and evaluation of head tracked auto-stereoscopic displays,"* 3DTV Conference: The True Vision - Capture, Transmission and Display of 3D Video (3DTV-CON), 2011 , vol., no., pp.1-4, 16-18 May 2011

[17] Lane, B., "Stereoscopic displays" in Proc. SPIE Processing and Display of Three-Dimensional Data, ed. J.J. Pearson, 0367, 20-32 (1982).

[18] Meyer, L., *"Monitor selection criteria for stereoscopic displays"* in Proc. SPIE Stereoscopic Displays and Applications III, 1669, 211-214 (1992).

[19] Chu, Y.-M., Chien, K.-W., Shieh, H.-P. D., Chang, J.-M., Hu, A., and Yang, V., *"3D Mobile Display Based on Dual Directional Lightguides"* in 4th International Display Manufacturing Conference, Taipei, Taiwan, 799-801 (2005).

[20] Hong, H.-K., Jang, J.-W., Lee, D.-G., Lim, M.-J., Shin, H.-H., *"Analysis of angular dependence of 3-D technology using polarized eyeglasses"* in Journal of the SID, 18(1), 8-12 (2010).

[21] Boher, P., Leroux, T., Bignon, T., Collomb-Patton, V., "Multispectral polarization viewing angle analysis of circular polarized stereoscopic 3D displays," in Proc. SPIE Stereoscopic Displays and Applications XXI, 7253, 0R1-0R12, 2010.

[22] Vivian K. Walworth, Louis Cincotta, Julius J. Scarpetti, *"Efficiency of Polarization Optics in Viewing Stereoscopic Images"*, Proc, SPIE 4297, Stereoscopic Displays and Virtual Reality Systems VIII, June 2001.

[23] Srivastava, A.K.; de Bougrenet de la Tocnaye, J.L.; Dupont, L.; , *"Liquid Crystal Active Glasses for 3D Cinema,"* Display Technology, Journal of , vol.6, no.10, pp.522-530, Oct. 2010.

[24] S.B. Steinman, "Amblyopia", Lecture 24, Vision science III, Binocular vision, Chapter 9, Adlers 9th edition.

[25] D. M. Hoffman, V. I. Karasev and M. S. Banks, "Temporal presentation protocols in stereoscopic displays: Flicker visibility, perceived motion, and perceived depth", Journal of Society for Information Display, Vol. 19, pp. 271-297, 2011.

[26] J. S. Lipscomb, W. L. Wooten, *"Reducing crosstalk between stereoscopic views,"* presented at Stereoscopic Displays and Applications V, published in Proceedings of SPIE Stereoscopic Displays and Virtual Reality Systems, vol. 2177, pp. 92-96, February 2004.

[27] J. Konrad, B. Lacotte, E. Dubois, *"Cancellation of image crosstalk in time-sequential displays of stereoscopic video"* in IEEE Transactions on Image Processing, vol. 9, no. 5, pp. 897-908, May 2000.

[28] A. J. Chang, H. J. Kim, J. W. Choi, K. Y. Yu, *"Ghosting reduction method for color anaglyphs"* in Proceedings of SPIE Stereoscopic Displays and Applications XIX, vol. 6803, pp. 68031G, January 2008.

General Conclusion and Perspectives

This thesis covered two main points in the field of stereoscopic vision: the liquid crystal shutters and 3D Dual View Technique. The engineering work in the first part was to define the best structure, liquid crystal and process of fabrication to improve the LC shutters and consequently the 3D active glasses. Always the aim was to enhance the 3D experience. Many solutions were tested, optically characterized and, the advantages and disadvantages of each one were pointed out. Besides, in cooperation with Université de Bretagne Occidentale (UBO) it was realized some polarimetric measurements using a Snapshot Muller Matrix polarimeter made by them. It was evidenced the capability of the polarimeter to characterize shutters based on liquid crystal giving important information about the behavior of the liquid crystal director. In the end, the 3D Dual View technique was implemented at Télécom Bretagne in reflective mode and in two different configurations. The biggest issue of the technique, the crosstalk, which leads to ghosting effects, was addressed and an algorithm of ghostbusting to overcome was proposed and tested. In partnership with the company Immersion, which has built the 3D Dual View in transmissive mode, it was also possible to characterize and to compare the ghosting effect.

Liquid Crystal Shutters

Different types of liquid crystal shutters have been fabricated in clean room environment. To define the quality and the viability of these shutters to be used in 3D active glasses, seven aspects were taken into account and characterized: contrast ratio, response time, texture, robustness, scattering, transmission and white dispersion. The surface stabilized ferroelectric liquid crystal has an excellent response time which makes it a good alternative to increase the residual light in 3D systems. However, the chevron structure due to the shrinkage of the layers leads to zigzag defects reducing the contrast increasing the ghosting effect. To overcome the chevron, a twisted structure by rubbing the top and the bottom substrates in angle was proposed. The hypothesis was to compress the layers of the liquid crystal in the smectic-A phase and avoid the shrinkage in the smectic-A to smectic-C transition. It was obtained samples free of chevron with high contrast ratio maintaining the good response time intrinsic to the ferroelectric liquid crystal, but the texture changes to roof-top and stripes after applying electric field for long periods. Further, the samples presented a very weak resistance against shocks and even a simple manipulation can damage the cell destroying the alignment of the liquid crystal. Thus, a mixture of liquid crystal and polymer was tested to improve the robustness. The polymer network increases the response time of the shutter, but the switching speed is well within the requirements for 3D viewing. One of the advantages is that the samples are less susceptible to shocks, but the formed polymer network scatters the light and the contrast ratio goes down. Finally, the nematic solution, which is the liquid crystal used in the commercial 3D active glasses, was studied. Two nematic liquid crystals, one with high birefringence and the other with low birefringence were mixed in order to increase the light transmission over the visible spectra without slowing down the shutter. We have achieved a shutter with good transmission without changing considerably the response time. Nematic

liquid crystals have been studied for many years and are already established on the 3D active glasses market. In the future, it would be interesting to develop the phase separation technique using a combination of a nematic liquid crystal and an epoxy resin. In this way, it could be possible to reduce the thickness of the liquid crystal layer in a shutter decreasing the response time. The shutters based on ferroelectric liquid crystal and its different configurations should be thoroughly investigated. It is necessary to overcome the fragility and the scattering issue in maintaining required response time by synthesizing new materials. X-Ray measurements in the twist configuration should be performed to understand the layer organization in smectic-A and in smectic-C phase.

Snapshot Muller Matrix Polarimeter

The main conclusion concerning the polarimetric measurement is that the polarimeter is capable to characterize and, consequently, give important information about the liquid crystal director, texture and, indirectly, the behavior of the smectic layer. We have done static and dynamic measurements in two samples with different textures. It can be seen the relation of the polarimetric properties with the director between the two addressed states in a roof-top/chevron and stripe texture. It was seen that the difference between the memory state and the address state in cells with roof-top/chevron texture is higher due to the chevron structure of the layers and the director switch in a flat trajectory. On the other hand, in a stripe texture the layers are straightened-up, the difference becomes lower and the trajectory of the director is almost circular. Besides, it was shown that there is a gradual change of the polarimetric parameters while the samples were switching from a chevron to a stripe texture. This evidenced the reversible case for in-plane switching and the irreversible phenomena in out-plane switching for the transition from chevron to bookshelf. Polarimetric measurements were performed with polymer stabilized ferroelectric liquid crystal cells. The elastic coupling becomes more important than the ferroelectric coupling when the polymer network is denser. The results of ellipiticity shown a non-uniform distribution of the bulk, but it cannot be confirmed with polarimetric measurements. Another hypothesis was that the polymer network masks de zigzag defects but in this case also the polarimetric measurements cannot give information about the bulk and the in-depth molecular distribution.

3D Dual View Technique

The final part to the thesis was a 3D application, popularly known as 3D Dual View, which is a three dimensional system where two viewers can share the vision of the same subject in 3D, but from different perspectives. In order to have two separated 3D images (four 2D images/four 2D video streams) without interfering with each other several methods using time, color and polarization multiplexing were proposed. A prototype was built at Télécom-Bretagne in reflective mode, using a silver screen in two different configurations: case 2.1 and case 2.2, both mixing polarization with time multiplexing. In case 2.1, the viewers were separated by polarization and the images were time multiplexed. Case 2.2, the viewers were separated in time and the images multiplexed by polarization. Another prototype was built at Immerssion in transmissive mode but for the case 2.1 only. Two methods to quantify the crosstalk, and consequentially the ghosting effect, were suggested. The first one using test

charts, but it cannot measure the ghosting in different locations of the screen and it can be subjective since the eye sensibility varies from person to person. The second method uses a chromameter to carry out the measurements. The latter was used in all the experiments performed in both cases and modes. The ghosting was measured for red, green and blue colors. Also, a ghosting ratio was defined and used to evaluate the ghosting effect distribution. In all the situations and colors the ghosting by polarization was the most harmful followed by the time ghosting. In transmissive mode the ghosting has a higher angular dependence in θ and φ than in reflective mode, which depends only on φ. Moreover, an algorithm of ghostbusting to eliminate the ghosting effect was proposed and implemented, but with the decreasing of contrast. An important observation that was highlighted concerning the two cases was the physiological aspects. The case 2.2 can cause amblyopia if the system is used for long periods with unbalanced projectors. The case 2.1 fatigues the eyes due to the unrelated ghosting effect and the presence of artifacts caused by moving objects. There is a scope to improve the 3D Dual View system as it has the potential in different domains. As stated before in Chapter 4, different devices (screen, polarisers, quarter-wave plates, shutters and projectors) should be tested to optimize the system. A tracking system has to be implemented to allow the projectors to display the images with the correct perspectives with respect to the viewer's position. Also, the ghostbusting has to be tested in real time using the tracking coordinates.

Finally, we have successfully demonstrated various liquid crystal shutters and the advantages and disadvantages of each one. A mixture of nematic liquid crystal was proved to be a good solution to improve the 3D active glasses. Polarimetric measurements on the shutters were made and the Muller Matrix Polarimeter has demonstrated to be a great tool to characterize and to describe surface stabilized ferroelectric liquid crystal with and without polymer. The 3D Dual View was built, the ghosting effect was characterized and was mitigate by a ghostbusting algorithm.

Appendix I:

Polarized Light and The Mueller Matrix

A regular light beam propagating in an isotropic medium is the sum of individual waves oscillating perpendicular to the travel direction without a preferred orientation. If all the waves vibrate in a parallel plane and in the same direction, this light is said to be polarized, i.e., it has a directional characteristic. Particularly, in this situation, the light is defined as linearly polarized. However, the light can be circularly or elliptically polarized.

The following subsections have the objective to present the definition of light polarization and the mathematical approach to understand the Jones Vector, the Mueller Matrix and, consequently, the SMMP.

Light Polarization

Polarization is the behaviour with time of the electric field vector of an electromagnetic wave observed at a fixed point in space. In order to quantify the polarization, it will be considered a transversal wave propagating in an isotropic material. Let +z to be the direction of propagation and $\vec{k}$ the propagation vector, the electric field of the propagating wave can be written as:

$$\begin{aligned} E_x(z,t) &= E_{0x}\cos(\varpi t - kz + \varphi_x) \\ E_y(z,t) &= E_{0y}\cos(\varpi t - kz + \varphi_y) \\ E_z(z,t) &= 0 \end{aligned}$$

where E_x, E_y and E_z are respectively the electric field components along x, y and z, ϖ is the angular frequency and φ_x, φ_y, $E_{\grave{a}x}$ and $E_{\grave{a}y}$ are the phases and the maximum amplitude of each component, respectively. Since we are looking for the electric field at fixed point in space and its behaviour, it can be assumed $z = 0$. For a general case, elliptical polarization, the amplitudes for de x and y components are different ($E_{0x} \neq E_{0y}$) and they are out of phase by an angle δ ($\varphi_x = \varphi_y - \delta$). Then, calculating $(E_x)^2 + (E_y)^2$, it can be written:

$$\left(\frac{E_x}{E_{0x}}\right)^2 + \left(\frac{E_y}{E_{0y}}\right)^2 = \cos^2(\varpi t + \varphi_x) + \cos^2(\varpi t + \varphi_x - \delta)$$

Above it is the equation of an ellipse with the major axis doing an angle α with respect to the x axis, more commonly defined as:

$$\left(\frac{E_x}{E_{0x}}\right)^2 + \left(\frac{E_y}{E_{0y}}\right)^2 - 2\left(\frac{E_x}{E_{0x}}\right)\left(\frac{E_y}{E_{0y}}\right)\cos(\delta) = \sin^2(\delta)$$

and the α as:

$$\alpha = \frac{1}{2}\tan^{-1}\left[\frac{2E_{0X}E_{0y}\cos\delta}{E_{0x}^2 - E_{0y}^2}\right]$$

In Figure 139, the description of the ellipse and its respective parameters.

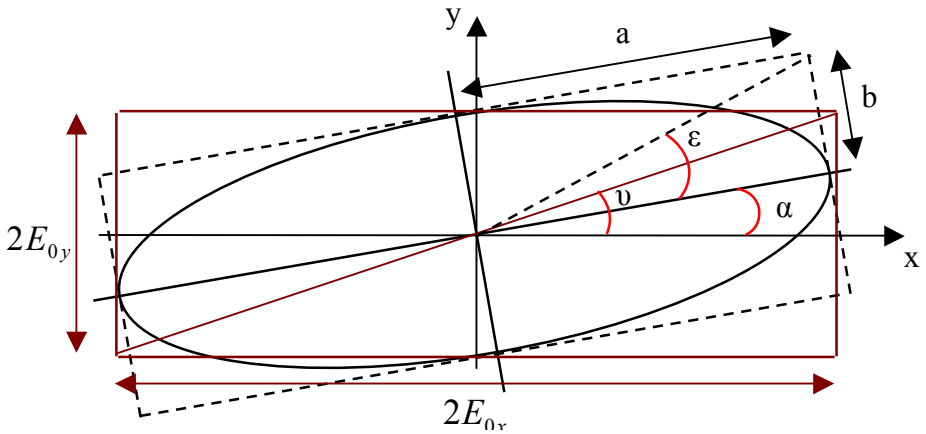

Figure 139 - Polarisation Ellipse

The parameters α, ε and υ are respectively the azimuth, ellipticity and the diagonal angle, a and b are the major and minor axis of the ellipse. From the ellipse case and according to equation X and X it is possible to obtain the circular and the linear polarization. If $\delta = \pi/2 \pm n\pi$ and $E_{\grave{a}x} = E_{\grave{a}y} = E_{\grave{a}}$ the wave is circularly polarized and if $\delta = \pm n\,\pi$ the wave is linear polarized. It is show in Figure 140 an example of the three types of polarization: elliptical, circular and linear.

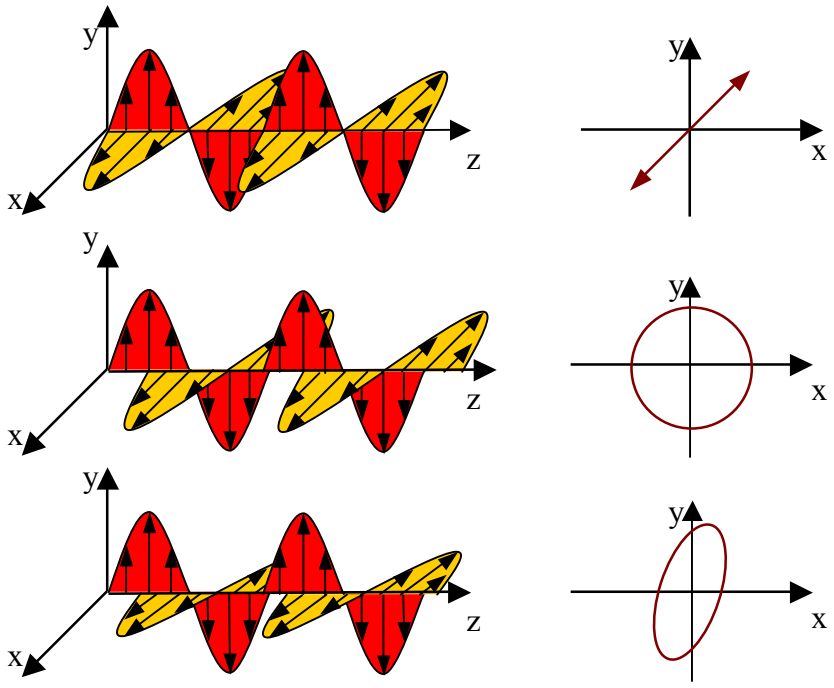

Figure 140 - Examples of polarisation states: linear (a), circular (b) and elliptical (c).

The Stokes Vector and the Mueller Matrix

The formal description of a light wave should be done by specifying the intensity, degree of polarization, plane of polarization and ellipticity of the radiation. Sir George Stokes [11], in 1852, proposed a set of four parameters to represent a polarized light based on the measurements of intensities by means of ideal polarizing components. First, the light intensity I_0 is measured without polarizing components. After, three intensities should be measured when the light passes through an ideal linear polarizer at 0 (I_{0^o}), 45 ($I_{\pm 45^o}$) and 90(I_{90^o}) degrees of orientation with respect to the coordinate system fixed to the light propagation direction. At last, the intensity is measured using ideal right (I_r) and left (I_l) circular polarisers. These steps, and consequently the measured intensities, allows to determine the Stokes parameters S_0, S_1, S_2 and S_3, it can be written as :

$$S = \begin{pmatrix} S_0 \\ S_1 \\ S_2 \\ S_3 \end{pmatrix} = \begin{pmatrix} I_0 \\ I_{0^o} - I_{90^0} \\ I_{45^o} - I_{-45^o} \\ I_r - I_l \end{pmatrix} = \begin{pmatrix} \langle E_{0x}^2 \rangle + \langle E_{0y}^2 \rangle \\ \langle E_{0x}^2 \rangle - \langle E_{0y}^2 \rangle \\ 2\langle E_{0x} E_{0y} \cos(\delta) \rangle \\ 2\langle E_{0x} E_{0y} \sin(\delta) \rangle \end{pmatrix}$$

where the symbol $\langle\ \rangle$ means the temporal and the spatial average of the intensity of the light beam in the detection system. Further, applying the time average definition to the polarization ellipse leads to the relation $S_0^2 = S_1^2 + S_2^2 + S_3^2$, which allows the representation of the polarization states on the Poincaré sphere of radius S_0 with S_1, S_2 and S_3 as the Cartesian coordinates.

For an ideal polarized light, it is possible to rewriting the Stokes vector, normalized by S_0, as a function of the ellipse variables ε, υ and α:

$$S = \begin{pmatrix} I \\ \cos(2\varepsilon)\cos(2\alpha) \\ \cos(2\varepsilon)\sin(2\alpha) \\ \sin(2\varepsilon) \end{pmatrix}$$

Furthermore, the Stokes vector can also describe partially polarized light [12]. In that case, it is defined a parameter *p* which represents the degree of polarization, given by:

$$p = \frac{\sqrt{S_1^2 + S_2^2 + S_3^2}}{S_0}$$

The degree of polarization *p* is equal to 1 for fully polarize light and equal to 0 for nonpolarized light. Stokes vector with *p* between 0 and 1 is for partially polarized light. Then, since the Stokes vector is able to characterize polarized light, or partially polarized light or unpolarized light, it is convenient to establish a matrices formalism relating the Stokes vector of a light beam leaving an optical device (S_e) and the Stokes vector of the input light beam (

S_i). Thus, Hans Mueller [13], in 1943, introduced the Mueller matrix (M) to represent a particular optical element through the determination of the Stokes Vector S_e and S_i. It is a 4x4 matrix where the coefficients contain all the polarimetric information on the optical system under study and the relation is written as:

$$S_e = (M).S_i = \begin{bmatrix} m_{00} & m_{01} & m_{02} & m_{03} \\ m_{10} & m_{11} & m_{12} & m_{13} \\ m_{20} & m_{21} & m_{22} & m_{23} \\ m_{30} & m_{31} & m_{32} & m_{33} \end{bmatrix}.S_i$$

The Mueller Matrix **M** of an optic device is the matrix which transforms an incident Stokes vector SE into the exiting Stokes vector SI. The Mueller matrix M (k,LAM) is a function of the direction of propagation and wavelength. The formalism involved can characterise the polarization in the way that it contains all the polarization properties like: diattenuation, retardance and depolarization. Also, with the Matrix Muller formalism, it is possible to study one optical system with n-devices placed in cascade and it can be written as:

$$S_e = [M_n]..[M_3][M_2][M_1]S_i$$

In the next section it will be presented the Mueller Matrix of the polarizing components used in the polarimeter.

Appendix II:

Publications in Peer Review Journals

- **SILVA, V N H**; BABILOTTE, P; DUBREUIL, M; RIVET, S; JEUNE, B LE; DUPONT, L. Characterization of the dynamics of surface stabilized ferroelectric liquid crystal under electric field by full optical snapshot matrix Mueller polarimeter. Optical Engineering (Bellingham. Print), v. 51, p. 123601, 2012.

- **SILVA, Vinicius**; STOENESCU, Daniel; NASSOUR, Théo; DE LA RIVIERE, Jean-Baptiste; DE BOUGRENET DE LA TOCNAYE, Jean-Louis. Ghosting impingements in 3D Dual-View projection systems. Journal of Displays Technology.

- BABILOTTE, P; **SILVA, V N H**; DUBREUIL, M; RIVET, S; JEUNE, B LE; DUPONT, L. Experimental study of the dynamic behaviour of twisted ferroelectric liquid crystal samples using snap-shot Mueller matrix polarimetry. Journal of Physics. D, Applied Physics (Print), v. 46, p. 125101, 2013.

- Philippe Babilotte; **SILVA, V. N. H**.; Matthieu Dubreuil; Sylvain Rivet; Laurent Dupont; Bernard Le Jeune. Impact of the concentration in polymer on the dynamic behavior of polymer stabilized Ferroelectric liquid crystal using Snap-shot Mueller matrix polarimetry. The European Physical Journal. E, Soft Matter (Print), 2013 (accepted for publication).

- Dubreuil, Matthieu ; Babilotte, Philippe ; **Silva, Vinicius N.H.** ; Rivet, Sylvain ; Le Jeune, Bernard ; Dupont, Laurent . Correlation between static and dynamic polarimetric properties and the texture of surface-stabilised ferroelectric liquid crystal cells. Liquid Crystals (Print), v. 1, p. 1-10, 2012.

Publications in International Conferences

- **SILVA, V. N. H**.; K. Sathaye; S. Dianne; RIBEIRO, R. M.; BARBERO, A. P. L. Cholesteric Liquid-Crystal Filters for Visible WDM Channels. In: 24th International Liquid Crystal Conference, 2012, Mainz. 24th International Liquid Crystal Conference, 2012. (Poster)

- S. Dianne; RIBEIRO, R. M.; BARBERO, A. P. L.; **SILVA, V. N. H.**; K. Sathaye; L. Dupont. Liquid-Crystal Filters for Visible WDM Channels over Polymer Optical Fibres. In: SEMINATEC 2012, 2012, São Bernardo do Campo. SEMINATEC 2012, 2012.

- S. Dianne; **SILVA, V. N. H.**; K. Sathaye; RIBEIRO, R. M.; BARBERO, A. P. L. Development of Cholesteric Liquid-Crystal Spectral Filters for Visible WDM Channels Over Polymer Optical Fibres. In: MOMAG 2012, 2012, João Pessoa. MOMAG 2012, 2012.

- J.-L. de Bougrenet de La Tocnaye ; L. Dupont ; D. Stoenescu ; K. Sathaye ; **SILVA, V. N. H.** Liquid Crystal for 3-D Active Glasses (invited). In: 3rd International Workshop on Liquid Crystals for Photonics LCP2010, 2010, Elche. 3rd International Workshop on Liquid Crystals

for Photonics, 2010. p. 23-24.